NOTICE

The quality of this microform is heavily dependent upon the quality of the original thesis submitted for microfilming. Every effort has been made to ensure the highest quality of reproduction possible.

If pages are missing, contact the university which granted the degree.

Some pages may have indistinct print especially if the original pages were typed with a poor typewriter ribbon or if the university sent us an inferior photocopy.

Reproduction in full or in part of this microform is governed by the Canadian Copyright Act, R.S.C. 1970, c. C-30, and subsequent amendments.

AVIS

La qualité de cette microforme dépend grandement de la qualité de la thèse soumise au microfilmage. Nous avons tout fait pour assurer une qualité supérieure de reproduction.

S'il manque des pages, veuillez communiquer avec l'université qui a conféré le grade.

La qualité d'impression de certaines pages peut laisser à désirer, surtout si les pages originales ont été dactylographiées à l'aide d'un ruban usé ou si l'université nous a fait parvenir une photocopie de qualité inférieure.

La reproduction, même partielle, de cette microforme est soumise à la Loi canadienne sur le droit d'auteur, SRC 1970, c. C-30, et ses amendements subséquents.

The Effect of Interface Properties on the Adhesion of Cement Paste to Various Substrates

by

Glendon B. Pye

Submitted in partial fulfillment of the
requirement for the degree of
Master of Applied Science

Department of Civil Engineering
University of Ottawa
Ottawa, Canada

ISBN 0-315-62308-X

Canada

UNIVERSITÉ D'OTTAWA
UNIVERSITY OF OTTAWA

ABSTRACT

This study deals with the adhesion of cement paste and modified cement paste systems to substrates of steel and glass for hydration times of up to seven days.

The bond strength of cement, clinker and C_3S paste in addition to cement paste systems containing salts ($NaNO_3$, $CaCl_2$, $Ca(C_3H_5O_2)_2.H_2O$) and silica fume was studied using a uniaxial tensile testing apparatus. A new term, interface fracture energy, was derived to provide a more meaningful basis for comparison of bond tests. This was necessary as the interfacial bond for all the paste systems was thickness dependent. A decrease in paste thickness resulted in an increase in bond failure stress.

Factors other than the deposition of CH and C-S-H at the interface may affect bond strength. Comparison of the bond strength data for the control paste and the C_3S and clinker pastes indicates that the effect of the hydration products resulting from gypsum reactions eg. sulphoaluminate phases, may be secondary. Physico-mechanical characteristics of the interface eg. geometry and size of inherent flaws may be important. The addition of the salts and silica fume did not consistantly increase the bond strength of the paste. It is inferred that factors other than CH crystal size are important.

Interface fracture energy, γ, reaches a maximum after one day, decreases at two days then remains relatively constant. The decrease in bond strength may be due to the pressure exerted by the formation of CH crystals in the interface. In general the interface fracture energy increased with a decrease in water-cement ratio. Other time and system dependent factors appear to affect the development of interface fracture energy. Values of γ for all systems studied range from 0.001 to 1.66 Jm^{-2} suggesting that van der Waal's forces of attraction are the primary binding forces.

ACKNOWLEGEMENTS

The author wishes to express his sincere appreciation to the following individuals:

To Dr. J.J. Beaudoin for his continuous support and encouragement as thesis supervisor.

To Messrs. R.E. Myers, G.W. Chan, E.G. Quinn, R. Lacroix, J. Margeson, H. Schultz, M. Arnott, G. Polomark, Ms. D. Charron and all the staff of the Building Materials Section at the Institute for Research in Construction for all their help and friendship.

To his parents and friends for their support and understanding.

TABLE OF CONTENTS

LIST OF FIGURES

LIST OF TABLES

LIST OF ABBREVIATIONS

BSE	backscatter electron
$Ca(C_3H_5O_2)_2.H_20$	calcium propionate (propionate)
$CaCl_2$	calcium chloride
$Ca(OH)_2$	calcium hydroxide
CH	calcium hydroxide
C-S-H	calcium silicate hydrate
ID	interior diameter
$NaNO_3$	sodium nitrate
RH	relative humidity
SEM	scanning electron microscopy
SF	silica fume
TGA	thermogravimetric analysis
w/c	water-cement ratio
γ	interface fracture energy

CHAPTER 1

INTRODUCTION

1.1 Portland Cement and Cement Paste

Concrete is one of the major construction materials used today. Its application varies from reinforced concrete slabs in buildings to material for patio stones and ship hulls. Several books have been written on the uses and properties of concrete and the following summary makes reference to them. Cement paste makes up 25-40% of the total volume of hardened concrete and is the material which holds together the coarse and fine aggregate to produce a cohesive mass. Portland cement is a hydraulic material, which sets and hardens to form cement paste in the presence of water. This process is called hydration.

Portland cement is produced from materials containing lime, silica, alumina and iron components, such as limestone, iron ore, chalk, sand, clay or shale. The materials are pulverized and combined to produce the correct chemical composition. The combining can use a wet or a dry process. The materials are ground and combined in a slurry in the wet process. The materials are processed without water in the dry process. The combined materials are fed into a large rotating kiln where the raw mix sinters and partly fuses into balls called clinker. The clinker is then cooled and subsequently ground to a fine powder to which gypsum is added, to control the setting time. This mixture is called portland cement.

Four compounds constitute 90% of the weight of portland cement; they are:

Tricalcium silicate: C_3S

Dicalcium silicate: C_2S

Tricalcium aluminate: C_3A

Tetracalcium aluminoferrite: C_4AF

The notation generally used by cement chemists for these compounds is adopted where: C=CaO, S=SiO_2, A=Al_2O_3 and F=Fe_2O_3. The different types of portland cement are

composed of different combinations of the cement minerals depending on the properties desired. The two calcium silicate compounds make up 75% of the weight of the portland cement and are the primary cementing compounds. The strength development of the cement paste during hydration parallels the behaviour of the C_3S and C_2S pastes. The silicates react with water to form calcium hydroxide (CH) and calcium silicate hydrate (C-S-H), which is the most important cementing compound in concrete. C_3A liberates large amounts of heat during hydration, but contributes slightly to paste strength. Flash set can occur unless adequate gypsum is added to the clinker. C_4AF reduces the clinkering temperature, hydrates rapidly and provides little contribution to the strength.

The heat of hydration of the cement paste is generated as a result of chemical reaction between the cement and water and is mainly dependent on the chemical composition of the cement. The extent of hydration of cement paste can be followed by several techniques[1,2]. These include:

a) estimation of the amount of CH in the paste

b) estimation of the amount of chemically combined water.

c) estimation of the depletion of anhydrous phases by X-ray diffraction methods

Limitations of these methods are discussed in the literature.

1.2 Bond Strength

Bond strength is an engineering property which, generally describes how well one material "sticks" to another. An understanding of the factors which influence bond strength is relevant for new developments in concrete technology. In the last decade demands for high performance concrete and improved cement based composites have increased. The properties of interface regions ie. fiber-paste, aggregate-paste, aggregate-mortar are central to the performance of these materials. The development of bond strength is intimately related to the nature of these interface zones. It is arguable,

therefore, that evaluations of bond strength should consider the impact of interface properties and microstructure on the fundamental meaning of the result.

Physicists have long been interested in the fundamentals of adhesion and the nature of the surface forces when solid surfaces are brought into close proximity. Analysis explaining "sticky" solid phenomena in terms of the interface energy of contact (γ) was advanced only in the 1970's[3]. The γ term is defined as the work done against surface attractions in breaking unit area of solid-solid interface. Estimates of γ for gelatine-glass interfaces are approximately 0.071 Jm^{-2}, the required magnitude for van der Waals attractions. These theories predict that adhesion force is not proportional to the contact area! Failure is progressive and considered to take place by a process akin to crack propagation. Failure force is described as being dependent on surface energy and not on strength. These arguments suggest the possibility that previous approaches for examining bond characteristics in cement systems merit re-examination.

Many researchers have described one or more of the vast number of bond tests available indicating that at present there is no one accepted standard permitting bond strength values to be compared equally. Few researchers have recognized or considered the implications of the dependence of cement paste bond on adhesive thickness. Schnittgrund observed this phenomena, ignored it, and completed his testing with only one paste thickness[4]. The thickness dependence of thin elastic films on the bond strength with rigid substrates was first discussed by Kendall[5]. He employed an energy approach and demonstrated that the bond strength of the thin film was dependent on the thickness of the film and other quantities. Griffith was the first to show that fracture of a solid depends not only on the geometry of the bond, but also on the surface energy of the solid and its elastic properties[6]. It was inferred, therefore, that any equation to calculate bond strength must include these properties. Meissner and Merrill investigated this problem by varying the thickness of the glue in a butt joint and found that the strength of the joint decreased as the glue thickness increased[7]. Kendall's approach involved obtaining an

expression for the total energy, U_T, in a strained butt joint. The characteristic dimension of the joint was termed, "a". For equilibrium fracture to occur the derivative of U_T with respect to, a, must equal zero. This condition means that the work done to break the bond is equal to the surface energy gain. The following derivation is given to illustrate the parameters which are relevant in a uniaxial bond test[8].

A thin elastic film of thickness , t, is assumed to be sandwiched between two rigid discs of diameter , 2a, to which a uniaxial tensile load P is applied.

Stress, σ, due to an applied tensile load P is given as: $\sigma = P/(\pi a^2)$

Axial deformation of the film, δ,leads to volume increase: $\Delta V = \pi a^2 \delta$

Volumetric strain $\varepsilon_V = \Delta V/V = \pi a^2 \delta/(\pi a^2 t) = \delta/t$

To a first approximation $\sigma = K \times \varepsilon_v$

where K=bulk modulus (for no lateral deflection this is not strictly true)

ie. $P/\pi a^2 = K\delta/t$

therefore $P = K\pi a^2 \delta/t$

or $\delta = Pt/(\pi a^2 K)$

stored energy = 1/2 force x deflection

$= P^2 t/2\pi K a^2$

Potential energy = $-P\delta$

$= -P \times Pt/(\pi a^2 K)$

$= -P^2 t/(\pi a^2 K)$

surface energy = $-\pi a^2 \gamma$

therefore total energy, $U_T = -\pi a^2 \gamma - P^2 t/2\pi K a^2$

$$\frac{dU_T}{da} = 0$$

therefore $-2\pi a\gamma + P^2 t/\pi K a^3 = 0$

$P^2 = 2\pi^2 a^4 K\gamma/t$ or $P/\pi a^2 = (2K\gamma/t)^{0.5}$ .....(1)

If equation (1) governs the bond strength phenomena in cement systems it is apparent that the applied load will be dependent on the thickness of the paste adhesive and independent of the properties of the rigid substrate or adherent. This is a primary postulate of this investigation. An estimate of γ, can also be obtained from analysis of bond failure stress versus thickness curves.

1.3 Engineering the Cement Paste/Substrate Interface

The cement paste/inclusion interface consists of a CH film deposited on the surface of the inclusion backed by a layer of C-S-H. The presence of the CH film is viewed by many researchers as the reason for lower than expected bond strengths between the cement paste and inclusions or substrates such as steel and glass. Some researchers have speculated that interface properties may be dependent on the size of the CH grains or crystallites in the interface region. It may be possible to produce a much stronger interface by controlling the CH crystal size. The concept of grain refinement has been utilized for many years in the production of steel, wherein the carbon is added to the iron to give the steel a much higher modulus of elasticity and toughness. Kung investigated the effect of $CaCl_2$ and $NaNO_3$ additions on CH grain size in C_3S pastes at 25° C. He found that the C_3S paste had a CH crystal density of 25.0 crystals/mm^2 while the $CaCl_2$ addition produced 9.0 and the $NaNO_3$ 14.5 crystals/mm^2 [9]. Ramachandran published data in which $Ca(C_3H_5O_2)_2.H_2O$ was added to C_3S pastes to modify the CH grain size resulting in a grain density of 14 crystals/mm^2 [10].

1.4 Scope of the Investigation

The determination of bond strength is by no means a simple endeavor as evidenced by the great number of bond tests in use throughout the world.

In this investigation, an attempt will be made to measure the bond strength of cement pastes adhered to substrates of glass and steel. Pastes with varying compositions will be examined. A uniaxial tensile bond apparatus will be employed to make the measurements. Relationships between bond strength and cement paste adhesive thickness

will be established. A new term, the interface fracture energy (γ), will be calculated for each paste system in an attempt to provide a more meaningful measure from which bond tests may be compared. Values of γ will be used to assess the nature of the bonds in the interface region between bulk cement paste matrix and the substrate. Scanning electron microscopy and backscattered image analysis techniques will be used to examine debonded surfaces with a view to establishing the failure mechanisms involved.

An effort will also be made to engineer the paste/substrate interface by attempting to change the size of the CH crystals found at the interface. Chemical compounds $NaNO_3$, $CaCl_2$, and $Ca(C_3H_5O_2)_2.H_2O$ will be used to alter the CH crystal size and silica fume will be used to inhibit the formation of CH at the interface. Clinker and C_3S pastes will also be studied. These pastes exclude the possibility of ettringite formation at the interface.

1.5 Objectives

The objectives of this study are:

1. To determine the effect of interface properties and hydration parameters on the bond strength of cement pastes to steel and glass substrates.
2. To utilize an energy approach to develop a relationship between bond strength and adhesive thickness and validate the relationship experimentally.
3. To investigate the applicability of an improved descriptor of interface properties eg. interface fracture energy.
4. Engineer the interface with different additives. Test the hypothesis that controlling CH crystal size at the interface will improve bond strength.

CHAPTER 2

LITERATURE REVIEW

2.1 Bond Tests

There are many bond tests in current use. The large number of different tests suggests that there are inherent difficulties in obtaining reliable values for bond strength. The following list compiled by Kuhlmann[11] gives examples of the wide variety of bond tests, with descriptions and test users.

A SUMMARY OF CONCRETE BOND TESTS
(EXCLUDING JIS TESTS)

TENSILE BOND

1) Direct Tensile

   a) Pipe Nipple Test

      Users : Dow Chemical, Reinhold Chemical, National Bureau of Standards

      Description : Under development by Dow Chemical;it is applicable to both laboratory prepared samples and field cores; reproducability is good; early age tests (24 hours) are possible.

   b) Pullout test (Lok-Test)

      Users : Trow, Ltd.; Dow Chemical

      Description - Developed for measuring overlay bond in the field; core drill cuts through overlay into base concrete; metal plate is glued to overlay surface and pulled off by mechanical device that measures tensile load; suitable also to lab; recommended by ACI 503.

2) Indirect Tensile (Split Tensile, modified ASTM C 496)

   User : Wiss, Janney & Elstner

   Description : Core is cut at interface such that a cylinder with bond plane between concretes is vertical axis of cylinder; specimen is mounted horizontally in testing machine with compression applied vertically to bond plane; measures tensile bond strength indirectly by compression test; suitable to both lab and field.

SHEAR BOND

1) Direct

   a) Guillotine

      Users : FHWA, NY DOT. -5026E; TRR 814; Ohio D.O.T.

      Description : A minimum 1" thick overlay on a 4" diameter conventional concrete guillotine apparatus; sample can either be lab prepared or a core from the field; problem can develop if bond interface is not on a plane at right angles to the axis of the cylinder.

   b) Flat Plate

      Users : Rohm & Haas

      Description - 2"x2"x1/2" thick mortar is cast onto a flat concrete surface in a compression machine.

   c) Arizona Slant Shear

      Users : FHWA RD-78-35

      Description - Conventional concrete cylinder is cut on a diagonal to serve as base; it is inserted in cylinder mold and material in question is applied to it; measures shear strength of interface indirectly by compression test; materials with different moduli of elasticity may affect results; suitable for lab only.

   d) Dow Pipe

      Users : Dow Chemical (formerly)

      Description : Sample preparation similar to Guillotine Test; assembly is inserted into pipe sleeve with interface aligned at end of pipe; mounted horizontally on compression machine, cap is sheared off with special semi-circular jig; same limitations as Guillotine Test.

2) Indirect

   a) Flexural Beam

      User : Pennsylvania State University

      Description : A standard flex beam mold is cast half depth with conventional concrete, cured, surface cleaned and overlayed with concrete to be tested; composite beam is then third point loaded on testing machine; shear stress at interface when failure occurs is calculated.

Other bond tests are briefly described:

Chana presented a realistic test method for determining bond stresses in reinforcing bars[12]. In the experiments both smooth and ribbed reinforcing bars are cast in concrete prisms at all four corners with 25mm cover. The bars are then pulled out of the prism with a loading jack and the maximum stress is calculated at the maximum load. These values were then compared to BS 8110 and proved to be very close to the standard values. Chana also referred to BS 4449, the British bond strength test, wherein a reinforcing bar is pulled out of the center of a concrete prism cast with heavy transverse steel to prevent splitting. The transverse steel causes the bond stress produced to be very high.

Nakayama and Beaudoin developed an overhanging beam method of calculating bond strength between steel and cement paste. A uniform coating of cement paste is applied to a flexible steel substrate[13,14]. The composite beam is then placed on supports so that the overhang is 0.46 times the midspan length negating the effect of any uniformly distributed weight changes in the paste. The resultant bond strength at a given hydration time is calculated from the sum of the midspan deflection values due to hydration at 100% RH and subsequent shrinkage at 0% RH.

Schnittgrund determined bond strength for cement paste and cement minerals by casting a 1.27 mm thick paste layer between the ends of two 76.2 mm steel bars[4]. The composite bars were tested in flexure using four point loading in a universal testing machine. The thickness of the paste between the bars was varied in his initial experiments. He found that bond strength of the cement paste increased with a decrease in thickness. Typical results are shown in Figure 2.1.

Sasse and Fiebrich described many bond tests; among those were two direct tensile strength tests[15]. In the first test a composite 160 mm diameter cylinder is formed by placing fresh concrete in a cylinder half filled with old concrete. The sample is then tested in tension to determine the bond developed between the new and old concrete. The second tensile test involved casting a 200 mm concrete cube between 100 mm square

Figure 2.1 Schnittgrund's Bond Strength Data

(from reference 4)

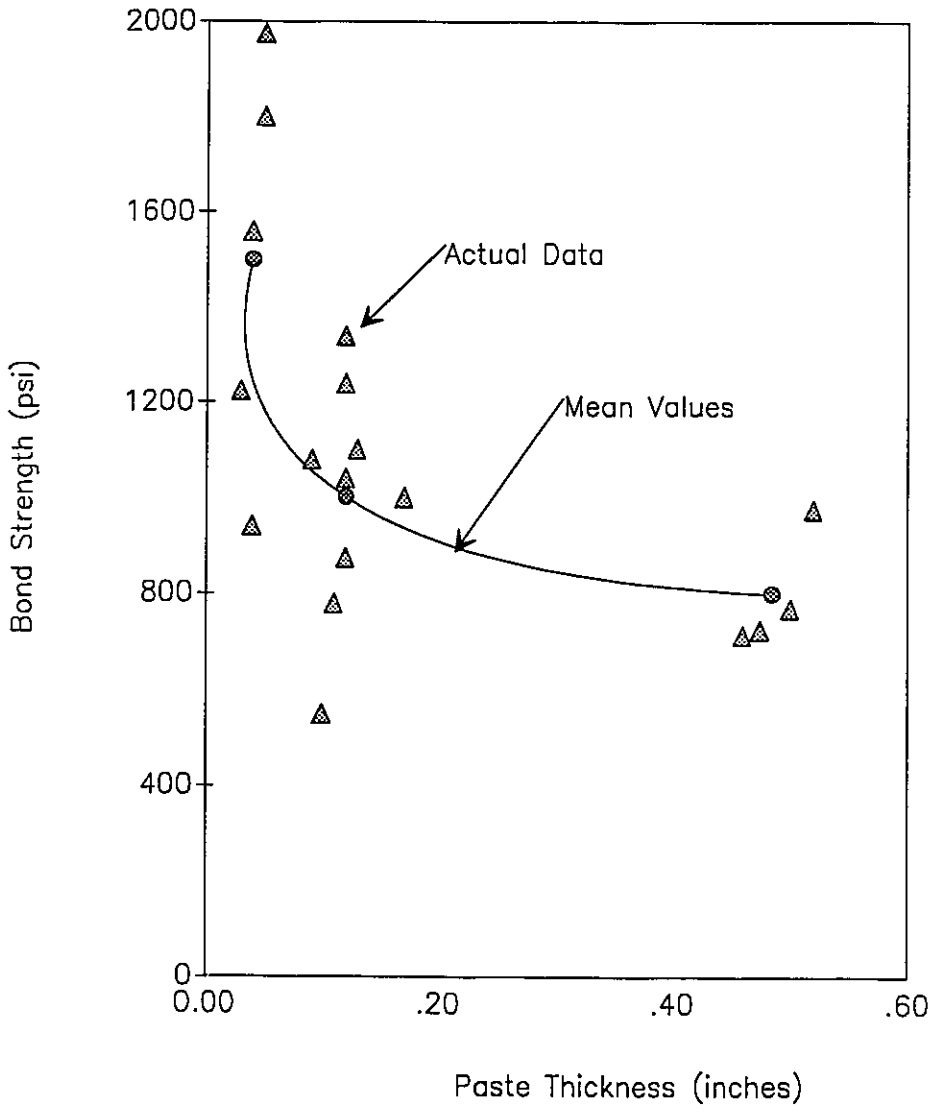

steel slabs. The specimen is tested in tension to determine the steel/concrete bond strength after curing.

Two very similar shear strength tests were also described by Sasse and Fiebrich. These tests involved casting new concrete over an old concrete surface, which had been cut at 30° to the vertical. Once the necessary curing had taken place the samples were failed in compression. The samples were either 100x100x300 mm prisms or cylinders 76.2 mm in diameter x 152.4 mm in length. Another shear test involved placing either one or two steel plates within a concrete prism and then failing the prism by placing a compressive force on the plate. A third type of shear test involved casting the bottom of a concrete cylinder against a steel plate and then loading the end of the cylinder, the steel plate and the concrete/steel interface on the cylinder, all in compression. The last shear tests involving steel plates all produced a value of concrete to steel bond strength.

2.2 Interface Regions- The Transition Zone

A zone of segregation is formed which is markedly different from the bulk matrix when cement paste is cast against a surface, or during the hydration of concrete at the mortar-aggregate interface. Maso described the formation of the transition zone in concrete as follows[16]:

> (1) In fresh-compacted concrete, a water film forms around the aggregate.
> (2) Migration of calcium, hydroxyl, sulfate and aluminate ions produced by the hydration of calcium sulfate and calcium aluminate compounds of portland cement, to the vicinity of the aggregate results in the nucleation of ettringite and $Ca(OH)_2$ crystals at the interface. This results in the formation of a porous network consisting of large crystals of these minerals which are not in close contact with the surface of the aggregate.
> (3) With the process of cement hydration, the formation of a second generation of crystals fills the empty spaces between the large crystals already present. This second generation of crystals, consisting of smaller

crystals of CSH, $Ca(OH)_2$ and ettringite helps to improve the density and strength of the transition phase.

Bentur, Diamond and Mindess have presented a detailed description of the interface zone[17]: A duplex film, 1 μm thick, is found adjacent to the aggregate surface. The film is composed of a layer of CH, with its c-axis perpendicular to the aggregate, backed by a layer of C-S-H gel one particle thick. The film is backed by a zone of massive $Ca(OH)_2$ with some porous regions. The third component of the interfacial zone consists of a porous mix of C-S-H gel, ettringite and large CH crystals of varying orientations. The entire thickness of this region varies between 50 μm-100 μm, depending on the w/c and admixtures present. Diamond attributed the formation of the duplex film to a rapid precipitation of a 0.5 μm thick layer after mixing was initiated[18]. Scrivener, Crumbie and Prah however, found no evidence of the duplex film nor of the CH layer deposited on the aggregate[19]. Monteiro and Mehta found the crystal morphology and the microstructure of the transition zone products differed from those in the bulk matrix due a higher w/c caused by bleeding[20]. Page detected a zone of high porosity, compared to the matrix, which followed the dense interfacial layer[21].

Bentur and Cohen detected a vacant interfacial zone at one day, despite hydration products forming a continuous network within the matrix[22]. This was attributed to inefficient packing of the cement grains around the aggregate as well as some bleeding and wall effects.

Monteiro and Mehta[20,23] as well as Page[21] suggest that the reason for such large crystals oriented with their c-axis perpendicular to the interface in the transition zone was due to the high porosity of the area caused by the localized increase in w/c. This additional space allows the crystals to develop more fully than in the matrix. Much work has been done concerning the orientation of the $Ca(OH)_2$ crystals within the transition zone. Grandet and Ollivier established an equation to determine the randomness of

crystal orientation using x-ray diffraction measurements[24]. Mehta and Bentur, Diamond and Mindess reported that the orientation of the $Ca(OH)_2$ decreased with distance from the interface, becoming essentially random at about 50 μm[25,17]. Detweiler and Monteiro found that the orientation of the crystals increased with time[24]. Studies by Page concluded that during hydration the duplex film becomes tied to the bulk matrix through deposition of $Ca(OH)_2$, ettringite and other hydration products[21].

2.3 Silica Fume and Other Supplementary Cementing Materials

Many researchers have explored the benefits of silica fume addition in cement systems. The general consensus seems to be that the addition of silica fume (SF), even as low as 5% (by weight of cement), improves the properties of the interfacial zone. Odler and Zurz as well as Monteiro and Mehta observed that the bonding characteristics of ordinary portland cement (OPC) increased with added SF[26,20]. Scrivener, Bentur and Pratt argued that this was due to the effects of SF on the microstructure of the transition zone[27]. Scrivener, Bentur and Pratt as well as Bentur, Goldman and Cohen suggest that use of silica fume results in better packing around inclusions and reduced bleeding in the transition zone[27,28]. Scrivener et al. also add that the SF has two effects on the cement system; firstly there is a water reducing effect wherein the silica fume addition provides greater workability for a given w/c and secondly an inherent effect which simply stated means the SF strengthens the cement system[27].

Many researchers have reported on the fact that the SF acts as an activating site for hydration where the SF reacts with CH to form C-S-H thereby producing a much denser transition zone[20,22,23,29,30,31]. In some cases the transition zone was decreased from 50 μm in the control to 8 μm in the SF specimen. Monteiro and Mehta however attribute the decrease in transition zone thickness to a decrease in w/c[20]. In many cases with silica fume addition it became difficult, if not impossible to identify an intermediate zone between the interface and the bulk matrix.

Odler and Zurz examined the failure surface at the rock-cement interface and found the addition of SF moved the failure plane further away from the interface[26]. In the control sample the failure took place between the duplex film and the CH and ettringite rich region.

Mehta investigated the addition of a bituminous flyash on the cement system, and found it had little influence on the consistency and setting characteristics of the reference mortar[25]. This flyash did however increase both the index of orientation of the CH at the interface and the thickness of the transition zone. Mehta and Monteiro added flyash, blast furnace slag, and limestone aggregate to various cement systems including Type K expansive cement and in all cases produced an interface with smaller and less preferentially oriented CH crystals[23].

2.4 Factors Affecting the Strength of the Transition Zone

It has been suggested by Nakayama and Beaudoin as well as Monteiro and Mehta that the transition zone is the weak link in the hydrated cement system[14,20]. It follows that a change in the properties of the transition zone can cause a change in the strength of the system. Mehta attributed the strength of the transition zone to van der Waal's forces of attraction[25]. At later ages he suggested that there may be chemical bonding at the aggregate surface. The many large CH crystals present near the interface would reduce adhesion due to van der Waal's forces as well as providing preferred cleavage sites due to their orientation. Nakayama and Beaudoin and Monteiro and Mehta contend that CH crystal growth may be the reason for low bond strengths at later ages. Monteiro also argues that it may be due to the ease of crack propagation through the oriented CH[14,32].

Grain size refinement of the CH where the large crystals are reduced in size or even eliminated may improve the interface strength[20].

Some researchers have concentrated on the effect of time on bond strength. Page surmised that the interface structure changes little after the first few days of curing since very little increase in bond is produced[21]. Bentur and Cohen encountered a relatively

straight fracture surface through the matrix at 28 days due to extremely brittle behaviour[22]. Beaudoin found that the bond strength increased with time to one day after which there was a reduction in bond strength until at least seven days[13]. Moavenzadeh and Bremner concluded that C-S-H gel adhered well to glass but CH inhibited a good bond[33].

Surface roughness has been found to affect the bond strength at the cement-aggregate interface. Hsu and Slate, Alexander, et al, and Zhuralev and Shteiert have all investigated the effect of surface roughness on bond and have reported that increased surface roughness increases bond strength[34-36].

CHAPTER 3

EXPERIMENTAL PROCEDURE

3.1 Description of Mixes

The cement paste mixes prepared for this study can be divided into five subsets:

1. Control mixes
2. Pastes containing added salts
3. C_3S pastes
4. Clinker pastes
5. Cement pastes containing silica fume additions

The control mixes consisted of cement pastes with w/c values of 0.30 and 0.35. The pastes with salt additives (w/c of 0.30 and 0.35) contained 2% of the salt by weight of cement. The C_3S systems were mixed at w/c 0.35 only. One system contained pure C_3S, while the second contained C_3S with 2% $NaNO_3$ (by weight of C_3S). The clinker and silica fume systems were mixed at two w/c, 0.30 and 0.35 (clinker is portland cement without gypsum). Silica fume systems contained combinations of cement and silica fume (10% by weight of cement) plus 0.3% superplasticiser (by weight of cement based on solids content), for improved workability. The cement used was a St. Mary's type 10 normal portland cement.

Mix compositions were chosen for the following reasons: The salt additives were intended to change the crystallite size of the portlandite precipitated at the matrix-substrate interface. C_3S is the major component of portland cement. The hydration products consist of C-S-H and CH. The C_3S pastes were studied in order to investigate interface properties for systems not containing sulphoaluminate phases. Silica fume pastes were selected to determine if cement matrices containing smaller quantities of CH had beneficial effects on the bond strength. Silica fume reacts with excess lime produced during hydration of portland cement.

The hydration times were chosen to be 1 and 2 days for all systems as well as two times less than one day for pastes containing salt additives and control paste systems. Some systems were also hydrated for seven days. Times less than one day were chosen at the mid-point and the maximum of the second peak on the heat of hydration curve . The curves were produced by using a conduction calorimeter. For data acquisition and processing, the calorimeter was interfaced with an Apple IIe microcomputer using a TaurusOne 12-bit analog-to-digital convertor and an Apple super-serial interface card.

3.2 Mix Preparation for Uniaxial Tensile Bond Test

All samples for the tensile bond test were mixed in a small, low speed mixer (Figure 3.1). The systems which contained salts or superplasticisers had the admixture added to the water before mixing. The silica fume was premixed with the cement to produce a homogeneous mixture.

The mixing process is described as follows: the mixing water (plus salt and superplasticiser) was added to the mixing bowl; the mixer was turned on and the cementitious material slowly added to the bowl so that no large lumps were formed. The sides of the bowl were scraped with the mixer still operating. Mixing was completed when a smooth paste was obtained. Approximately 50 g of cementitious material were used for each mix.

3.3 Preparation of Uniaxial Tensile Bond Test Specimens

The uniaxial tensile bond test was performed on a paste sandwich which consisted of two brass cubes between which was a layer of the paste to be tested (Figure 3.2). Each cube had an appropriate substrate (glass or steel) epoxied to one face. Some specimens were made using steel cubes thus eliminating the necessity to epoxy the substrate to one face. There was no significant difference in the results. After it was mixed the paste was placed on a plexiglass sheet before it was applied to the substrate. The substrate was cleaned with acetone before application of the paste after which a knife was used to spread a thin layer of paste on the substrate. The paste layers were pushed together to

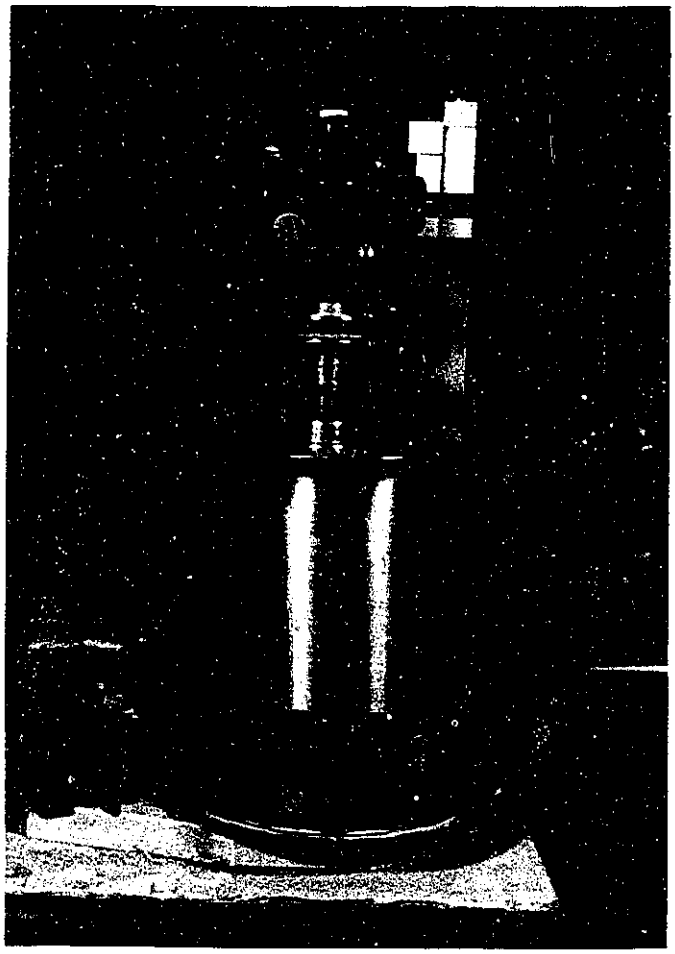

Figure 3.1 Low Speed Mixer Used for Sample Preparation

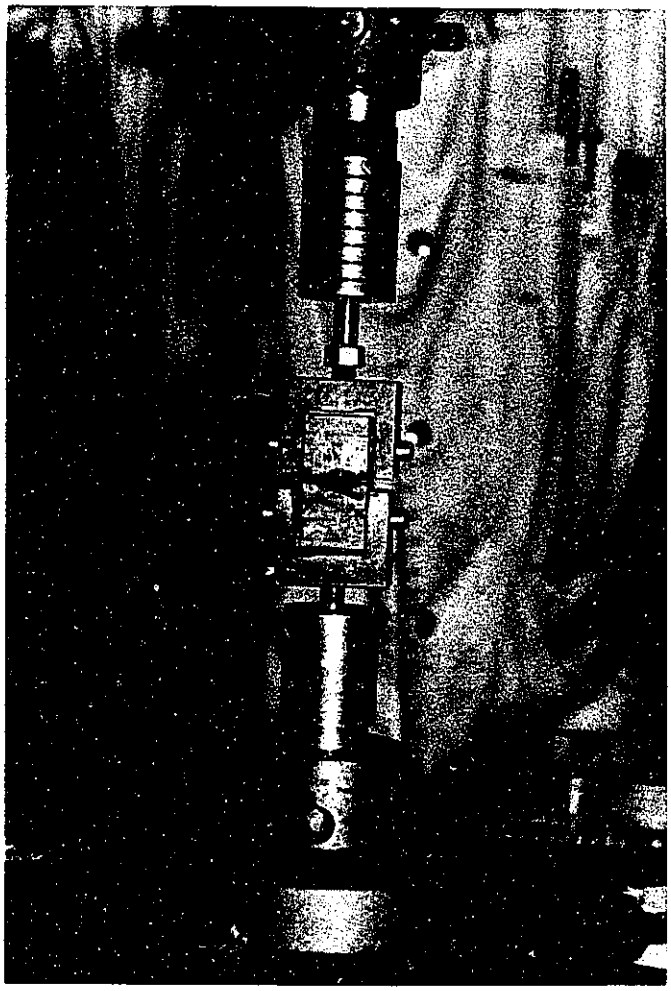

Figure 3.2 Uniaxial Bond Specimen in Testing Apparatus

form one layer after both substrates were coated. The various thicknesses necessary for the experiment were produced by varying the thickness of the paste applied to the various substrates. The completed "sandwich" was then placed in a mould which allowed the sample to be perfectly aligned (ie. a constant thickness of paste throughout).

3.4 Retention of Samples for Microscopy Studies

For each system and hydration time, at least three failed paste samples and accompanying substrates were kept for further analysis. These samples were marked and sealed in a vacuum container until needed.

3.5 Description of Uniaxial Tensile Bond Test

The tensile test apparatus consisted of two holders which connected into the Instron 1122 Testing Machine. The latter was interfaced with an IBM compatible PC for data acquisition. The bottom holder of the apparatus was fixed, but the top holder was allowed two degrees of freedom. The tensile bond test sample was connected by pins to the testing apparatus and a screw attachment on the upper head was used to take up the slack in the apparatus. The testing program was initiated on the computer and the sample was loaded with a cross-head speed of 2 mm/min. The computer recorded the maximum load for each sample tested and after each test the paste sample was removed from the substrate and the thickness measured and recorded. Comments on the condition of the paste or substrate were noted.

The tensile test results were plotted on a graph of bond failure stress vs thickness. A computer software package was then used to produce a best fit exponential curve and r-value for the data. A value of fracture energy was calculated using equation (1) at 11 points along the best fit curve. The 11 values were then averaged to give the fracture energy value for the system. The r-value was compared to tabulated r-values with the appropriate sample size and level of confidence to determine the significance of the best fit curve.

3.6 Thermogravimetric Analysis

Determination of non-evaporable water and CH content was made by thermogravimetric analysis (TGA) on bulk paste samples. The analysis was performed on a DuPont 9900 Thermal Analyzer with computerized data acquisition. Samples were taken from the bulk sample after failure. The samples were vacuum dried at 110° C for 3 hours, and ground to a fine powder in a mortar and pestle. The test method consisted of heating a 150 mg sample from room temperature to 1000° C at a rate of 20° C/min. Non-evaporable water estimates were based on the weight loss between 110° and 1000° C. The lime content was calculated using the weight loss data between 400° and 500° C.

3.7 Modulus of Elasticity Determinations

The modulus of elasticity for each system at each curing time was needed to determine the fracture energy. For each system a paste mix was cast into a 3.2 mm ID plexiglass tube. After demoulding at approximately 4 hours three discs 1.27 mm thick were cut on a low speed Isomet saw. The discs were then tested individually using the apparatus shown in Figure 3.3.

The testing procedure consisted of centrally loading the circular plate specimens and recording the resulting deflection. The modulus of elasticity was determined by substituting the appropriate values into equation (2), for a centrally loaded circular plate supported at three points[37]. The value used was the average of three values for each system.

$$E = \frac{1.192 \times 10^{6} \times P}{\delta \times (t^{3})} \qquad (2)$$

E = modulus of elasticity in Pascals
P = load in grams
δ = deflection from dial gauge in mm
t = thickness of sample in mm

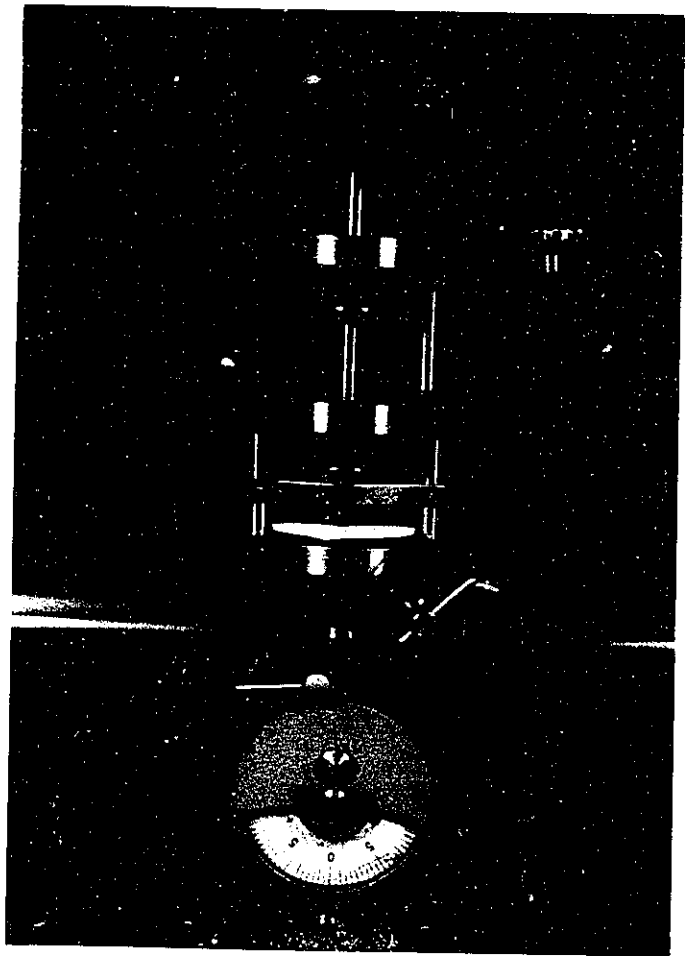

Figure 3.3 Modulus of Elasticity Testing Apparatus

3.8 Porosity Determination

Samples of cement paste and cement paste with calcium propionate addition, both at w/c=0.35, were used for mercury porosimetry determinations at all hydration times. An American Instruments Company porosimeter was used. The value used to represent the porosity of the sample was the maximum porosity obtained during the test. The porosity values of pastes with silica fume and $CaCl_2$ additions were obtained from the literature. The porosity values for cement clinker paste were assumed to be the same as the normal cement paste.

3.9 Scanning Electron Microscopy

Paste and substrate samples observed with the scanning electron microscope (SEM) were sputter coated with gold before examination. The SEM used was a Cambridge Stereoscan 250 with a TN-5500 X-Ray Analyzer and a backscatter electron detector (BSE).

The first SEM task was to determine the amount of cover on each substrate using an image analyzing program in conjunction with the BSE. Three values of surface cover were taken for each substrate and the results were averaged. The BSE could only be used with the steel substrates since in the glass substrates the silica present in both the substrate and the surface cover could not be differentiated. Throughout the coverage analysis, elemental scans were made of the substrate surface to assist in the identification of the hydration products present.

The second SEM task was to determine if there were any patterns in hydration product deposition at the interface as well as to obtain a more detailed description of the hydration products, composition and morphology. Magnifications used ranged from 100X to 5000X.

3.10 Surface Roughness Determination

Surface roughness measurements were made to determine the relative roughness of the two substrates. The roughness determination was performed on a Rank Tallysurf 4

roughness testing machine. The testing machine consisted of a stylus which is dragged across the surface of the substrate. The signal from the stylus was relayed to a chart recorder which plotted the surface roughness profile of the substrate.

CHAPTER 4

EXPERIMENTAL RESULTS

4.1 Conduction Calorimetry

The calorimetry curves shown in Figures 4.1 and 4.2 were used to determine the two hydration times less than two days which would be used in the experiments. Setting usually occurs at a time associated with the ascending portion of the second heat peak. Most of the CH is precipitated during this period. The two test times were chosen to reflect the relative amounts of CH formed at early hydration times in each system. From the curves it can be seen that calcium propionate is a retarder which delays the occurrence of the second heat peak in the acceleratory period of the cement paste by about two hours. Sodium nitrate did not appreciably affect the characteristics of the heat curves for the paste, while the appearance of the second heat peak for calcium chloride was accelerated by two hours. An increase in w/c caused a slight increase in the time associated with the second heat peak of up to 30 minutes. The early hydration times used for testing are shown in Table 4.1.

Table 4.1 Early Hydration Times for Control Pastes and Pastes with Salt Additives

	Cement		$NaNO_3$		$CaCl_2$		Propionate	
	w/c		w/c		w/c		w/c	
	0.30	0.35	0.30	0.35	0.30	0.35	0.30	0.35
Midpeak	4h	4h	4h	4h	3h	3.5h	5.5h	5.5h
Peak	6.5h	7h	6.5h	7h	5h	5.5h	9h	9h

4.2 Calcium Hydroxide Determination

The amount of calcium hydroxide present in the paste is expressed as a percentage of the paste weight and is adjusted for the amount of carbonation which has occurred. The TGA curves for each control paste and paste system containing salt additives, at all hydration times of interest are shown in Appendix A.

Figure 4.1 Calorimeter Curves for Control and Pastes Containing Salt Additives

w/c=0.30

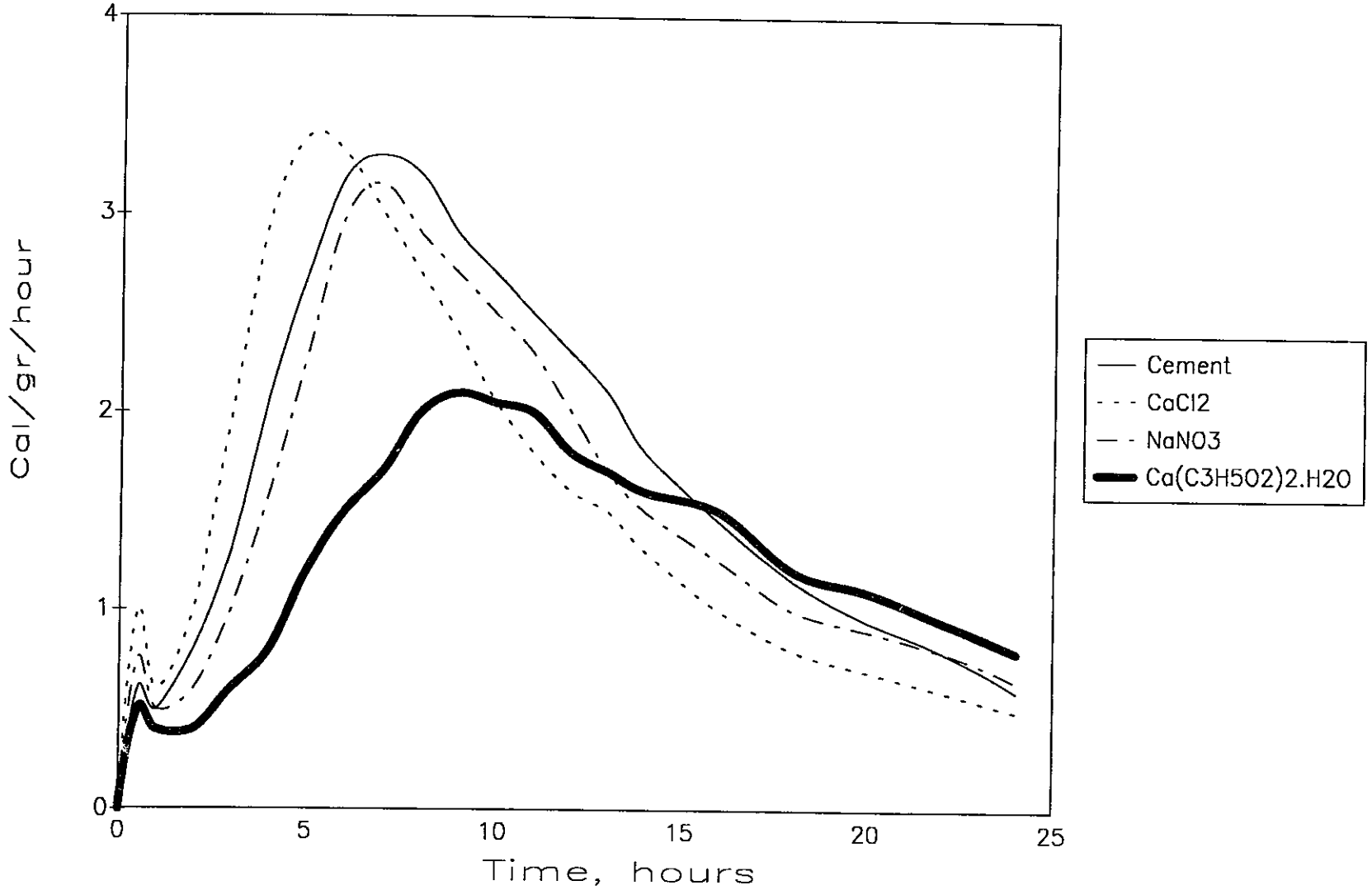

Figure 4.2 Calorimeter Curves for Control and Pastes Containing Salt Additives

w/c=0.35

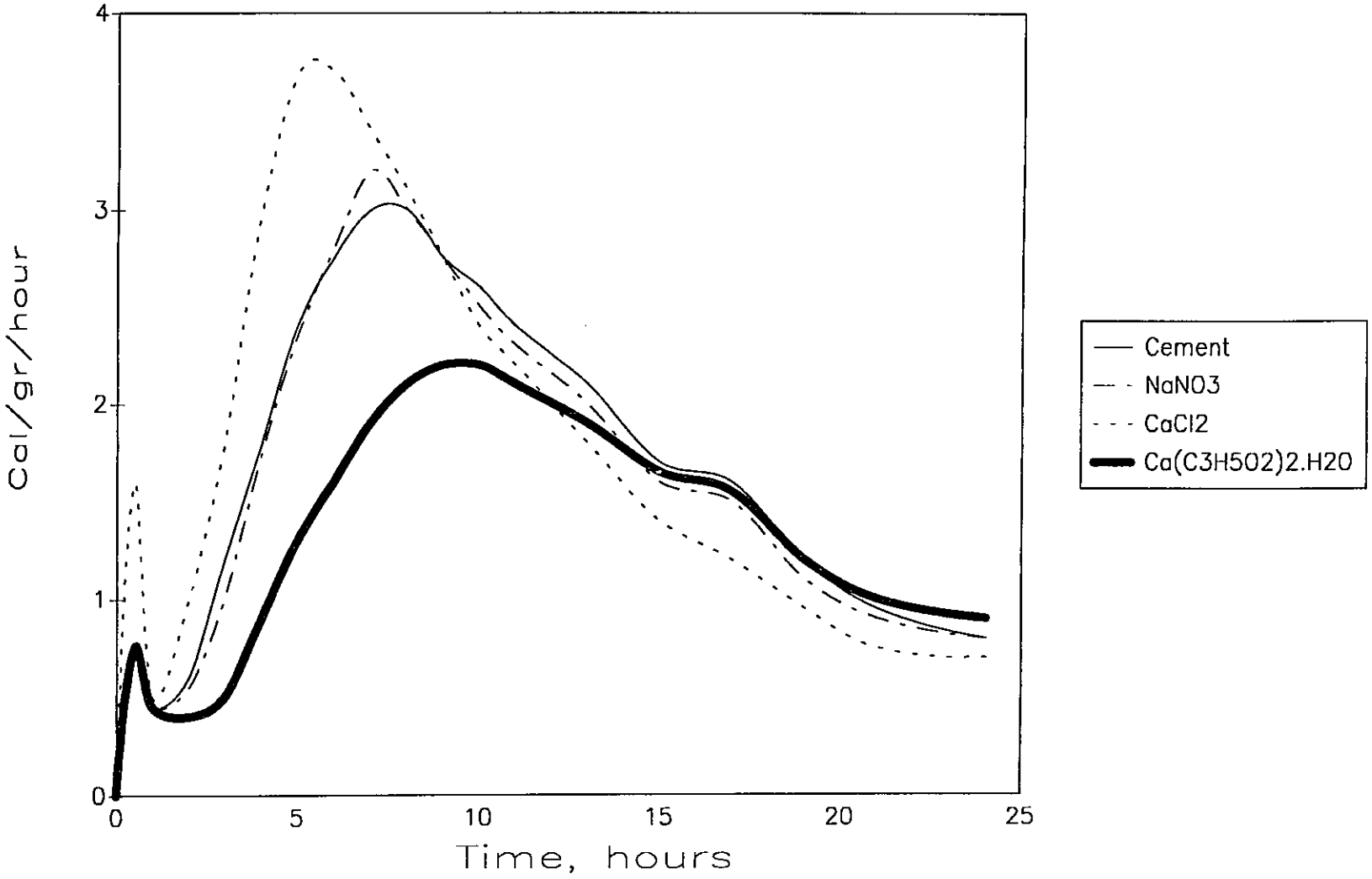

The TGA results for the calcium hydroxide determination are found in Table 4.2. The percentage of $Ca(OH)_2$ present in the samples increased with time of hydration. The sodium nitrate and calcium propionate additions at w/c=0.30 produced less CH than the corresponding control system, while $CaCl_2$ and calcium propionate additions at w/c=0.35 produced more CH than the controls.

Pure paste systems and those containing propionate and chloride produced more CH at w/c=0.30 than at w/c=0.35 at hydration times less than one day. The $NaNO_3$ showed little effect due to w/c.

Table 4.2 $Ca(OH)_2$ Contents for Salt Systems

	CH (%)		CH (%)
Cement 0.30		$NaNO_3$ 0.30	
3.5h	3.27	3.5h	2.96
6.5h	4.54	6.5h	3.34
1 day	8.81	1 day	8.87
2 days	11.69	2 days	10.51
7 days	12.57	7 days	11.55
Cement 0.35		$NaNO_3$ 0.35	
4h	2.47	4 h	2.71
7h	3.77	7 h	3.51
1 day	8.26	1 day	7.82
2 days	11.44	2 days	10.76
7 days	12.21	7 days	12.15
$CaCl_2$ 0.30		Propionate 0.30	
3h	2.92	5 h	2.18
5h	5.36	9 h	4.68
1 day	11.29	1 day	8.48
2 days	12.54	2 days	10.66
$CaCl_2$ 0.35		Propionate 0.35	
3.5h	2.53	5 h	2.75
5.5h	5.17	9 h	4.62
1 day	11.75	1 day	9.22
2 days	13.51	2 days	11.18

4.3 Non-Evaporable Water Determination

Non-evaporable water is often used as a measure of degree of hydration and is calculated as the percentage weight loss, based on ignited weight, obtained after heating

the paste to 1000° C, after preheating to remove the evaporable water. The greater the non-evaporable water content , the greater the degree of hydration.

The non-evaporable water determinations given in Table 4.3 were calculated from the TGA curves given in Appendix A. For all systems the non-evaporable water increased with increased hydration. The paste system containing $NaNO_3$ had less water, compared to the control, at times less than one day and at seven days. The paste systems containing $CaCl_2$ at both water-cement ratios had values greater than the control for all hydration times. The calcium propionate paste at w/c=0.35 also had values greater than the control at all hydration times, except at two days. The control pastes contained more non-evaporable water than the paste containing calcium propionate (w/c=0.30) at all hydration times.

4.4 Modulus of Elasticity

The modulus of elasticity values for each system are shown in Table 4.4. As expected the modulus of elasticity for each system increased with increased hydration. The modulus values for silica fume pastes were taken from published literature. Values at the earliest hydration times for the systems containing salt additives could not be obtained due to testing difficulties. For the pastes containing $NaNO_3$,$CaCl_2$ and calcium propionate (w/c=0.30) the control systems had higher values at times earlier than one day. At advanced times pastes containing salt additives exhibited higher modulus values. The calcium propionate paste (w/c=0.35) had higher modulus values than the control at all hydration times.

Table 4.3 Non-evaporable Water Content for Salt Systems

	Non-evap Water (%)
Cement 0.30	
3.5h	3.33
6.5h	4.68
1 day	10.33
2 days	11.51
7 days	13.81
Cement 0.35	
4h	2.12
7h	3.75
1 day	9.28
2 days	12.40
7 days	14.18
$CaCl_2$ 0.30	
3h	4.74
5h	5.80
1 day	11.99
2 days	13.19
$CaCl_2$ 0.35	
3.5h	4.24
5.5h	6.27
1 day	12.10
2 days	13.74

	Non-evap Water (%)
$NaNO_3$ 0.30	
3.5h	3.73
6.5h	4.33
1 day	8.12
2 days	10.78
7 days	16.48
$NaNO_3$ 0.35	
4 h	3.67
7 h	4.64
1 day	8.90
2 days	11.08
7 days	17.53
Propionate 0.30	
5 h	2.47
9 h	4.47
1 day	8.41
2 days	10.66
Propionate 0.35	
5 h	3.34
9 h	4.55
1 day	10.22
2 days	11.82

Table 4.4 Modulus of Elasticity Values for Salt Systems (MPA 10^4)

Cement

0.30		0.35	
6.5h	0.448	7h	0.302
1d	1.169	1d	0.880
2d	1.636	2d	1.464
7d	2.472	7d	2.009

$NaNO_3$

0.30		0.35	
6.5h	0.182	7h	0.165
1d	1.333	1d	1.137
2d	1.911	2d	1.544
7d	2.619	7d	2.073

$CaCl_2$

0.30		0.35	
5h	0.186	5.5h	0.142
1d	1.460	1d	1.221
2d	2.090	2d	1.615

Propionate

0.30		0.35	
9h	0.138	9h	0.323
1d	1.269	1d	1.292
2d	1.922	2d	1.916

Silica Fume

0.30		0.35	
1d	1.553	1d	1.325
2d	1.828	2d	1.585
7d	2.293	7d	2.005

C_3S

0.35	
1d	0.862
2d	1.416
7d	2.036

4.5 Porosity

The relationship between porosity and compressive strength of cement paste is well documented. Compressive strength increases exponentially as the porosity decreases. The existence of such a relationship between porosity and bond strength or surface fracture energy is unknown.

The porosity values shown in Table 4.5 are the porosity values from obtained this investigation or from the literature[38,39]. As hydration time increases the pore structure of the paste becomes finer and the porosity decreases. An increase in water-cement ratio results in increased porosity for the paste.

Table 4.5 Porosity Values, %, for Cement Paste Systems

	Cement			Silica Fume	
	w/c=0.30	w/c=0.35		w/c=0.30	w/c=0.35
1d	30.3	35.0	1d	28.9	33.7
2d	29.1	33.2	2d	27.3	32.0
7d	25.0	28.6	7d	22.9	27.0

	$CaCl_2$			Clinker	
	w/c=0.30	w/c=0.35		w/c=0.30	w/c=0.35
1d	29.8	33.6	1d	30.3	35.0
2d	26.8	29.4	2d	29.1	33.2

4.6 Roughness Measurements

The surface roughness values obtained for the glass and steel substrates are meant to provide an indication of the relative roughness of the two substrates. The roughness parameter was not included in any of the calculations of interface bond failure stress or interface fracture energy. The surface roughness plots for the two substrates are shown in Figure 4.3. The surface of the glass was essentially smooth with asperity heights <0.01 μm, while the steel surface had asperity heights <0.1 μm. Both the steel and glass substrates are smooth relative to aggregate surfaces.

4.7 Bond Strength

Bond strength vs. paste thickness curves obtained with the raw data for the $NaNO_3$ paste system (w/c=0.30, 1 day, glass substrate) and cement paste (w/c=0.30, 2

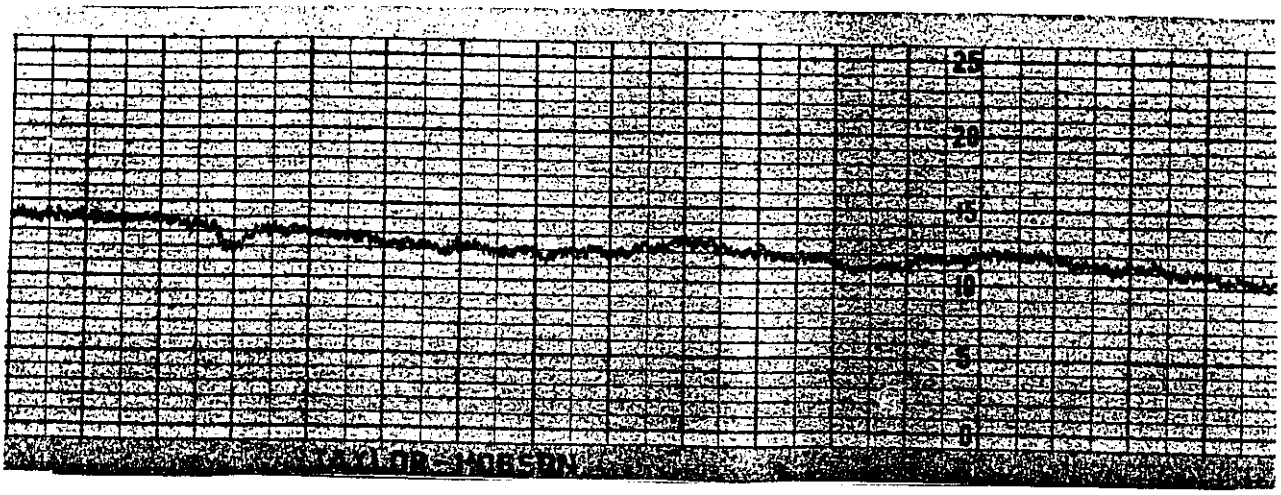

a) Glass substrate

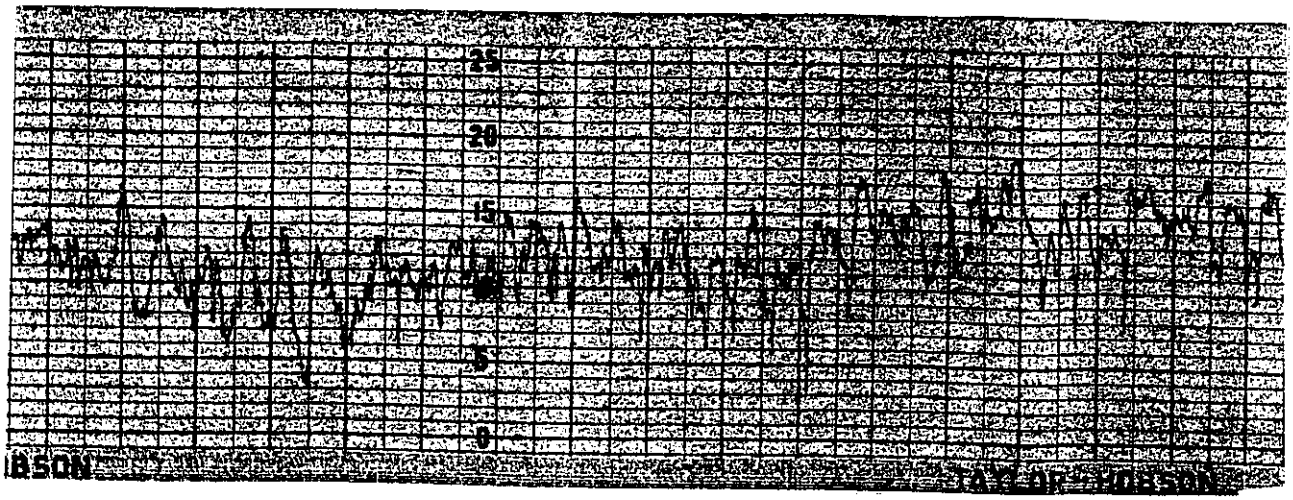

b) Steel substrate

Figure 4.3 Roughness Plots for Substrates (1 vertical division=0,02μm)

days, steel substrate) are plotted in Figures 4.4 and 4.5. Regression curves have been calculated from the raw data for all systems at all hydration times studied. This data is found in Appendix B. The regression curves (bond strength vs paste thickness) for the individual cement paste systems are plotted in Figures 4.6 to 4.33. A correlation coefficient, r ($0 \leq r \leq 1$), was calculated for each regression curve. The r value is a measure of how well the calculated curve fits the data points with higher values of r meaning a better "fit". The calculated value of r was then compared to tabulated values of r for the number of degrees of freedom for the curve and the level of significance, to determine the suitability of the regression curve in describing the raw data[40]. Table 4.6 gives the correlation coefficient values for each system and hydration time as well as the level of significance which it passes.

Most systems showed increases in strength with hydration time, except at seven days where the bond strength may have been less than the two , or even the one day strength. The exceptions are the following systems on the steel substrate: cement, $NaNO_3$ (w/c=0.30) and silica fume (w/c=0.35). The one day strength, however, was greater than the two day strength for the following systems; Steel substrate: cement (w/c=0.30), $NaNO_3$, $CaCl_2$, propionate (w/c=0.30), silica fume (w/c=0.30); glass substrate: cement (w/c=0.30), $NaNO_3$ (w/c=0.30), $CaCl_2$, clinker, silica fume (w/c=0.35). In general an increase in water-cement ratio resulted in a decrease in bond strength.

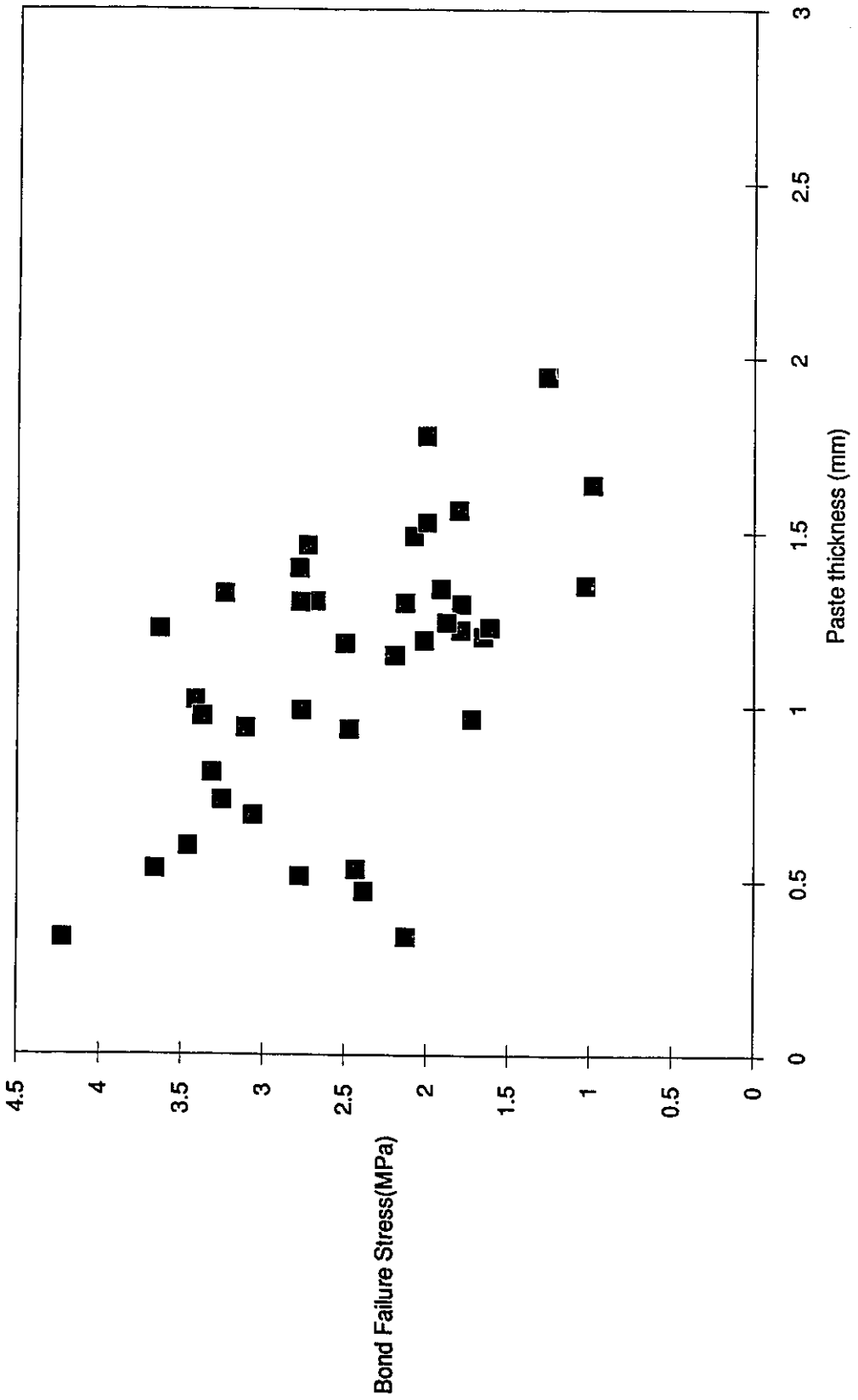

Figure 4.4 Raw Data for Cement Paste +2%NaNO3, w/c=0.30, glass substrate

Figure 4.5 Raw Data for Cement Paste, w/c=0.30, 2 days, steel substrate

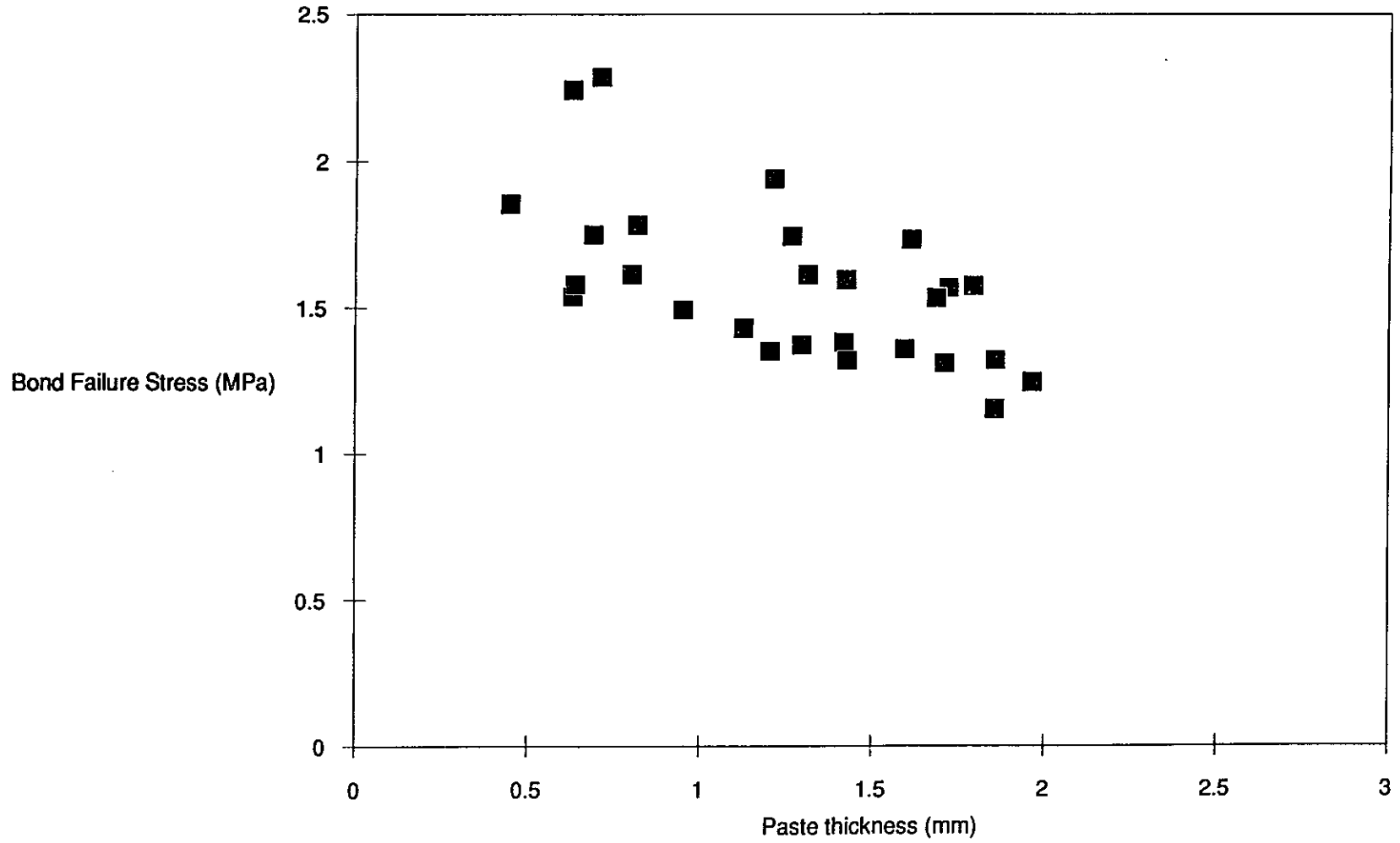

Figure 4.6 Cement paste, w/c=0.30, steel substrate

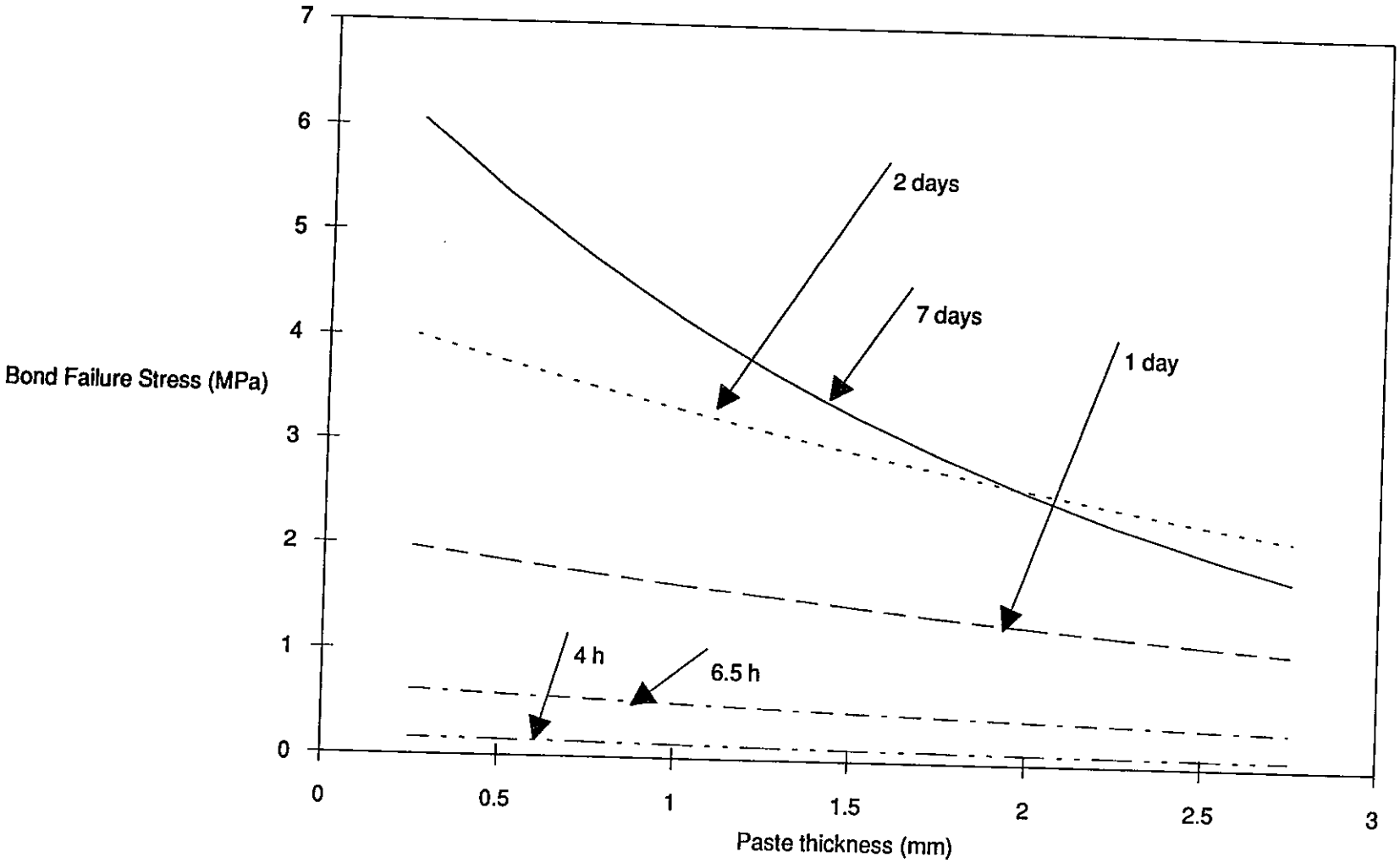

Figure 4.7 Cement paste, w/c=0.35, steel substrate

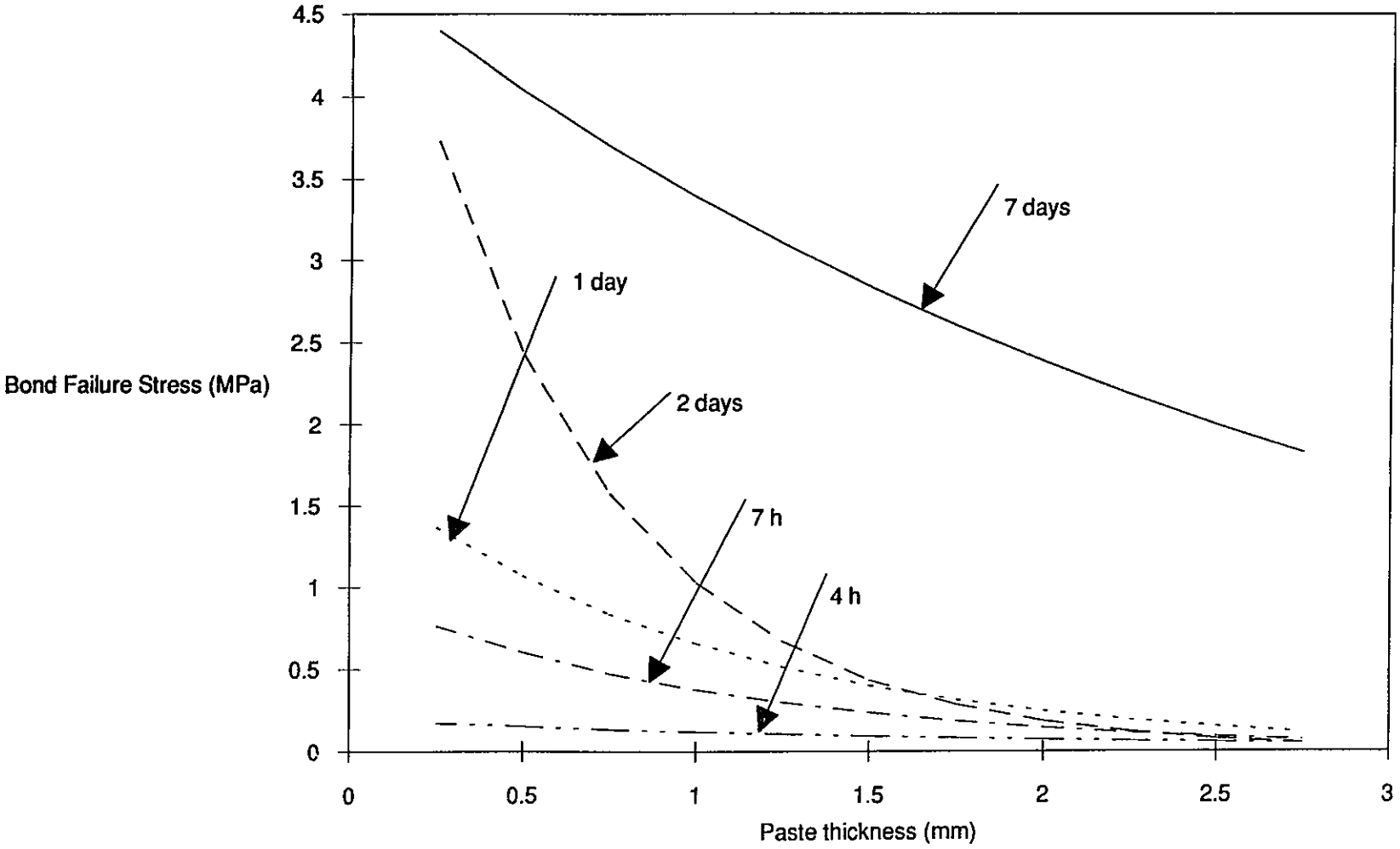

Figure 4.8 Cement paste, w/c=0.30, glass substrate

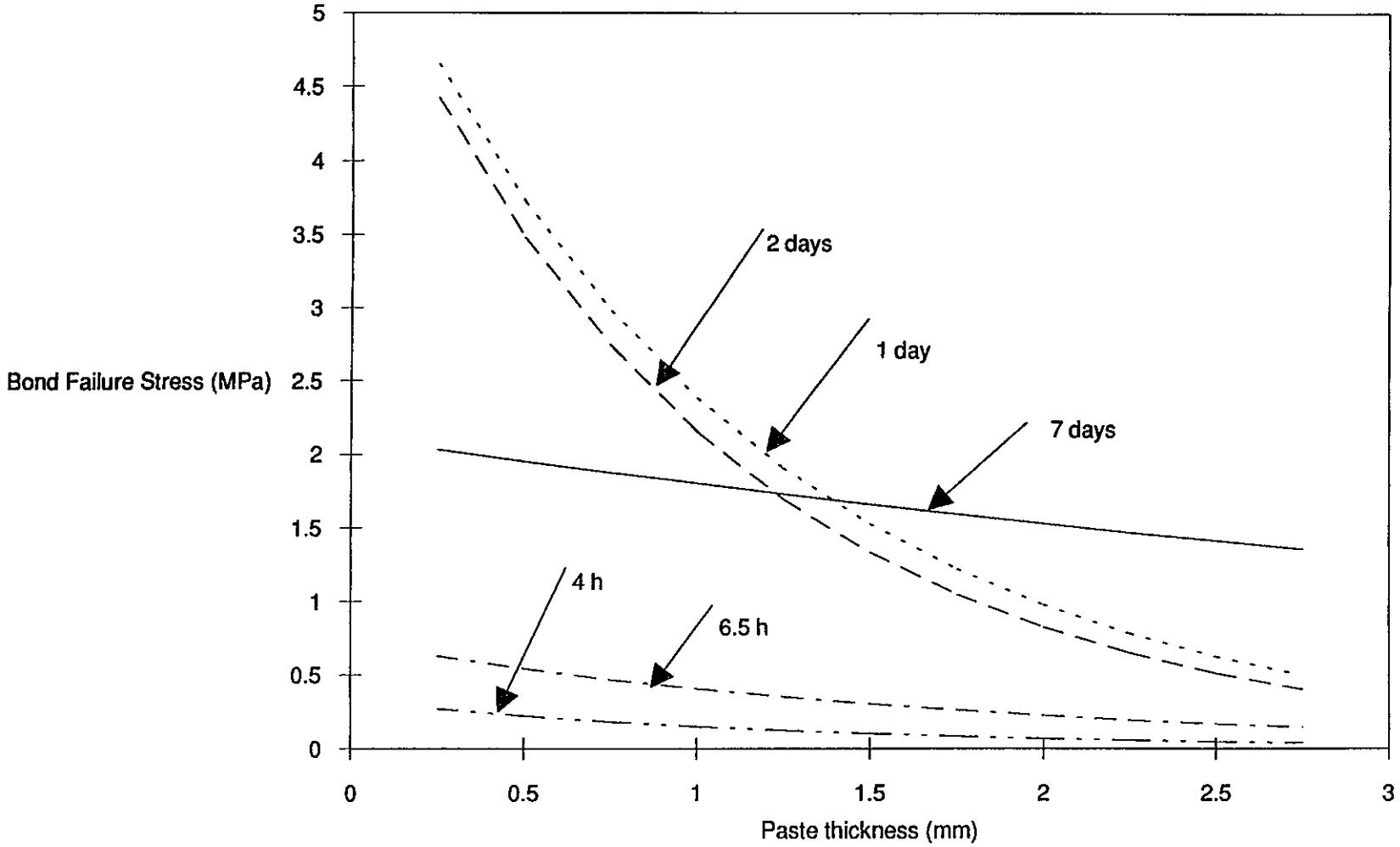

Figure 4.9 Cement paste, w/c=0.35, glass substrate

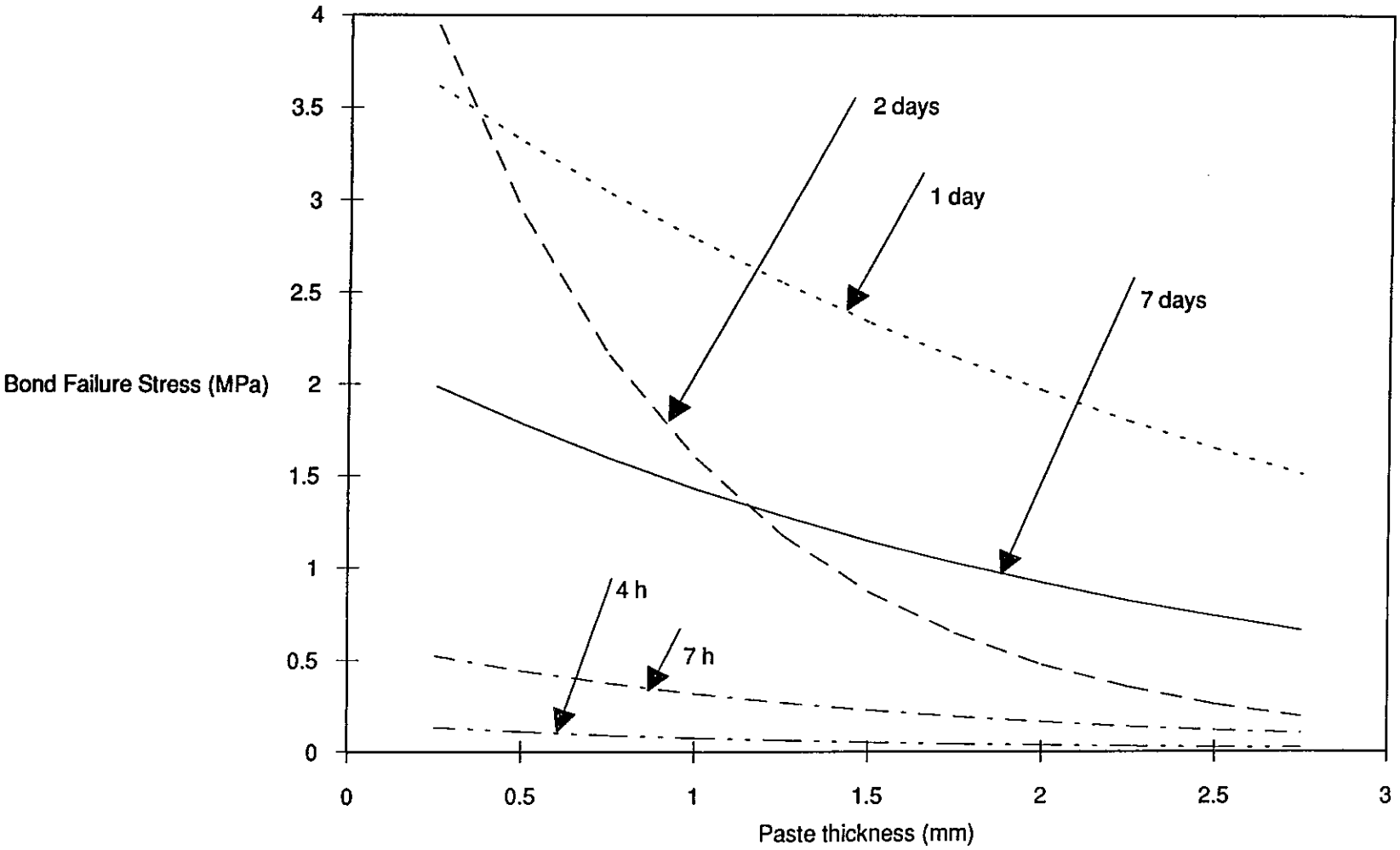

Figure 4.10 Cement+2% Sodium Nitrate, w/c=0.30, steel substrate

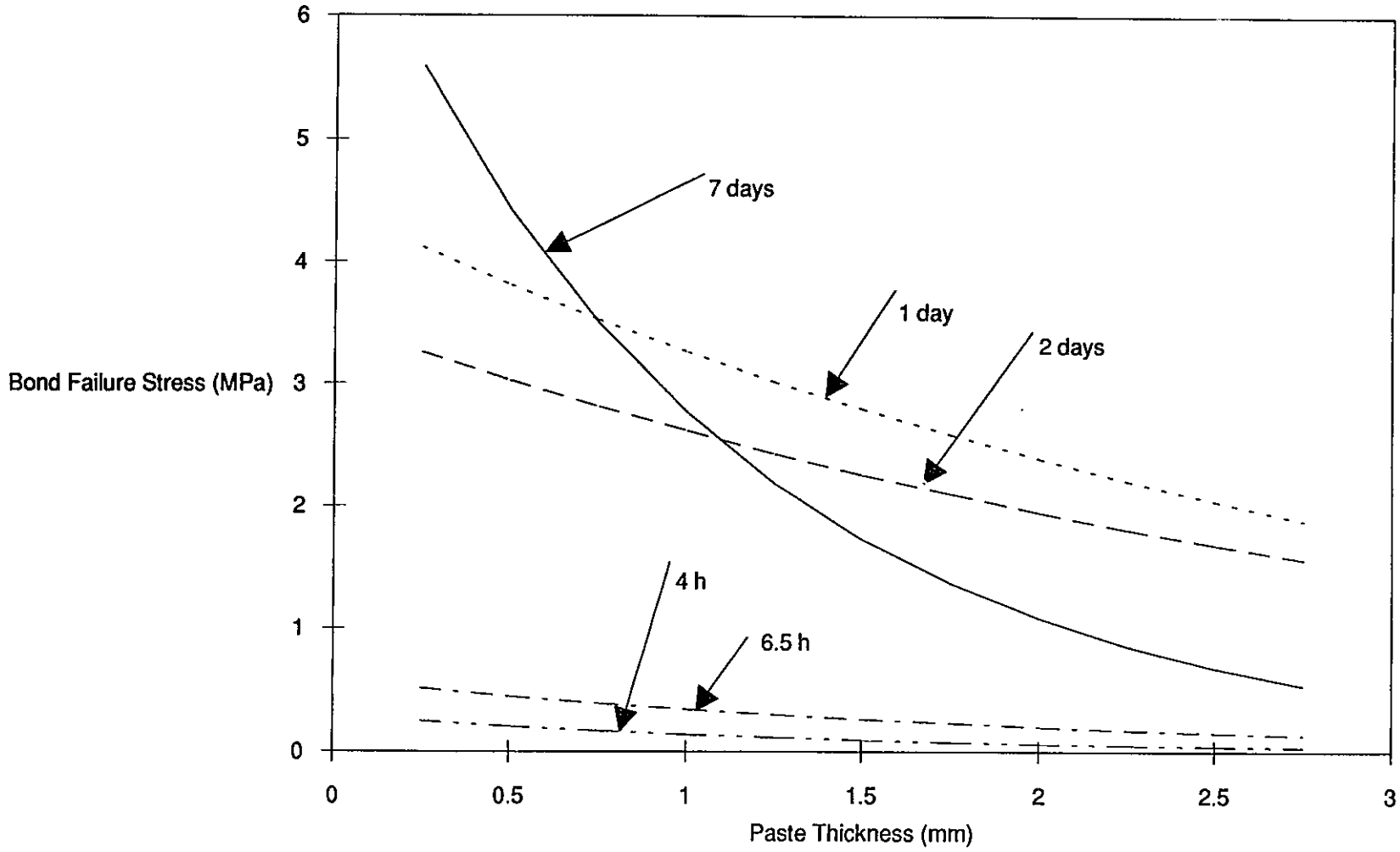

Figure 4.11 Cement+3% Sodium Nitrate, w/c=0.35, steel substrate

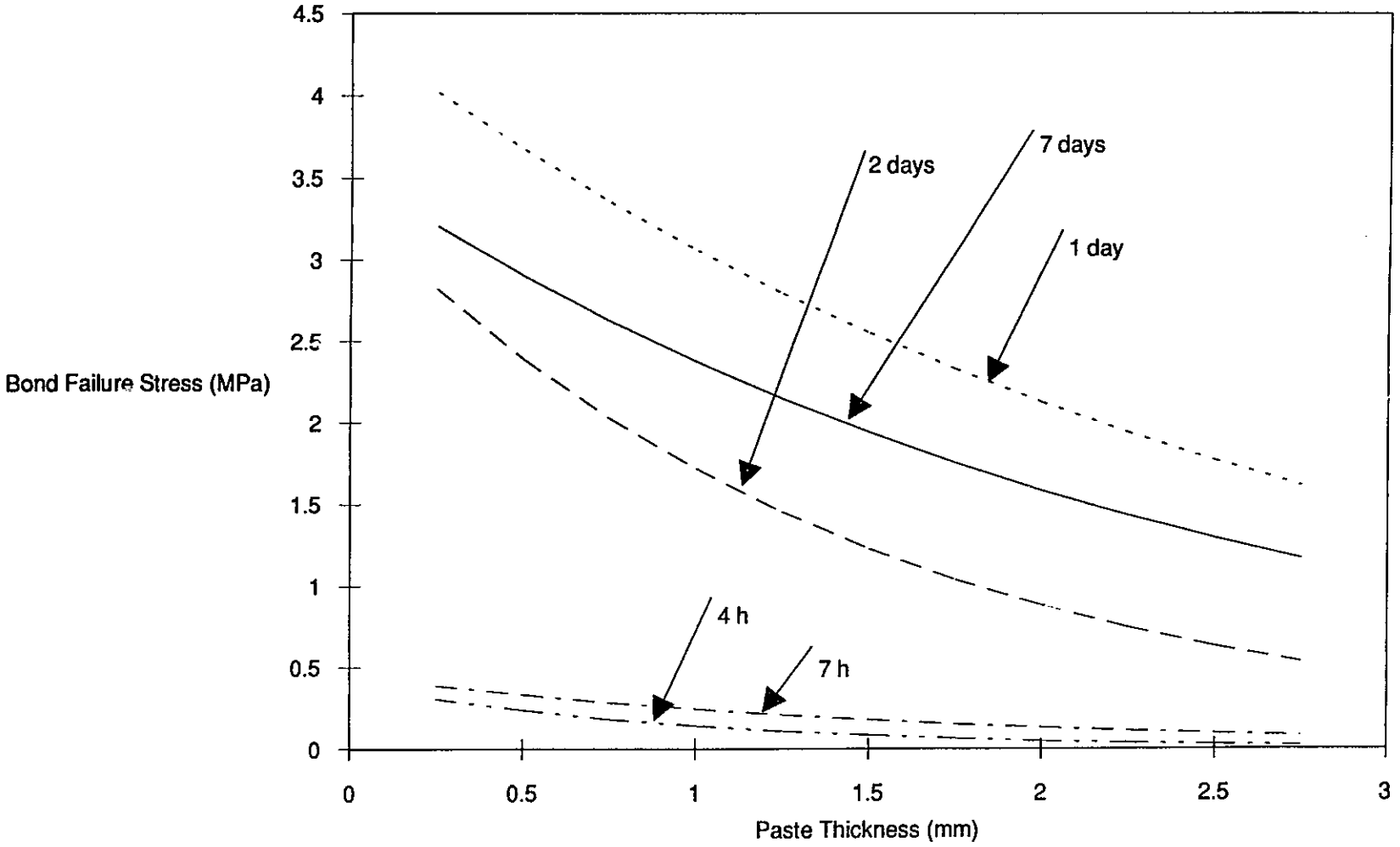

Figure 4.12 Cement+2% Sodium Nitrate, w/c=0.30, glass substrate

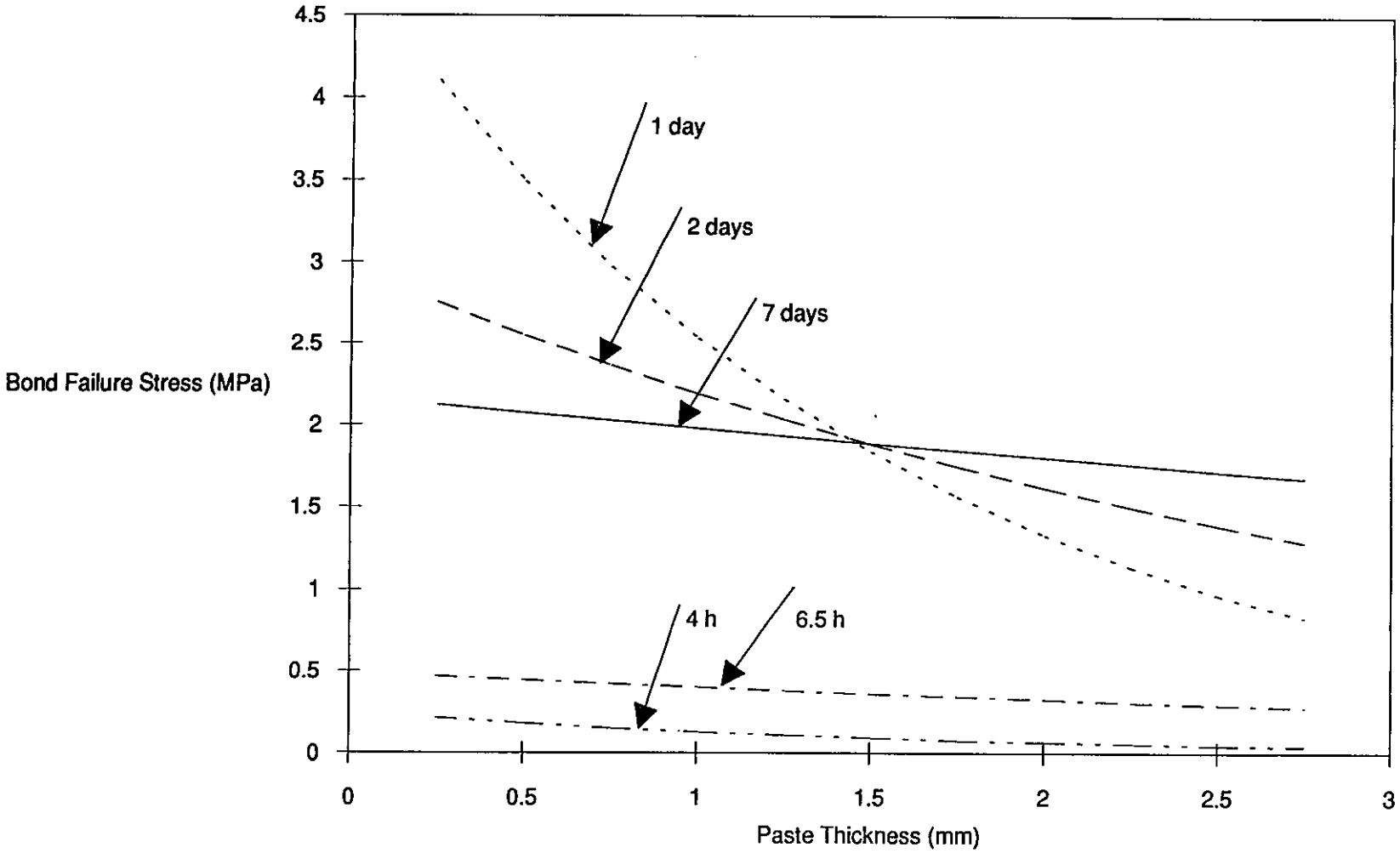

Figure 4.13 Cement+2% Sodium Nitrate, w/c=0.35, glass substrate

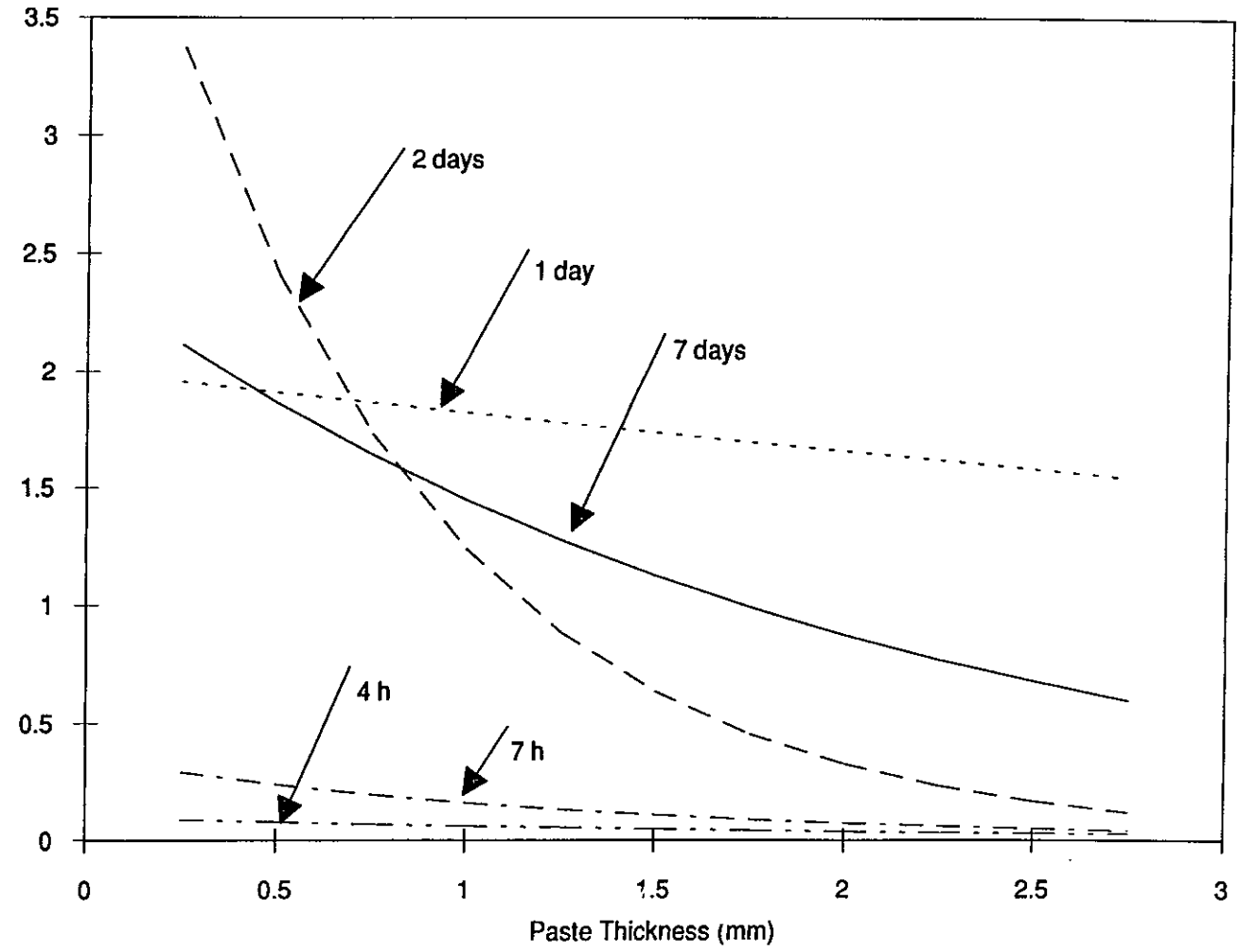

Figure 4.14 Cement+2% Calcium Chloride, w/c=0.30, steel substrate

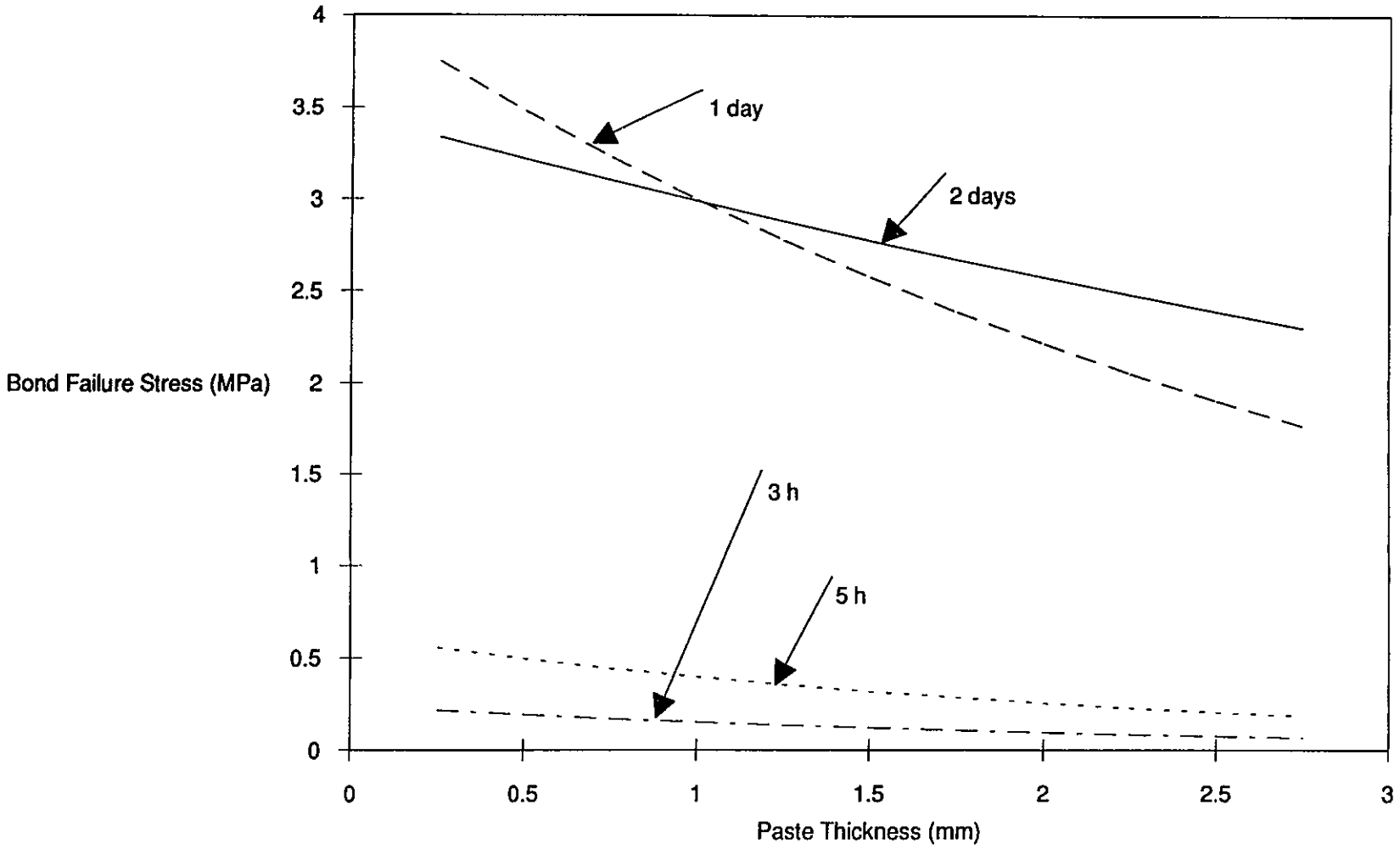

Figure 4.15 Cement+2% Calcium Chloride, w/c=0.35, steel substrate

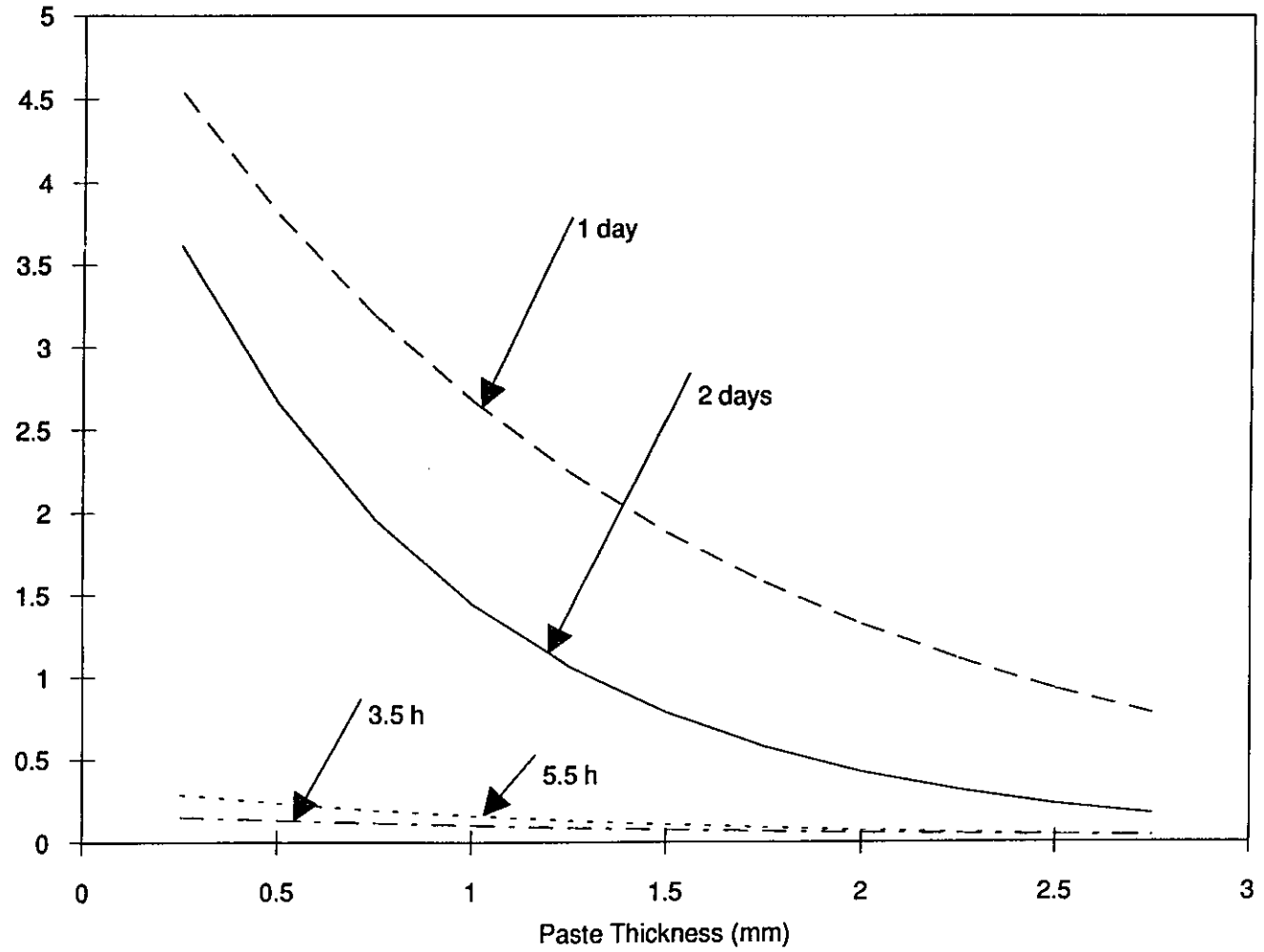

Figure 4.16 Cement+2% Calcium Chloride, w/c=0.30, glass substrate

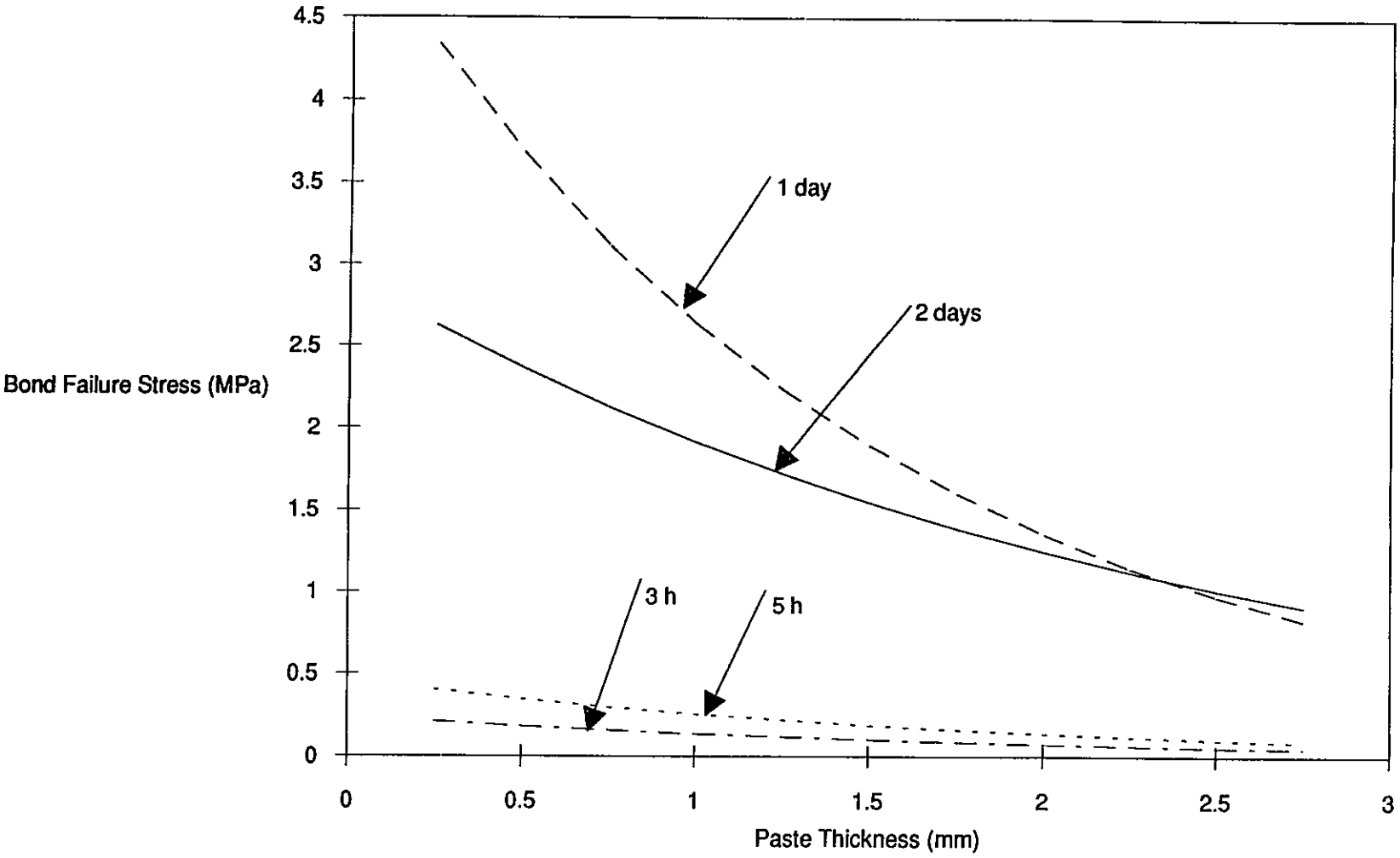

Figure 4.17 Cement+2% Calcium Chloride, w/c=0.35, glass substrate

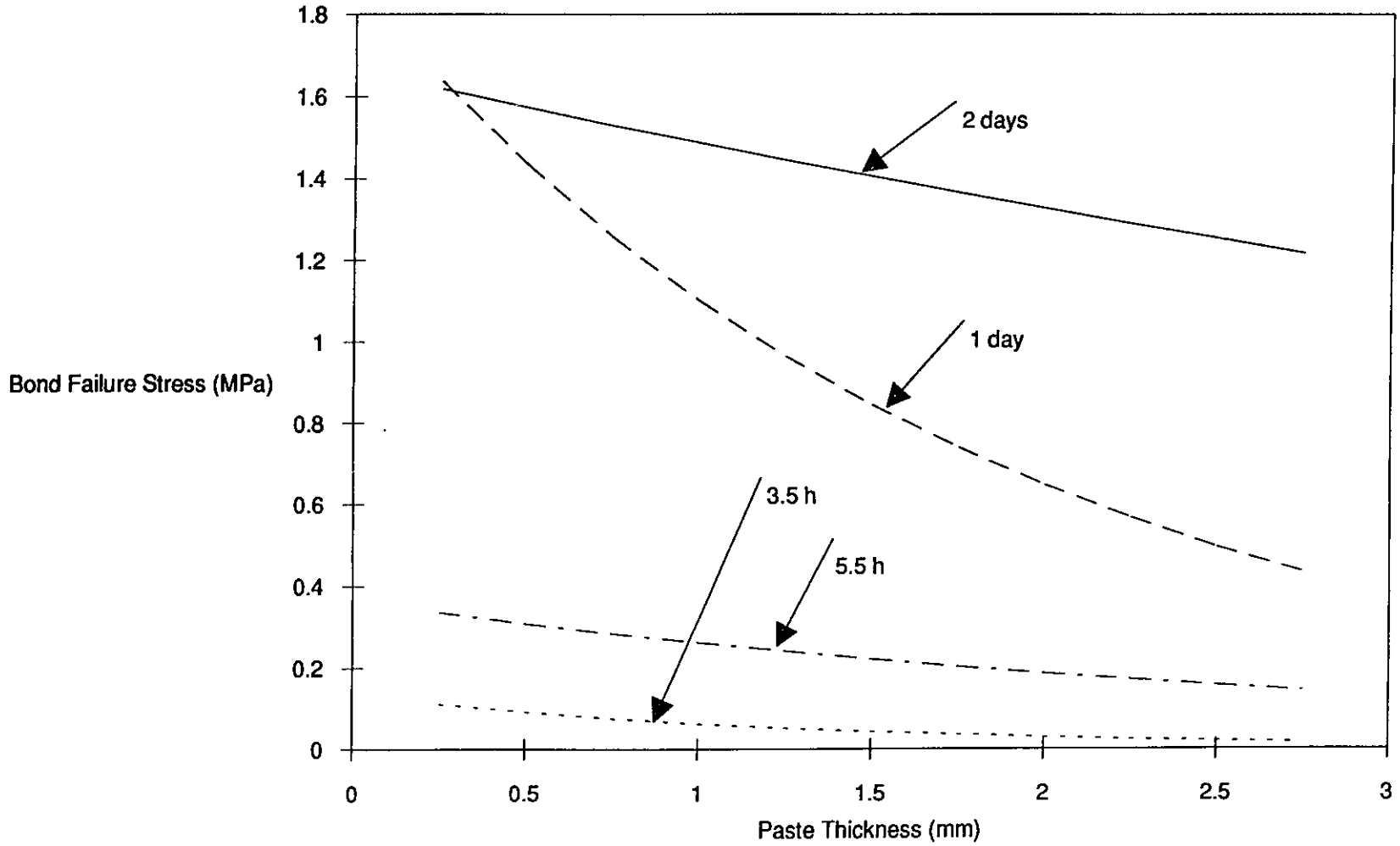

Figure 4.18 Cement+2% Calcium Propionate, w/c=0.30, steel substrate

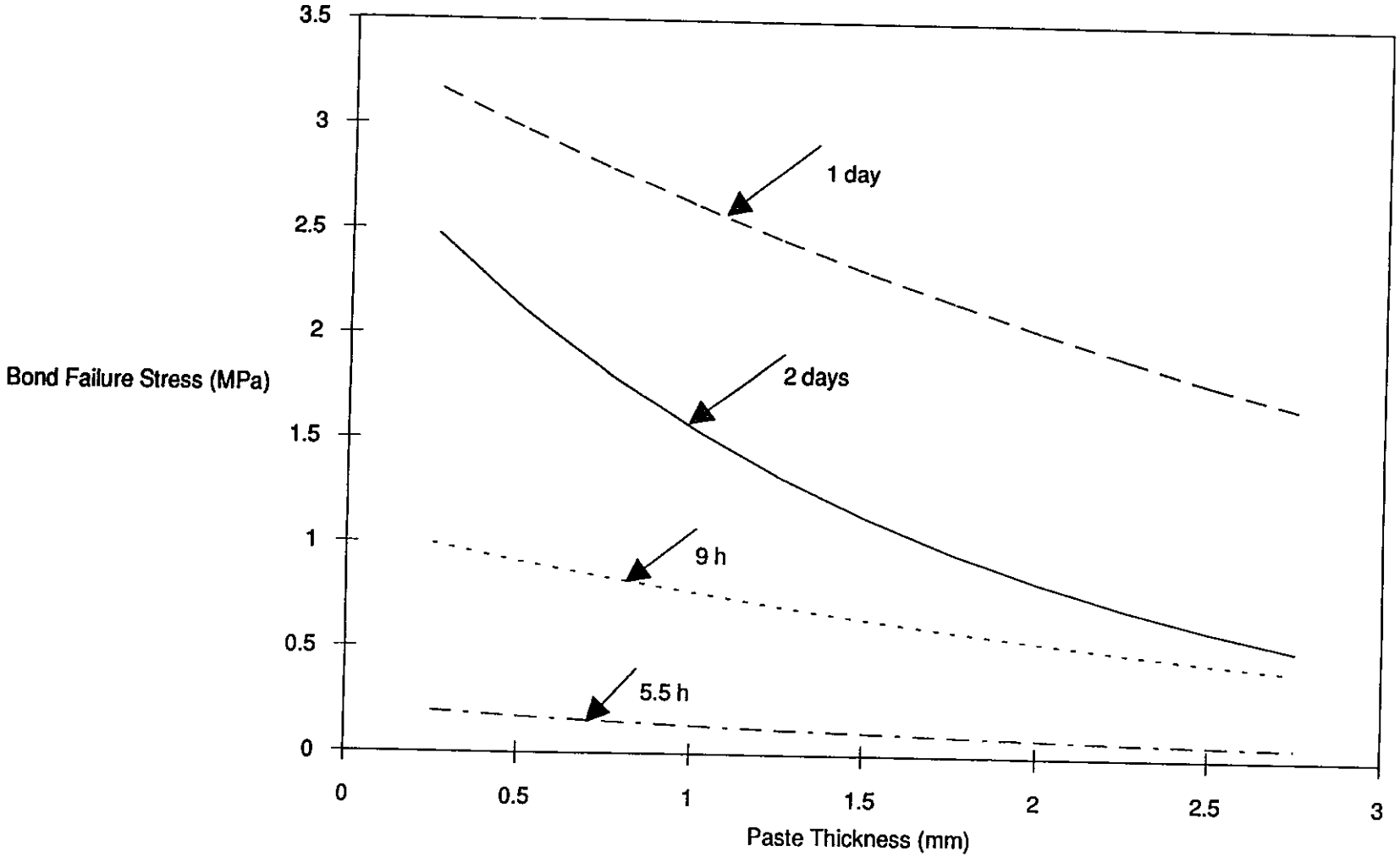

Figure 4.19 Cement+2% Calcium Propionate, w/c=0.35, steel substrate

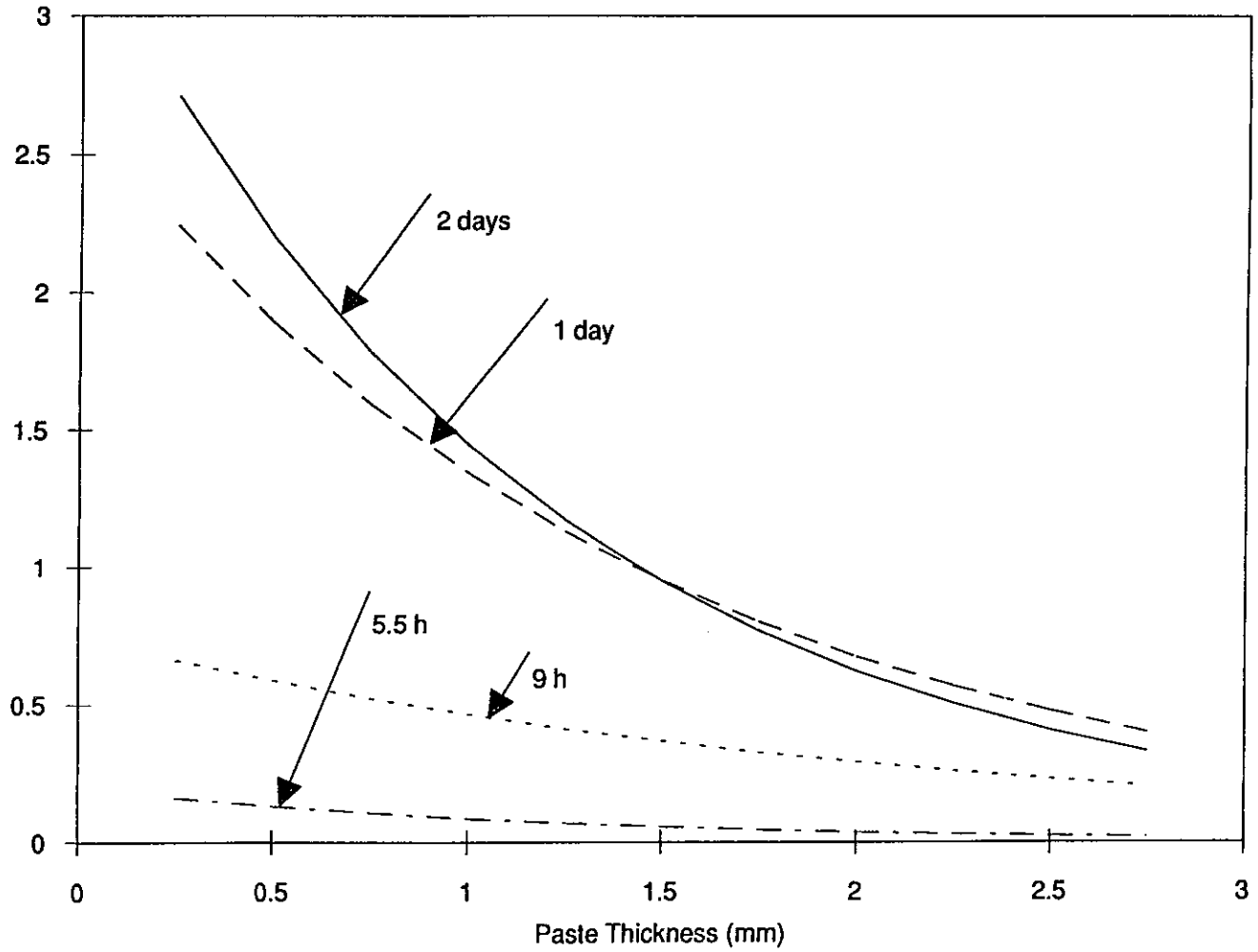

Figure 4.20 Cement+2% Calcium Propionate, w/c=0.30, glass substrate

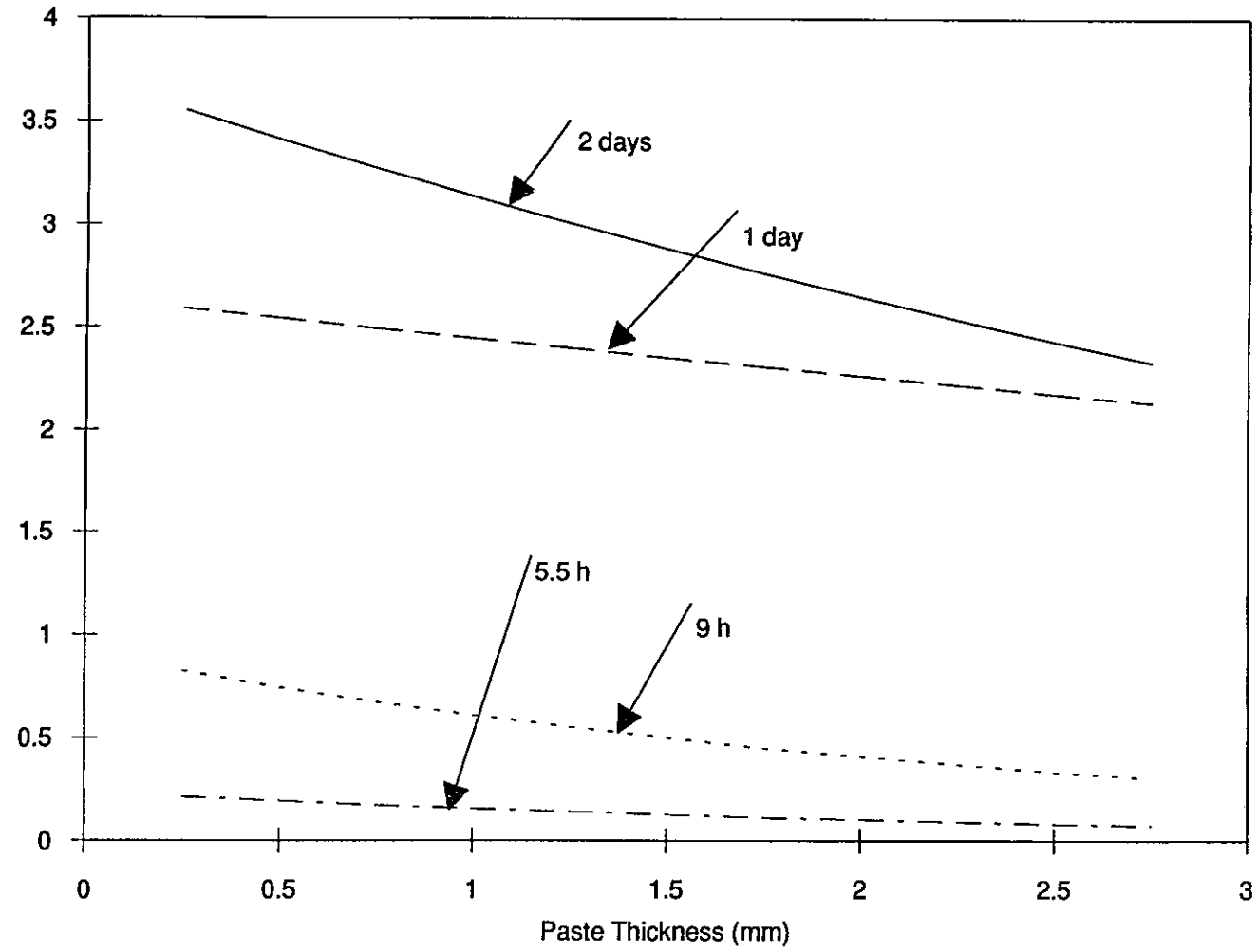

Figure 4.21 Cement+2% Calcium Propionate, w/c=0.35, glass substrate

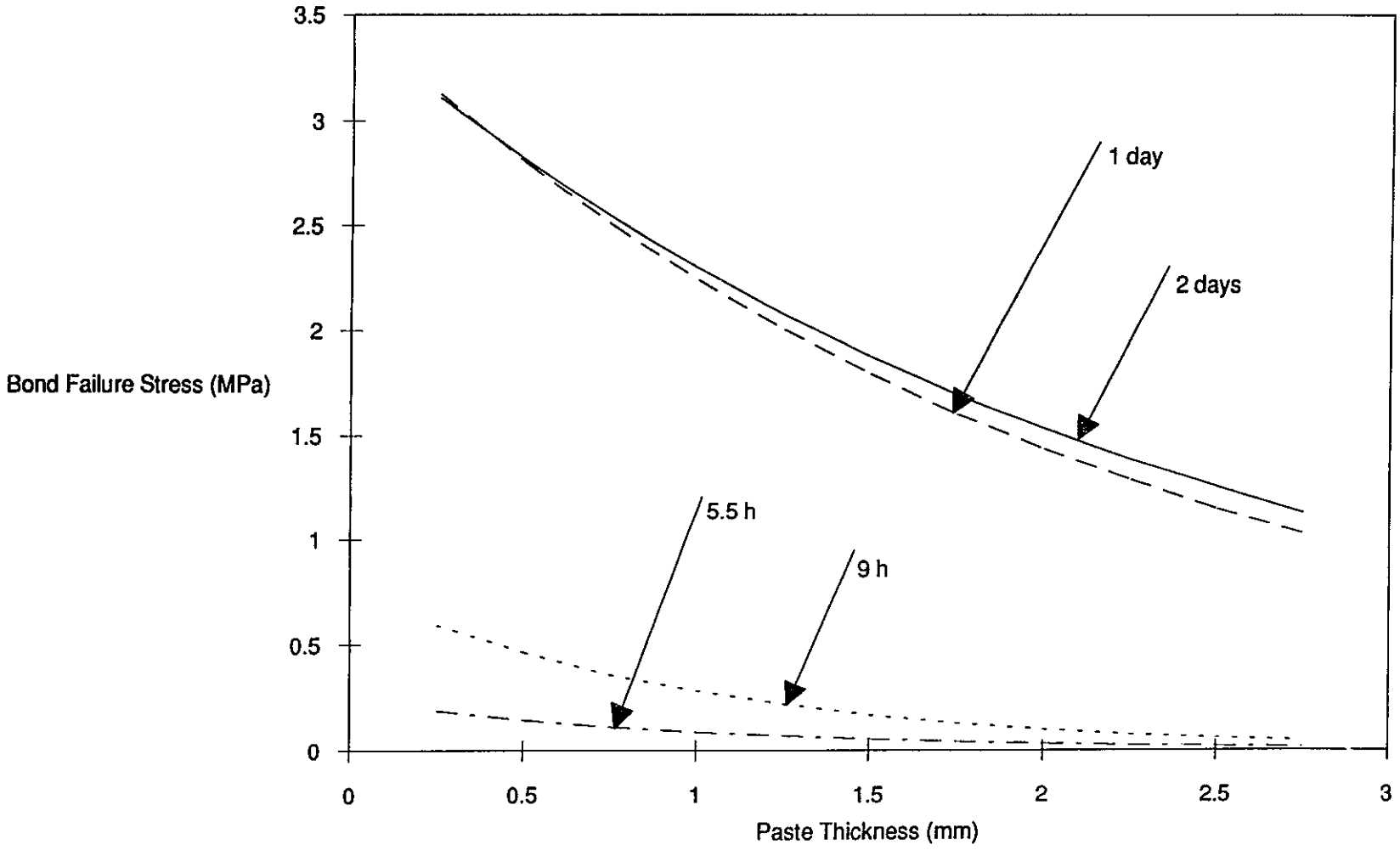

Figure 4.22 Cement+10% Silica Fume, w/c=0.30, steel substrate

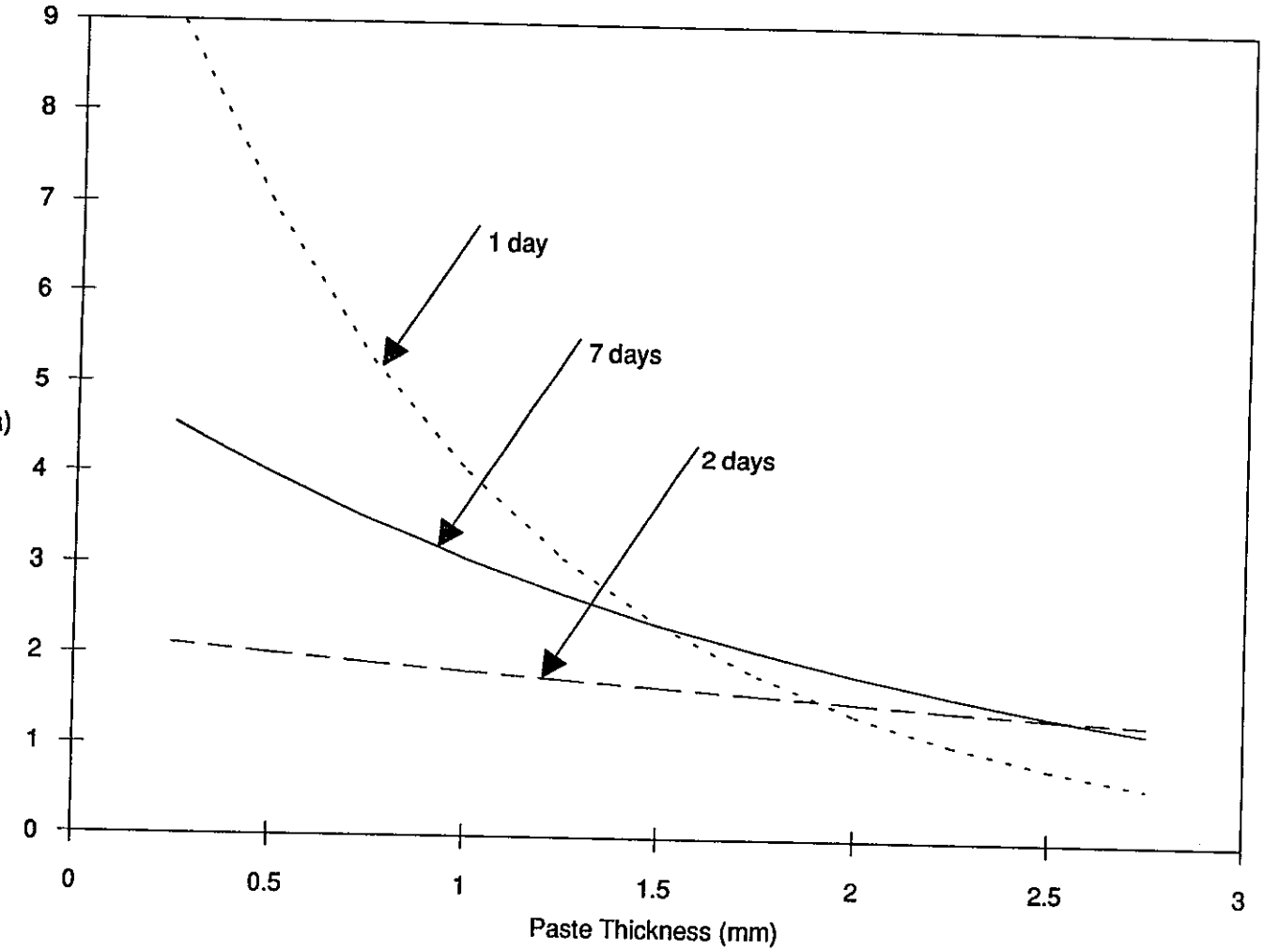

Figure 4.23 Cement+10% Silica Fume, w/c=0.35, steel substrate

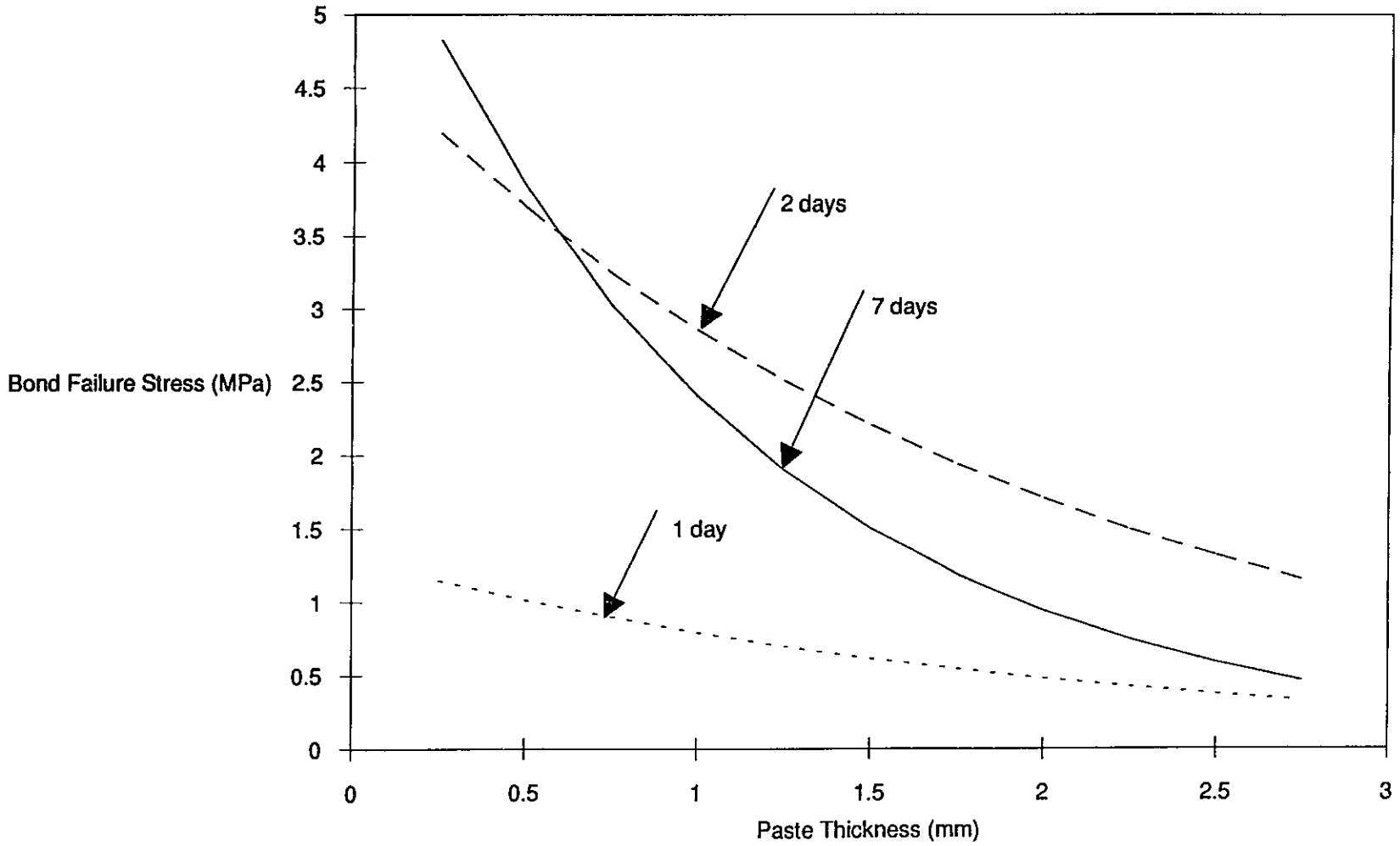

Figure 4.24 Cement+10% Silica Fume, w/c=0.30, glass substrate

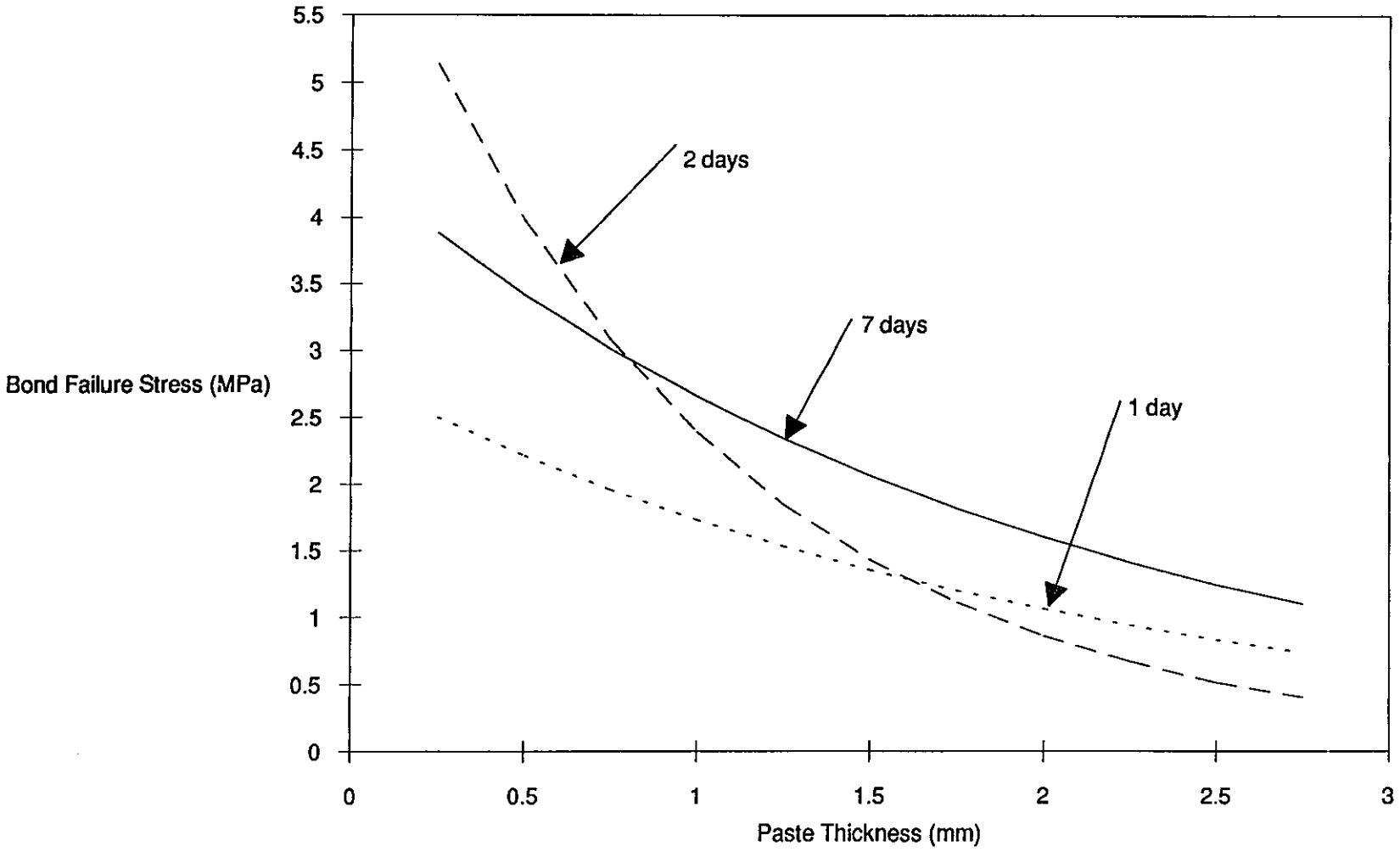

Figure 4.25 Cement+10% Silica Fume, w/c=0.35, glass substrate

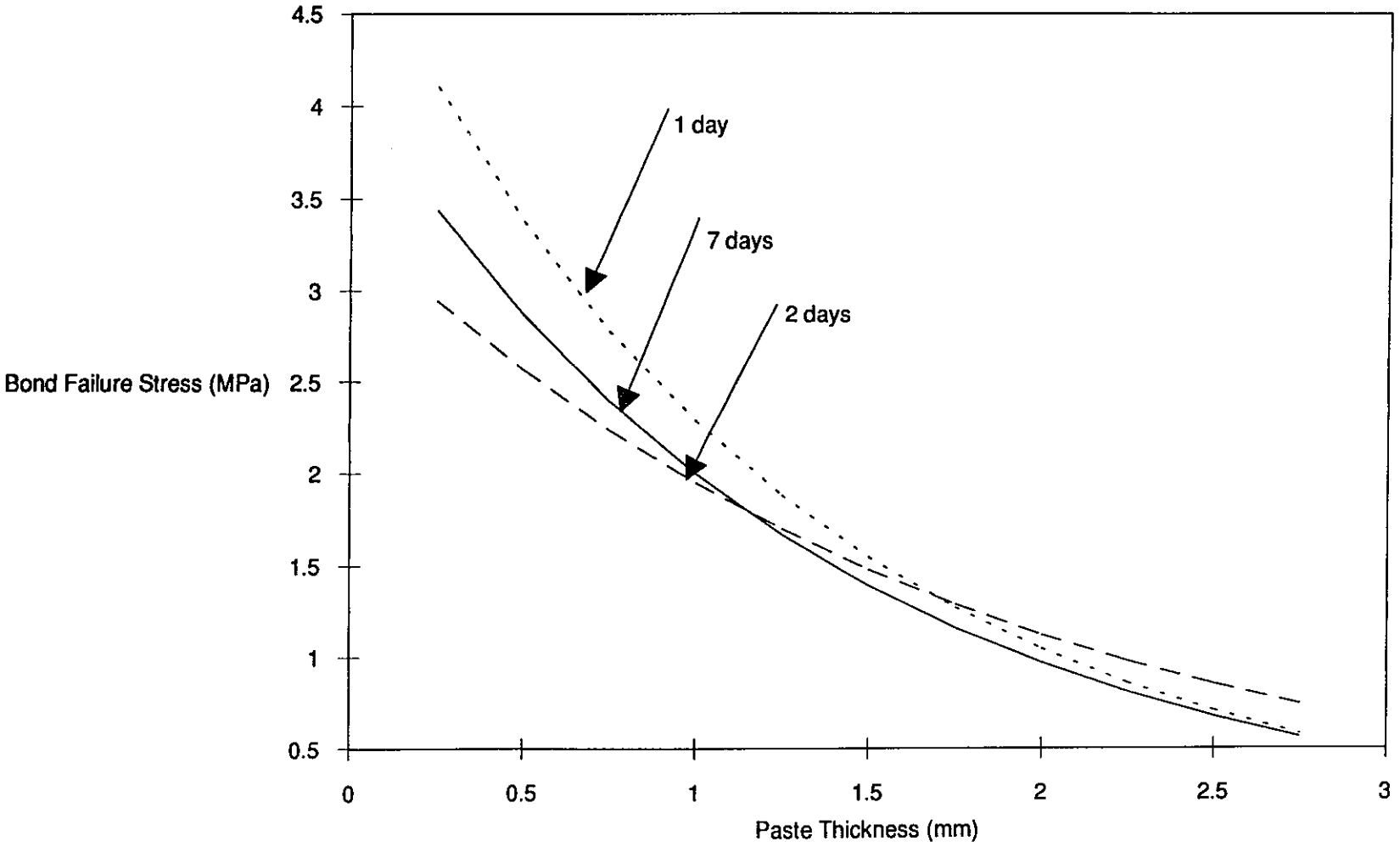

Figure 4.26 Clinker, w/c=0.30, steel substrate

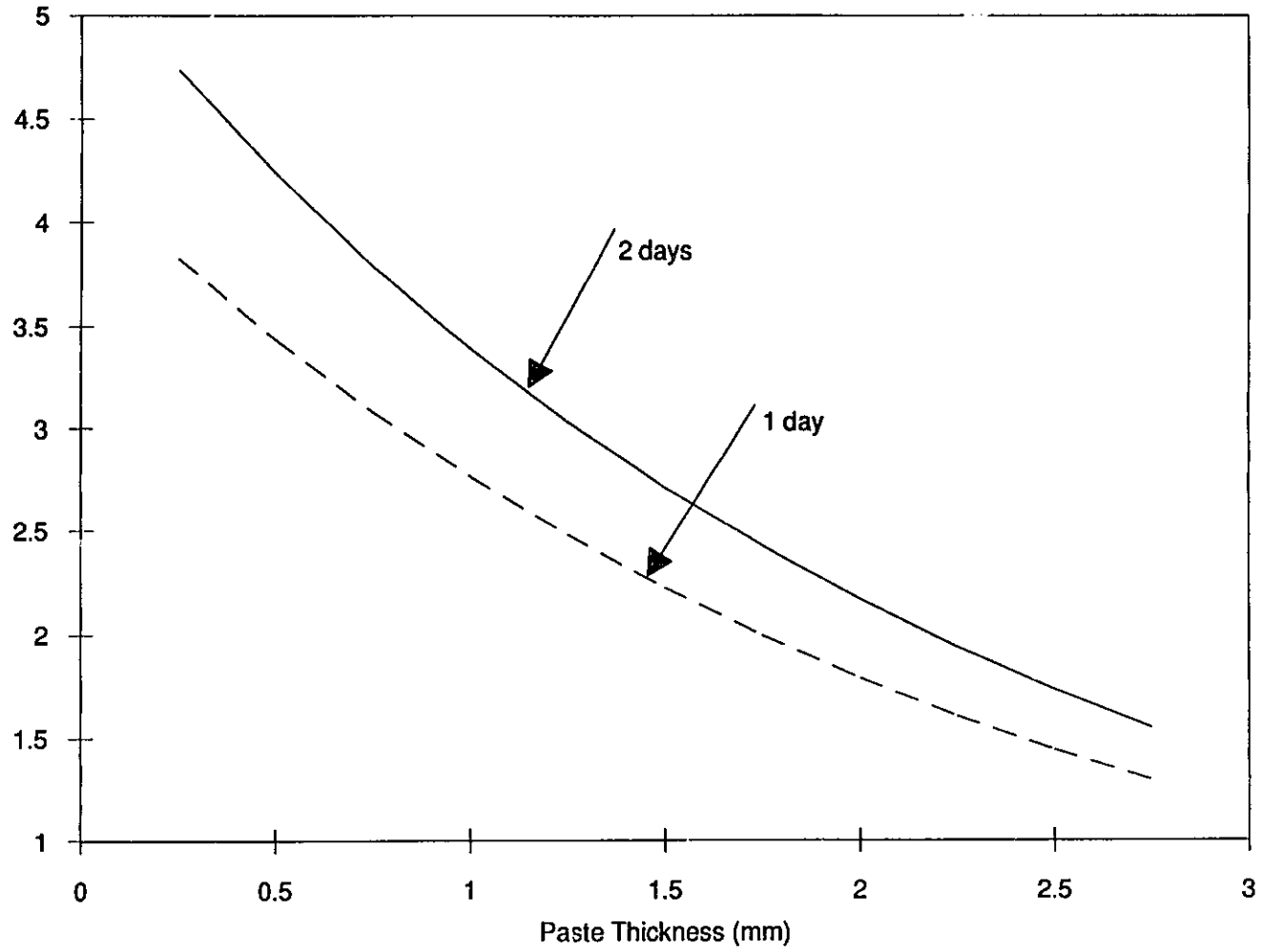

Figure 4.27 Clinker, w/c=0.35, steel substrate

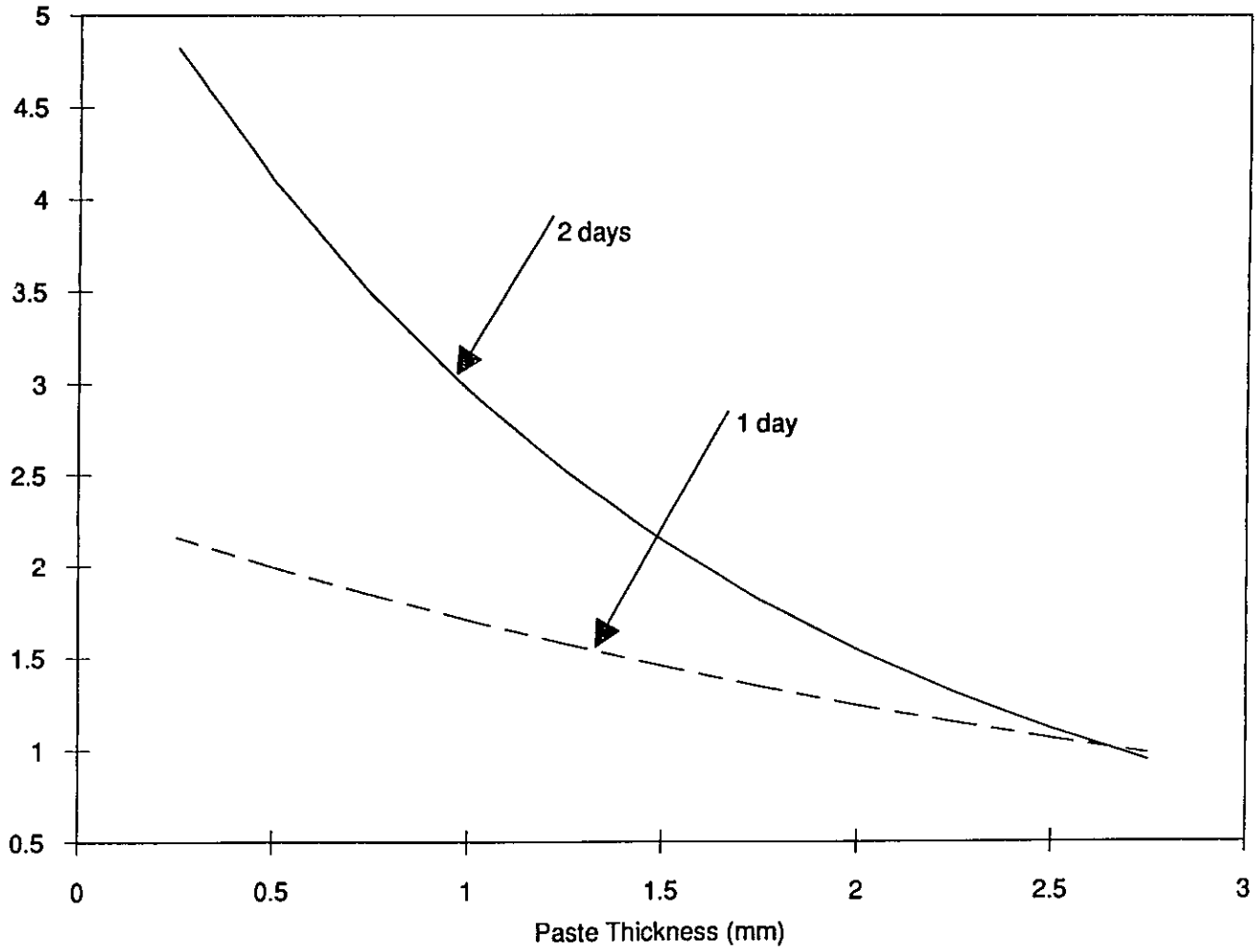

Figure 4.28 Clinker, w/c=0.30, glass substrate

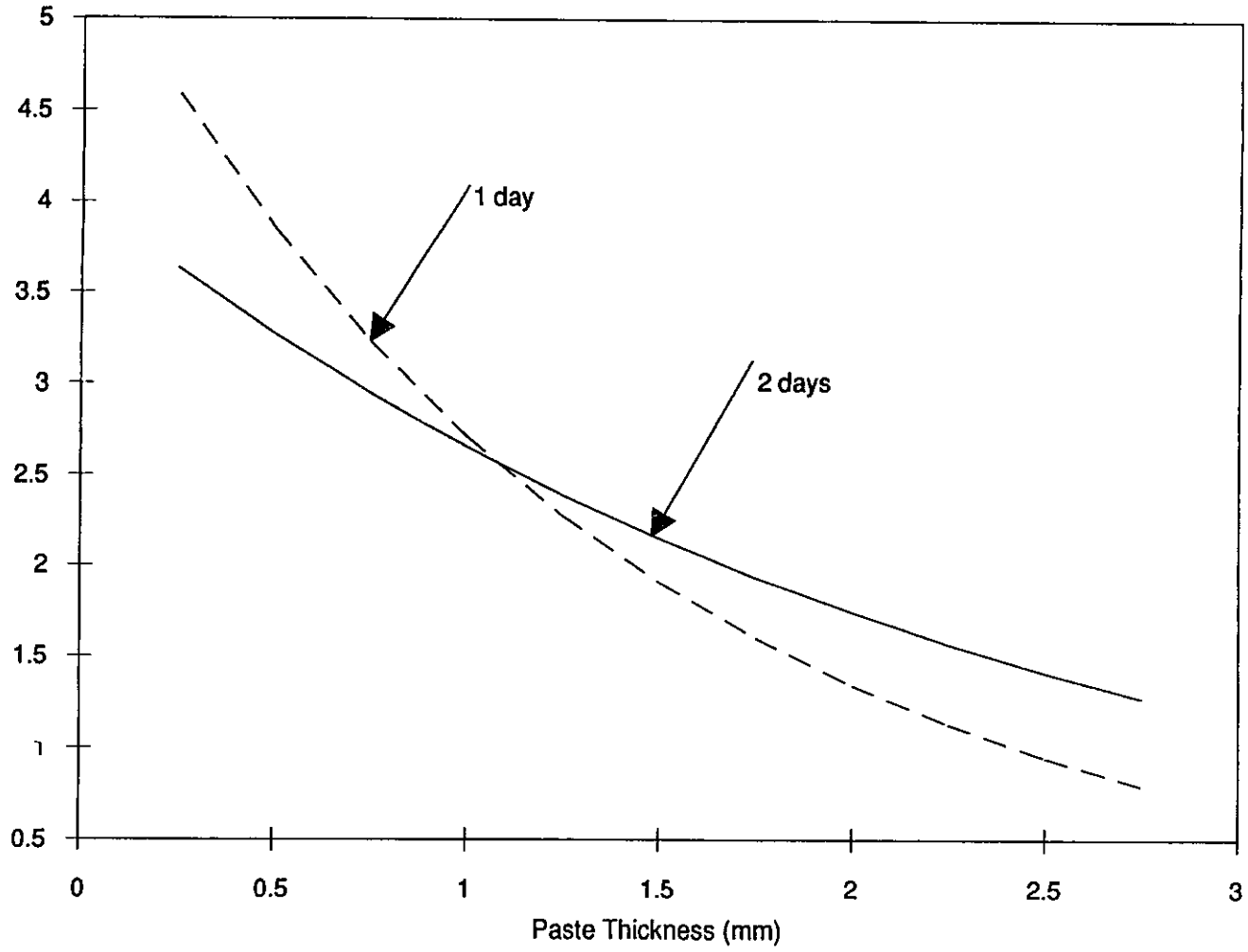

Figure 4.29 Clinker, w/c=0.35, glass substrate

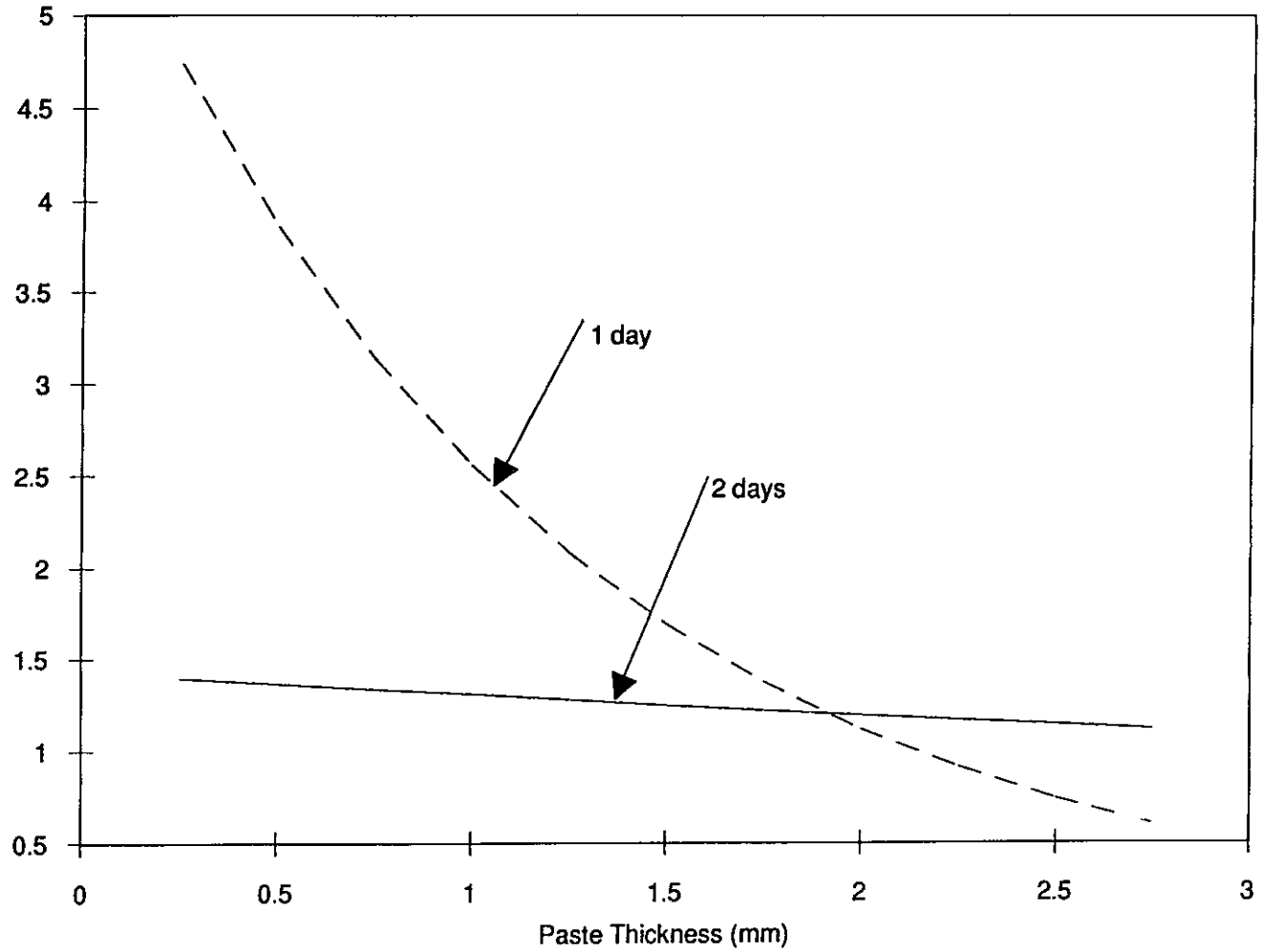

Figure 4.30 C3S, w/c=0.35, steel substrate

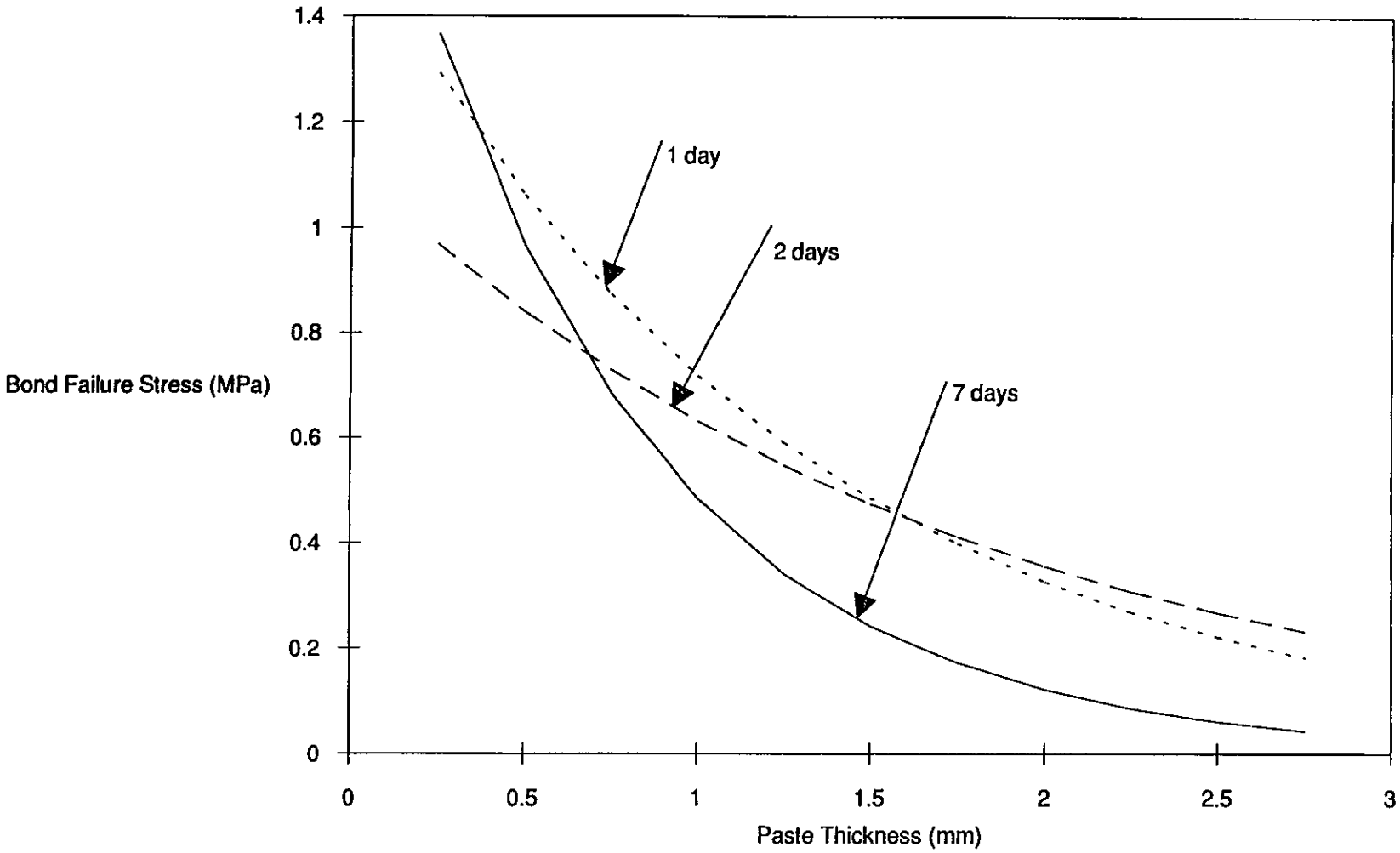

Figure 4.31 C3S, w/c=0.35, glass substrate

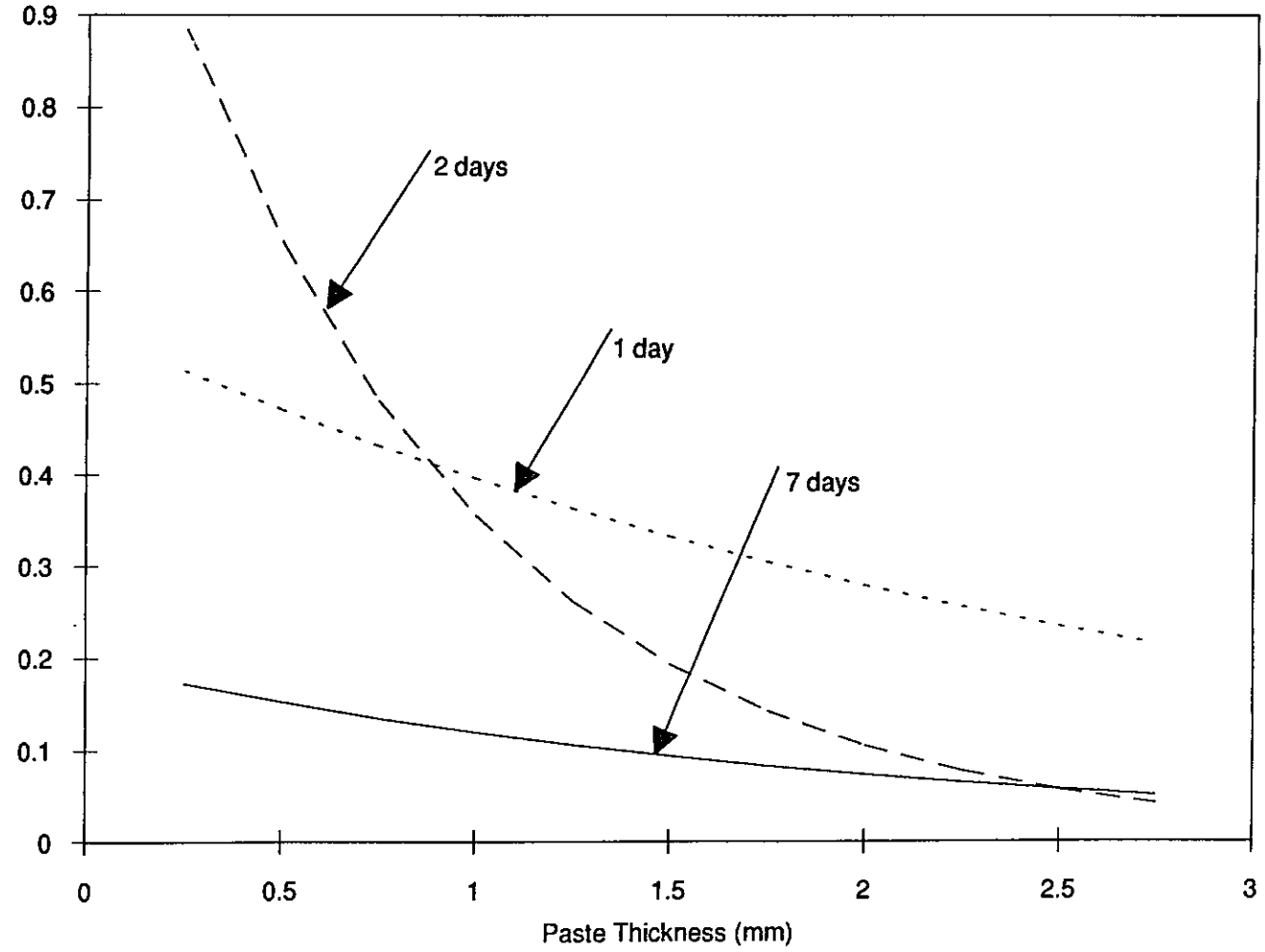

Figure 4.32 C3S+2% Sodium Nitrate, w/c=0.35, steel substrate

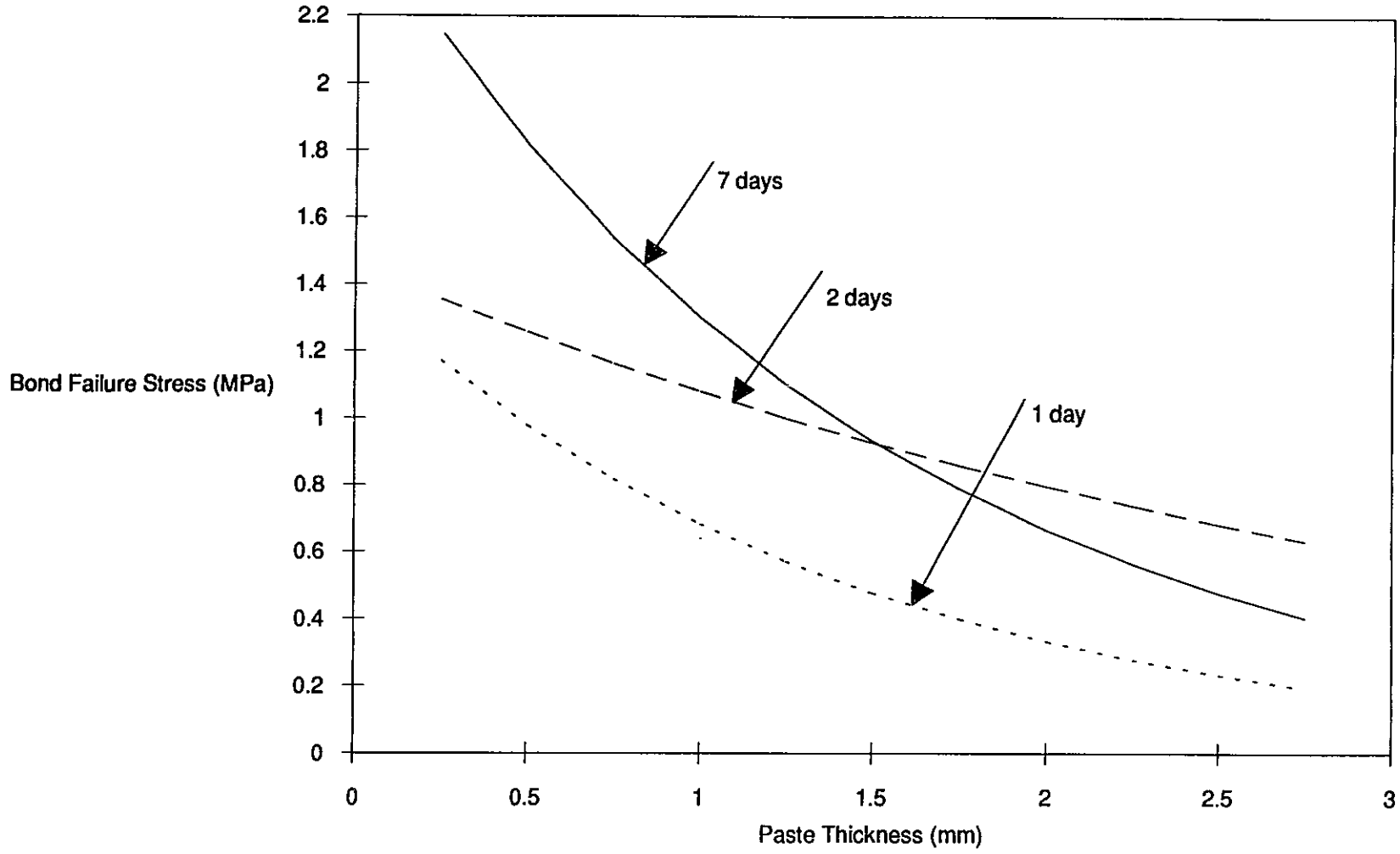

Figure 4.33 C3S+2% Sodium Nitrate, w/c=0.35, glass substrate

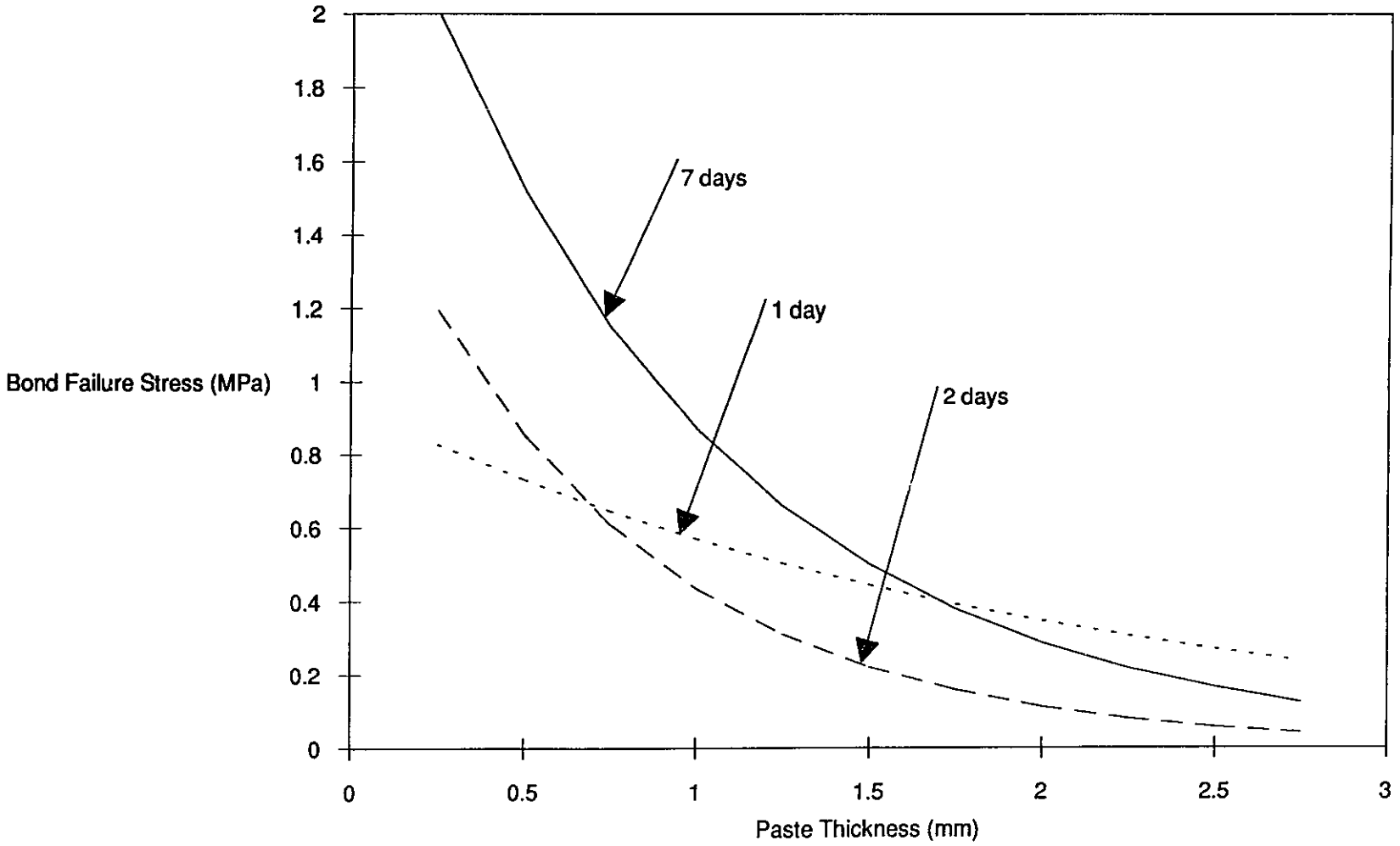

Table 4.6 Bond Strength vs Cement Paste Adhesive Thickness Curves Correlation Coefficients and Level of Significance

Steel Substrate					Glass Substrate				
System		# of val	r	Lvl Sign.	System		# of val	r	Lvl Sign.
Cement	4h	28	0.67	1%	Cement	4h	25	0.79	1%
w/c=0.30	7h	27	0.50	1%	w/c=0.30	7h	26	0.55	1%
	1d	41	0.38	5%		1d	24	0.59	1%
	2d	27	0.64	1%		2d	28	0.72	1%
	7d	24	0.77	1%		7d	28	0.58	1%
Cement	4h	27	0.64	1%	Cement	4h	20	0.78	1%
w/c=0.35	7h	23	0.77	1%	w/c=0.35	7h	32	0.68	1%
	1d	32	0.59	1%		1d	18	0.63	1%
	2d	22	0.81	1%		2d	28	0.76	1%
	7d	21	0.69	1%		7d	12	0.63	1%
$NaNO_3$	4h	33	0.80	1%	$NaNO_3$	4h	32	0.80	1%
w/c=0.30	7h	38	0.69	1%	w/c=0.30	7h	37	0.51	1%
	1d	53	0.62	1%		1d	29	0.80	1%
	2d	23	0.67	1%		2d	31	0.57	1%
	7d	27	0.76	1%		7d	10	0.39	--
$NaNO_3$	4h	21	0.84	1%	$NaNO_3$	4h	27	0.55	1%
w/c=0.35	7h	25	0.70	1%	w/c=0.35	7h	26	0.77	1%
	1d	22	0.57	1%		1d	36	0.26	--
	2d	24	0.55	1%		2d	31	0.78	1%
	7d	10	0.71	5%		7d	6	0.60	--
$CaCl_2$	3h	35	0.79	1%	$CaCl_2$	3h	23	0.63	1%
w/c=0.30	5h	27	0.79	1%	w/c=0.30	5h	23	0.68	1%
	1d	43	0.50	1%		1d	23	0.75	1%
	2d	25	0.23	--		2d	21	0.66	1%
$CaCl_2$	3h	36	0.77	1%	$CaCl_2$	3h	25	0.63	1%
w/c=0.35	5h	24	0.80	1%	w/c=0.35	5h	30	0.63	1%
	1d	55	0.54	1%		1d	33	0.73	1%
	2d	73	0.60	1%		2d	21	0.32	--
Propion.	5h	28	0.68	1%	Propion.	5h	21	0.72	1%
w/c=0.30	9h	36	0.72	1%	w/c=0.30	9h	30	0.65	1%
	1d	55	0.33	1%		1d	28	0.15	--
	2d	40	0.67	1%		2d	25	0.57	1%
Propion.	5h	25	0.81	1%	Propion.	5h	20	0.84	1%
w/c=0.35	9h	32	0.62	1%	w/c=0.35	9h	27	0.79	1%
	1d	34	0.43	5%		1d	23	0.54	1%
	2d	34	0.62	1%		2d	22	0.78	1%
Silica F	1d	15	0.83	1%	Silica F	1d	29	0.65	1%
w/c=0.30	2d	19	0.47	5%	w/c=0.30	2d	27	0.77	1%
	7d	13	0.71	1%		7d	8	0.77	5%
Silica F	1d	26	0.75	1%	Silica F	1d	24	0.78	1%
w/c=0.35	2d	13	0.68	5%	w/c=0.35	2d	27	0.72	1%
	7d	14	0.81	1%		7d	12	0.79	1%

Table 4.6 Continued

		Steel Substrate					Glass Substrate		
System		# of val	r	Lvl Sign	System		# of val	r	Lvl Sign
Clinker	1d	45	0.67	1%	Clinker	1d	45	0.81	1%
w/c=0.30	2d	28	0.82	1%	w/c=0.30	2d	33	0.81	1%
Clinker	1d	8	0.75	5%	Clinker	1d	15	0.78	1%
w/c=0.35	2d	20	0.77	1%	w/c=0.35	2d	24	0.25	--
C_3S	1d	13	0.80	1%	C_3S	1d	14	0.40	--
w/c=0.35	2d	6	0.69	--	w/c=0.35	2d	4	0.84	--
	7d	10	0.80	1%		7d	15	0.41	--
C_3S+$NaNO_3$	1d	10	0.70	5%	C_3S+$NaNO_3$	1d	19	0.66	1%
w/c=0.35	2d	5	0.70	--	w/c=0.35	2d	13	0.82	1%
	7d	6	0.52	--		7d	19	0.79	1%

Note: Hydration times of less than one day have been rounded, # of val=number of data points used in the regression, Lvl Sign=level of significance which the regression passes, Silica F=silica fume.

A comparison of bond strength results for the various systems to the controls shows that on the steel substrate at w/c=0.30 cement paste had the lowest bond strength values at one day, two days and the hydration time associated with the midpeak of the heat of hydration curve. Comparison at w/c=0.35 indicated that the differences in results for the paste systems did not show any clear trend. The C_3S paste produced consistently low values (0.2-1.4 MPa), while the addition of $NaNO_3$ to the C_3S system increased the paste bond strength.

The cement paste system at w/c=0.30 debonded at higher stresses on the glass substrate than all other systems at the time associated with the midpeak of the heat of hydration curve and at one and two days. The cement paste (w/c=0.35) was highest only at two days, while the C_3S paste with $NaNO_3$ addition once again was stronger than the plain C_3S paste.

An examination of the differences in bond strength between the two substrates reveals little difference in bond strength for all systems at hydration times of less than one day. The clinker paste exhibits greater bond strength on the steel at both one and two days, but all other systems showed no affinity for one substrate over the other.

4.8 Interface Fracture Energy

The interface fracture energy terms for all systems are shown in Table 4.7. In general the interface fracture energy increased from the time associated with the midpoint of the heat of hydration curve (3h to 5h) until one day, then decreased at two days. At seven days the interface fracture energy increases for the steel substrate, but for the glass substrate it decreases. Interface fracture energy data indicate that an increase in w/c results in a decrease of fracture energy.

A comparison of interface fracture energy values for the two substrates showed that the paste containing $NaNO_3$ (w/c=0.35) and $CaCl_2$ (w/c=0.30) had higher values on the steel substrate at all hydration times. The same was true of the silica fume pastes (w/c=0.30) for the glass substrate. Cement paste (w/c=0.30) required more energy to debond on the steel substrate, except at two days. Pastes containing $NaNO_3$ (w/c=0.30) and silica fume (w/c=0.35) also had higher values on the steel but at times greater than seven hours and one day respectively. The pastes containing calcium propionate had higher interface fracture energy values on the glass after hydration of more than nine hours.

A comparison between the systems at each hydration time shows that no one system consistently produced higher interface fracture energy values than the other systems at all hydration times. The cement paste control system on the steel substrate produced the highest values for both water-cement ratios at seven days. The calcium propionate system exhibited greater interface fracture energy values on the glass substrate at two days with both water-cement ratios. The highest value of interface fracture energy, 1.66 Jm^{-2}, is obtained with the silica fume system adhered to the glass substrate.

Table 4.7 Interface Fracture Energy Values for all Systems (J/m^2)

Interface Fracture Energy Values for Steel Substrate

	Cement		$NaNO_3$		$CaCl_2$		Propionate	
	0.30	0.35	0.30	0.35	0.30	0.35	0.30	0.35
Peak	0.074	0.035	0.055	0.029	0.082	0.014	0.448	0.062
1d	1.17	0.037	0.871	0.844	0.680	0.464	0.636	0.112
2d	0.191	0.076	0.400	0.154	0.585	0.102	0.103	0.083
7d	0.652	0.593	0.221	0.267	-----	-----	-----	-----

	Silica Fume		Clinker		C_3S
	0.30	0.35	0.30	0.35	0.35
1d	0.062	0.030	0.062	0.083	0.062
2d	0.112	0.315	0.112	0.267	0.112
7d	0.083	0.149	-----	-----	0.083

Interface Fracture Energy Values for Glass Substrate

	Cement		$NaNO_3$		$CaCl_2$		Propionate	
	0.30	0.35	0.30	0.35	0.30	0.35	0.30	0.35
Peak	0.031	0.027	0.109	0.012	0.029	0.051	0.265	0.019
1d	0.368	0.920	0.394	0.436	0.385	0.087	0.723	0.368
2d	0.214	0.137	0.278	0.062	0.169	0.198	0.677	0.271
7d	0.176	0.097	0.072	0.224	-----	-----	-----	-----

	Silica Fume		Clinker		C_3S
	0.30	0.35	0.30	0.35	0.35
1d	1.660	0.210	0.499	0.568	0.499
2d	0.380	0.143	0.417	0.176	0.006
7d	0.305	0.108	-----	-----	0.001

4.9 Microscopy

4.9.1 Substrate Coverage

The amount of transition zone material retained on the substrate relative to substrate area after sample failure is defined as substrate coverage. The surface coverage was measured using an image analysis program in conjunction with the SEM and BSE detector. The image analysis program calculated the relative amount of substrate area covered.

The values of substrate coverage shown in Table 4.8 show a decrease in cover with increased hydration time. In general the first two hydration times produced cover values close to 100% and at later ages the glass substrates exhibited greater cover than

the steel. A comparison of all systems with the controls shows that at times of one day and longer, for the steel substrate, the salt and silica fume cement paste systems have higher coverage. The clinker and C_3S systems have less coverage. For the glass substrate the $NaNO_3$, C_3S and silica fume paste systems (w/c=0.30) all had greater coverage than the controls. The $CaCl_2$ paste produced less cover, while the calcium propionate and silica fume pastes (w/c=0.35) had coverage patterns similar to the control. The clinker comparison was not considered due to insufficient data.

A comparison between the substrates, within the systems showed the coverage was greater on the glass than on the steel for the following paste systems: $CaCl_2$ (w/c=0.35), calcium propionate (w/c=0.35), silica fume (w/c=0.30), C_3S, clinker and cement (except at seven days). The steel substrate had greater coverage at two days and later for the $NaNO_3$ paste systems, while for calcium propionate (w/c=0.30) coverage on the steel was greater, except at two days.

A comparison can be made within the systems and between w/c. The cement, $NaNO_3$ and silica fume paste systems all had more cover with a w/c=0.30 for the steel substrate. The $CaCl_2$ and calcium propionate systems showed little difference with w/c. The $CaCl_2$ and calcium propionate systems (w/c=0.30) exhibited greater coverage at all times except two days for the glass substrate. The cement paste control (w/c=0.35) had the largest coverage at less than one day, while $NaNO_3$ (w/c=0.30) and silica fume pastes (w/c=0.35) produced better coverage at most times.

Table 4.8 Percentage Coverage on Substrates for all Systems

% Coverage for Steel Substrate

	Cement		$NaNO_3$		$CaCl_2$		Propionate	
	0.3	0.35	0.3	0.35	0.3	0.35	0.3	0.35
Mid	100	93.6	74.0	58.2	80.2	72.1	100	99.0
Peak	72.5	76.7	57.4	58.1	59.7	53.2	100	98.5
1d	65.9	19.8	77.0	33.6	68.6	40.8	89.4	30.8
2d	50.1	---	73.4	78.7	37.1	37.7	22.6	27.3
7d	38.6	28.6	61.4	50.3	---	---	---	---

	Silica Fume		Clinker		C_3S	$C3S+NaNO_3$
	0.3	0.35	0.3	0.35	0.35	0.35
1d	65.3	84.1	49.1	65.9	16.0	17.7
2d	24.4	75.2	40.7	25.2	23.6	19.1
7d	---	23.6	---	---	35.3	17.9

% Coverage for Glass Substrate

	Cement		$NaNO_3$		$CaCl_2$		Propionate	
	0.3	0.35	0.3	0.35	0.3	0.35	0.3	0.35
Mid	100	100	100	100	100	100	100	100
Peak	98.0	97.8	---	100	100	100	100	100
1d	100	---	80.0	64.0	54.7	53.8	60.2	51.9
2d	51.0	43.9	67.4	54.3	33.1	38.2	47.9	49.1
7d	19.1	11.7	51.4	31.3	---	---	---	---

	Silica Fume		Clinker		C_3S	$C_3S+NaNO_3$
	0.3	0.35	0.3	0.35	0.35	0.35
1d	76.6	67.1	---	80.1	100	71.8
2d	54.4	21.2	---	62.4	61.7	67.6
7d	22.4	45.0	---	---	51.8	41.2

*Note: Mid refers to the hydration time associated with midpeak of the heat of hydration curve. Peak refers to the maximum value of heat of hydration on the same curve. Actual times are given in section 4.1. A strikethrough means the value was not available.

4.9.2 SEM Micrographs

The low magnification photos, some of which are shown in Figures 4.34-4.40, were used to determine the amount of cover on the substrate. The high magnification photos, Figures 4.41-4.46 were utilized for examination of the fracture surface microstructure in an attempt to link observed bond strength with the condition of the failure surface. The photos are labelled with the system name, water-cement ratio,

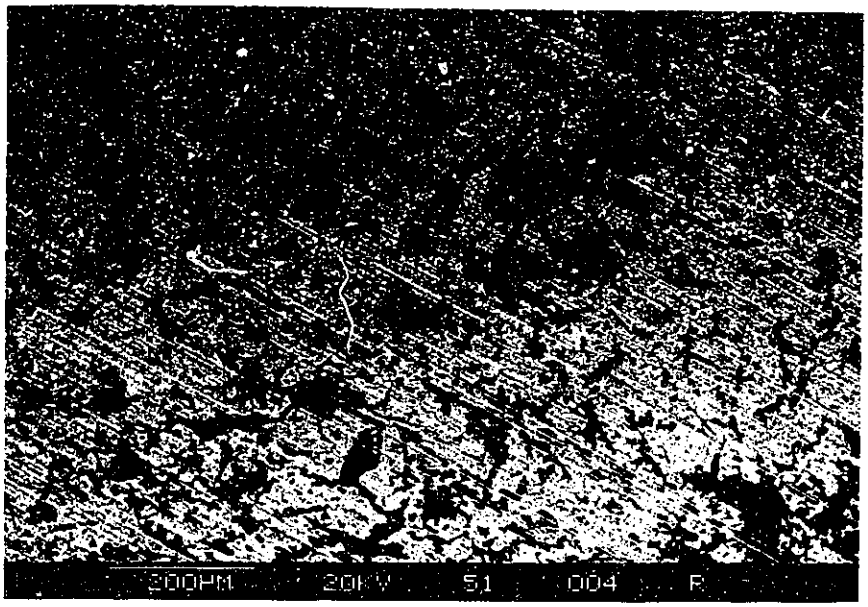

a) Cement, w/c=0.30, 2 days, steel substrate

b) Cement, w/c=0.30, 1 day, glass substrate

Figure 4.34

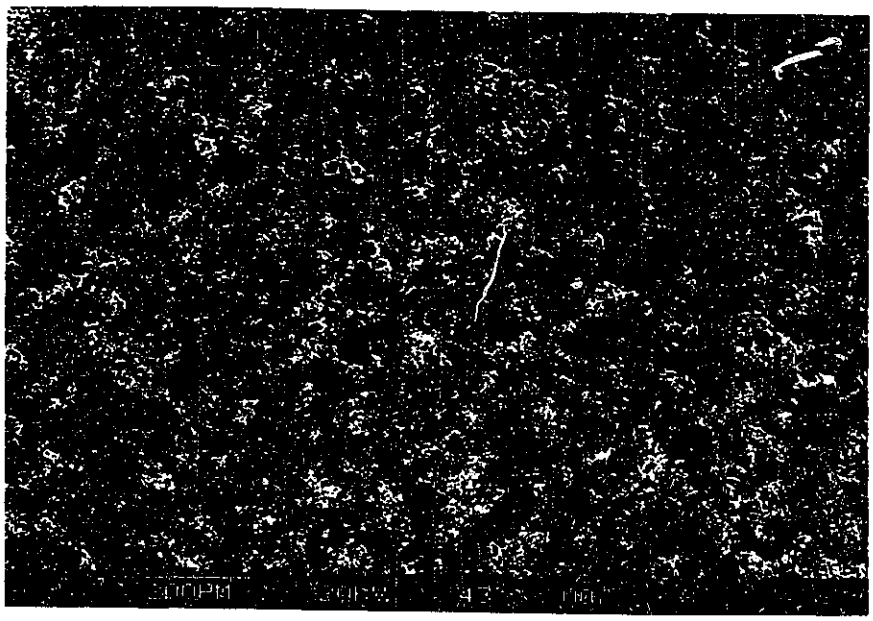

a) Cement+2% $NaNO_3$, w/c=0.35, 1 day, glass substrate

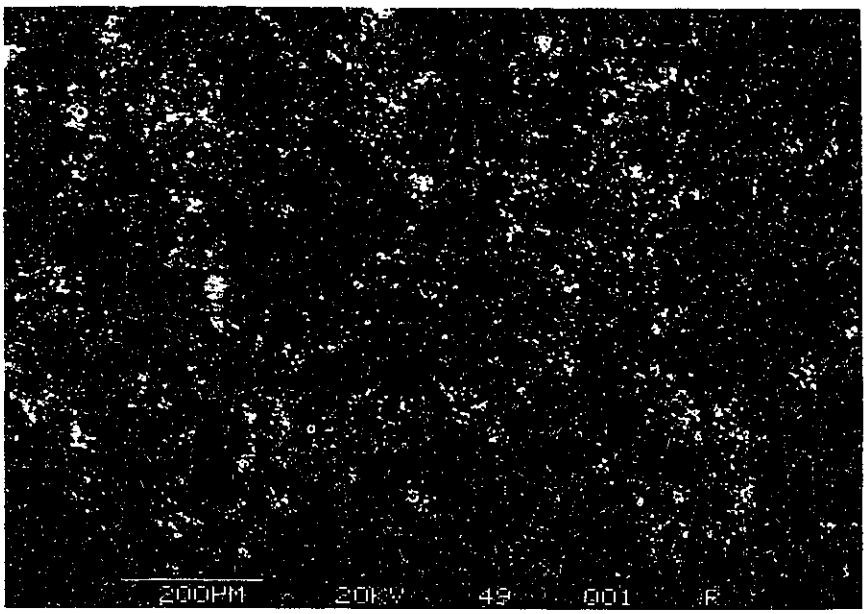

b) C_3S, w/c=0.35, 2 days, glass substrate

Figure 4.35

a) Cement+2% $NaNO_3$, w/c=0.30, 2 days, glass substrate

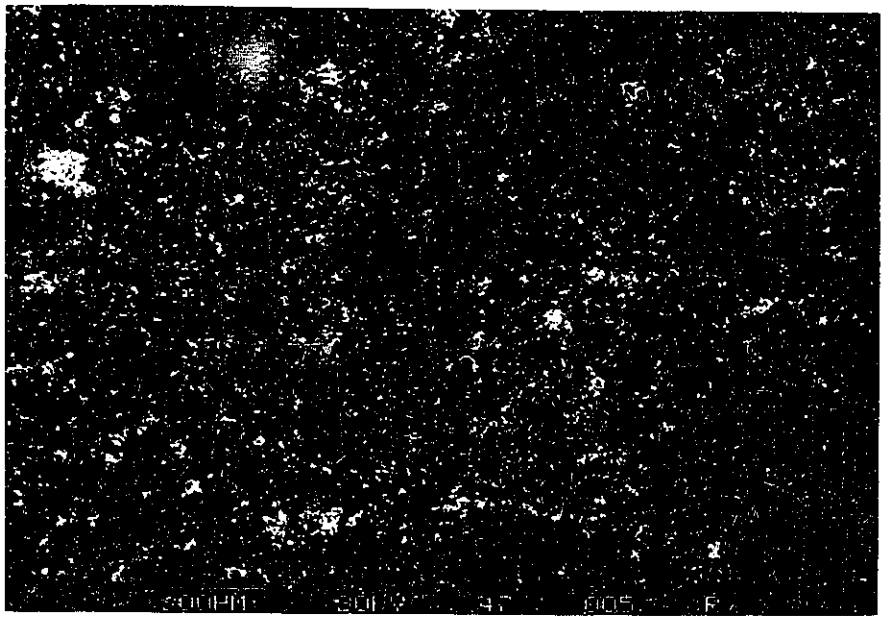

b) Cement+10% Silica Fume, w/c=0.30, 1 day, glass substrate

Figure 4.36

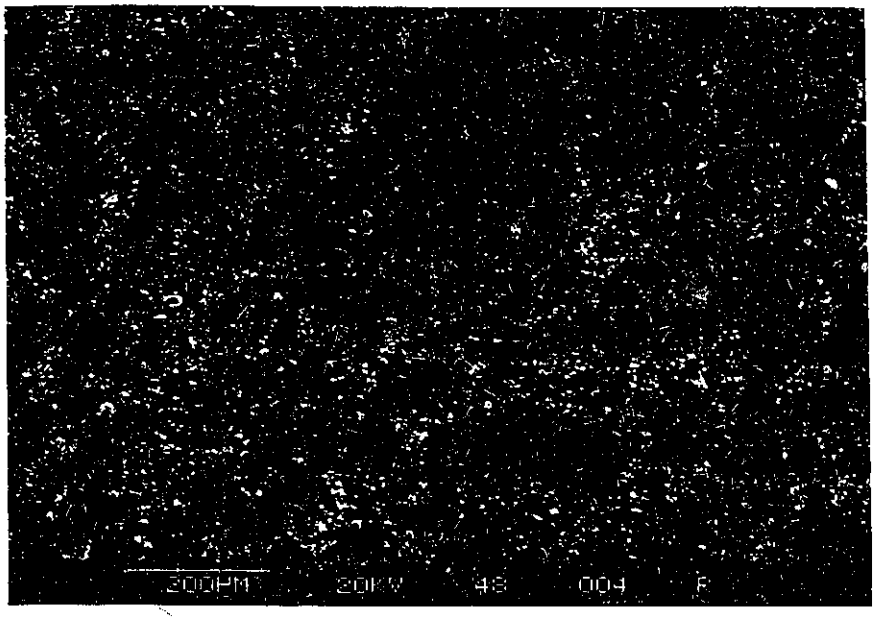

a) C_3S+2% $NaNO_3$, w/c=0.35, 1 day, glass substrate

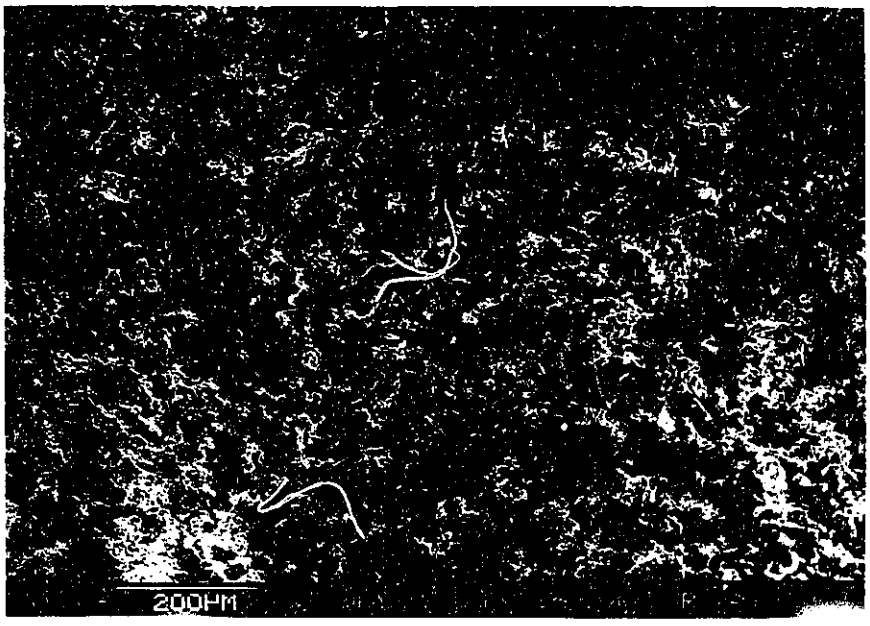

b) Cement+2% $Ca(C_3H_5O_2)_2.H_20$, w/c=0.30, 1 day, glass susbstrate

Figure 4.37

a) Cement+2% $CaCl_2$, w/c=0.35, 2 days, glass substrate

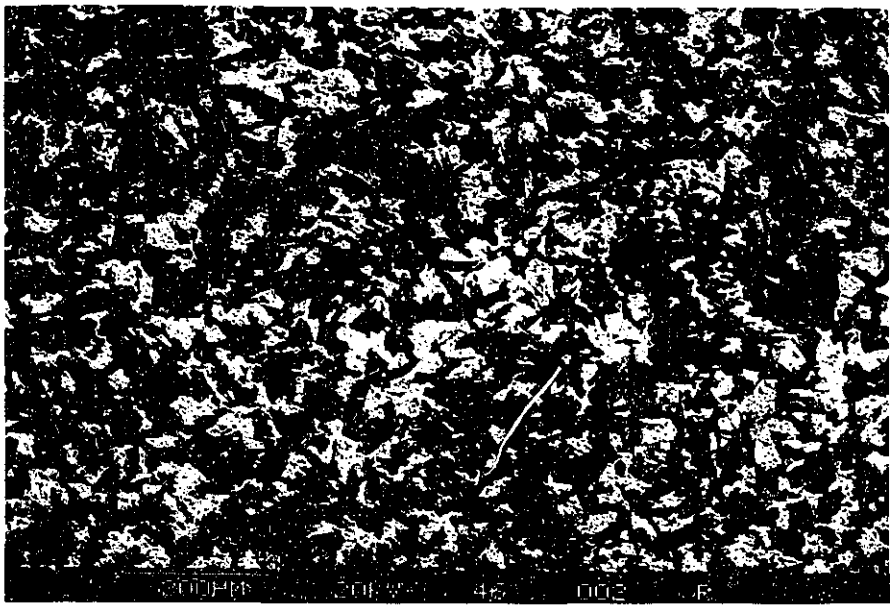

b) Cement+2% $Ca(C_3H_5O_2)_2.H_2O$, w/c=0.30, 2 days, glass substrate

Figure 4.38

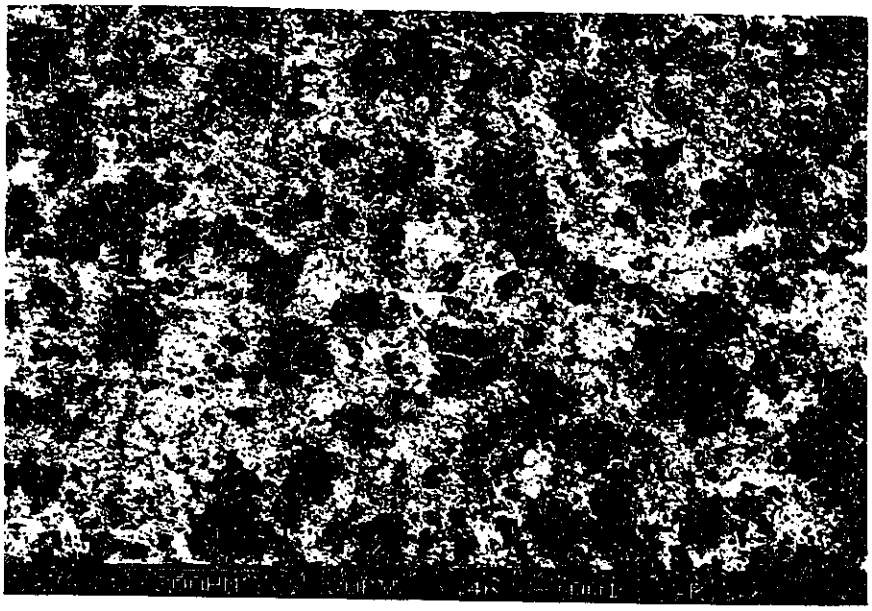

a) Cement+2% $CaCl_2$, w/c=0.30, 1 day, glass substrate

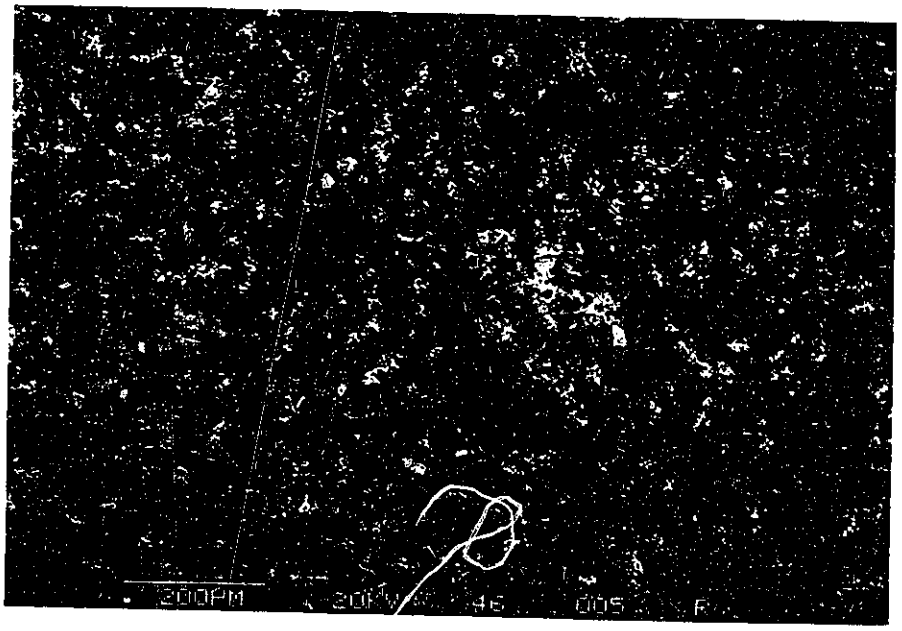

b) Cement+2% $Ca(C_3H_5O_2)_2.H_2O$, w/c=0.35, 2 days, glass substrate

Figure 4.39

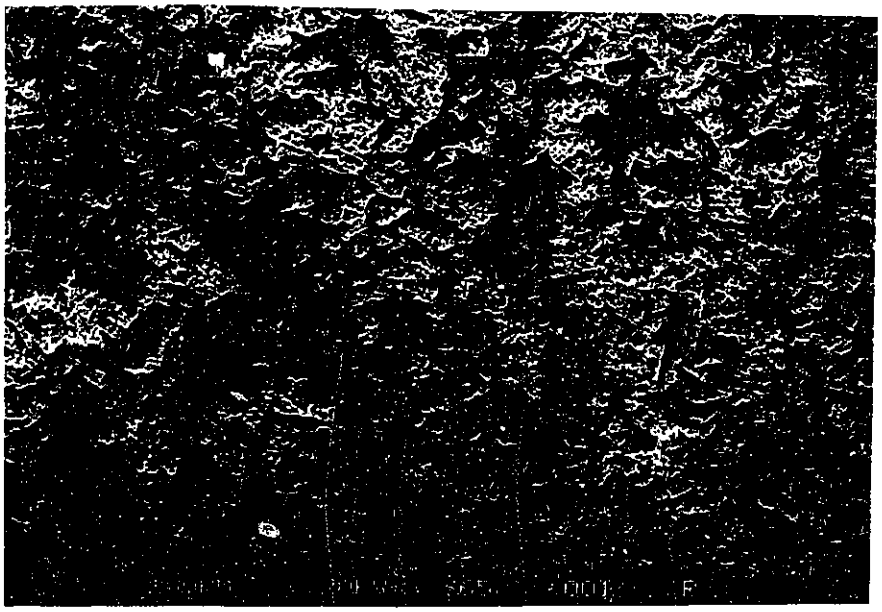

a) Cement, w/c=0.35, 2 days, paste off glass substrate

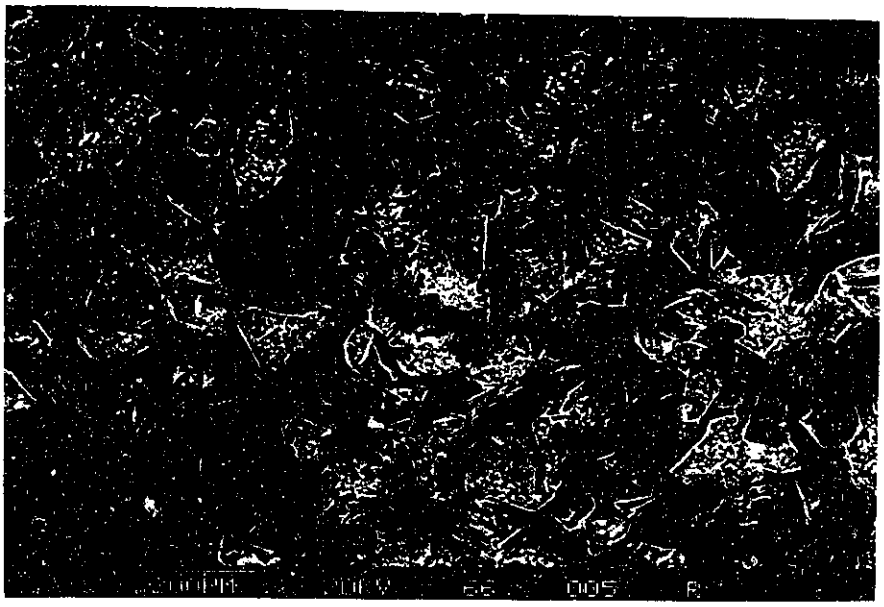

b) Cement+2% $Ca(C_3H_5O_2)_2.H_2O$, w/c=0.30, 1 day, paste off glass substrate

Figure 4.40

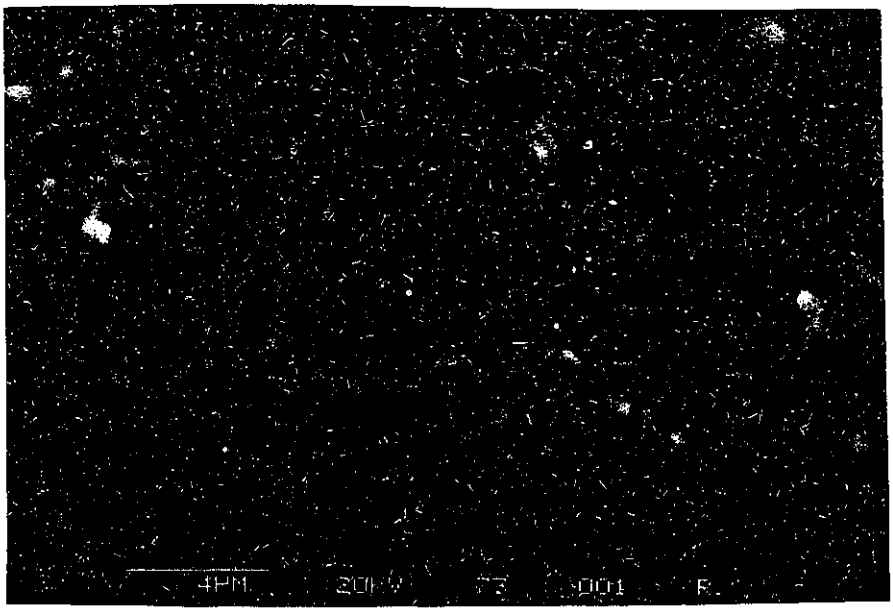

a) Cement+2% $NaNO_3$, w/c=0.35, 7 days, steel substrate

b) C_3S+2% $NaNO_3$, w/c=0.35, 2 days, paste off steel substrate

Figure 4.41

a) Cement, w/c=0.30, 7 days, paste off steel substrate

b) Cement+2% $Ca(C_3H_5O_2)_2.H_2O$, w/c=0.35, 1 day, paste off glass substrate

Figure 4.42

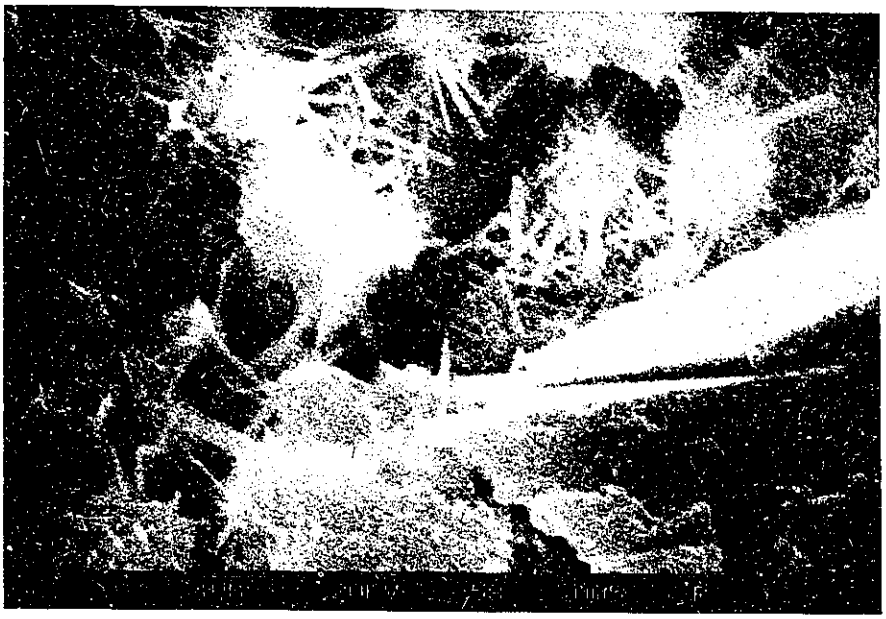

a) Cement+2% $NaNO_3$, w/c=0.35, 2 days, paste off steel substrate

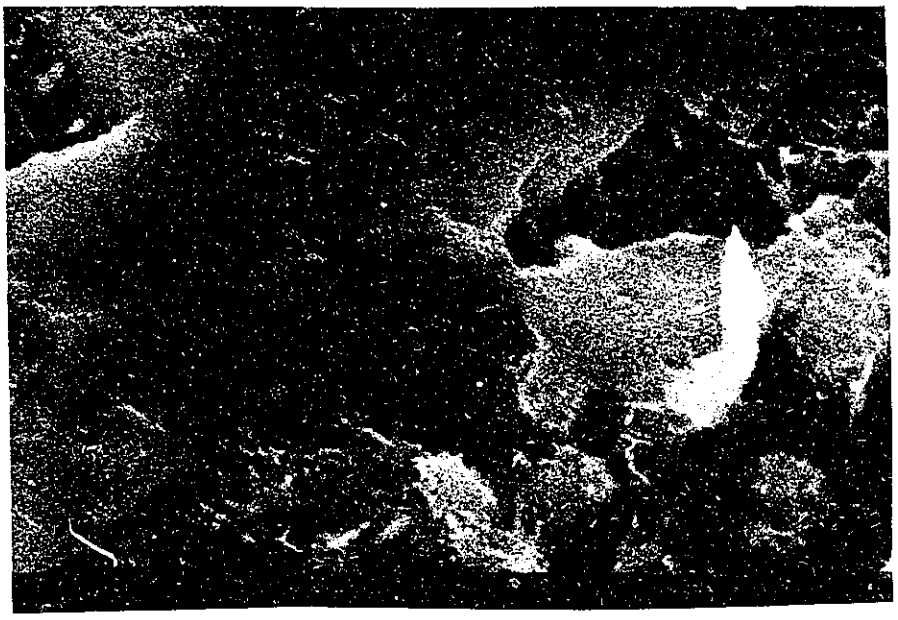

b) Cement, w/c=0.35, 7 days, paste off steel substrate

Figure 4.43

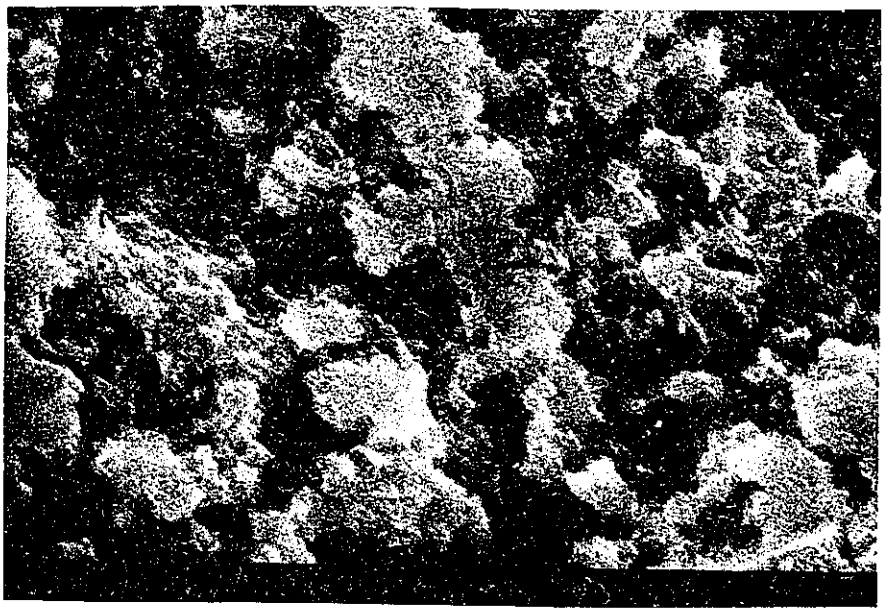

a) Cement+10% Silica Fume, w/c=0.30, 7 days, paste off steel substrate

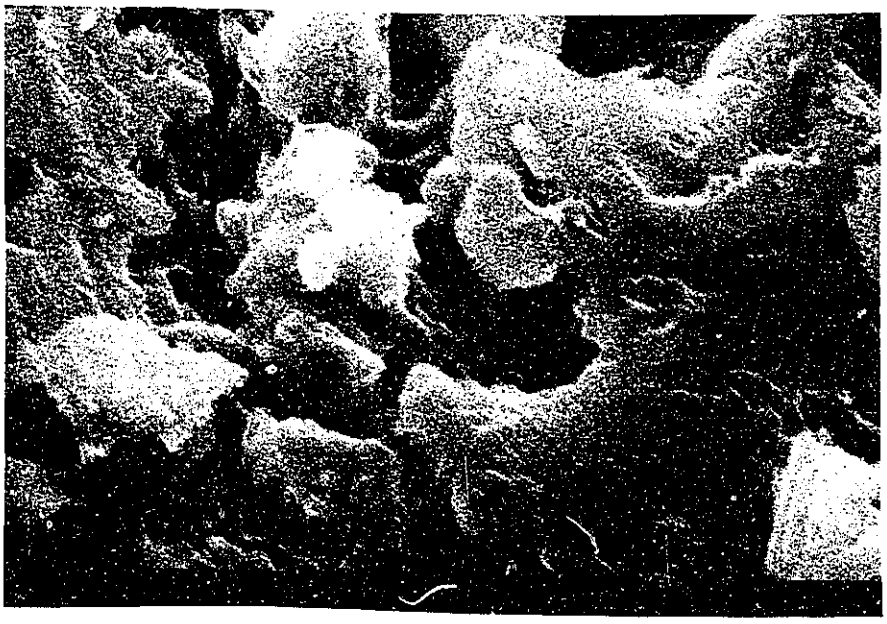

b) Clinker, w/c=0.35, 2 days, paste off steel substrate

Figure 4.44

a) Clinker, w/c=0.30, 1 day, paste off steel substrate

b) C_3S, w/c=0.35, 7 days, paste off steel substrate

Figure 4.45

C_3S, w/c=0.35, 7 days, paste off glass substrate

Figure 4.46

hydration time and the side of the fracture (paste side or substrate side) from which the photo was taken.

At hydration times less than one day, the surfaces of the substrates were generally fully covered with a thick layer or film containing large nodules of paste. At one and two days hydration time the fracture surface was much cleaner, although some one day samples still contained large nodules. At low magnifications (100X) patterns were formed on the glass by material left adhering after the bond failure. These patterns ranged from a distribution of rod-like clear areas on the substrate, to circular or even triangular clear patterns. At high magnifications (5000X) the failure surfaces at one and two days revealed cleaved surfaces and surfaces containing groups of particles less than 4 μm in size with much porosity present. At seven days in the cement and $NaNO_3$ paste systems ettringite needles could be seen in the high magnification micrographs.

Consideration of the bond fracture stress data with respect to the microstructural information presented on the micrographs indicates that the hydration times associated with the greatest bond fracture stress (within a system) are likely to produce a cleaved fracture when viewed at high magnification. The hydration times associated with lower bond stress values were found to correlate with fracture surfaces characterized by particles in the 4 μm range.

4.10 Comparison of Substrate Coverage to Paste Properties

The factors affecting the amount of coverage present on the substrate subsequent to failure are unknown. The possibility exists that amount of cover is dependent on a paste property and time. Substrate surface coverage is plotted against CH content of the paste in Figures 4.47 and 4.48. An increase in CH content is followed by a decrease in substrate surface coverage for both substrates. The relationship between surface coverage and CH is linear in a very narrow band between four and eleven percent CH for the glass substrate. Substrate surface coverage is plotted against non-evaporable water content in Figures 4.49 and 4.50. An increase in non-evaporable water results in a

Figure 4.47 Substrate Surface Coverage vs CH, steel substrate

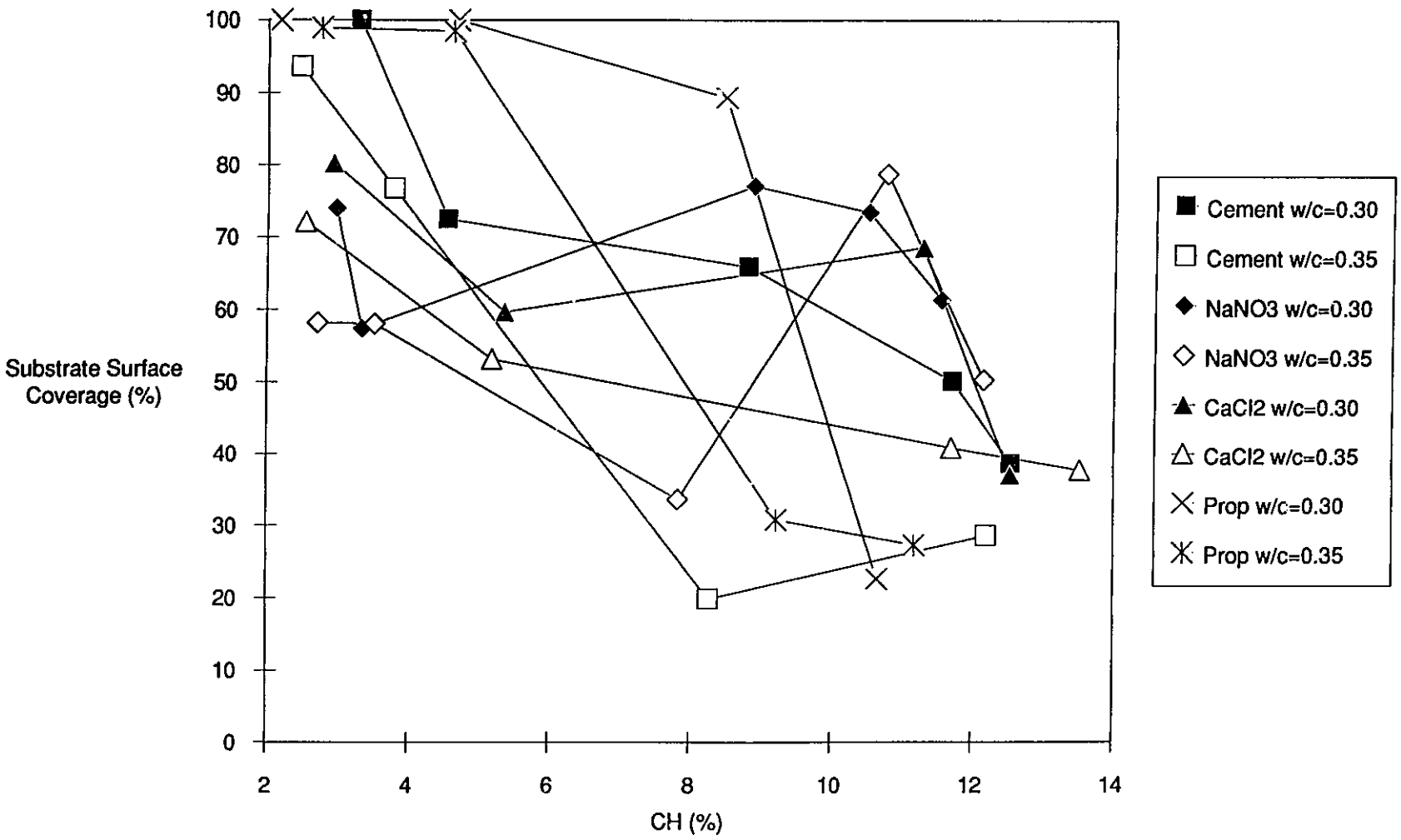

Figure 4.48 Substrate Surface Coverage vs CH, glass substrate

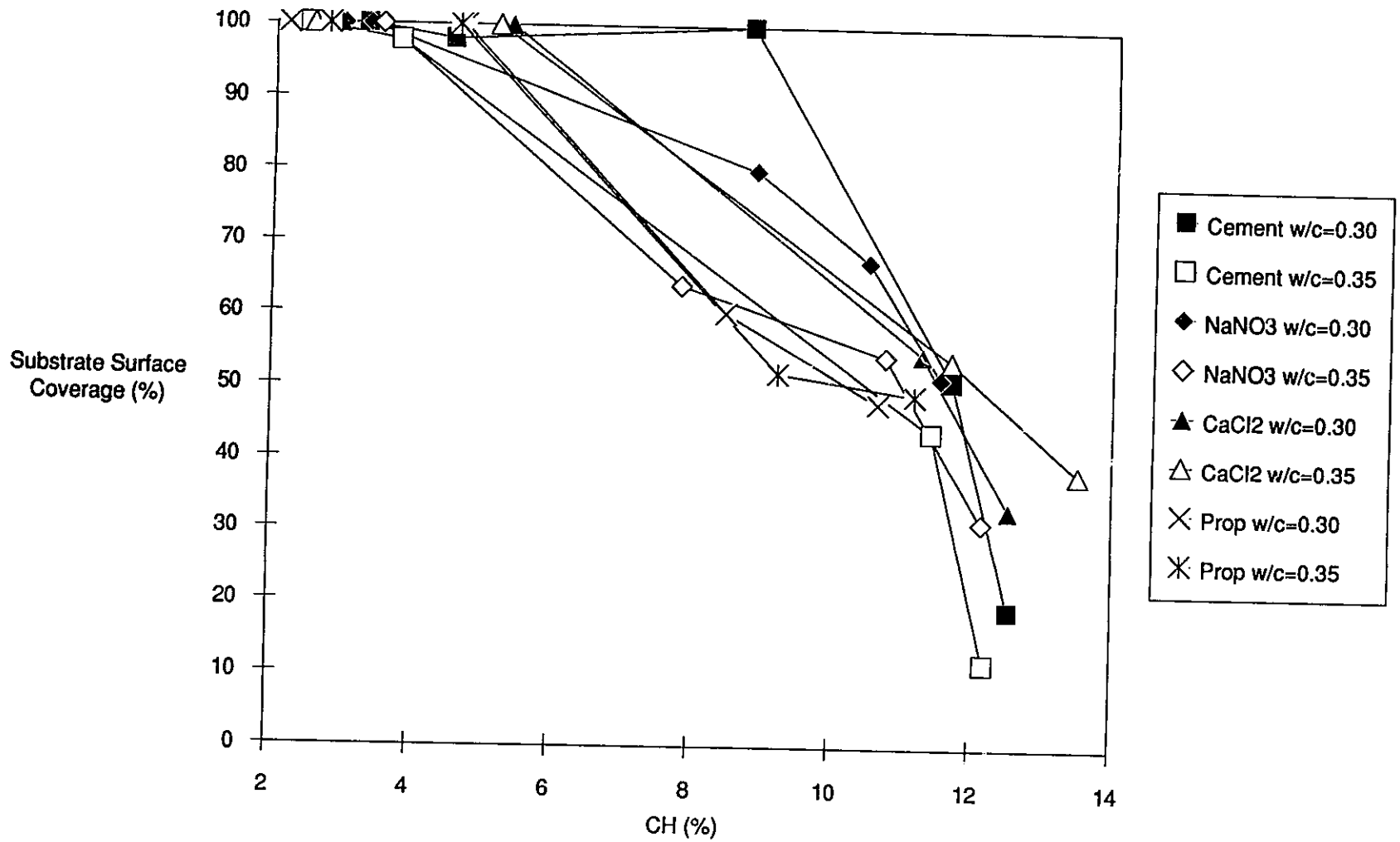

Figure 4.49 Substrate Surface Coverage vs Non-evaporable Water, steel substrate

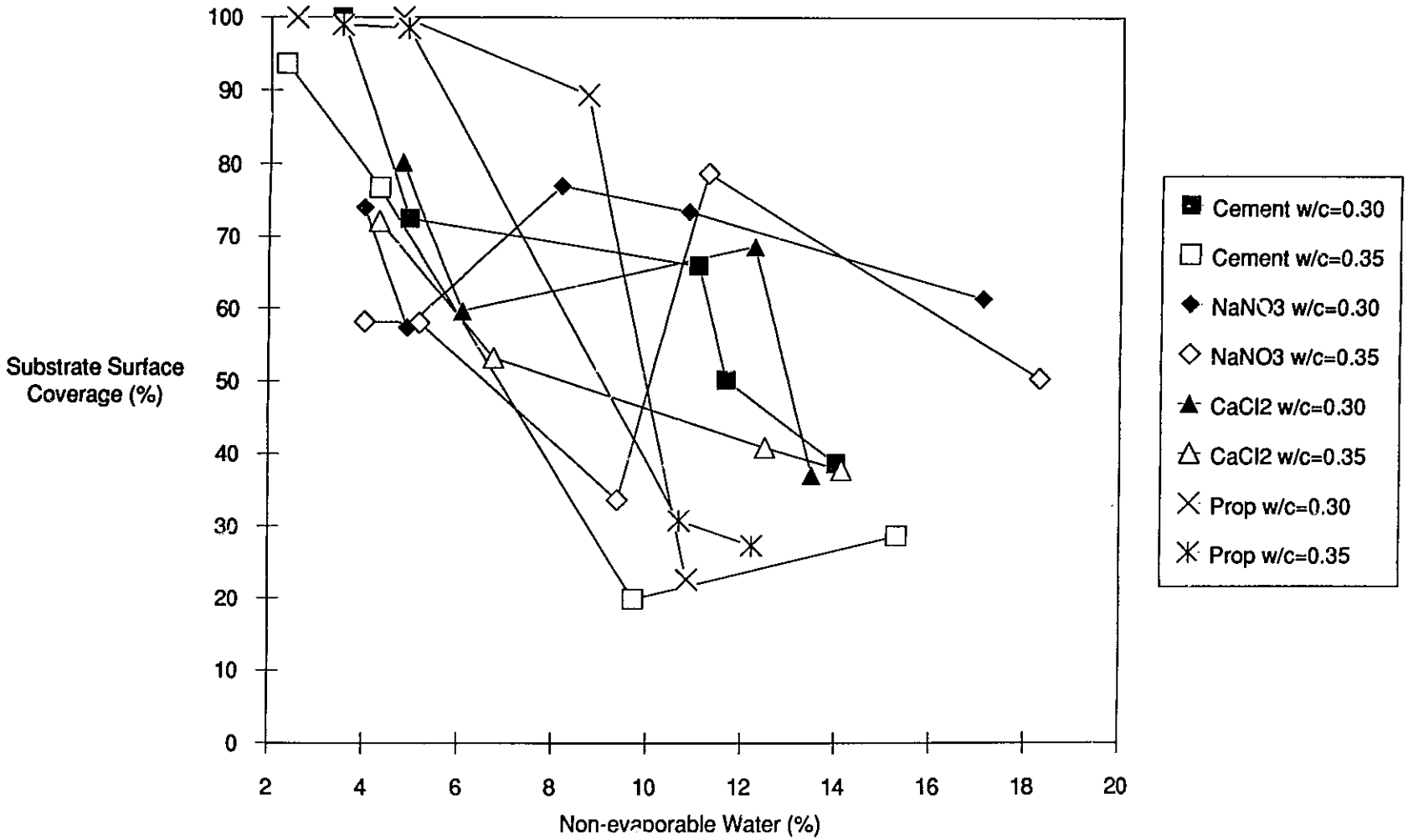

Figure 4.50 Substrate Surface Coverage vs Non-evaporable Water, glass substrate

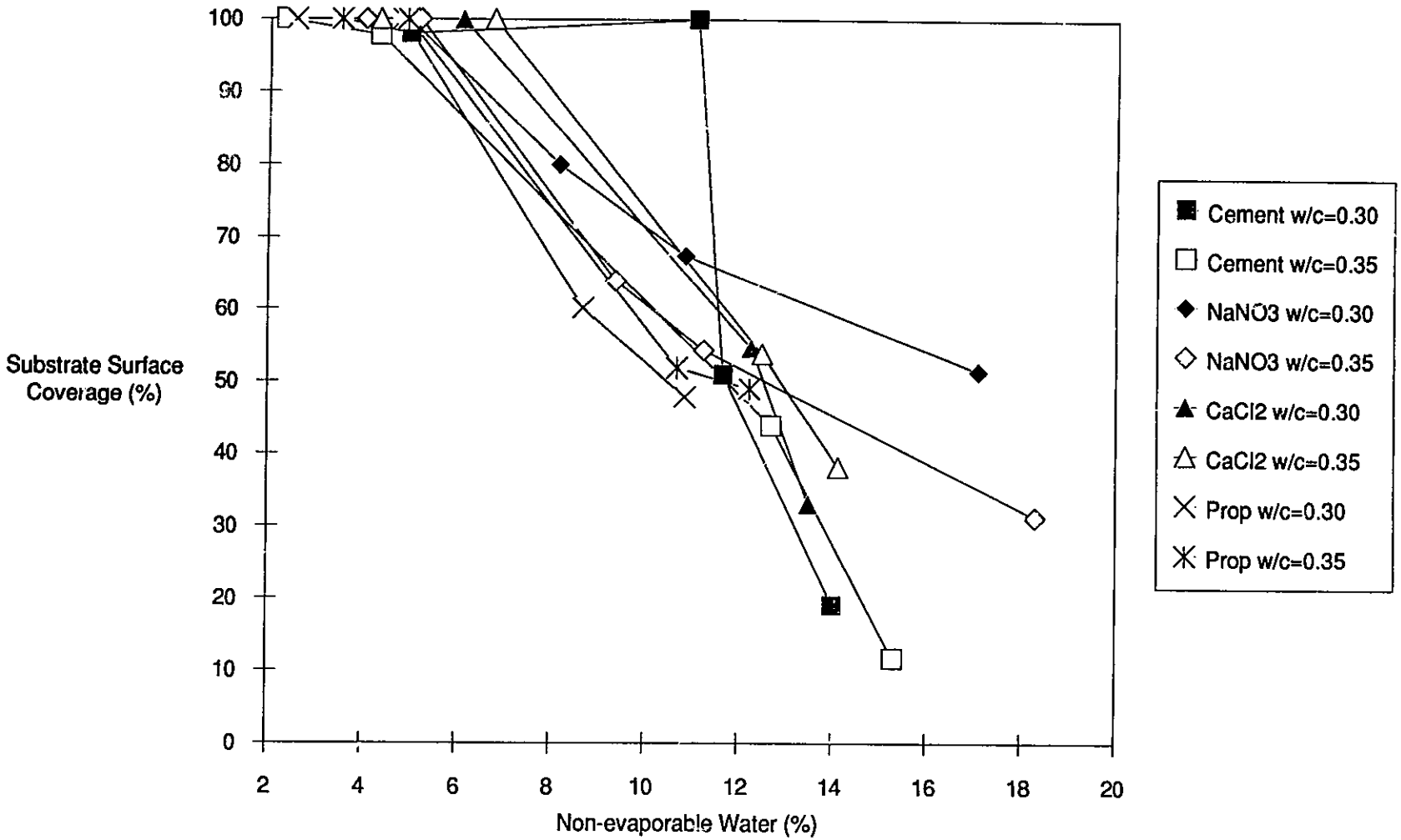

Figure 4.51 Substrate Surface Coverage vs Porosity, steel substrate

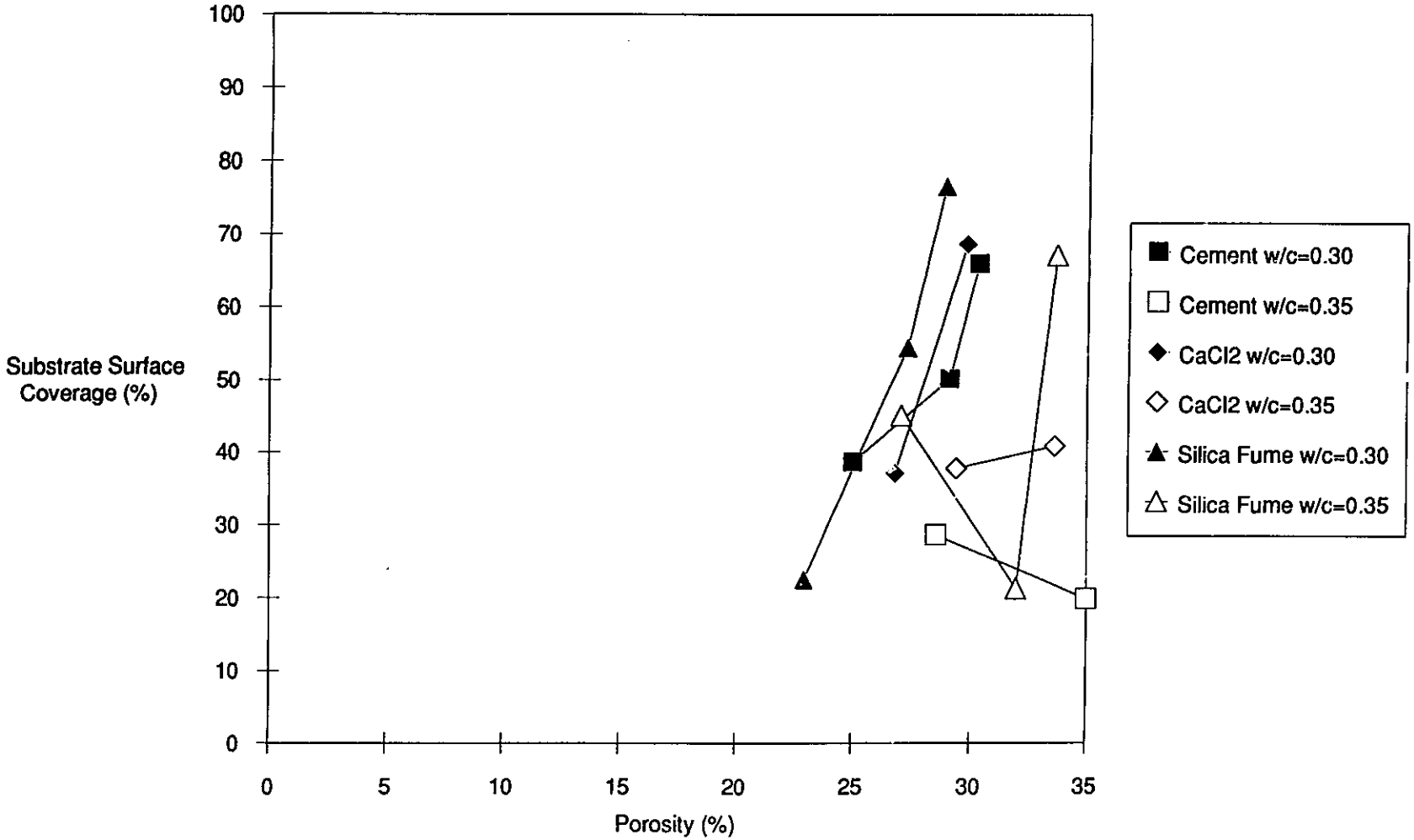

Figure 4.52 Substrate Surface Coverage vs Porosity, glass substrate

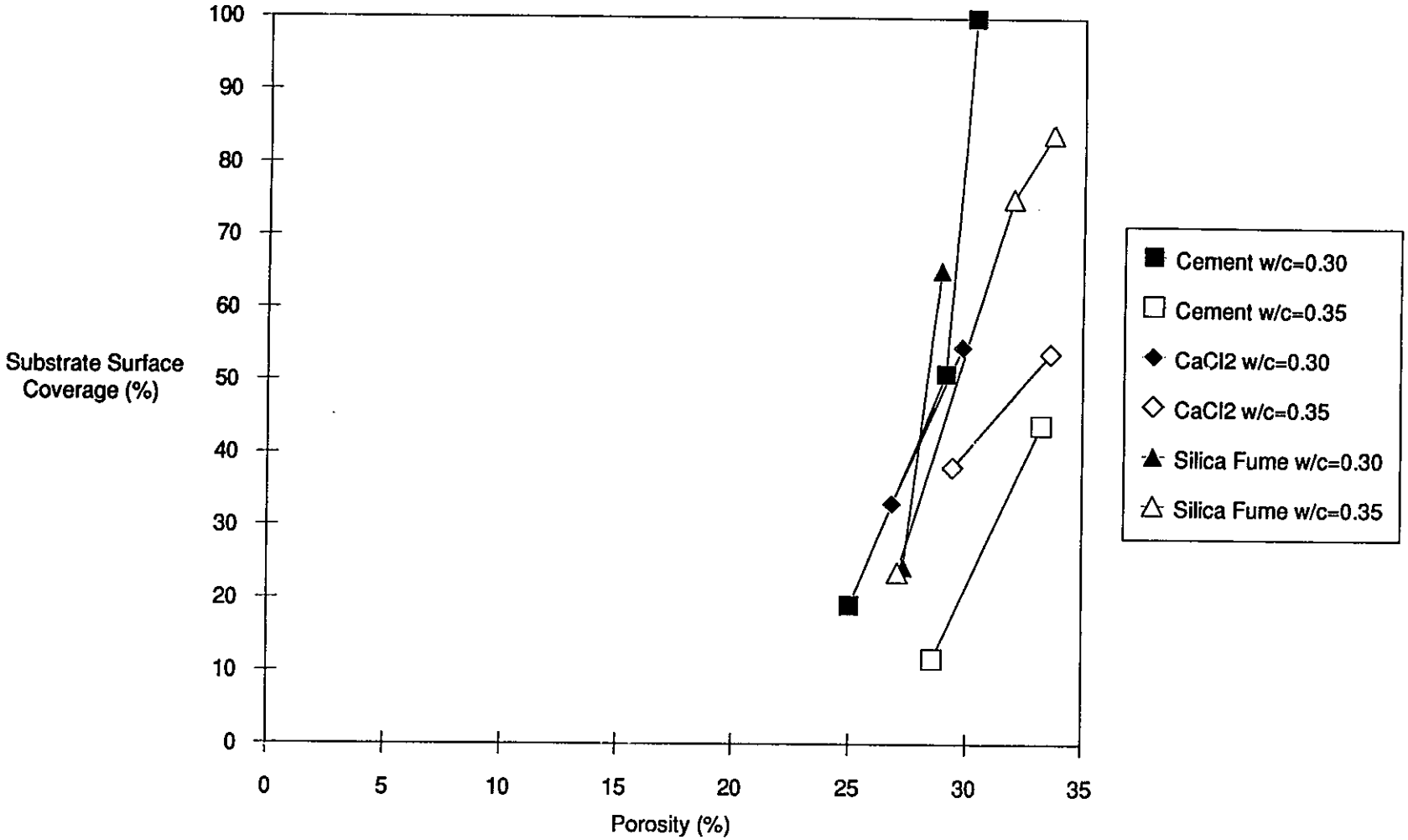

decrease in substrate cover and once again a linear band exists for the glass substrate, where, between four and twelve percent non-evaporable water a linear decrease in substrate coverage is observed. The relationship between substrate surface coverage and paste porosity is illustrated in Figures 4.51 and 4.52. The curves indicate an increase in porosity results in increased substrate coverage, although the silica fume w/c=0.35 and cement w/c=0.35 systems on the steel substrate show a reduction in coverage with an increase in porosity

4.11 Comparison of Interface Fracture Energy to Paste Properties

The relationship between porosity and compressive strength for cement pastes is well documented[1,41,42,43]. It was thought that a relationship might exist between the interface fracture energy and the porosity of the cement paste systems examined. Figures 4.53 and 4.54 are plots of the interface fracture energy vs. porosity values for the four systems for which porosity values are known. Porosity increases with interface fracture energy for the glass substrate. This relationship is unique for each system, although for all systems a point is reached where a small increase in porosity results in a large increase in the energy required for fracture. The plot for the steel substrate does not indicate a trend which is applicable to all systems. Three systems , however, show an increase in interface fracture energy resulting from a decrease in porosity.

Figures 4.55 and 4.56 are plots of the interface fracture energy vs. CH content of the paste for each substrate. Figures 4.57 and 4.58 are plots of the interface fracture energy vs. non-evaporable water of the pastes. Both of these sets of curves are similar in nature to the interface fracture energy vs. time plots, in which the fracture energy increases to a peak and then declines. For the 'CH' curves the fracture energy peak occurs between six and nine percent CH, depending on the system. The non-evaporable water plots show the maximum fracture energy is achieved with a non-evaporable water content between eight and eleven percent, depending on the system.

Figure 4.53 Interface Fracture Energy vs Porosity, steel substrate

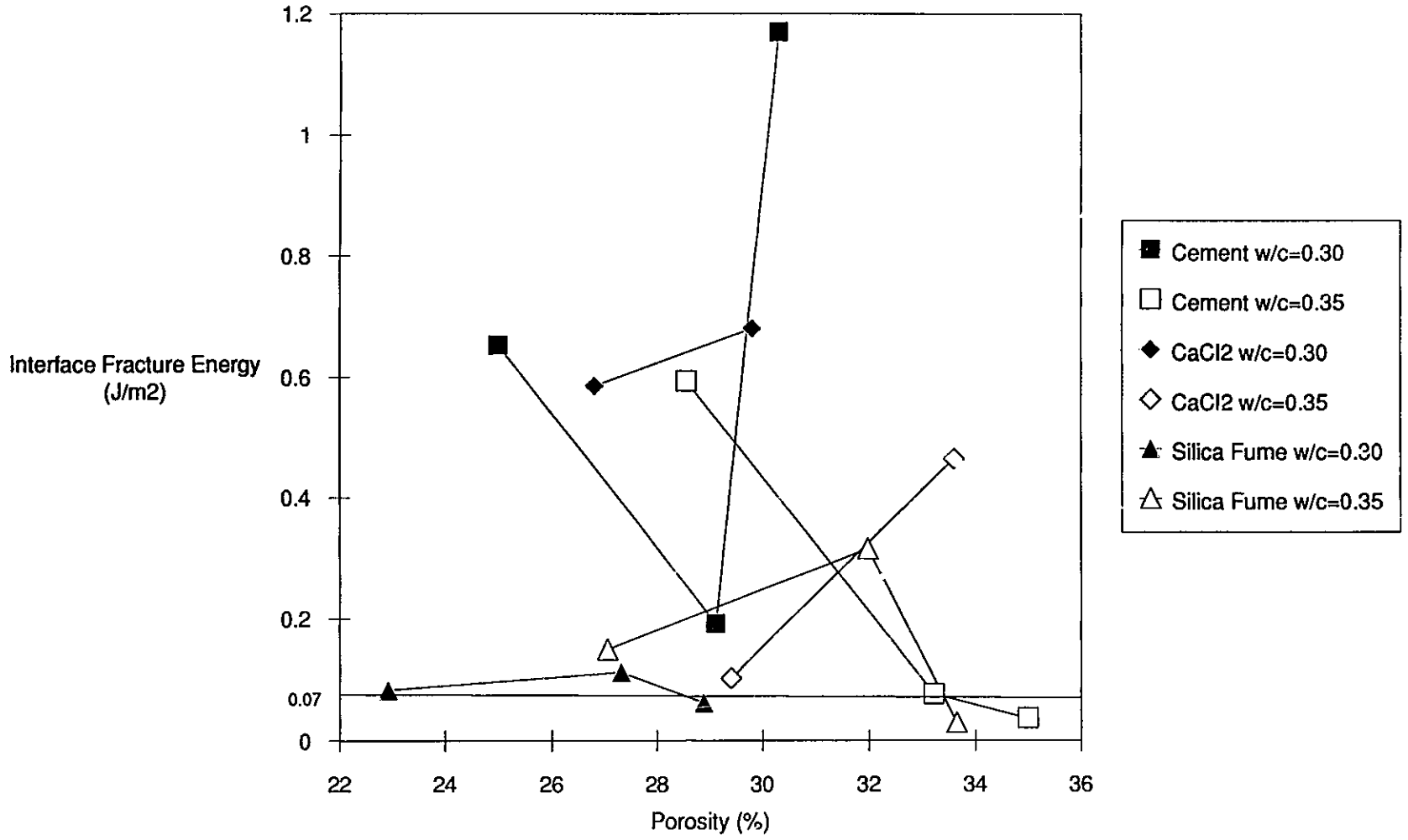

Hydration proceeds from R to L. 1st pt.: 1 day; 2nd pt.: 2 days; 3rd pt.(if plotted): 7 days.

Figure 4.54 Interface Fracture Energy vs Porosity, glass substrate

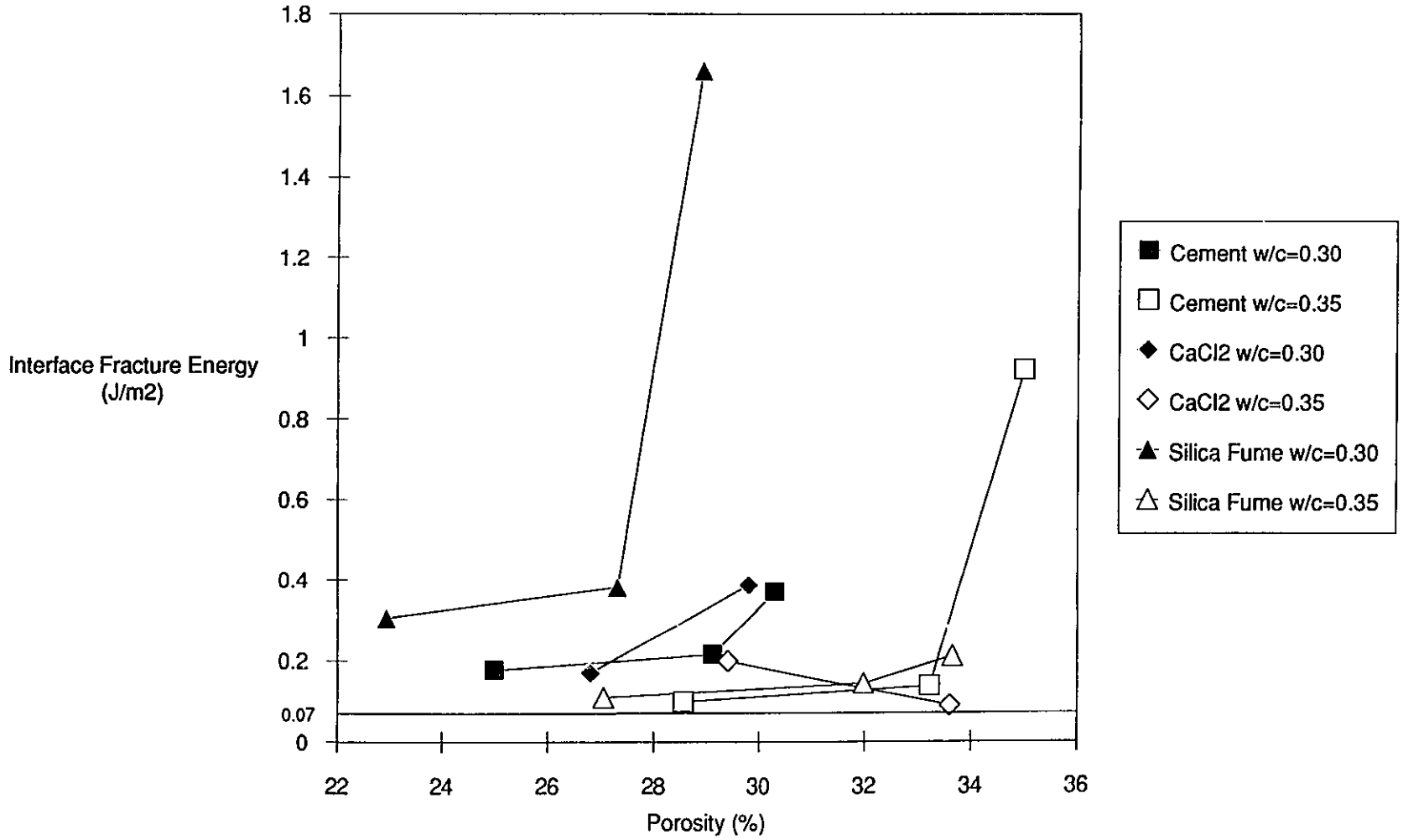

Hydration proceeds from R to L. 1st pt.: 1 day; 2nd pt.: 2 days; 3rd pt.(if plotted): 7 days.

Figure 4.55 Interface Fracture Energy vs. CH, steel substrate

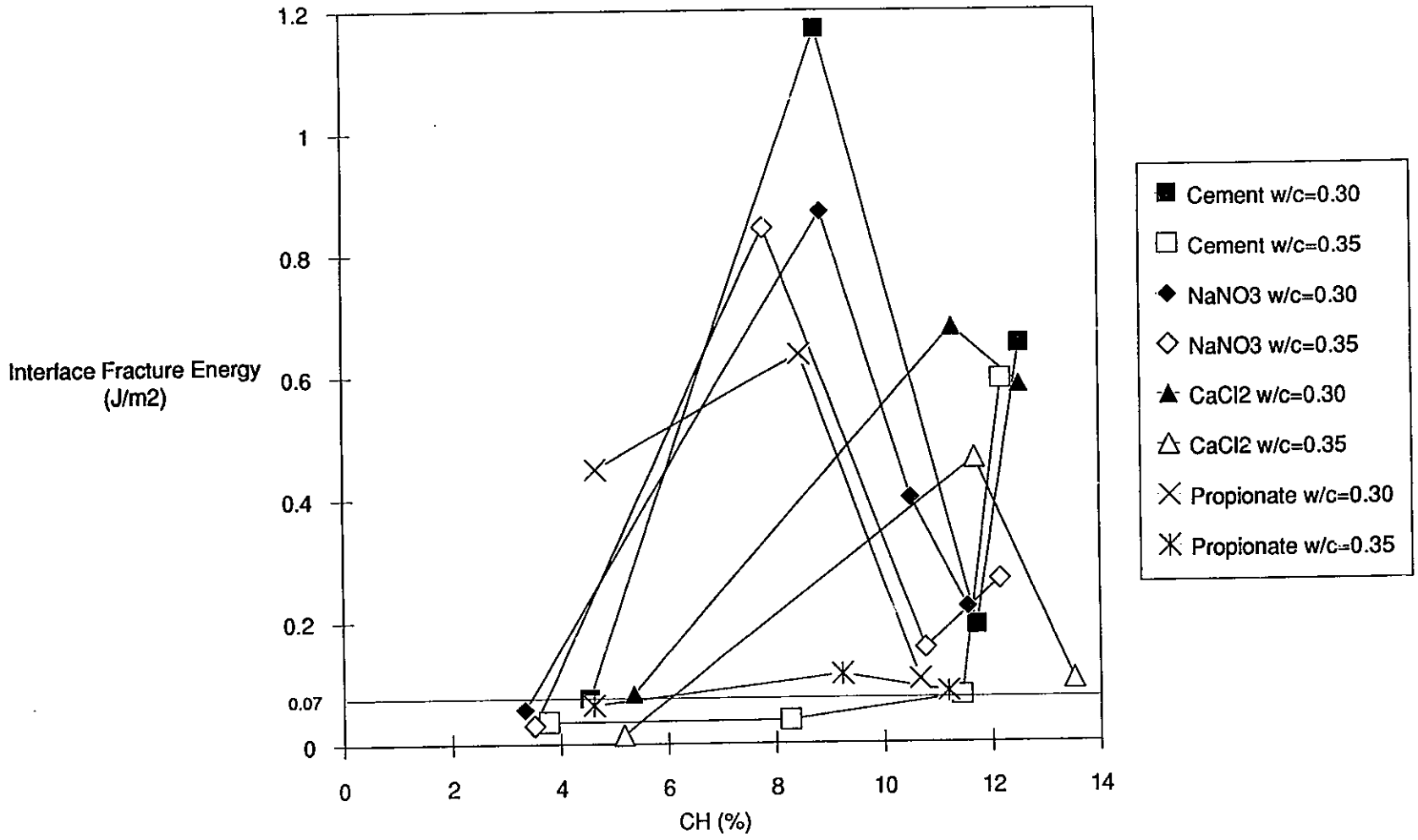

Hydration proceeds from L to R. 1st pt.: time at peak of second heat of hydration curve; 2nd pt.: 1 day; 3rd pt.: 2 days; 4th pt.(if plotted):7 days.

Figure 4.56 Interface Fracture Energy vs. CH, glass substrate

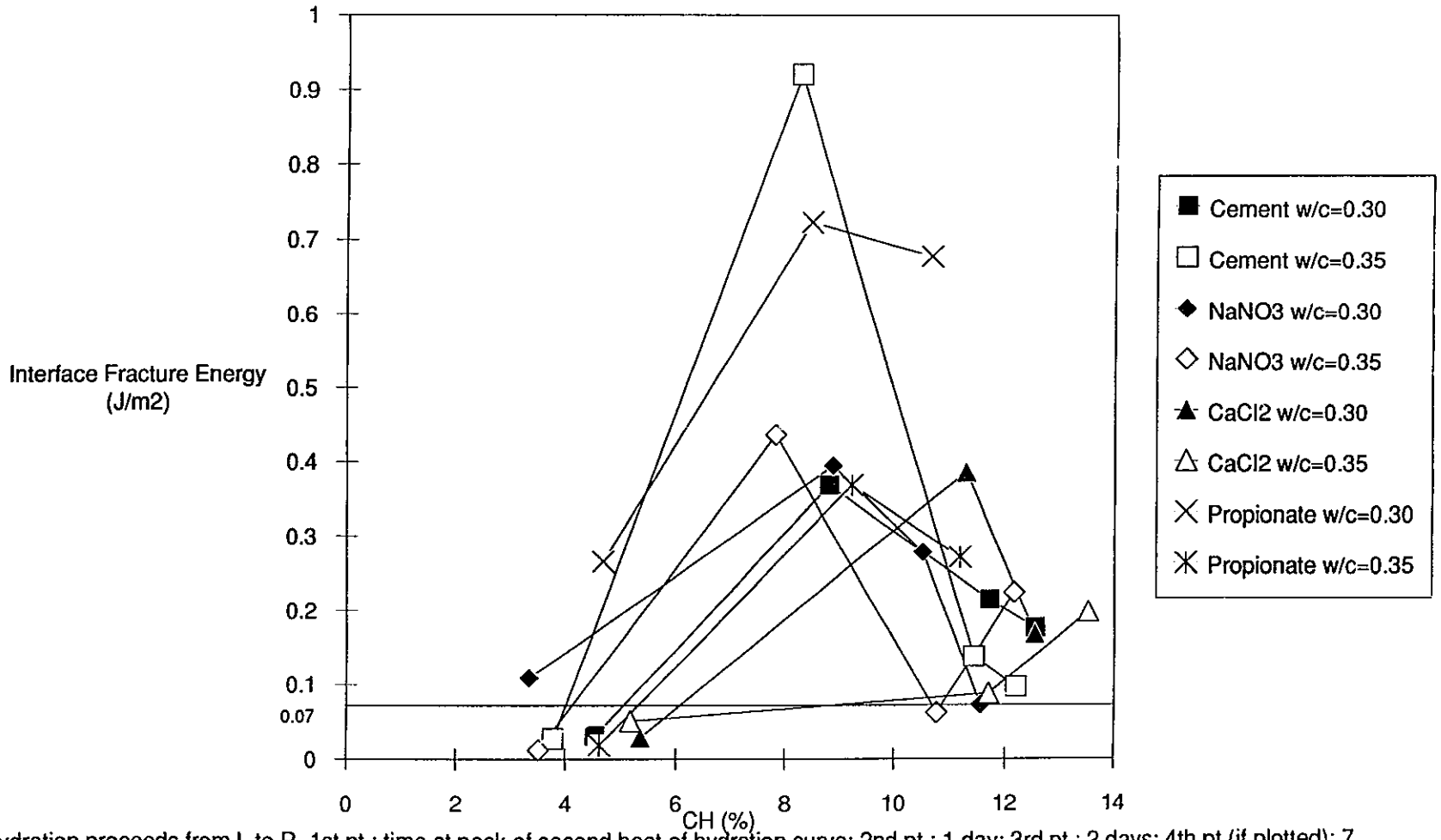

Hydration proceeds from L to R. 1st pt.: time at peak of second heat of hydration curve; 2nd pt.: 1 day; 3rd pt.: 2 days; 4th pt.(if plotted): 7 days.

Figure 4.57 Interface Fracture Energy vs. Non-evaporable water, steel substrate

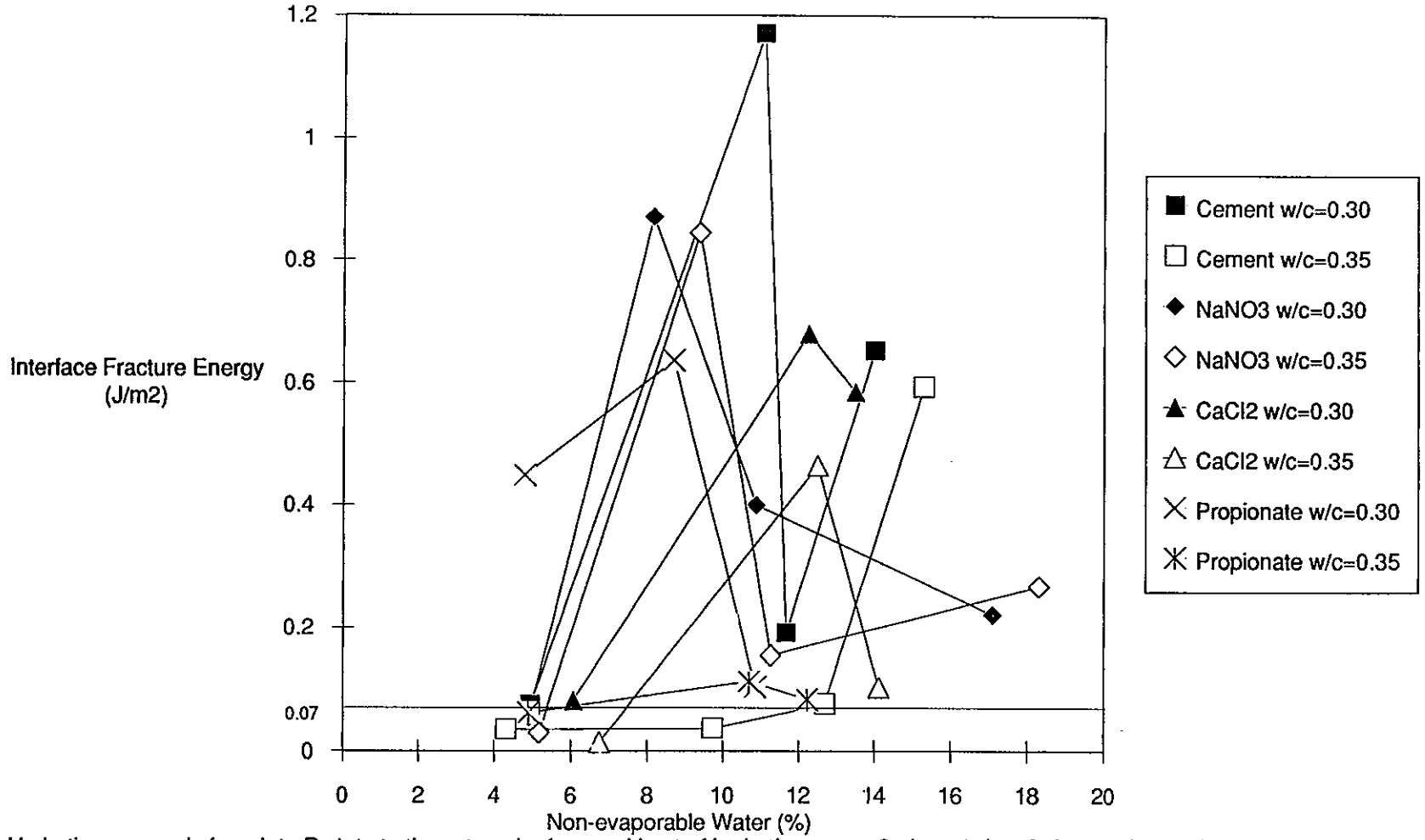

Hydration proceeds from L to R. 1st pt.: time at peak of second heat of hydration curve; 2nd pt.: 1 day; 3rd pt.: 2 days; 4th pt.(if plotted): 7 days.

Figure 4.58 Interface Fracture Energy vs. Non-evaporable water, glass substrate

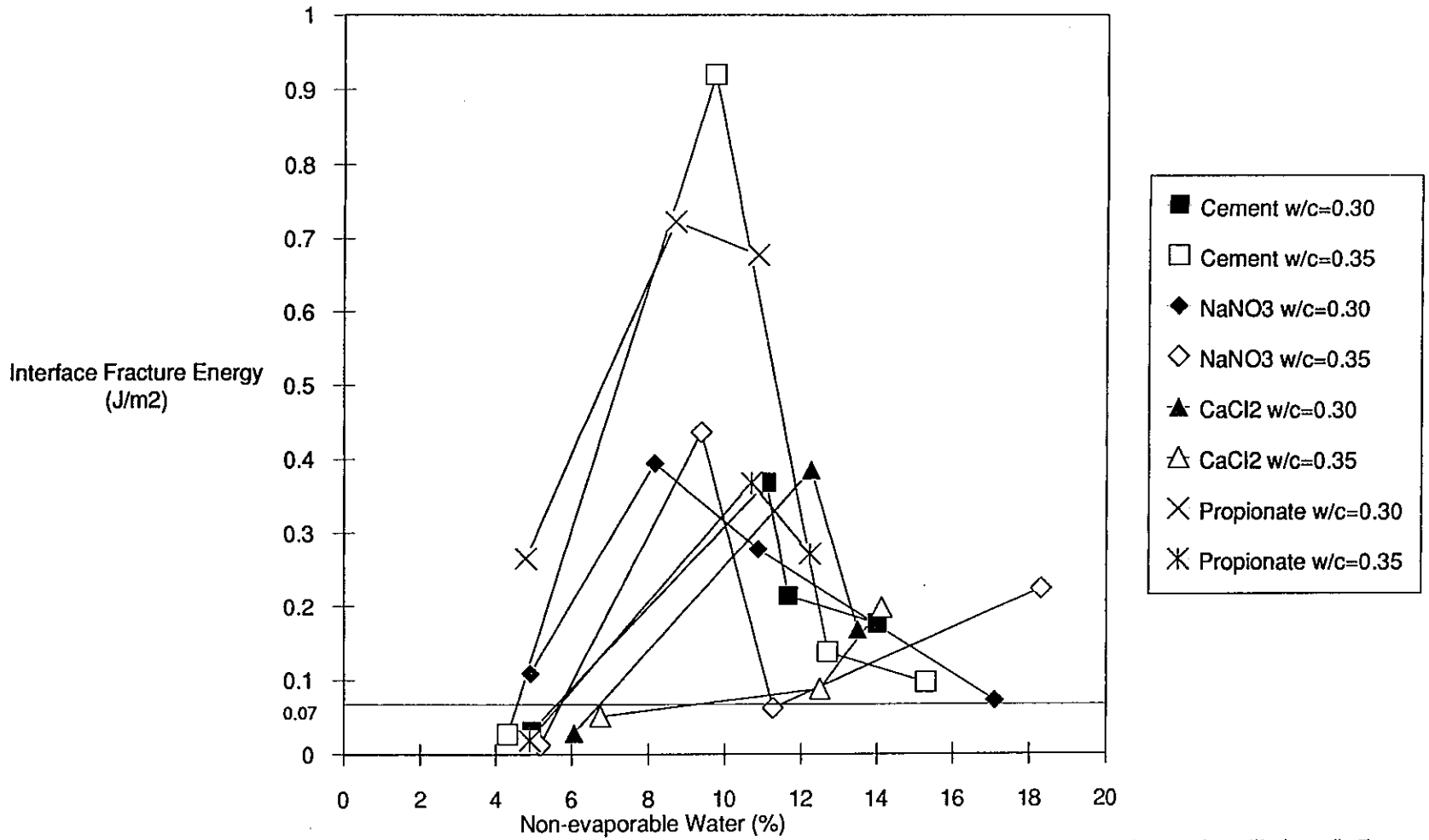

Hydration proceeds from L to R. 1st pt.: time at peak of second heat of hydration curve; 2nd pt.: 1 day; 3rd pt.: 2 days; 4th pt.(if plotted): 7 days.

CHAPTER 5

DISCUSSION OF RESULTS

5.1 Interface Bond Stress

The interface bond stress calculation is used in conventional testing. There is therefore some merit in directly comparing some test results plotted as bond failure stress/paste thickness curves prior to discussion of interface fracture energy.

All the paste systems tested exhibited a thickness dependence of the interface bond failure stress. A decrease in paste adhesive thickness generally resulted in an increase in bond stress.

Equation (1) expressing bond failure stress as a function of bulk modulus, interface fracture energy and cement paste adhesive thickness effectively describes the experimental data. The principal conclusion is that applied stress at failure is not "a priori" descriptor of the quality of the adhesive bond in cement composite systems. The implication that factors other than contact area are important in determining bond strength at first seems surprising. If the failure process is viewed as progressive it is appropriate to treat it using an energy approach - the major argument of this thesis. Surface energy then is proposed as the superior descriptor and "material" property for describing the nature of the cement paste - substrate bond.

Some paste systems showed a more dramatic increase in bond stress with a decrease in paste sample thickness while others exhibited a very gradual bond stress gain with decreasing thickness. The difference in the shape of the curves could simply be due to the number of data points in the low thickness region that were used in the regression calculation. The relatively flat curves may be a result of very few data points being available at the low thickness values (less than 0.5 mm). It is possible that a larger population of data points at lower thickness values would have resulted in steeper curves as the paste thickness decreased in this range.

The level of significance data for the individual curves indicates that generally the regression curves provide a very good description of the raw data. About 85% of the regression curves meet the 1 % level of significance when comparing the calculated correlation coefficients to tabulated values. The curves which did not meet either the 1 % or 5 % level of significance had fewer data points to calculate the regression curve from, although the few points which were available still showed that the bond strength exhibited a strong thickness dependence.

Many systems produced one day strengths that were greater than the two day and in some cases even the seven day strengths. The reason for this will be discussed in the discussion of interface fracture energy.

Bond strengths for the salt systems, particularly the systems with $NaNO_3$ and $CaCl_2$ additions were greater than the control paste for the steel substrate at a majority of the hydration times. The plain cement systems were generally stronger on the glass substrate. A global assessment of the data generally indicates that the salt additions to the cement did not significantly increase the bond strength of the paste.

The clinker paste was found to have very similar bond strength values to the control on both substrates, suggesting that the addition of gypsum to cement does not contribute significantly, to the development of bond strength. The paste with silica fume additions performed much as the cement clinker did, in that bond strength was neither consistently stronger nor weaker than the control. It was anticipated that the silica fume paste would show an increase in strength over the control. This may indeed be the case at ages greater than 7 days as densification of the interfacial zone may require additional time.

A comparison of the plain cement paste systems to the C_3S systems shows that the cement paste systems always produced greater bond strengths than the C_3S pastes. This would imply that factors other than the deposition of CH and C-S-H at the interface can affect bond strength. The sulphoaluminate phases formed in the presence of gypsum

do not appear to be a significant factor (clinker paste results). This would suggest that physical factors eg. morphology, crystal size and pore structure of the interface materials may be more favorable for bond strength development in cement systems than in C_3S systems.

5.2 Interface Fracture Energy

The graphs of interface fracture energy vs. CH and non-evaporable water content both indicate that the maximum interface fracture energy is achieved within a range of values for both quantities. Plots of interface fracture energy vs. time indicate that the interface fracture energy reaches its maximum after one day of hydration, decreases to two days and then remains relatively constant. It is argued that a loss of bond strength following strength gain could be due to pressure generated by CH crystal growth. Visual evidence for CH crystal growth in cement systems has been reported[40]. The same interface fracture energy pattern is found in the silica fume systems. Reaction of the silica fume consumes CH, but does not eliminate its presence from the transition zone. The silica fume may not react quickly enough to prevent CH crystal pressure from resulting in an interface fracture energy decrease.

It is apparent that the complex factors affecting the development of interface fracture energy (γ) are time and system dependent. It is generally true that an increase in water-cement ratio weakens the interface resulting in lower values of γ. This is not unexpected as porosity generally weakens a material. There are however anomalies. Examples include silica fume (steel, 2 days), cement paste (glass, 1 day), and $NaNO_3$ paste (glass, 1 day, 7 days) where values of γ are greater for the higher w/c ratio systems. The values of γ, 0.315, 0.920, 0.436 and 0.224 Jm^{-2} are all in excess of 0.07 Jm^{-2}, a value indicative of van der Waal's type bonding. It is inferred that the possibility of chemical bonding processes making a contribution to these higher values exists. This argument is somewhat tenuous as chemical bonds are generally associated with values of

γ approaching 5 Jm^{-2}. Glass , a silicate system, is a more likely substrate candidate for possible chemical interaction.

It is difficult to assess the transient affect of CH crystal size on bond strength. The highest values of γ was obtained with silica fume (glass, 1.66 Jm^{-2}) which refines CH crystal structure. This result is consistent with a strategy to refine the CH structure in the transition zone. This maximum effect is lost, however, at 2 and 7 days. At several hydration times salt addition decreases the value of γ in concert with the hypothesis that initially larger crystals of CH weaken the interface. The reverse, however, is also true suggesting that the role of CH crystal size is secondary. The size and nature of the flaws at CH interfaces or boundaries may govern progressive failure. It is possible then that crack growth at the interface is also dependent on the extent to which the transition zone matrix is composed of minor amounts of C-S-H and sulphoaluminate phases provided the latter alter the nature of crystal boundaries or crack tips. These postulates are also useful to explain anomalies in the γ versus porosity results. Results with the steel substrate generally follow expectations ie. γ decreases with porosity. The high result with cement paste (w/c=0.30) and $CaCl_2$ paste (w/c=0.30,0.35) may be a result of flaw geometry modification at specific hydration times. Results with the glass substrate are generally anomalous ie. increases in γ are observed with porosity. Large increases for cement paste (w/c=0.35) and silica fume paste (w/c=0.30) at high porosities further suggests the possibility that chemical interaction can modify factors affecting crack initiation. It is concluded that although more research is needed to significantly affect practice, the fracture energy concept has merit. Chemical modification of interfaces to improve bond strength needs further exploration. Controlling CH crystal size at the interface is probably of secondary importance.

It is recognized that surface roughness would have the effect of increasing the value of γ. This is not directly accounted for in the calculations. The γ term therefore includes this effect. Surface roughness measurements were made on both the steel and

glass substrates. The glass was essentially "smooth" with asperity heights of <0.01 μm. The steel surface had asperity heights <0.1 μm. It is argued that the effects of surface roughness in these experiments is likely minimal. In general terms the values of γ for glass were not significantly lower than those for steel given the 10 fold difference in surface roughness. The glass surface, essentially smooth, can be considered a zero roughness surface. Both glass and steel substrates in these experiments are smooth relative to aggregate surfaces.

5.3 SEM Micrographs

The analysis of the SEM micrographs at low magnifications (100X) provides a qualitative estimate of the rate of strength development at the interface, in the transition zone matrix. At hydration times of less than one day a large amount of material is left on the substrate after failure for most systems. This suggests the transition zone is weaker than both the paste matrix and the bond to the substrate. At later ages as the paste strength increases decreasing amounts of material are left on the substrate after bond failure indicating that the interfacial zone is increasing in strength relative to the bond with the substrate. The curves expressing substrate coverage versus CH, non-evaporable water and porosity are similar in character. There is an initial period of little change followed by a linear change. This initial period is much greater for the glass substrate in the case of both CH and non-evaporable water. Surface coverage generally increases with porosity indicating that strength of the transition zone is dependent on this parameter.

Examination of the high magnification micrographs (5000X) indicated that in the systems in which the one day bond strength was higher than the two day or even the seven day strength the fracture surface at one day was usually a very clean or cleaved. All the fracture energy was expended in breaking a true adhesive bond. The strength of the transition zone exceeded this value. This coincides with the formation of a continuous layer of hydration products as opposed to a group of small particles containing significant

porosity. It is concluded that the backscattered electron image analysis can be a useful tool for studying interfaces in cement systems.

CHAPTER 6

CONCLUSIONS AND RECOMMENDATIONS

This study focused on the elucidation of the nature of bond strength development of cement pastes. The effect of various additives on cement paste bond to steel and glass substrates was determined. A uniaxial bond test was applied to establish the relationship between bond strength and cement paste adhesive thickness. A new term, the interface fracture energy, γ, is derived and calculated for the cement paste systems at hydration times of up to seven days. Three salts, $NaNO_3$, $CaCl_2$ and $Ca(C_3H_5O_2)_2.H_2O$ as well as silica fume were added to the cement paste to engineer the properties of the interface through alteration of the size and amount of CH in the interfacial zone. C_3S and clinker pastes were also tested to determine the effect of eliminating some of the mineral phases present in cement.

6.1 Conclusions

A number of conclusions pertaining to the nature of the cement paste-substrate adhesive bond and bond strength can be derived from this investigation. The interfacial bond failure stress for all the paste systems was thickness dependent. A decrease in paste adhesive thickness generally resulted in an increase in bond stress. Bond failure stress is not the best descriptor of the quality of the cement paste-substrate bond. A new term, the interface fracture energy (equation 1) is more appropriate due to the progressive failure of the bond. Analysis based on an energy approach is suggested as most appropriate.

Factors other than the deposition of CH and C-S-H at the interface can affect bond strength. This is inferred from the results of experiments with clinker pastes, C_3S pastes and pastes with salt additions. The bond strength of the clinker paste showed little difference when compared to the controls suggesting that products resulting from gypsum reactions eg. the sulphoaluminate phases, may have little affect bond strength. The addition of the salts did not consistently increase the bond strength of the paste. The plain cement systems consistently had greater bond strengths than the C_3S pastes.

Interface fracture energy, γ, reaches its maximum value after one day of hydration, decreases at two days then remains relatively constant. The loss of bond strength may be due to pressure generated by the formation of CH crystals. In general interface fracture energy increases with a decrease in water-cement ratio, although it is apparent that other time and system dependent factors affect its energy development. There was no significant difference in the values of γ for the two substrates even though the steel substrate was ten times rougher than the glass substrate. Values of γ for all the systems studied range from 0.001 to 1.66 Jm^{-2} suggesting that van der Waal's forces of attraction are the primary binding forces.

Backscattered electron image analysis can be a useful tool for examining cement system interfaces. Image analysis showed that at less than one day large amounts of material were left on the substrate after failure suggesting that the transition zone is weaker than both the paste matrix and the paste-substrate bond. At later ages the interfacial zone increases in strength relative to the paste-substrate bond since decreasing amounts of material are left on the substrate. The one day fracture surface , viewed at high magnification (5000X), appeared clean or cleaved for the pastes which had their highest bond strength at one day.

6.2 Recommendations

Interface fracture energy is a more meaningful descriptor of cement paste bond strength than bond stress determined by conventional tests. More research however is needed to significantly affect practice and adoption of an energy approach for bond stress determination. Engineering cement paste bond strength through chemical modification of the interfacial zone needs further exploration. Other chemicals or techniques such as thermal shocking to decrease the size of the CH crystals may be appropriate.

REFERENCES

1. Neville, A.M., "Properties of Concrete", 3rd edition, Pitman, 1981, pp. 1-63.

2. "Design and Control of Concrete Mixes", Metric Edition, Canadian Portland Cement Association, 1981, pp. 7-23.

3. Kendall, K., "The Adhesion and Surface Energy of Elastic Solids", J. Phys. D:Appl. Phys., Vol. 4, 1971, pp. 1186-1195.

4. Schnittgrund, G.D., "Bond Strength Between Cement Hydrates and Steel", Ph.D. Thesis, University of Illinois at Urbana-Champaign, 1975.

5. Kendall, K., "Sticky Solids", Contemporary Physics, Vol. 21, No.3, 1980, pp. 277-297.

6. Griffith, A.A., Phil. Trans., No. 221A, 1920, pp. 163-198.

7. Meissner, H.P., and Merrill, E.W., ASTM Bulletin No. 151, 1948, pp. 80-83.

8. Kendall, K., (Personal correspondence, 1990).

9. Kung, J.H., "Drying Shrinkage and Microstructure of Hydrated Calcium Silicates", Ph.D. Thesis, University of Illinois at Urbana-Champaign, 1978, pp. 65.

10. Ramachandran, V.S., "Concrete Admixtures Handbook", Noyes Publications, Park Ridge, NJ, 1984, pp.63.

11. Kuhlmann, L.A., Correspondence to members of ASTM T.G. on Polymer Modified Concrete, October 18, 1988.

12. Chana, P.S., " A Test Method to Establish Realistic Bond Stresses", Magazine of Concrete Research, Vol. 42, No. 151, 1990, pp. 83-90.

13. Nakayama, M.and Beaudoin, J.J., "A Novel Technique for Determining Bond Strength Development between Cement Paste and Steel", Cement and Concrete Research, Vol. 17, No. 3, 1987, pp. 478-488.

14. Nakayama, M.and Beaudoin, J.J., "Bond Strength Development Between Latex-Modified Cement Paste and Steel", Prepared for submission to Cement and Concrete Research, December 1986.

15. Sasse, H.R. and Fiebrich, M., "Bonding of Polymer Materials to Concrete", Materials and Structures, Research and Testing, RILEM, Vol. 16, No. 94, July/August 1983, pp. 293-301.

16. Maso, J., "The Bond Between Aggregates and Hydrated Cement Paste", Proceedings 7th International Congress on Chemistry of Cement, 1980, Vol. 1, pp. VII 3-10.

17. Bentur, A., Diamond, S. and Mindess, S., "The Microstructure of the Steel Fibre-cement Interface", Journal of Materials Science, Vol 20, 1985, pp. 3610-3620.

18. Diamond, S., "The Microstructures of Cement Paste in Concrete", 8th International Congress on the Chemistry of Cement, Communications, Vol. I, pp. 122-147.

19. Scrivener, K.L., Crumbie, A.K. and Pratt, P.L., "A Study of the Interfacial Region Between Cement Paste and Aggregate in Concrete", Bonding in Cementitious Composites, Mindess, S. and Shah, S.P., editors, Materials Research Society Symposium Proceedings, Vol. 114, 1987, pp. 87-95.

20. Monteiro, P.J.M. and Mehta, P.K., "Improvement of the Aggregate-Cement Paste Transition Zone by Grain Refinement of Hydration Products", 8th International Congress on the Chemistry of Cement, Communications, THEME 2, Vol. III,pp 433-437.

21. Page, C.L., "Microstructural Features of the Interfaces in Fibre Cement Composites", Composites, April, 1982, pp. 140-144.

22. Bentur, A. and Cohen, M.D., "Effect of Condensed Silica Fume on the Microstructure of the Interfacial Zone in Portland Cement Mortars", Journal of the American Ceramics Society, Vol. 70, No. 10, 1987, pp. 738-743.

23. Mehta, P.K. and Monteiro, P.J.M., "Effect of Aggregate , Cement, and Mineral Admixtures on the Microstructure of the Transition Zone", Bonding in Cementitious Composites, Mindess, S. and Shah, S.P., editors, Materials Research Society Symposium Proceedings, Vol. 114, 1987, pp.65-75.

24. Detweiler, R.J., Monteiro, P.J.M., Wenk, H-R and Zhong, Z., "Texture of Calcium Hydroxide Near the Cement Paste-Aggregate Interface", Cement and Concrete Research, Vol. 18, 1988, pp. 823-829.

25. Alexander, K.M., Wardlaw, J. and Gilbert, D.J., "Aggregate Cement Bond, Cement Paste Strength, and the Strength of Concrete", Proceedings International Conference on the Structure of Concrete, Cement and Concrete Association, London, 1968, pp. 59-81.

26. Odler, I. and Zurz, A., "Structure and Bond Strength of Cement-Aggregate Interfaces", Bonding in Cementitious Composites, Mindess, S. and Shah, S.P., editors, Materials Research Society Symposium Proceedings, Vol. 114, 1987, pp.21-27.

27. Scrivener, K.L., Bentur, A. and Pratt, P.L., "Quantitative Characterization of the Transition Zone in High Strength Concretes", Advances in Cement Research, Vol. 1, No. 4, October 1988, pp. 230-237.

28. Bentur, A., Goldman, A. and Cohen, M.D., "The Contribution of the Transition Zone to the Strength of High Quality Silica Fume Concretes", Bonding in Cementitious Composites, Mindess, S. and Shah, S.P., editors, Materials Research Society Symposium Proceedings, Vol. 114, 1987, pp. 97-103.

29. Zhi-Yuan, C. and Xio-Zhong, Z., "Investigations on the Zinc/Hydrated-Cement-Paste Interfacial Zone", 8th International Congress on the Chemistry of Cement, Communications, THEME 2, Vol. III,pp 444-448.

30. Jia, W., Baoyuan, L., Songshan, X. and Zhongwei, W., "Improvement of Paste-Aggregate Interface By Adding Silica Fume", 8th International Congress on the Chemistry of Cement, Communications, THEME 2, Vol. III, pp. 460-465.

31. Monteiro, P.J.M, Gjorv, O.E. and Mehta, P.K., "Effect of Condensed Silica Fume On the Steel-Cement Paste Transition Zone", Cement and Concrete Research, Vol. 19, 1989, pp. 114-123.

32. Monteiro, P.J.M. and Mehta, P.K.. "The Transition Zone Between Aggregate and Type K Expansive Cement", Cement and Concrete Research, Vol. 16, 1986, pp. 111-114.

33. Moavenzadeh, F. and Bremner, T.W., "Fracture of Portland Cement Concrete", Structure, Solid Mechanics and Engineering Design, Proceedings Southampton, 1969, Civil Engineering Materials Conference (Ed. M. Te'eni), Wiley, NY, 1971.

34. Hsu, T.T.C.and Slate, F.O., "Tensile Bond Strength Between Aggregate and Cement Paste or Mortar", Journal of the American Concrete Institute, 1963, pp. 465-486.

35. Alexander, K.M. and Wardlaw, J., and Gilbert, J., "Aggregate-Cement Bond, Cement Paste Strength, and the Strength of Concrete", The Structure of Concrete, The Cement and Concrete Association, London, 1968, pp. 59-81.

36. Zhuravlev, V.F. and Shteiert, N.P., "Cohesion of Hardened Cement with Various Materials", Tsement, Vol 18, 1952, pp. 17-19.

37. Timoshenko, S., and Woinowsky-Krieger, S., Theory of Plates and Shells, McGraw-Hill, 1959, pp. 67.

38. Malhotra, V.M., Ramachandran, V.S., Feldman, R.F. and Aitcin, "Condensed Silica Fume in Concrete", CRC Press, Boca Raton, Fl., 1987.

39. Ramachandran, V.S. and Feldman, R.F., "Time-Dependent and Intrinsic Characteristics of Portland Cement Hydrated in the Presence of Calcium Chloride", Il Cemento, Vol. 75, No. 3, 1978, pp. 311-322.

40. Kennedy, J.B. and Neville, A.M., Basic Statistical Methods for Engineers & Scientists, 2nd edition, Dun-Donnelley Publisher, New York, NY, 1976.

41. Ramachandran, V.S., Feldman, R.F. and Beaudoin, J.J., Concrete Science, Heyden, London, 1981, pp. 193.

42. Advances in Cement Technology, Gnosh, S.N., ed., Pergammon, Oxford, 1983, pp. 454.

43. Sorka, I. , Portland Cement Paste and Concrete, MacMillan, London, 1979, pp. 75.

Appendix A

Thermogravimetric Curves

Note: On the top left hand corner of each graph is a heading labeled "SAMPLE NAME". The information in this heading is aa follows: system, w/c, hydration time. The systems are abbreviated as noted bellow.

Cement = Only Type 10 Portland Cement

CaCl2 = Cement + 2% $CaCl_2$

NaNO3 = Cement + 2% $NaNO_3$

Propionate = Cement + 2% $Ca(C_3H_5O_2)_2.H_2O$

Sample: Cement 0.30, 4h
Size: 137.9530 mg
Method: RT-1000 20 DEG/MIN

TGA

File: A:GLEN.01
Operator: GBP
Run Date: 02/12/90 15:50

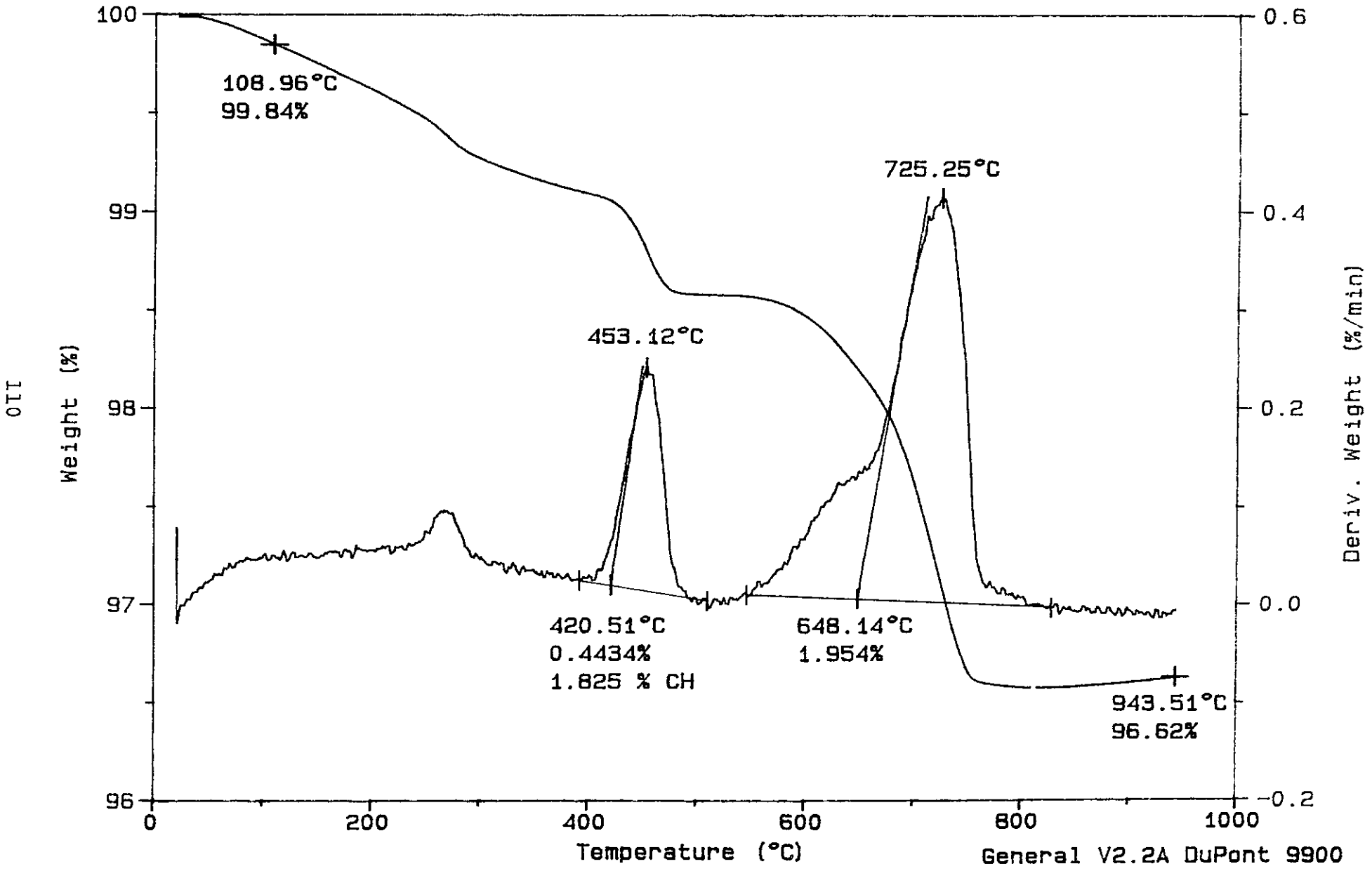

Sample: Cement 0.30, 6.5h
Size: 152.8260 mg
Method: RT-1000 20 DEG/MIN

TGA

File: A:GLEN.02
Operator: GBP
Run Date: 02/13/90 07:25

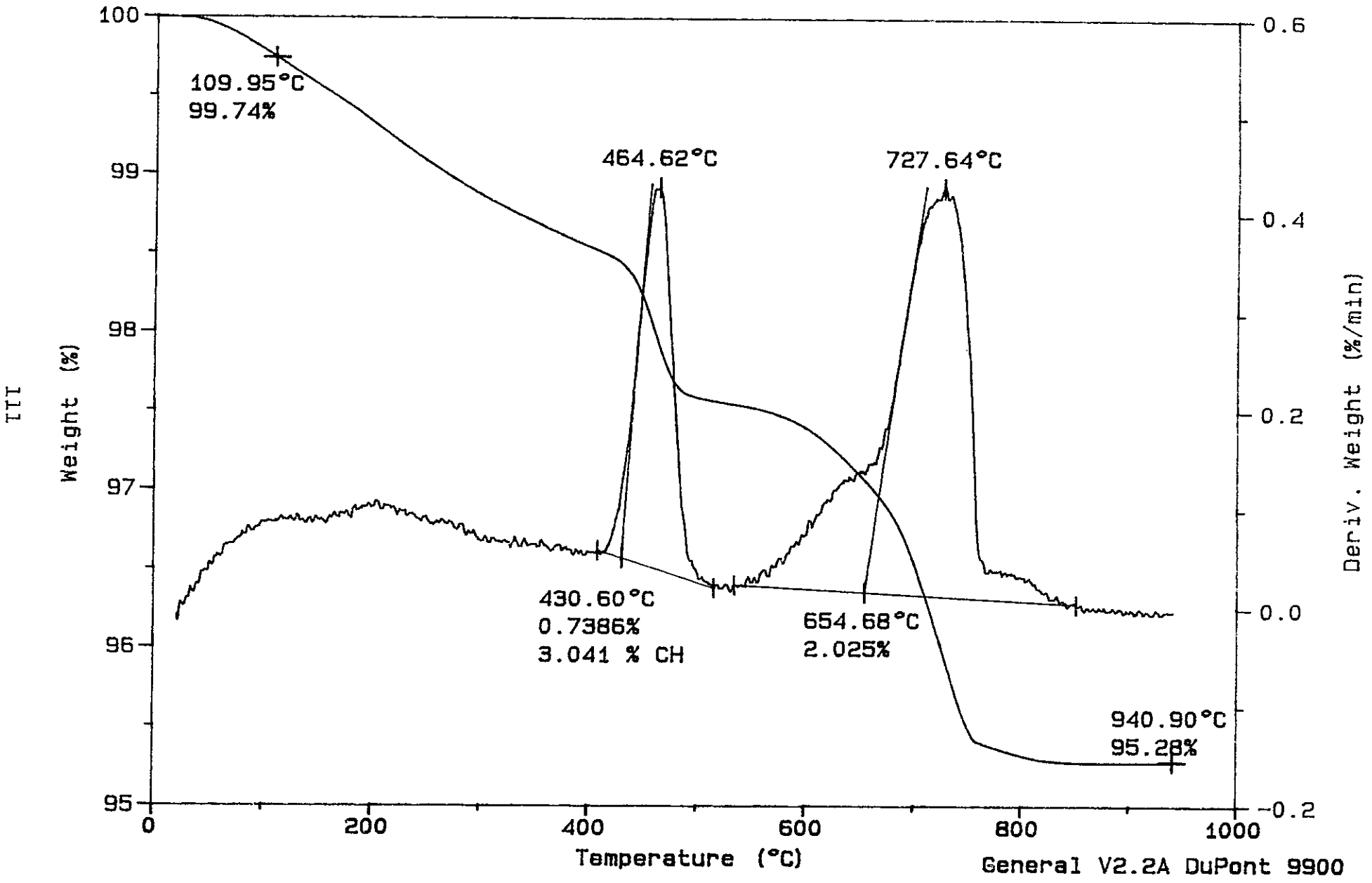

General V2.2A DuPont 9900

Sample: CEMENT, 0.30, 1 DAY
Size: 144.5790 mg
Method: RT-1000 20 DEG/MIN
Comment: AIR, 100 ml/min

TGA

File: A:GLEN.05
Operator: GBP
Run Date: 02/13/90 12:37

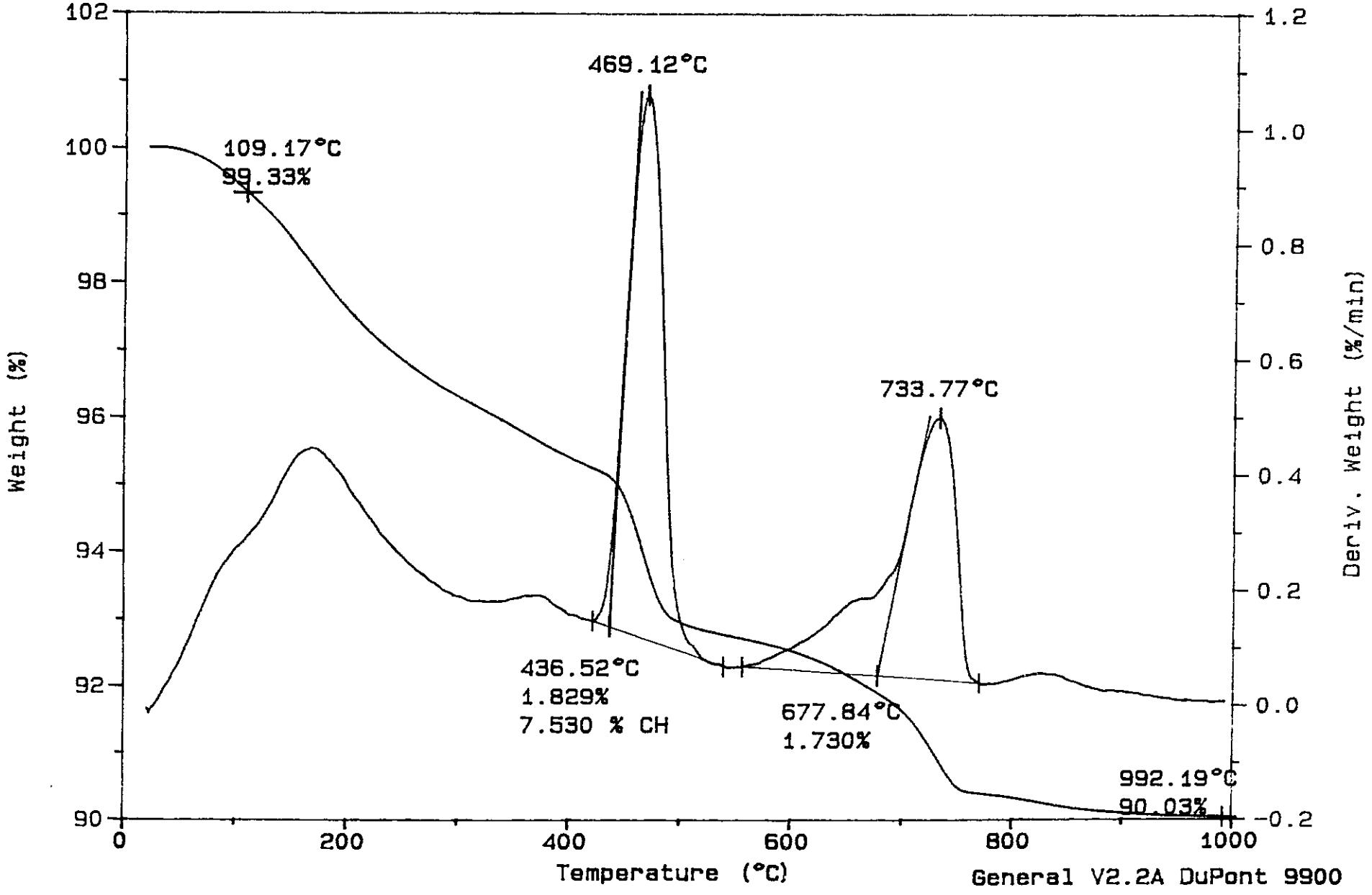

General V2.2A DuPont 9900

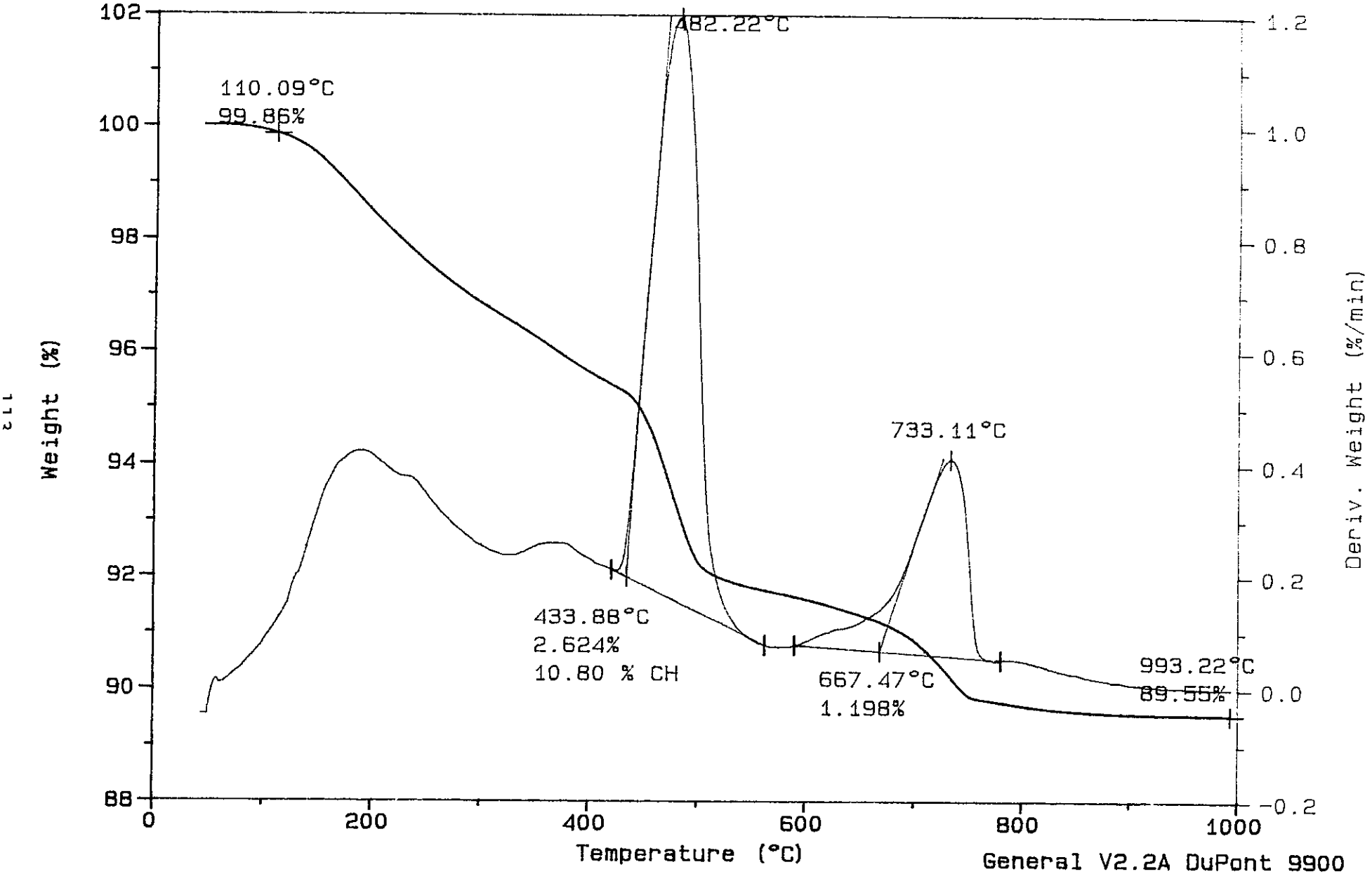
Sample: CEMENT, 0.30, 2 DAYS
Size: 180.5280 mg
Method: RT-1000 20 DEG/MIN
Comment: AIR, 100 ml/min
TGA
File: A:GLEN.07
Operator: GBP
Run Date: 02/13/90 15:43
482.22°C
110.09°C
99.86%
733.11°C
433.88°C
2.624%
10.80 % CH
667.47°C
1.198%
993.22°C
89.55%
Weight (%)
Deriv. Weight (%/min)
Temperature (°C)
General V2.2A DuPont 9900

Sample: CEMENT, 0.30, 7 DAYS
Size: 143.0300 mg
Method: RT-1000 20 DEG/MIN
Comment: AIR, 100 ml/min

TGA

File: A:GLEN.15
Operator: GBP
Run Date: 02/15/90 09:55

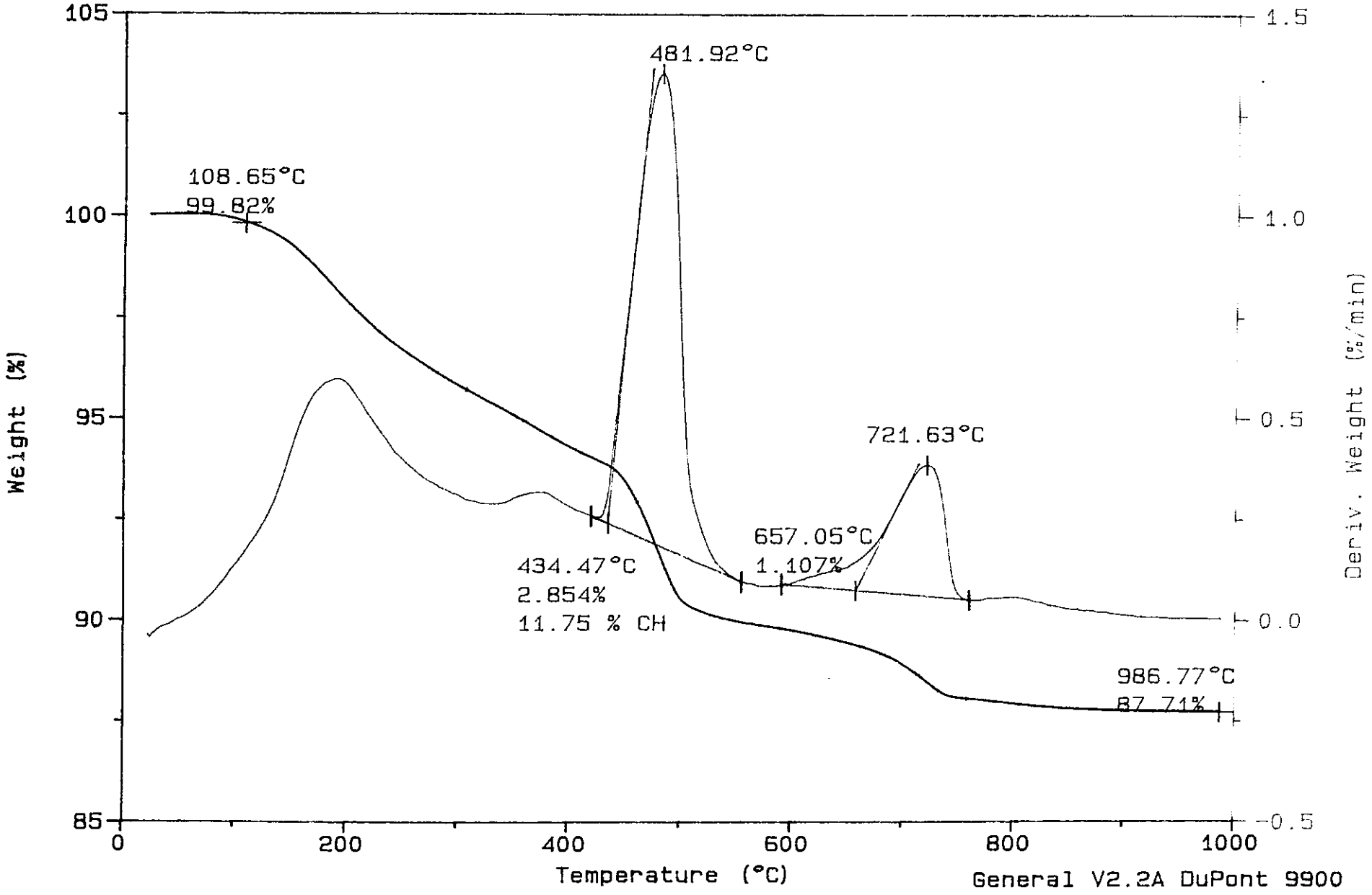

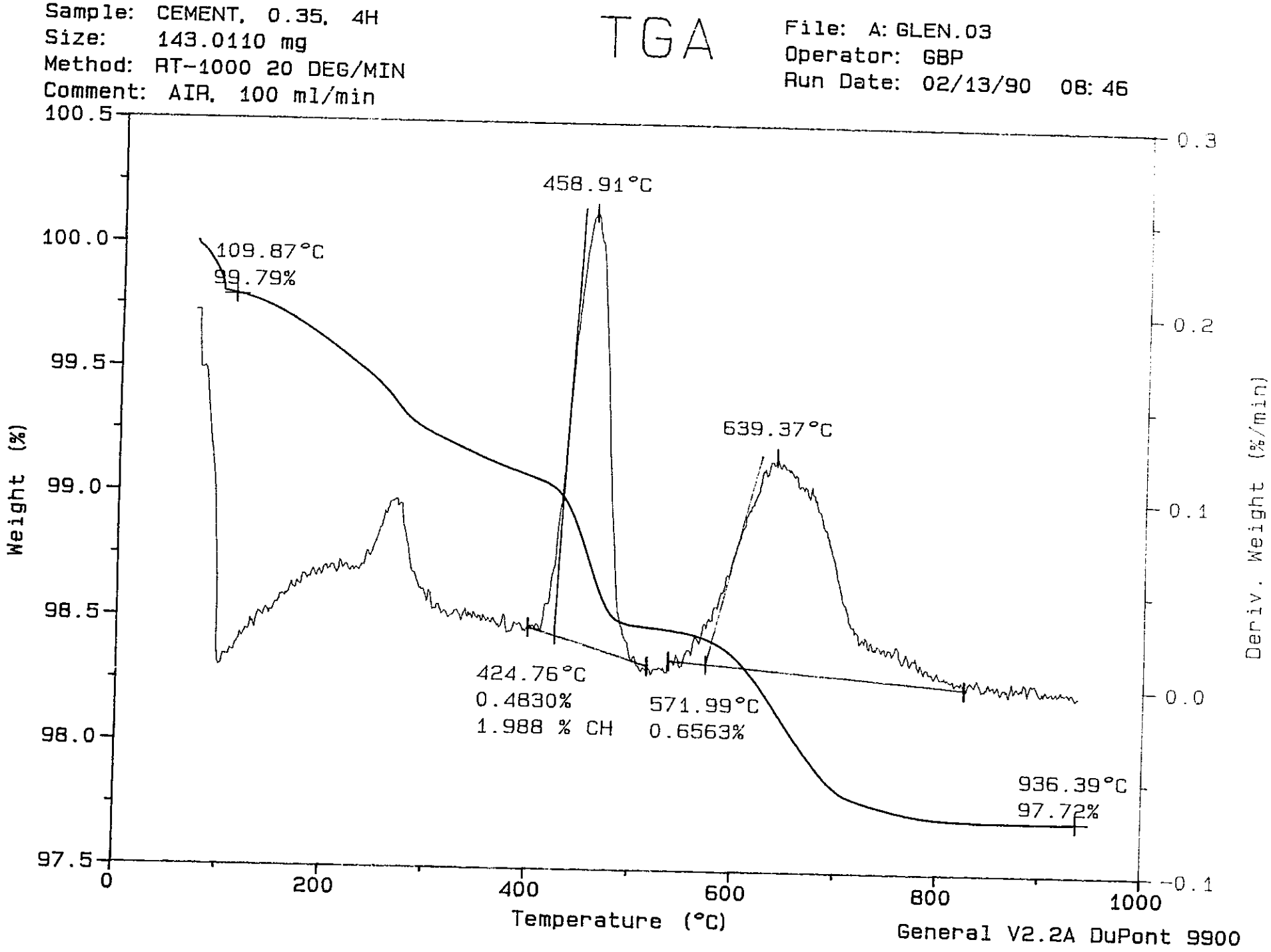
Sample: CEMENT, 0.35, 4H
Size: 143.0110 mg
Method: RT-1000 20 DEG/MIN
Comment: AIR, 100 ml/min
TGA
File: A:GLEN.03
Operator: GBP
Run Date: 02/13/90 08:46
458.91°C
109.87°C
99.79%
639.37°C
424.76°C
0.4830%
1.988 % CH
571.99°C
0.6563%
936.39°C
97.72%
Weight (%)
Deriv. Weight (%/min)
Temperature (°C)
General V2.2A DuPont 9900

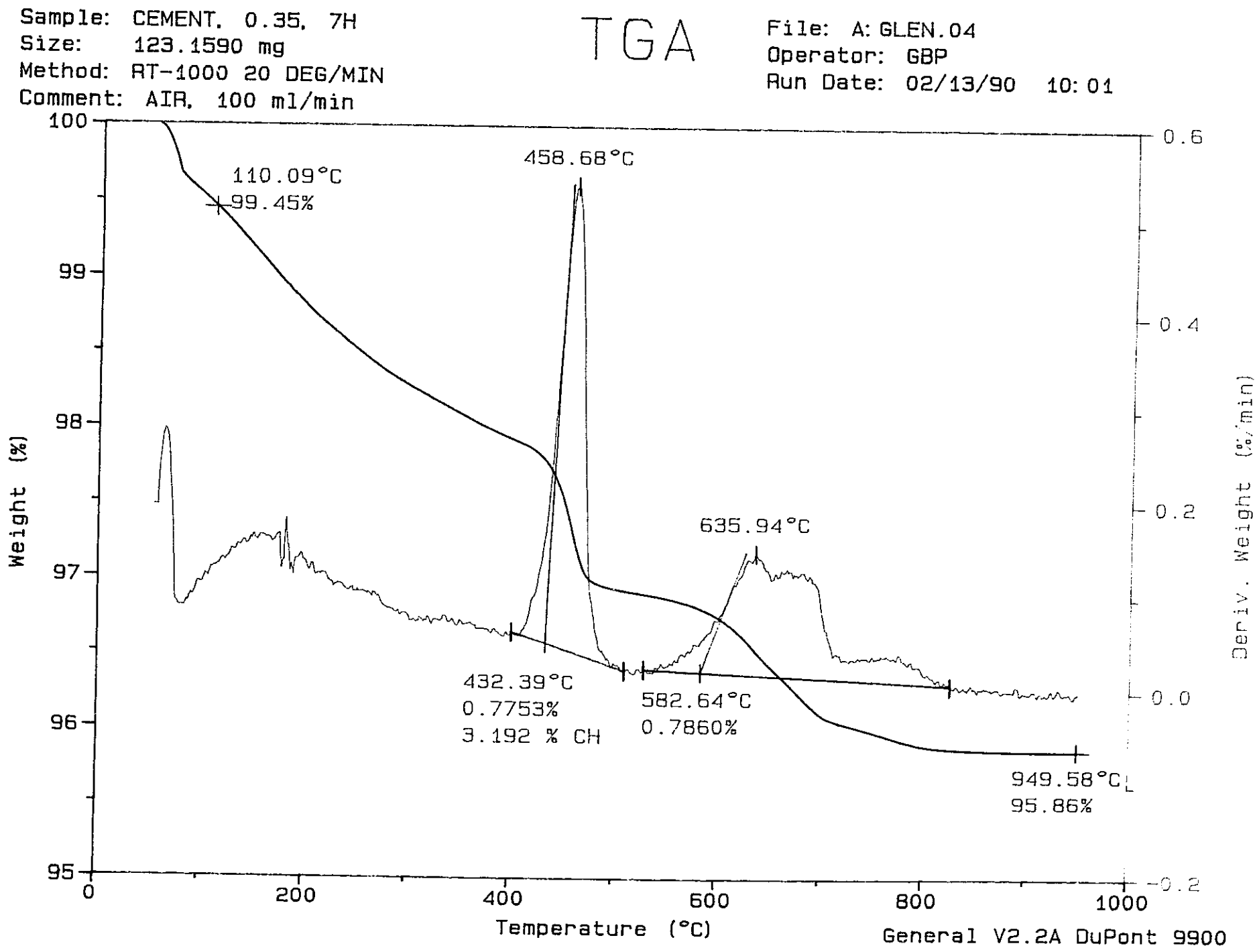
Sample: CEMENT, 0.35, 7H
Size: 123.1590 mg
Method: RT-1000 20 DEG/MIN
Comment: AIR, 100 ml/min
TGA
File: A:GLEN.04
Operator: GBP
Run Date: 02/13/90 10:01
110.09°C
99.45%
458.68°C
635.94°C
432.39°C
0.7753%
3.192 % CH
582.64°C
0.7860%
949.58°C
95.86%
Weight (%)
Deriv. Weight (%/min)
Temperature (°C)
General V2.2A DuPont 9900

Sample: CEMENT, 0.35, 1 DAY
Size: 145.4860 mg
Method: RT-1000 20 DEG/MIN
Comment: AIR, 100 ml/min

TGA

File: A:GLEN.06
Operator: GBP
Run Date: 02/13/90 14:16

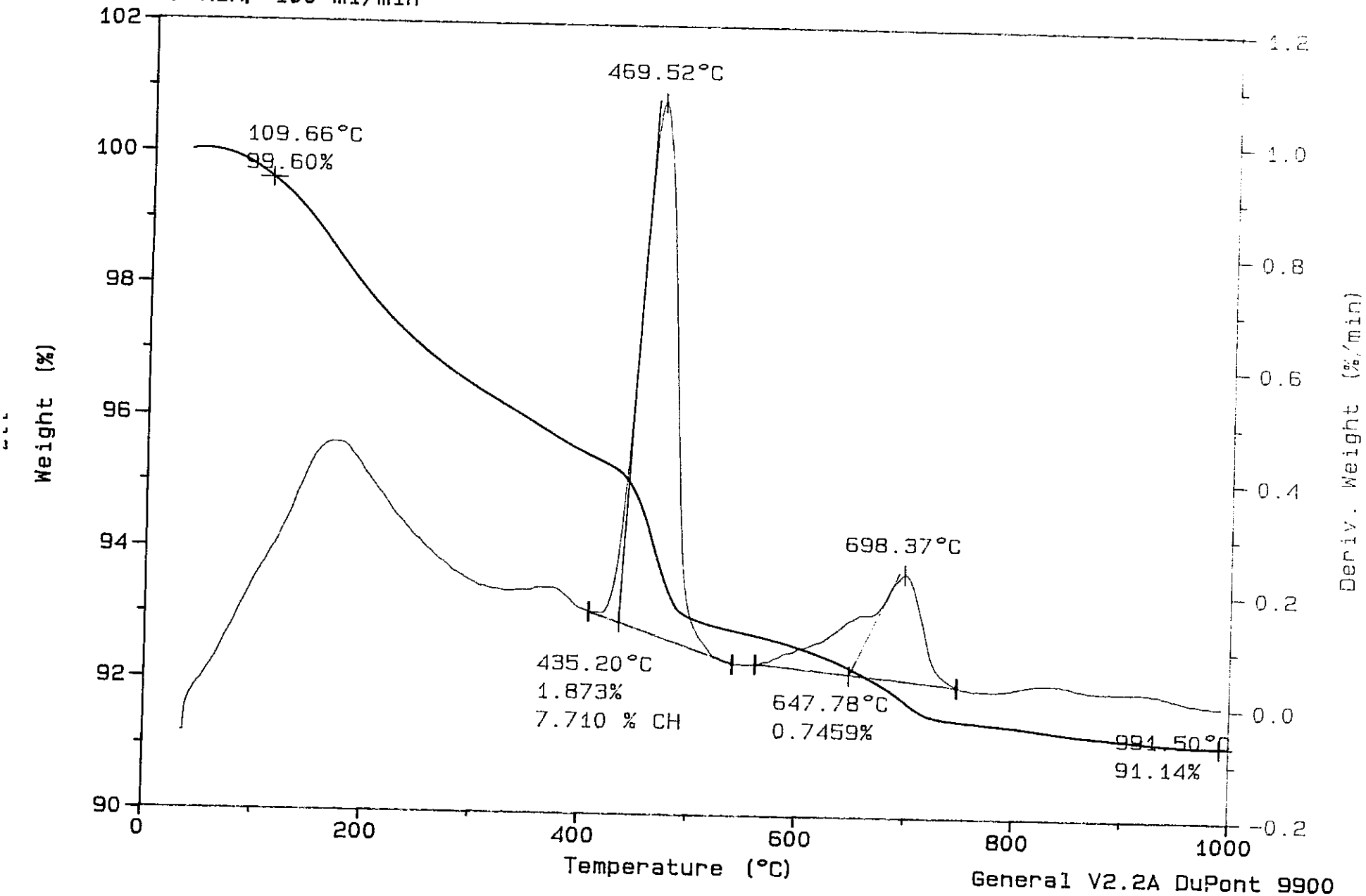

General V2.2A DuPont 9900

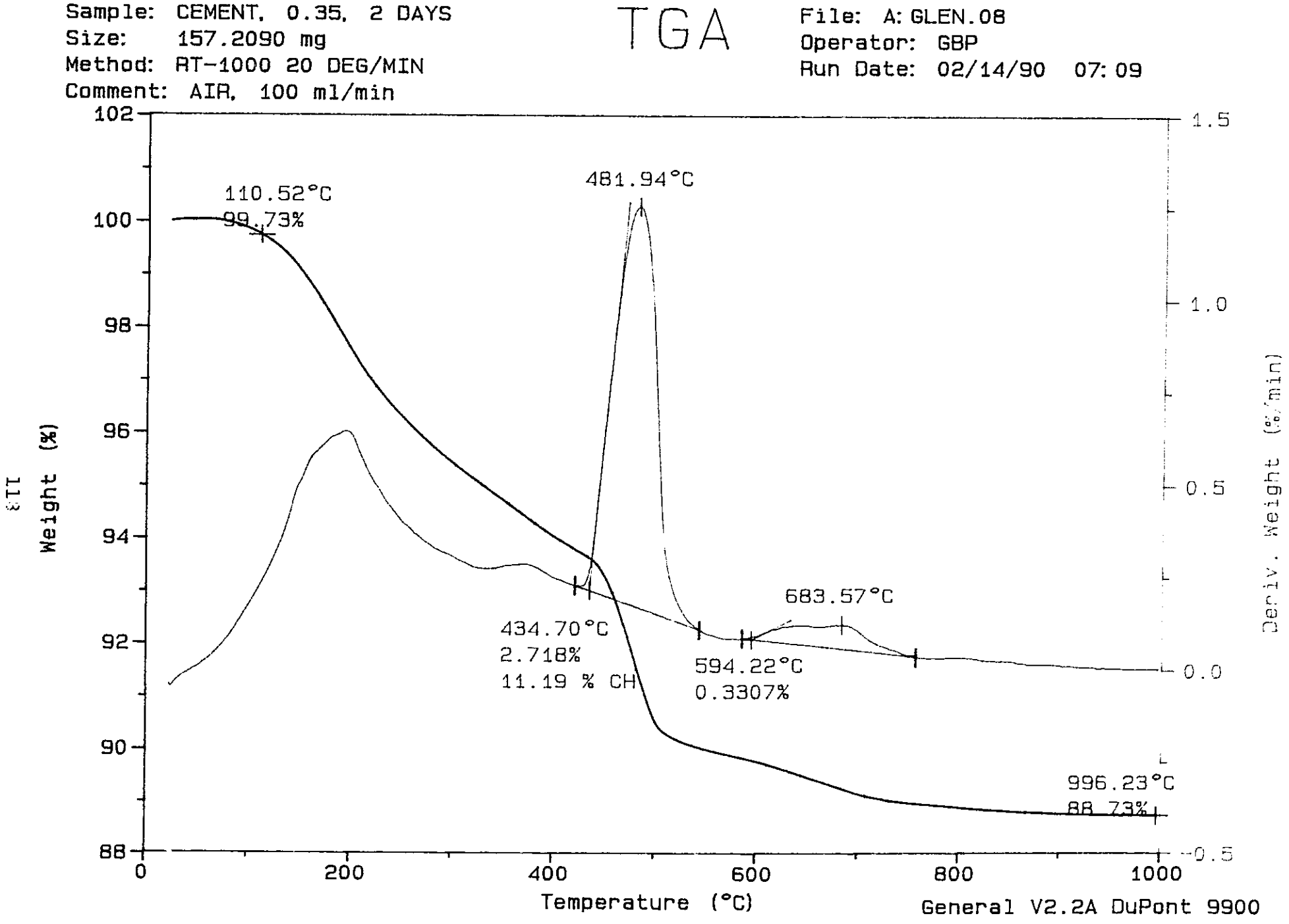
Sample: CEMENT, 0.35, 2 DAYS
Size: 157.2090 mg
Method: RT-1000 20 DEG/MIN
Comment: AIR, 100 ml/min
TGA
File: A:GLEN.08
Operator: GBP
Run Date: 02/14/90 07:09
110.52°C
99.73%
481.94°C
434.70°C
2.718%
11.19 % CH
683.57°C
594.22°C
0.3307%
996.23°C
88.73%
Weight (%)
Deriv. Weight (%/min)
Temperature (°C)
General V2.2A DuPont 9900

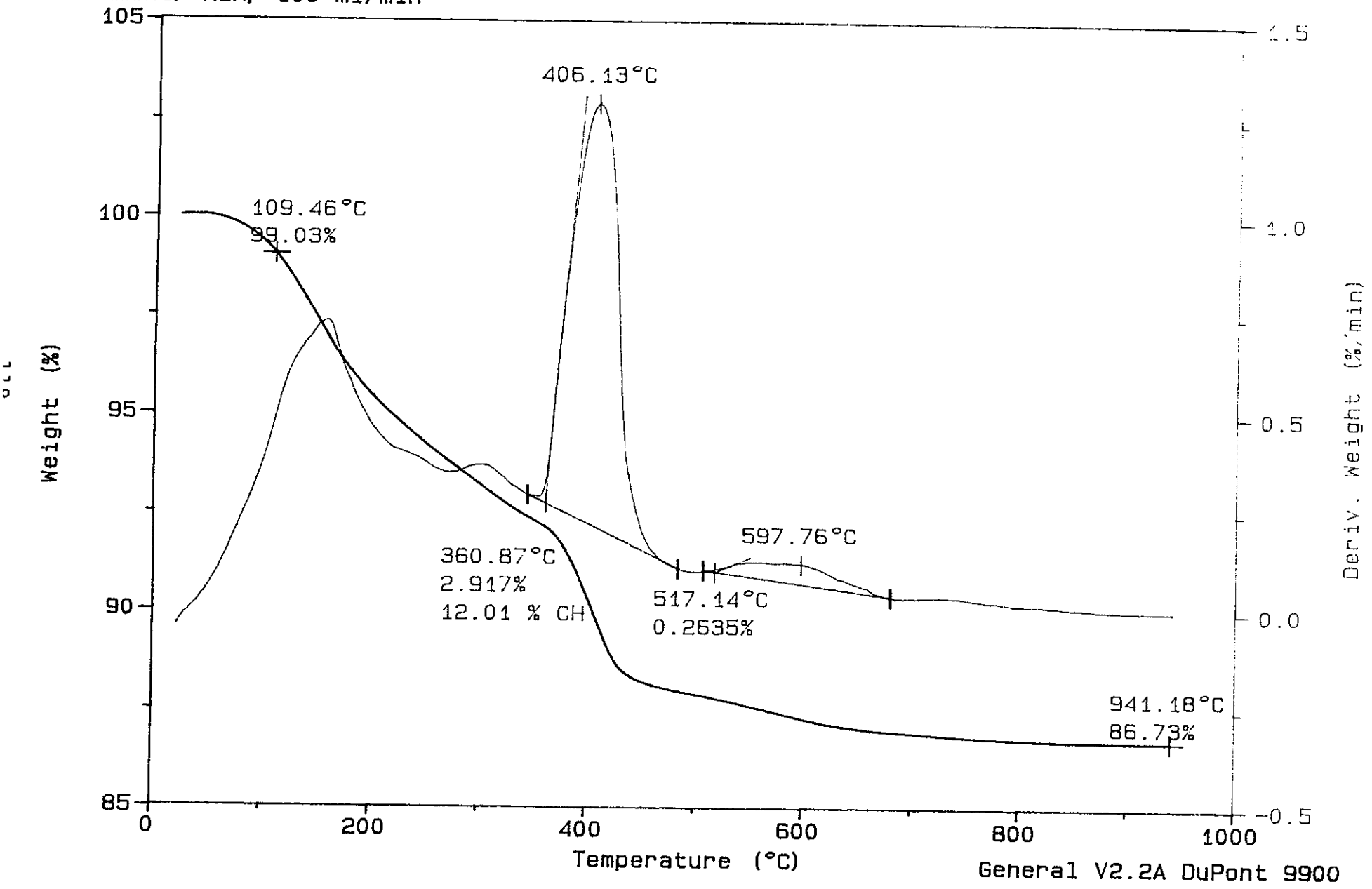
Sample: CEMENT, 0.35, 7 DAYS
Size: 161.9330 mg
Method: RT-1000 20 DEG/MIN
Comment: AIR, 100 ml/min
TGA
File: A:GLEN.16
Operator: GBP
Run Date: 02/15/90 13:55
406.13°C
109.46°C
99.03%
360.87°C
2.917%
12.01 % CH
517.14°C
0.2635%
597.76°C
941.18°C
86.73%
Weight (%)
Deriv. Weight (%/min)
Temperature (°C)
General V2.2A DuPont 9900

Sample: NaNO3 0.30, 3.5H
Size: 152.3550 mg
Method: RT-1000 20 DEG/MIN
Comment: N2 100 ML/MIN

TGA

File: A:GLEN.01
Operator: GBP
Run Date: 03/19/90 06:29

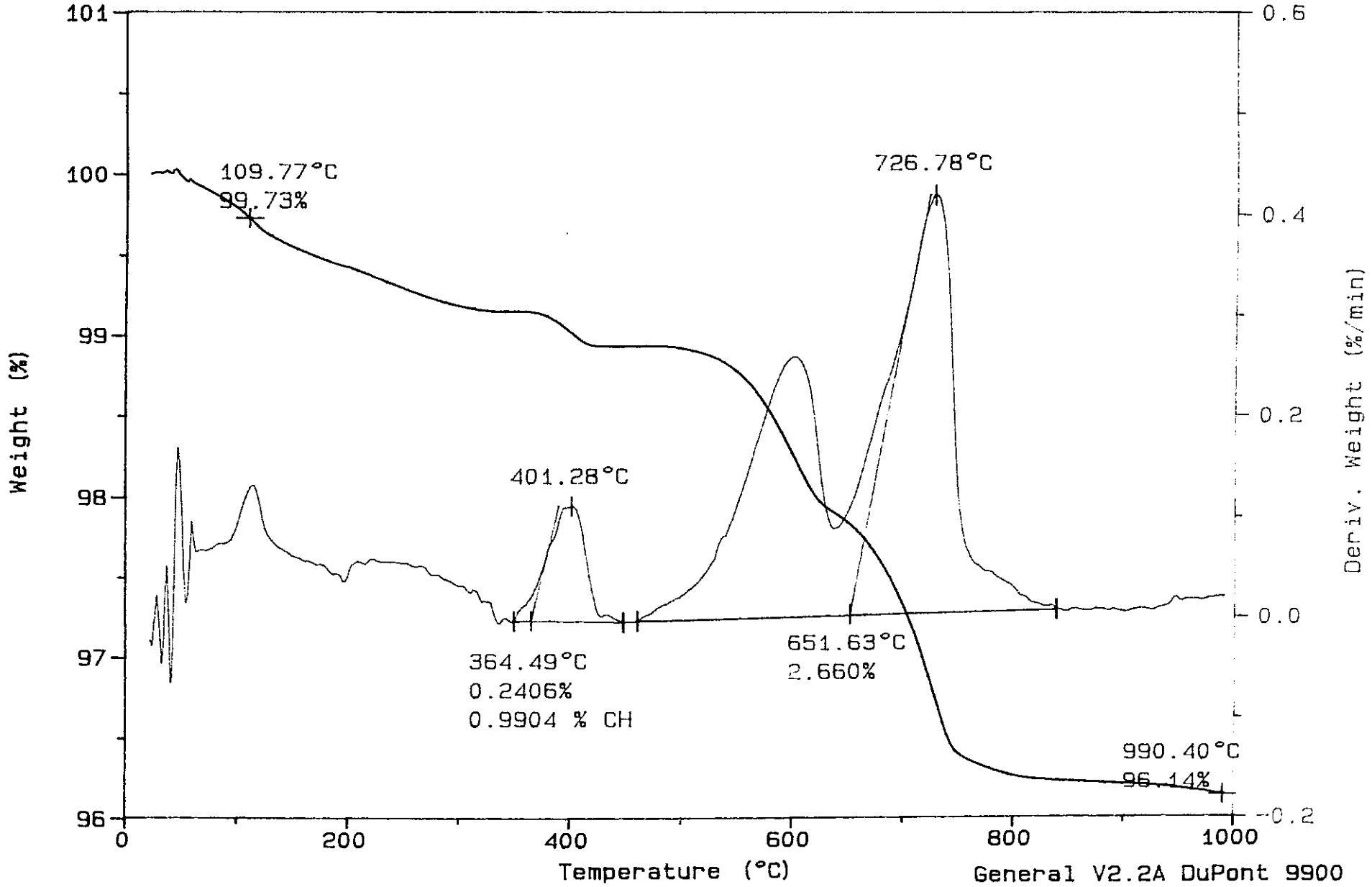

General V2.2A DuPont 9900

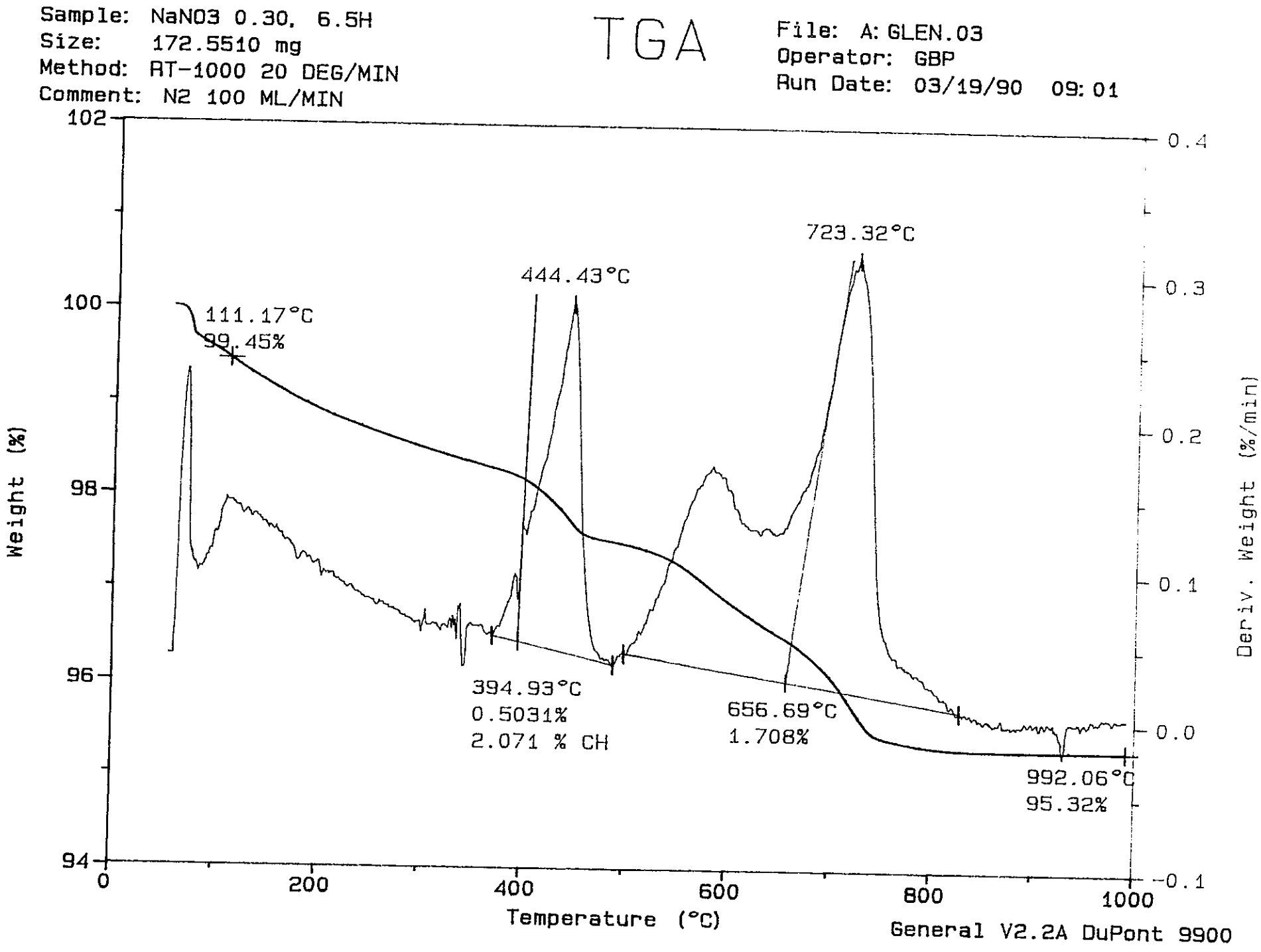
Sample: NaNO3 0.30, 6.5H
Size: 172.5510 mg
Method: RT-1000 20 DEG/MIN
Comment: N2 100 ML/MIN
TGA
File: A:GLEN.03
Operator: GBP
Run Date: 03/19/90 09:01
111.17°C
99.45%
444.43°C
723.32°C
394.93°C
0.5031%
2.071 % CH
656.69°C
1.708%
992.06°C
95.32%
Weight (%)
Deriv. Weight (%/min)
Temperature (°C)
General V2.2A DuPont 9900

Sample: NaNO3 0.30, 1 day
Size: 159.9060 mg
Method: RT-1000 20 DEG/MIN
Comment: N2 100 ML/MIN

TGA

File: A:GLEN.05
Operator: GBP
Run Date: 03/19/90 12:33

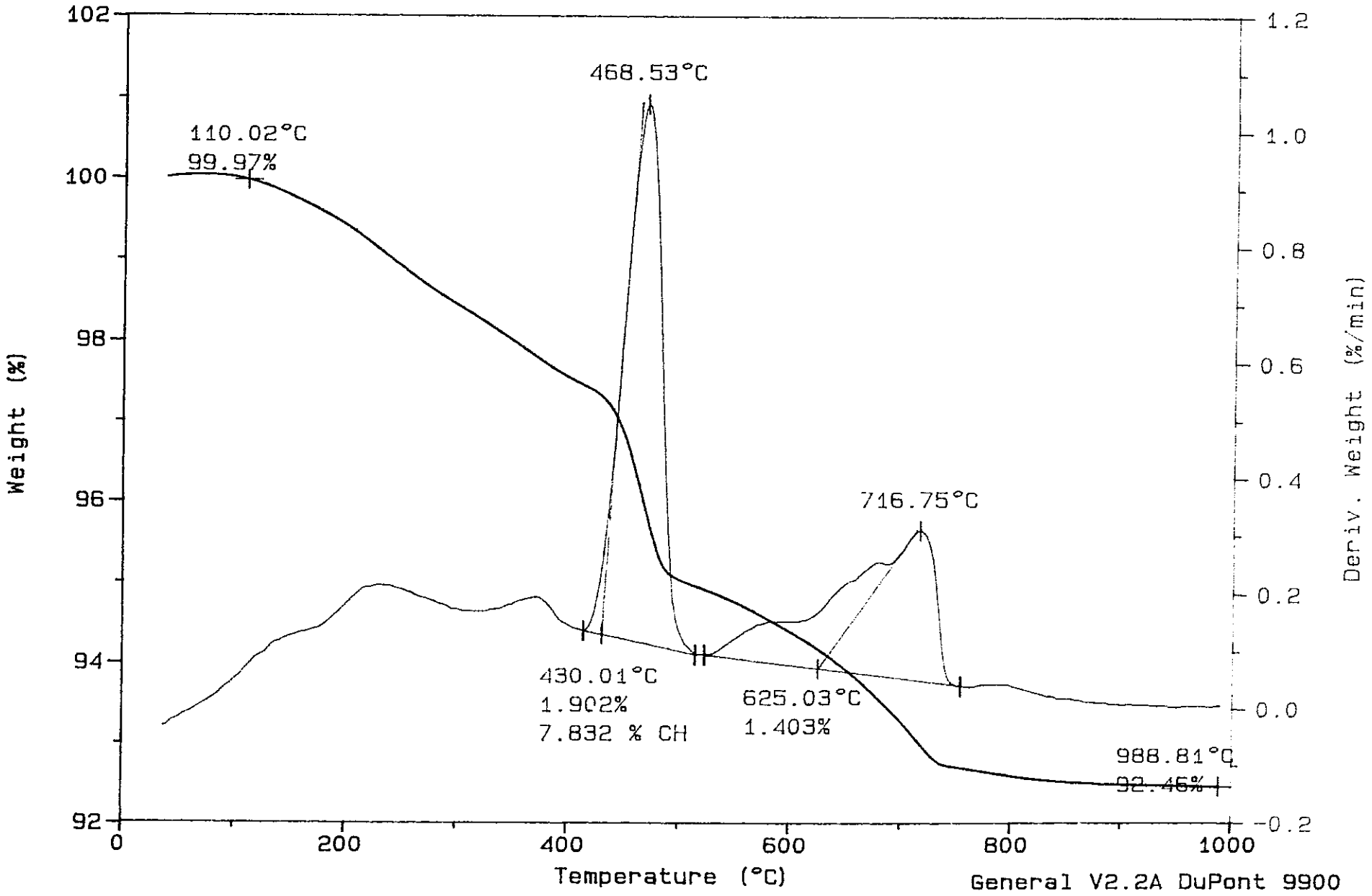

General V2.2A DuPont 9900

Sample: NaNO3 0.30, 2 days
Size: 160.7110 mg
Method: RT-1000 20 DEG/MIN
Comment: N2 100 ML/MIN

TGA

File: A:GLEN.07
Operator: GBP
Run Date: 03/20/90 05:38

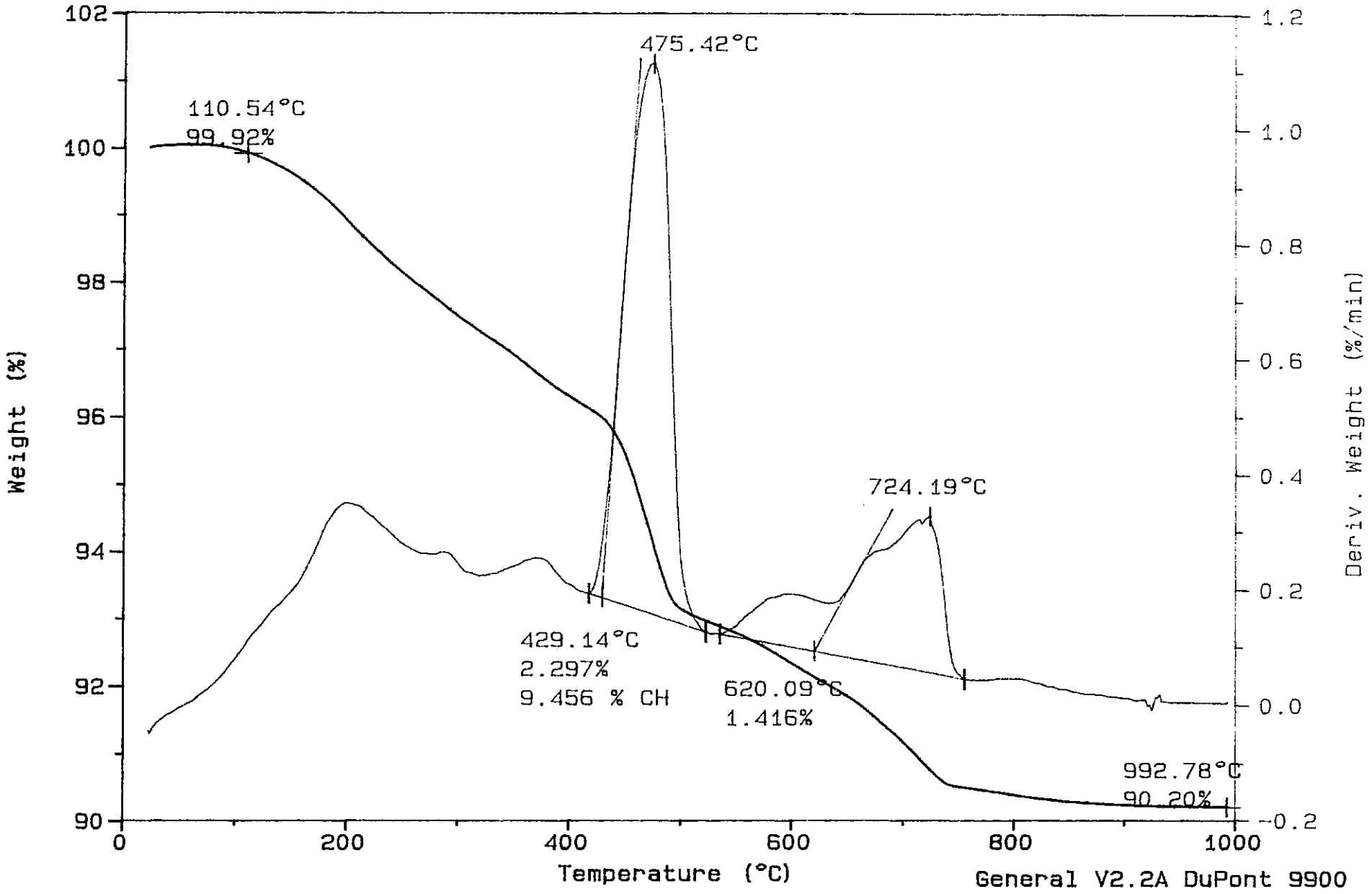

General V2.2A DuPont 9900

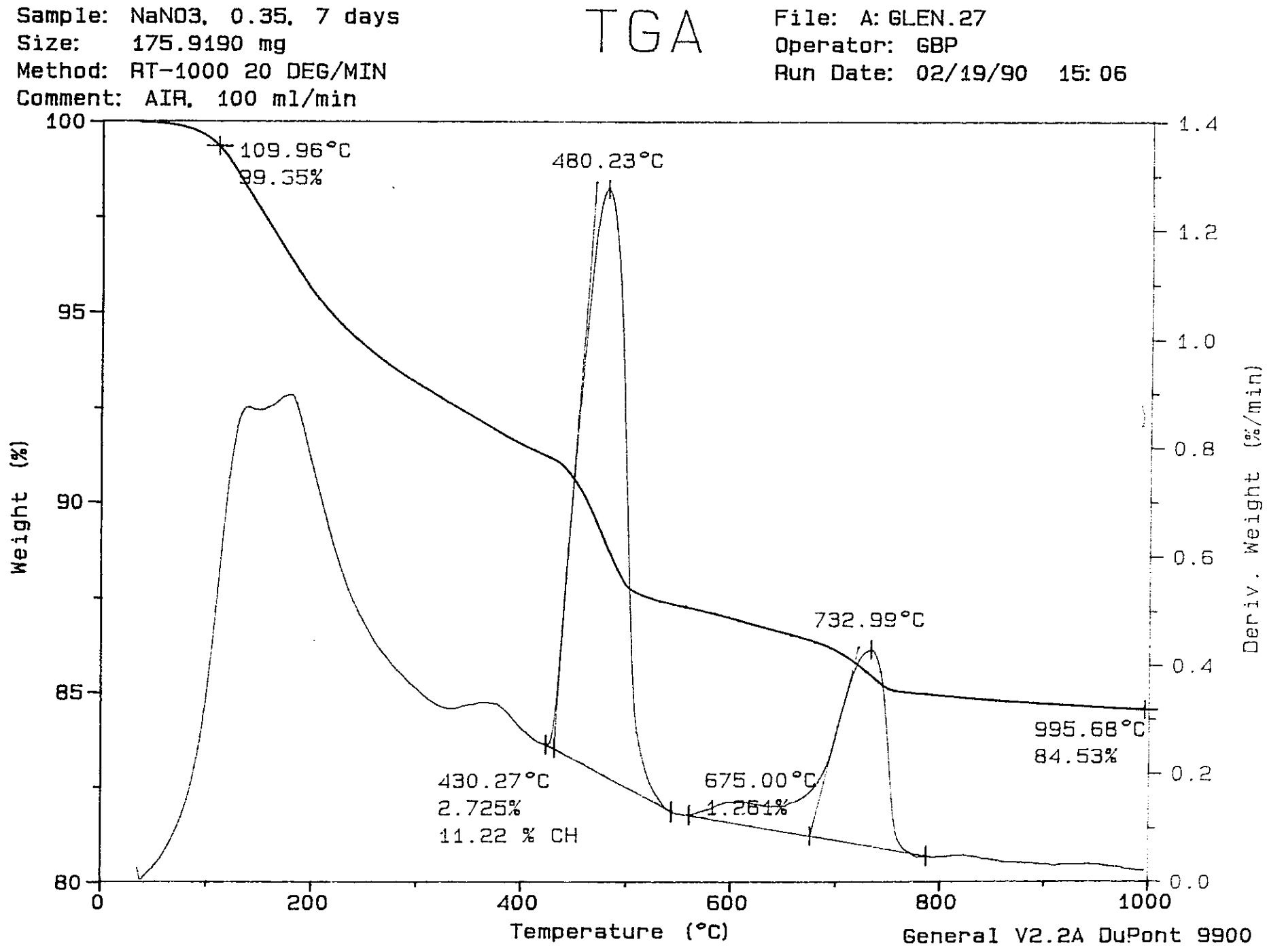
Sample: NaNO3, 0.35, 7 days
Size: 175.9190 mg
Method: RT-1000 20 DEG/MIN
Comment: AIR, 100 ml/min
TGA
File: A:GLEN.27
Operator: GBP
Run Date: 02/19/90 15:06
109.96°C
99.35%
480.23°C
732.99°C
995.68°C
84.53%
430.27°C
2.725%
11.22 % CH
675.00°C
1.261%
Weight (%)
Deriv. Weight (%/min)
Temperature (°C)
General V2.2A DuPont 9900

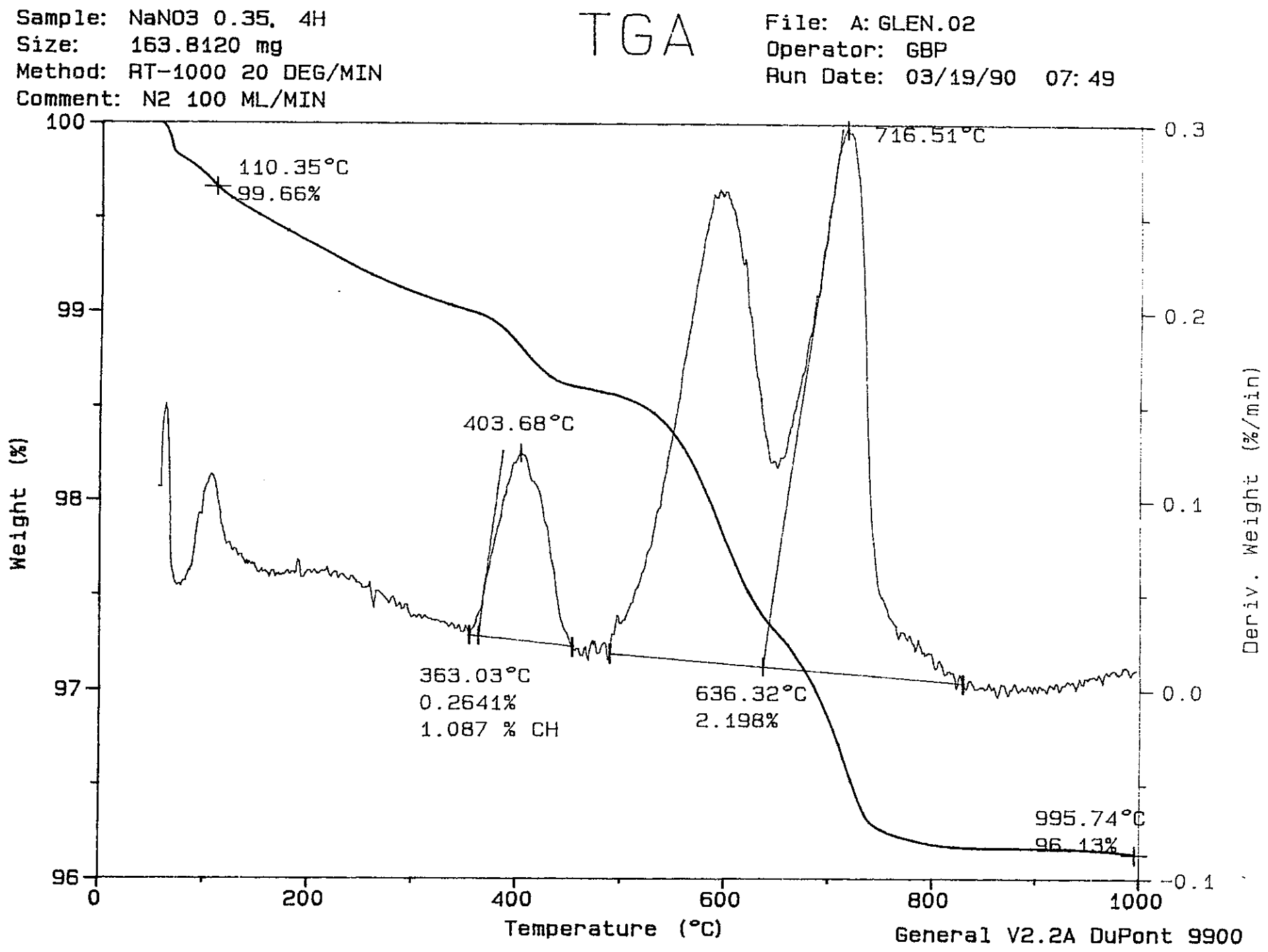
Sample: NaNO3 0.35, 4H
Size: 163.8120 mg
Method: RT-1000 20 DEG/MIN
Comment: N2 100 ML/MIN
TGA
File: A:GLEN.02
Operator: GBP
Run Date: 03/19/90 07:49
110.35°C
99.66%
403.68°C
363.03°C
0.2641%
1.087 % CH
636.32°C
2.198%
716.51°C
995.74°C
96.13%
Weight (%)
Deriv. Weight (%/min)
Temperature (°C)
General V2.2A DuPont 9900

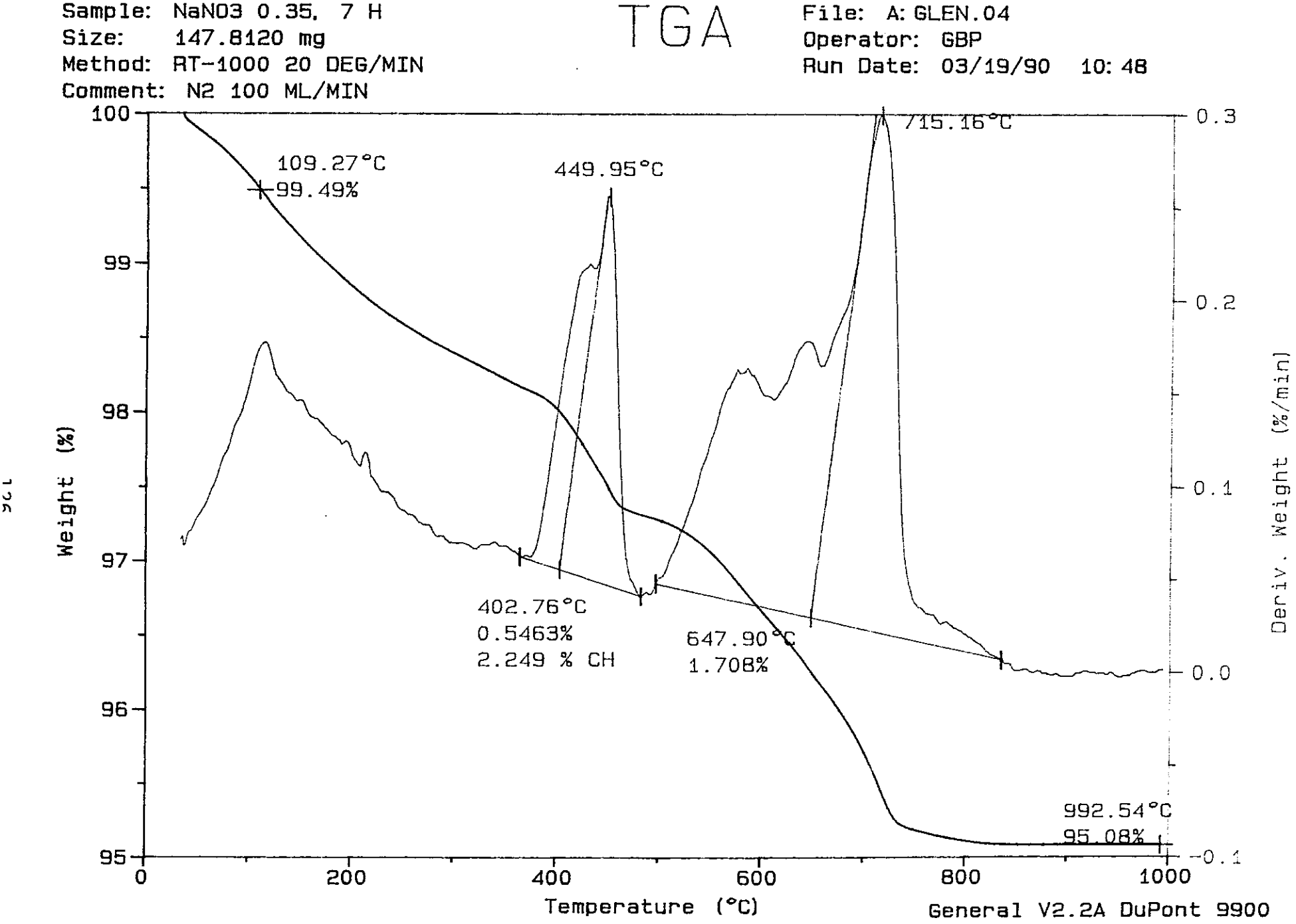
Sample: NaNO3 0.35, 7 H
Size: 147.8120 mg
Method: RT-1000 20 DEG/MIN
Comment: N2 100 ML/MIN
TGA
File: A:GLEN.04
Operator: GBP
Run Date: 03/19/90 10:48
109.27°C
99.49%
449.95°C
715.16°C
402.76°C
0.5463%
2.249 % CH
647.90°C
1.708%
992.54°C
95.08%
Weight (%)
Deriv. Weight (%/min)
Temperature (°C)
General V2.2A DuPont 9900

Sample: NaNO3 0.35, 1 day
Size: 151.0590 mg
Method: RT-1000 20 DEG/MIN
Comment: N2 100 ML/MIN

TGA

File: A:GLEN.06
Operator: GBP
Run Date: 03/19/90 13:46

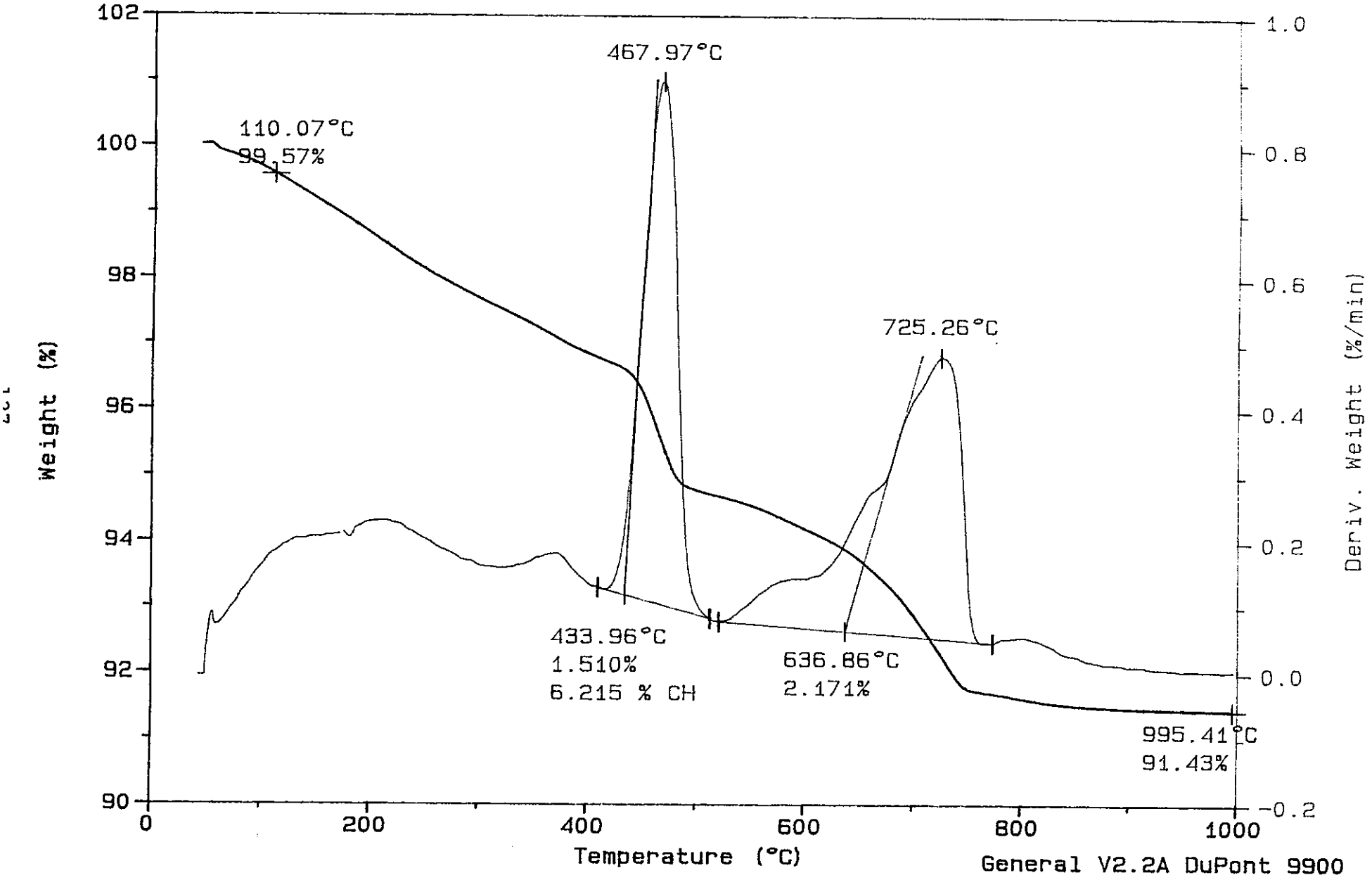

General V2.2A DuPont 9900

Sample: NaNO3 0.35, 2 days
Size: 157.7240 mg
Method: RT-1000 20 DEG/MIN
Comment: AIR 100 ML/MIN

TGA

File: A:GLEN.08
Operator: GBP
Run Date: 03/20/90 06:49

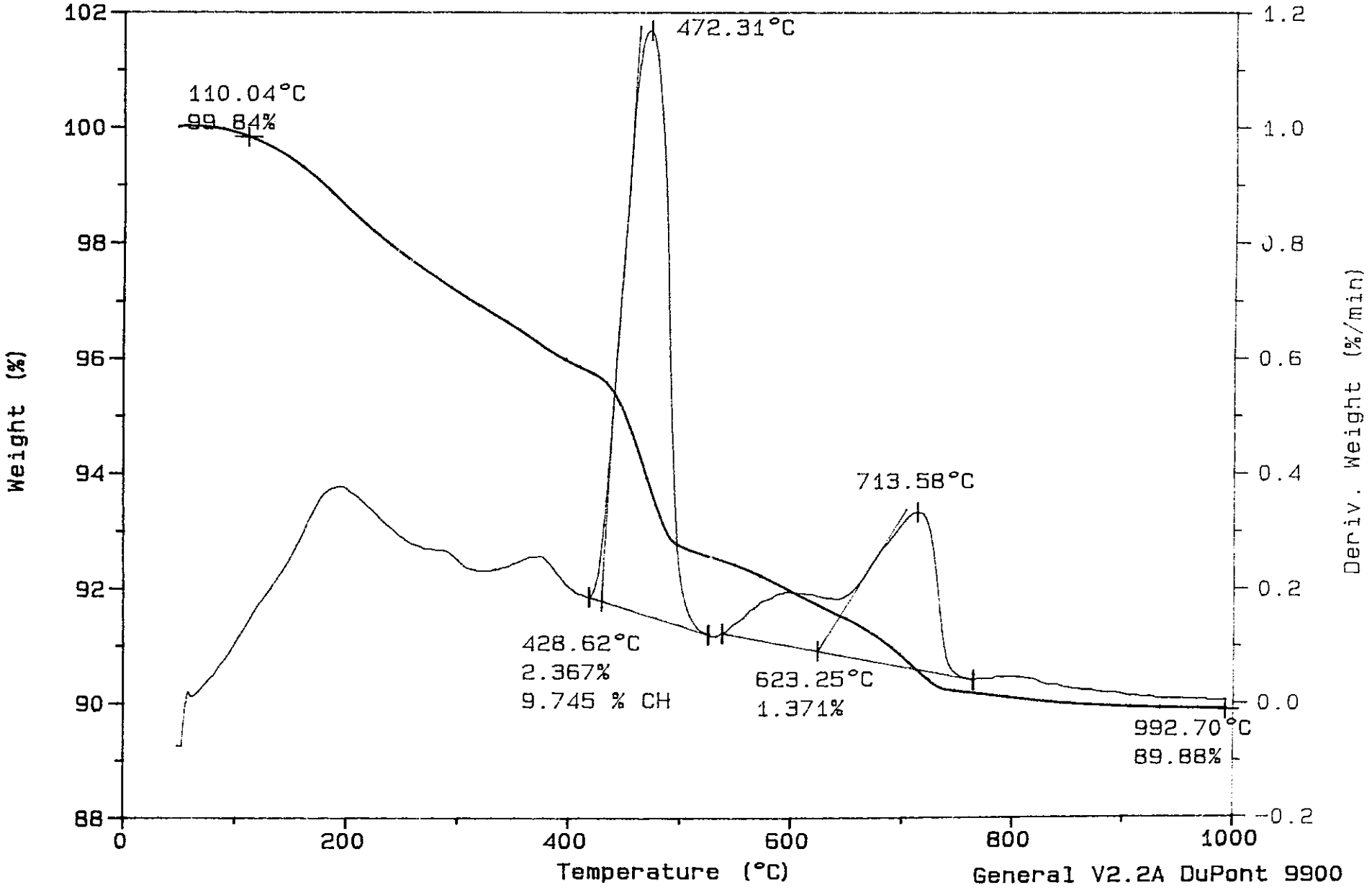

General V2.2A DuPont 9900

Sample: NaNO3, 0.30, 7 days
Size: 170.4410 mg
Method: RT-1000 20 DEG/MIN
Comment: AIR, 100 ml/min

TGA

File: A:GLEN.26
Operator: GBP
Run Date: 02/19/90 13:42

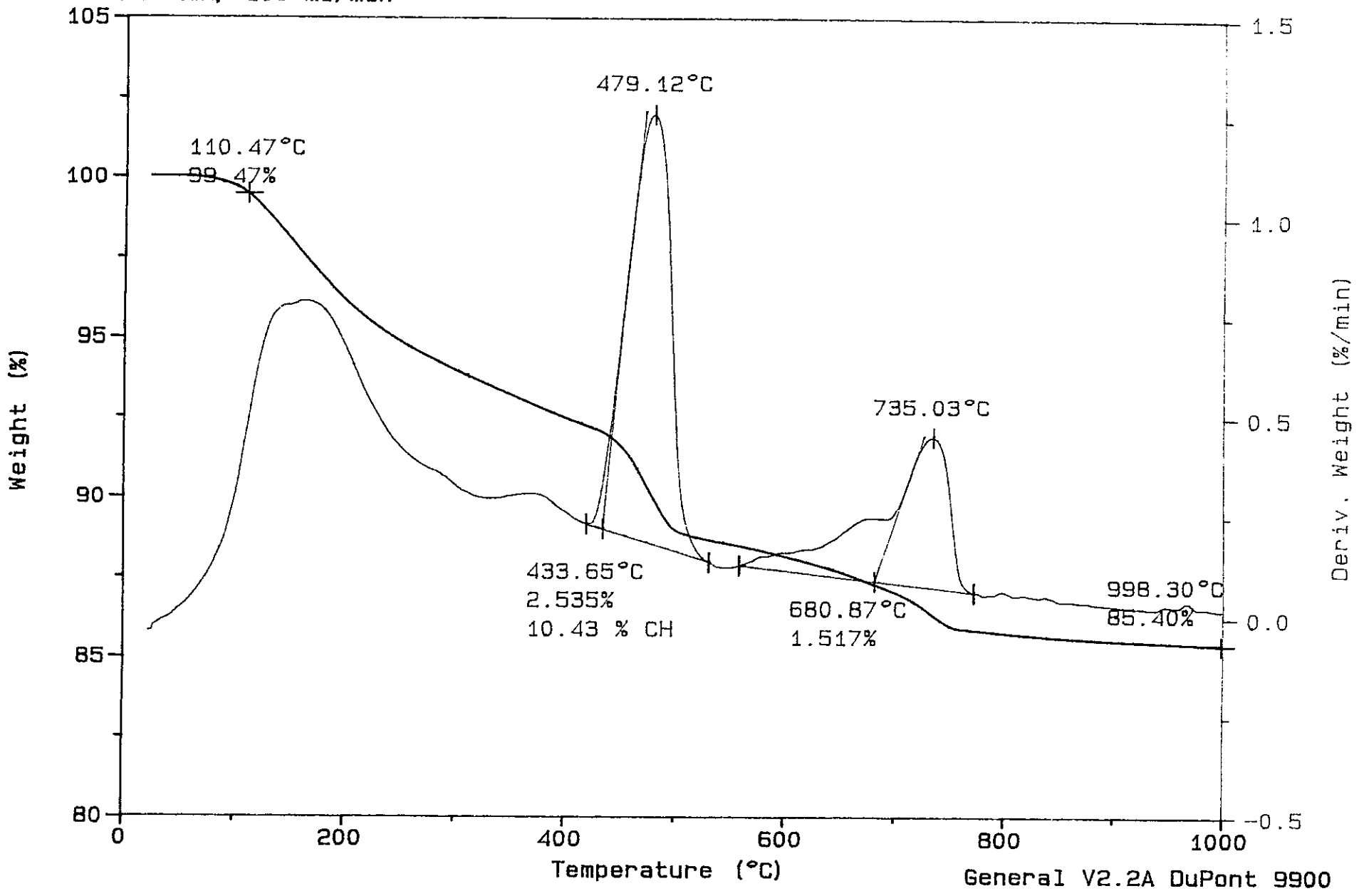

General V2.2A DuPont 9900

Sample: CaCl2, 0.30, 3 H
Size: 176.6070 mg
Method: RT-1000 20 DEG/MIN
Comment: AIR, 100 ml/min

TGA

File: A:GLEN.28
Operator: GBP
Run Date: 02/21/90 10:07

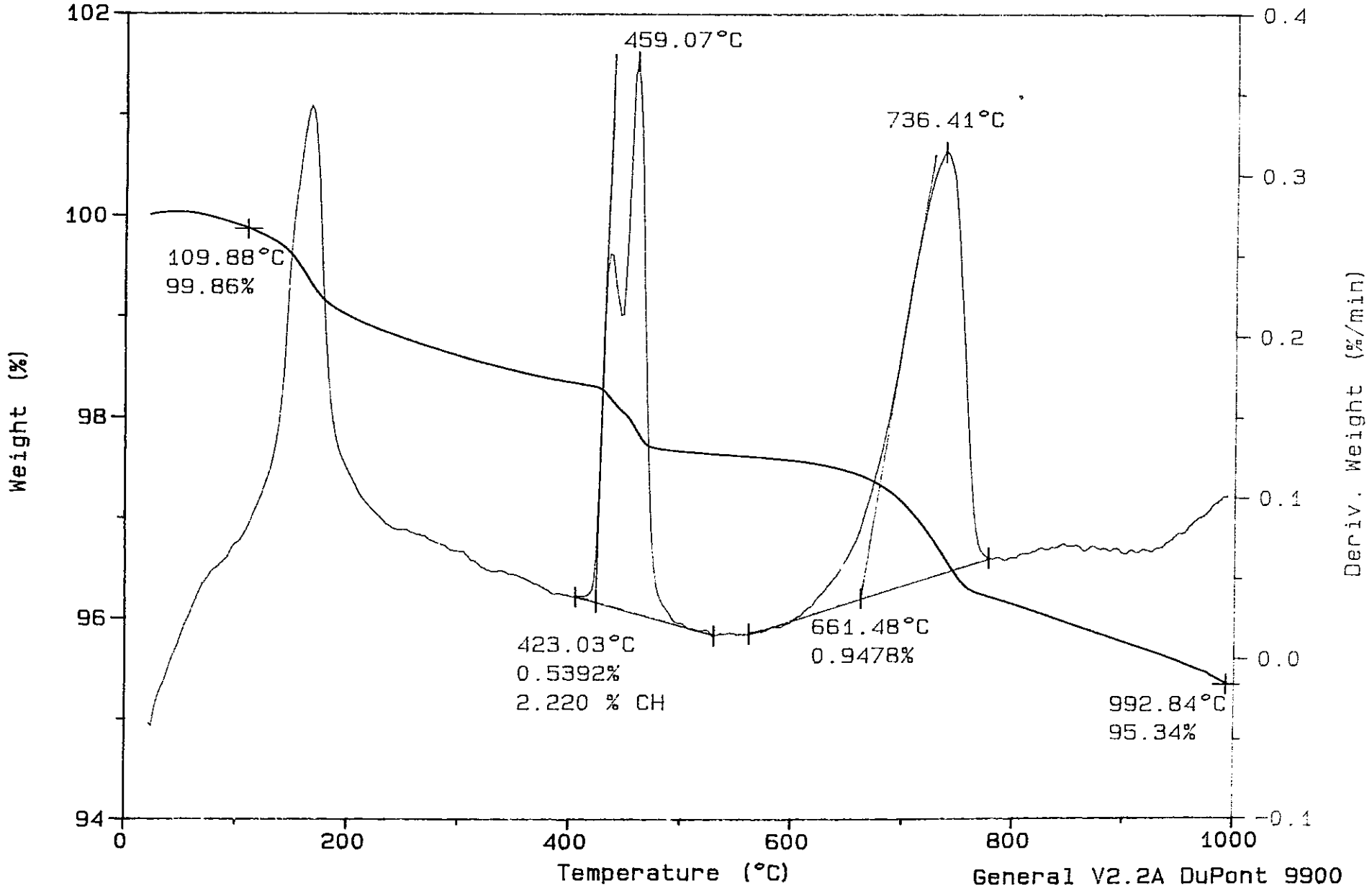

General V2.2A DuPont 9900

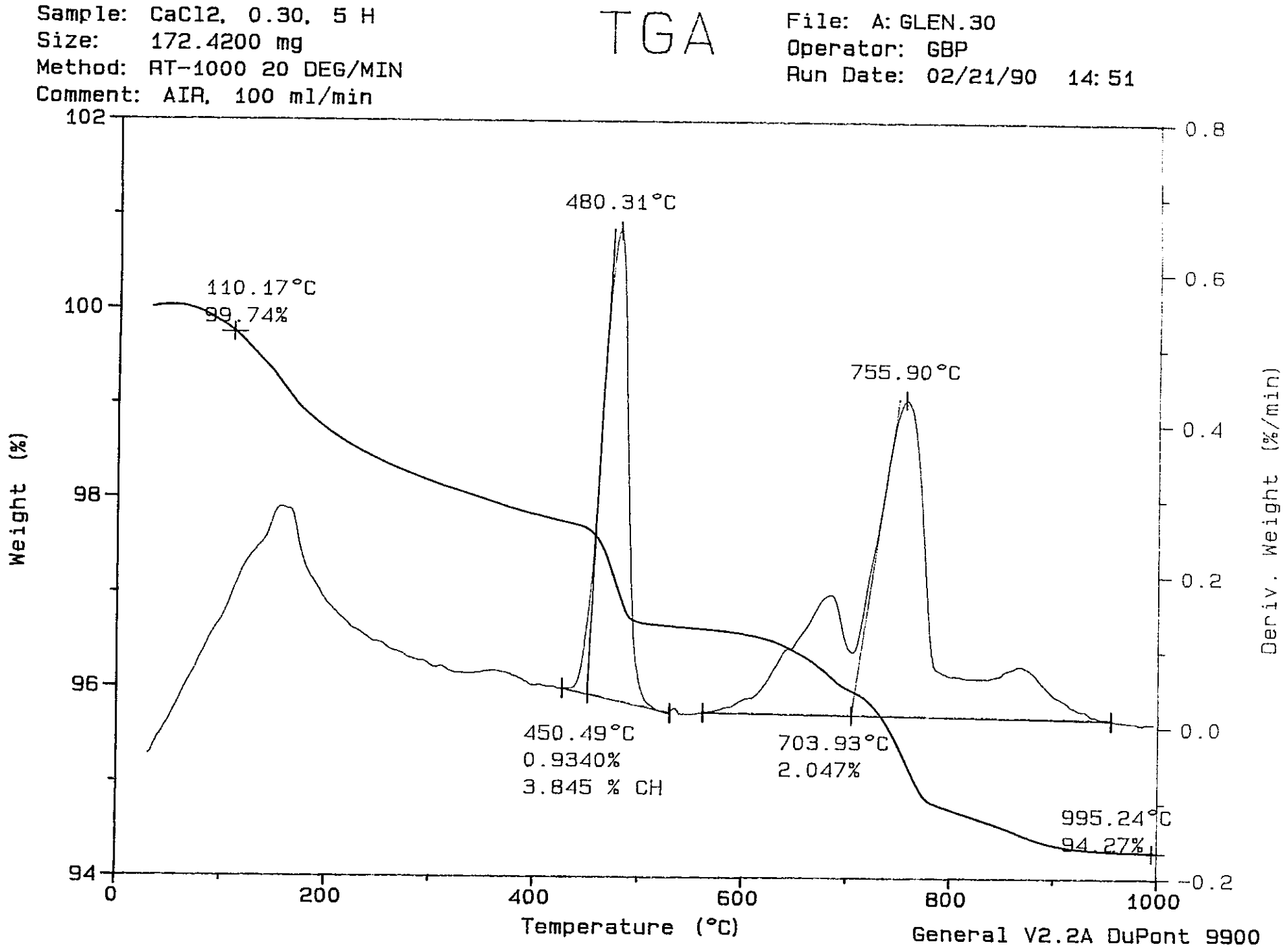
Sample: CaCl2, 0.30, 5 H
Size: 172.4200 mg
Method: RT-1000 20 DEG/MIN
Comment: AIR, 100 ml/min
TGA
File: A:GLEN.30
Operator: GBP
Run Date: 02/21/90 14:51
480.31°C
110.17°C
99.74%
755.90°C
450.49°C
0.9340%
3.845 % CH
703.93°C
2.047%
995.24°C
94.27%
Weight (%)
Deriv. Weight (%/min)
Temperature (°C)
General V2.2A DuPont 9900

Sample: CaCl2, 0.30, 1 DAY
Size: 185.7000 mg
Method: RT-1000 20 DEG/MIN
Comment: AIR, 100 ml/min

TGA

File: A:GLEN.32
Operator: GBP
Run Date: 02/22/90 07:44

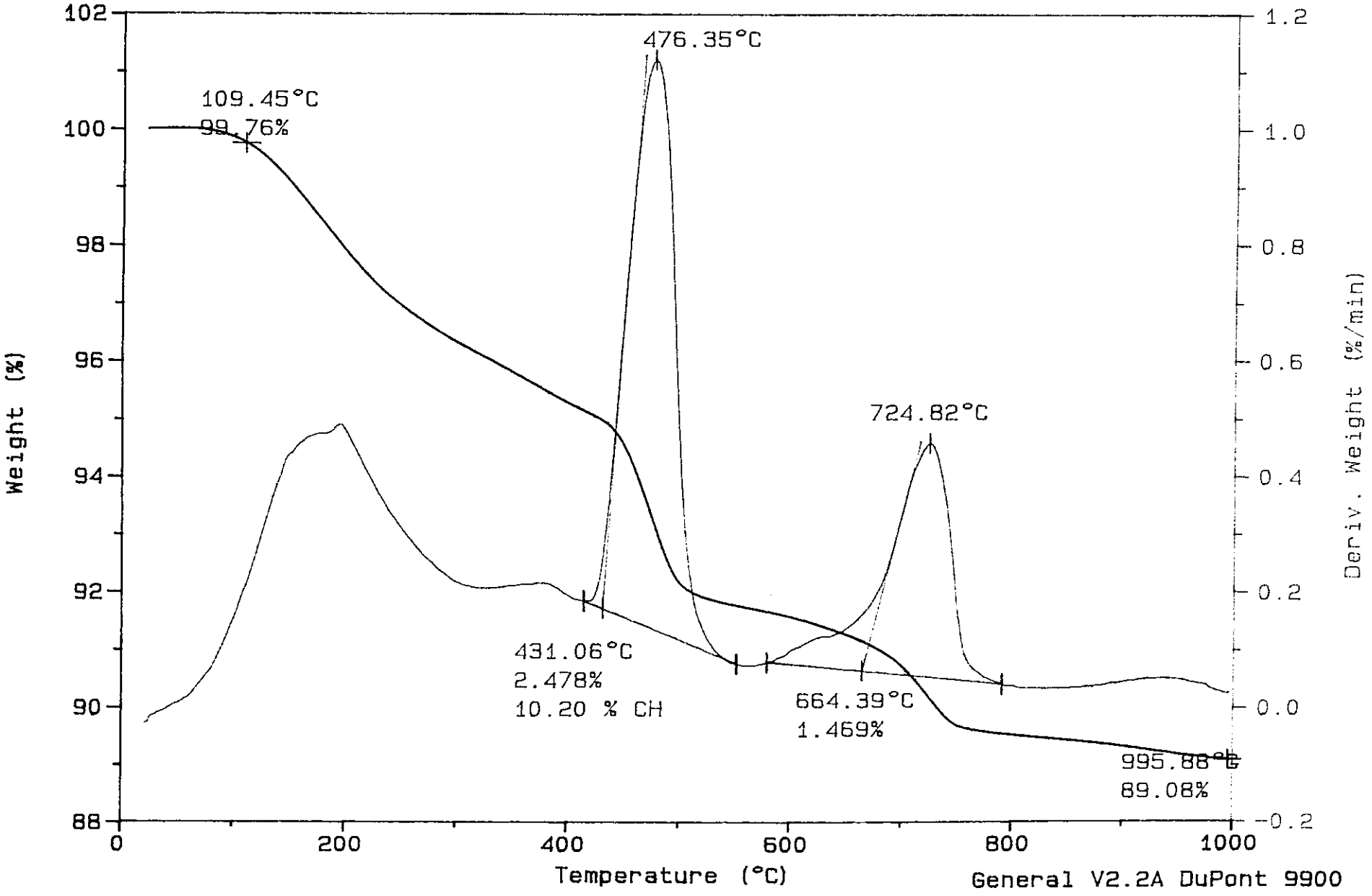

General V2.2A DuPont 9900

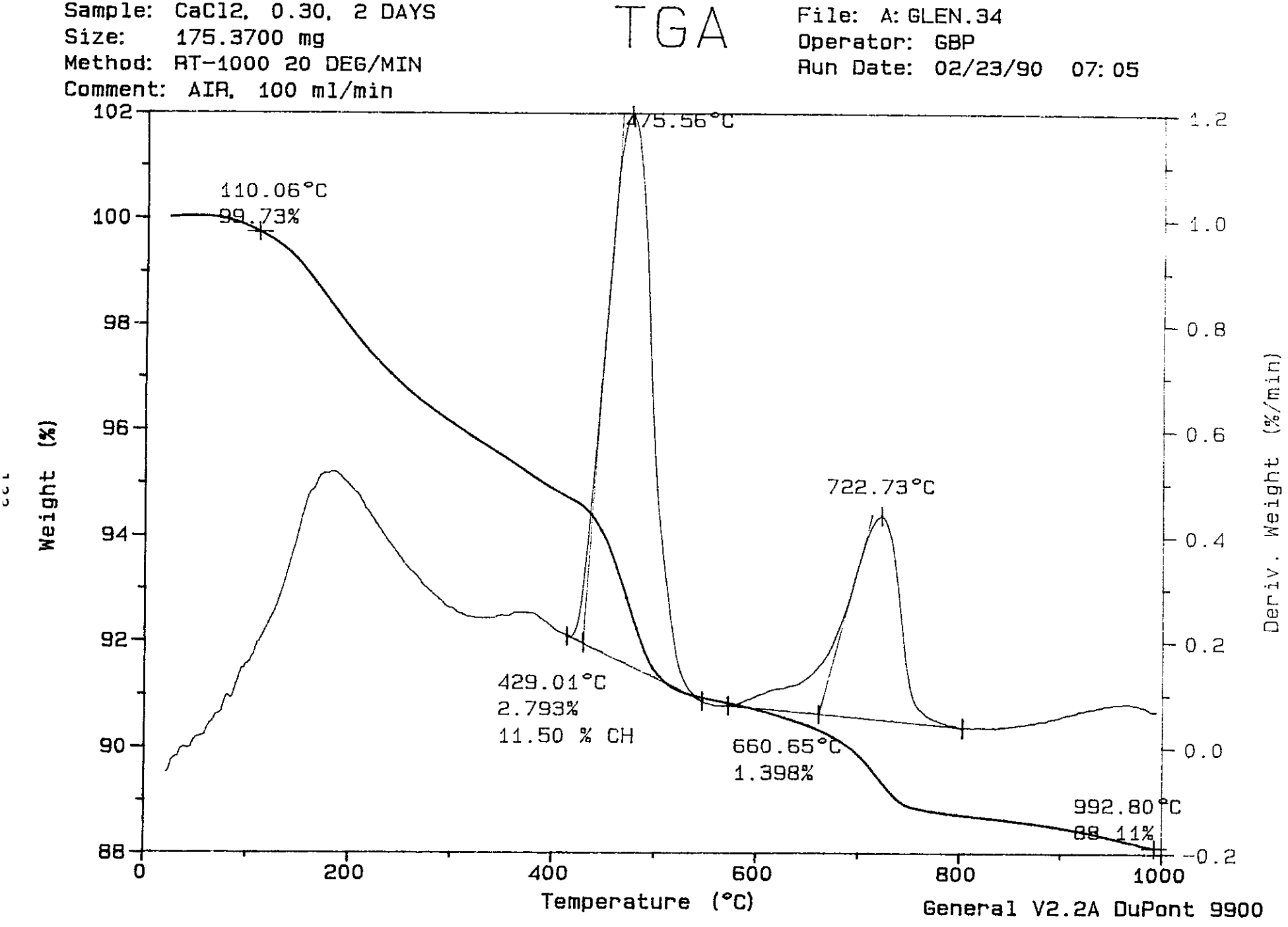
Sample: CaCl2, 0.30, 2 DAYS
Size: 175.3700 mg
Method: RT-1000 20 DEG/MIN
Comment: AIR, 100 ml/min
TGA
File: A:GLEN.34
Operator: GBP
Run Date: 02/23/90 07:05
475.56°C
110.06°C
99.73%
722.73°C
429.01°C
2.793%
11.50 % CH
660.65°C
1.398%
992.80°C
88.11%
Weight (%)
Deriv. Weight (%/min)
Temperature (°C)
General V2.2A DuPont 9900

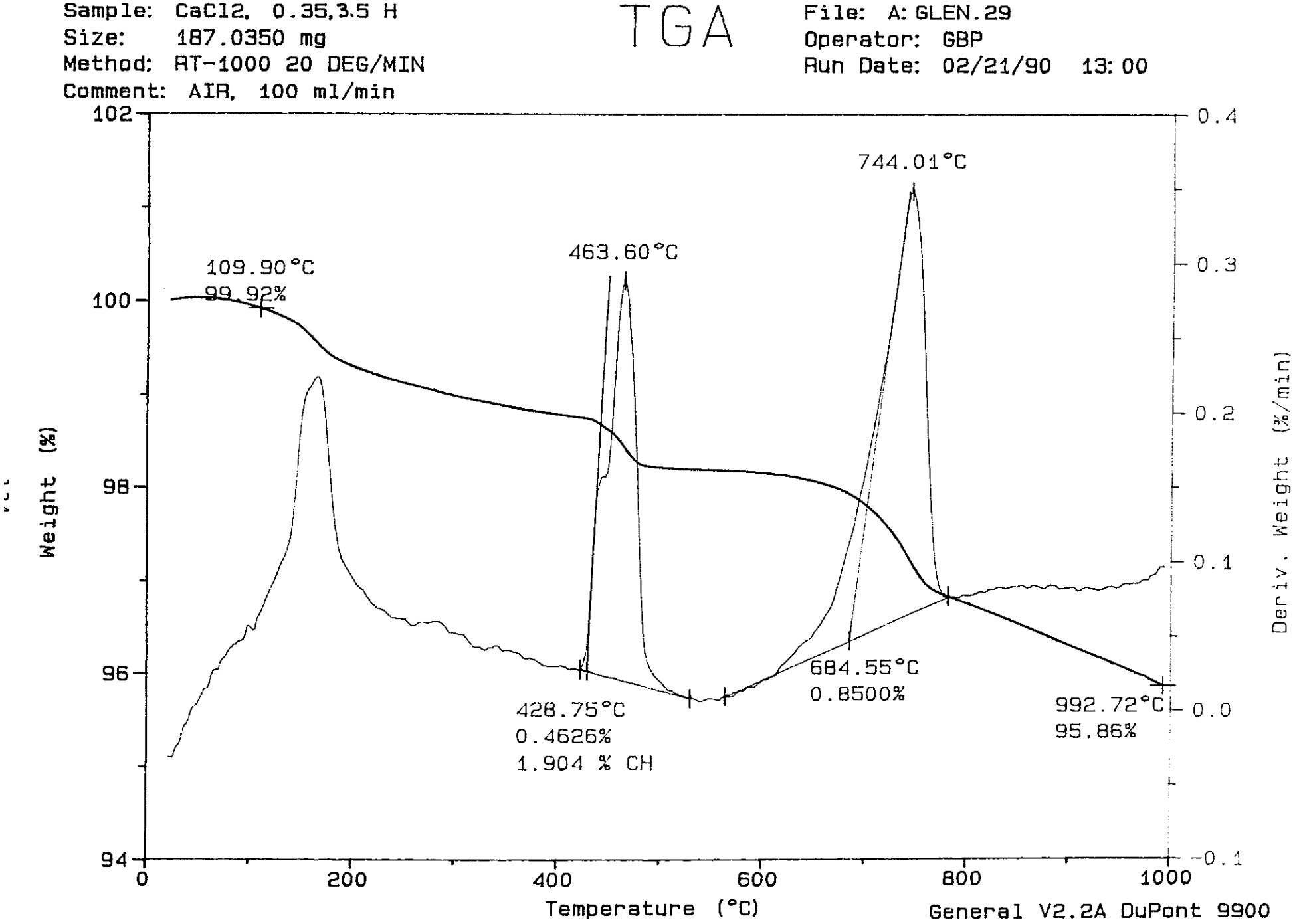
Sample: CaCl2, 0.35,3.5 H
Size: 187.0350 mg
Method: RT-1000 20 DEG/MIN
Comment: AIR, 100 ml/min
TGA
File: A:GLEN.29
Operator: GBP
Run Date: 02/21/90 13:00
109.90°C
99.92%
463.60°C
744.01°C
428.75°C
0.4626%
1.904 % CH
684.55°C
0.8500%
992.72°C
95.86%
Weight (%)
Deriv. Weight (%/min)
Temperature (°C)
General V2.2A DuPont 9900

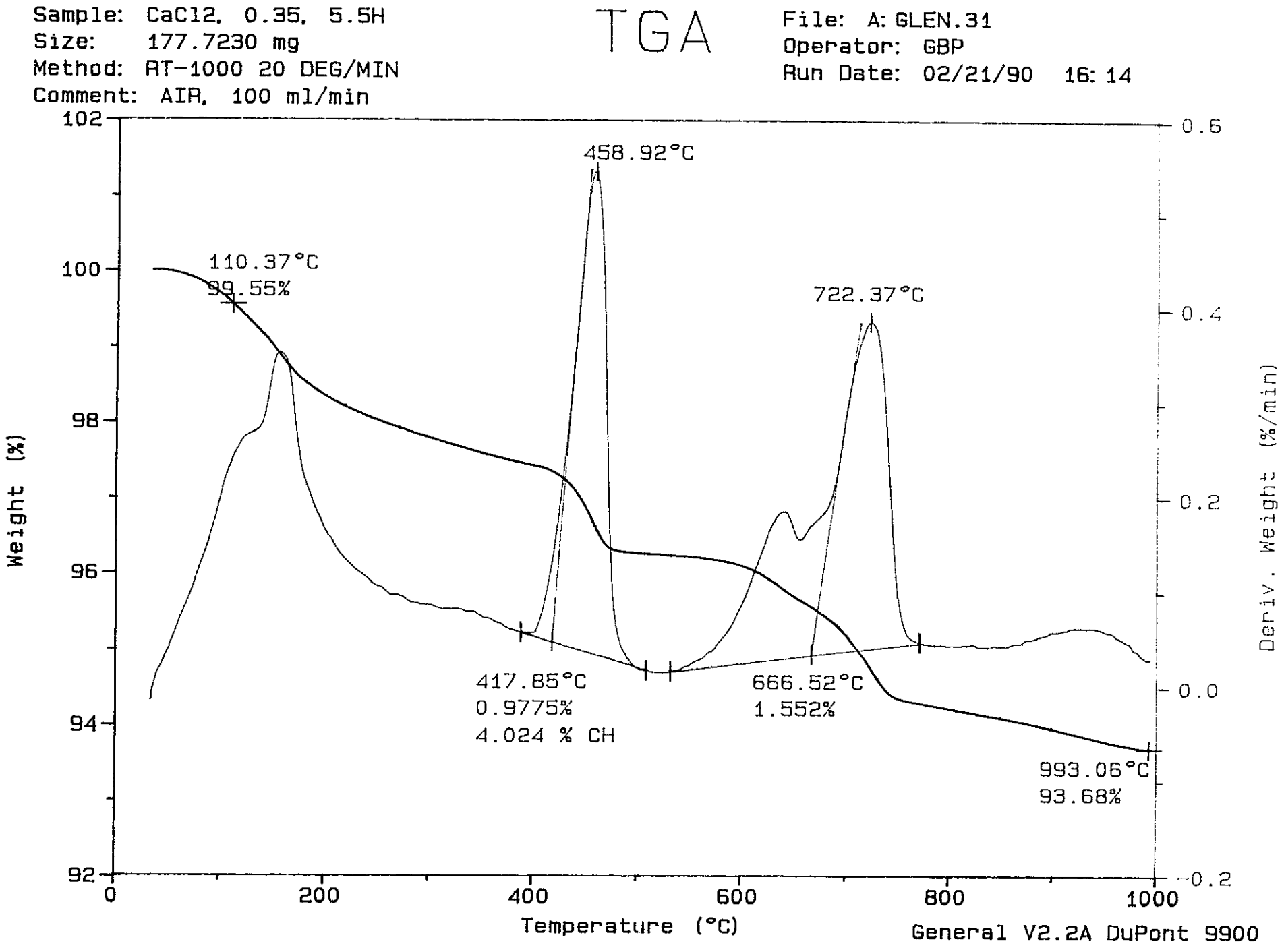
Sample: CaCl2, 0.35, 5.5H
Size: 177.7230 mg
Method: RT-1000 20 DEG/MIN
Comment: AIR, 100 ml/min
TGA
File: A:GLEN.31
Operator: GBP
Run Date: 02/21/90 16:14
458.92°C
110.37°C
99.55%
722.37°C
417.85°C
0.9775%
4.024 % CH
666.52°C
1.552%
993.06°C
93.68%
Weight (%)
Deriv. Weight (%/min)
Temperature (°C)
General V2.2A DuPont 9900

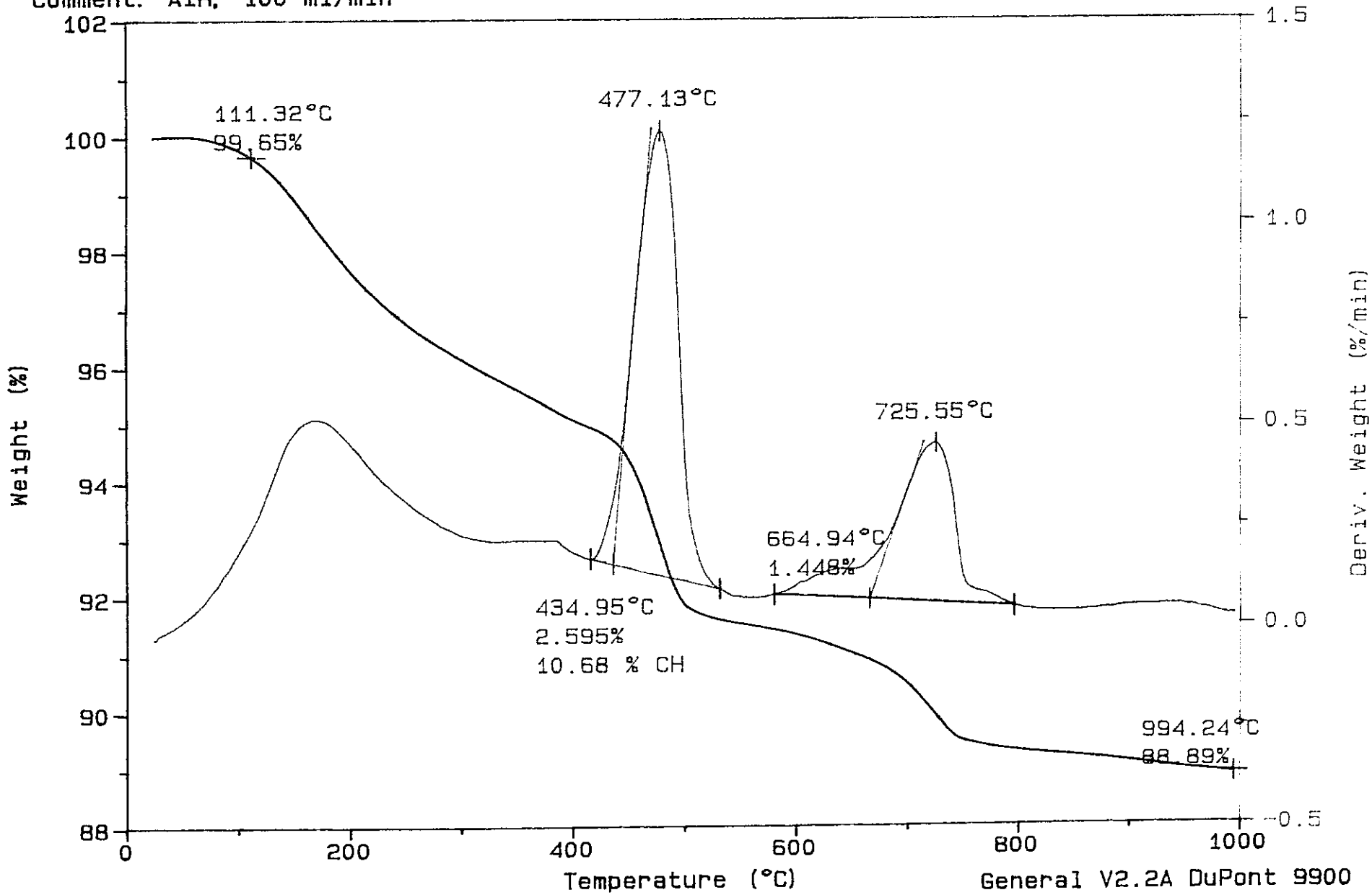
Sample: CaCl2, 0.35, 1 DAY
Size: 180.2530 mg
Method: RT-1000 20 DEG/MIN
Comment: AIR, 100 ml/min
TGA
File: A:GLEN.33
Operator: GBP
Run Date: 02/22/90 10:08
111.32°C
99.65%
477.13°C
725.55°C
664.94°C
1.448%
434.95°C
2.595%
10.68 % CH
994.24°C
88.89%
Weight (%)
Deriv. Weight (%/min)
Temperature (°C)
General V2.2A DuPont 9900

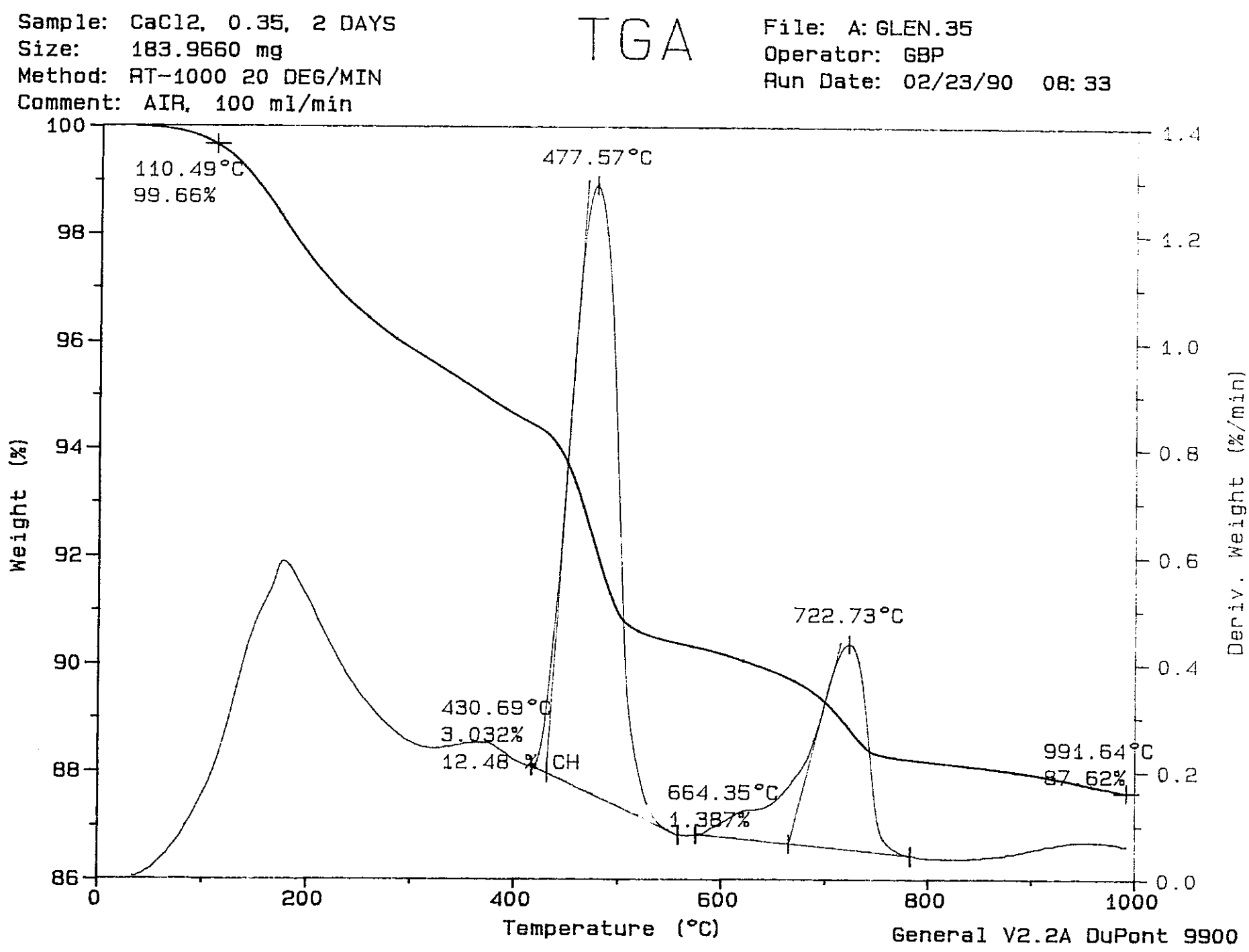
Sample: CaCl2, 0.35, 2 DAYS
Size: 183.9660 mg
Method: RT-1000 20 DEG/MIN
Comment: AIR, 100 ml/min
TGA
File: A:GLEN.35
Operator: GBP
Run Date: 02/23/90 08:33
110.49°C
99.66%
477.57°C
722.73°C
430.69°C
3.032%
12.48 % CH
664.35°C
1.387%
991.64°C
87.62%
Weight (%)
Deriv. Weight (%/min)
Temperature (°C)
General V2.2A DuPont 9900

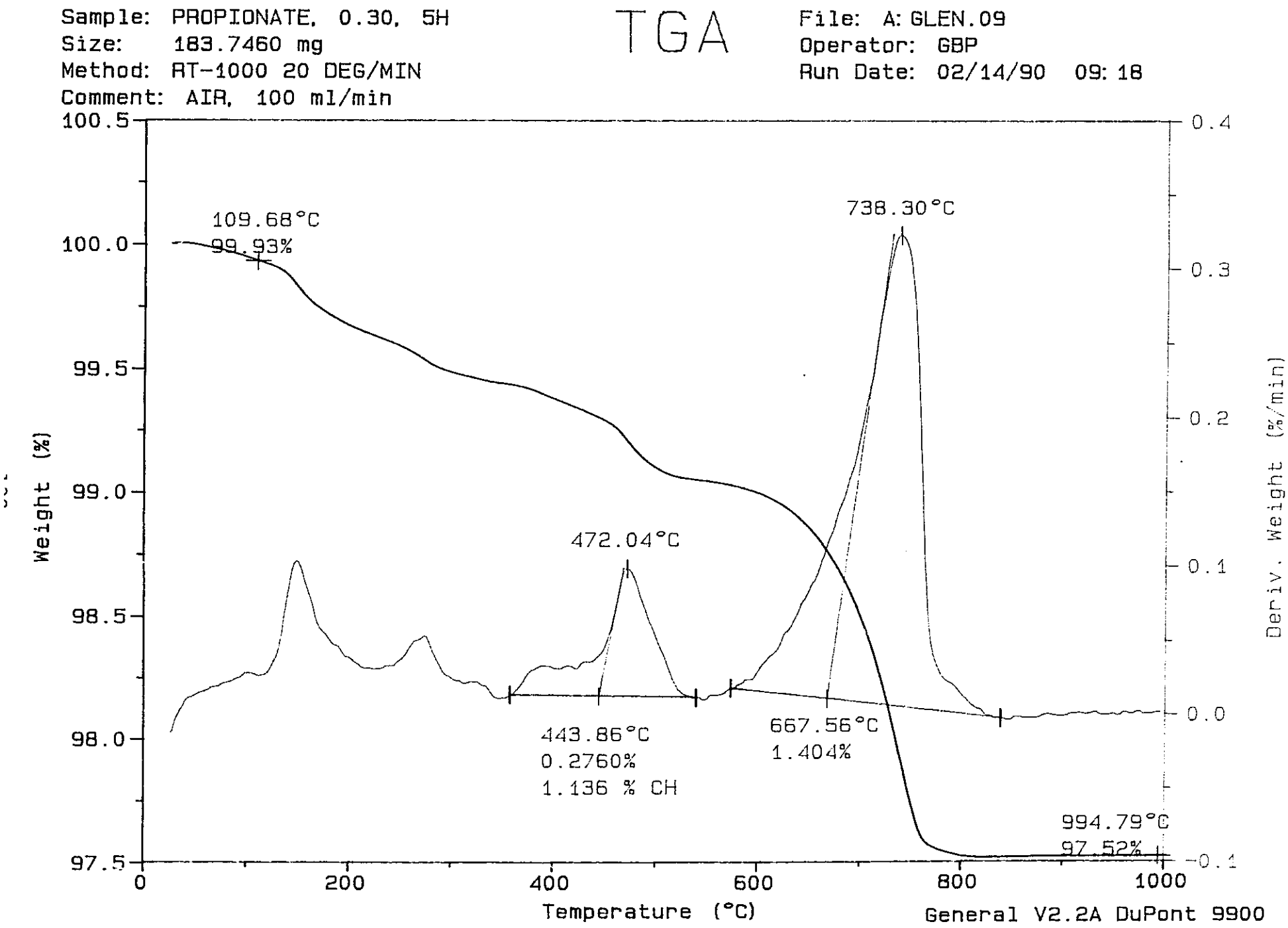
Sample: PROPIONATE, 0.30, 5H
Size: 183.7460 mg
Method: RT-1000 20 DEG/MIN
Comment: AIR, 100 ml/min
TGA
File: A:GLEN.09
Operator: GBP
Run Date: 02/14/90 09:18
109.68°C
99.93%
738.30°C
472.04°C
443.86°C
0.2760%
1.136 % CH
667.56°C
1.404%
994.79°C
97.52%
Weight (%)
Deriv. Weight (%/min)
Temperature (°C)
General V2.2A DuPont 9900

Sample: PROPIONATE, 0.30, 9 H
Size: 140.1330 mg
Method: RT-1000 20 DEG/MIN
Comment: AIR, 100 ml/min

TGA

File: A:GLEN.11
Operator: GBP
Run Date: 02/14/90 12:38

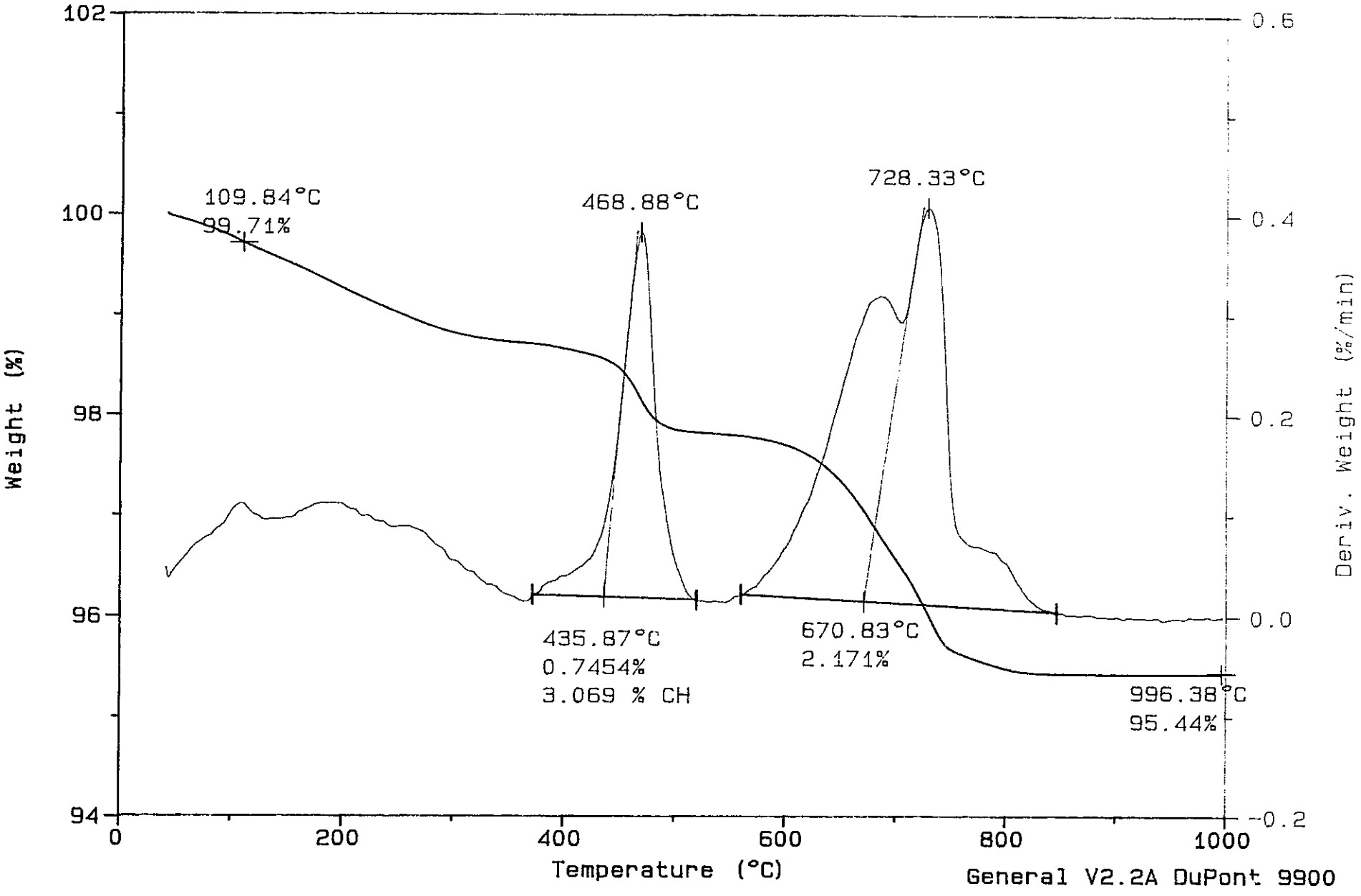

General V2.2A DuPont 9900

Sample: PROPIONATE, 0.30, 1 DAY
Size: 155.3090 mg
Method: RT-1000 20 DEG/MIN
Comment: AIR, 100 ml/min

TGA

File: A:GLEN.12
Operator: GBP
Run Date: 02/14/90 14:11

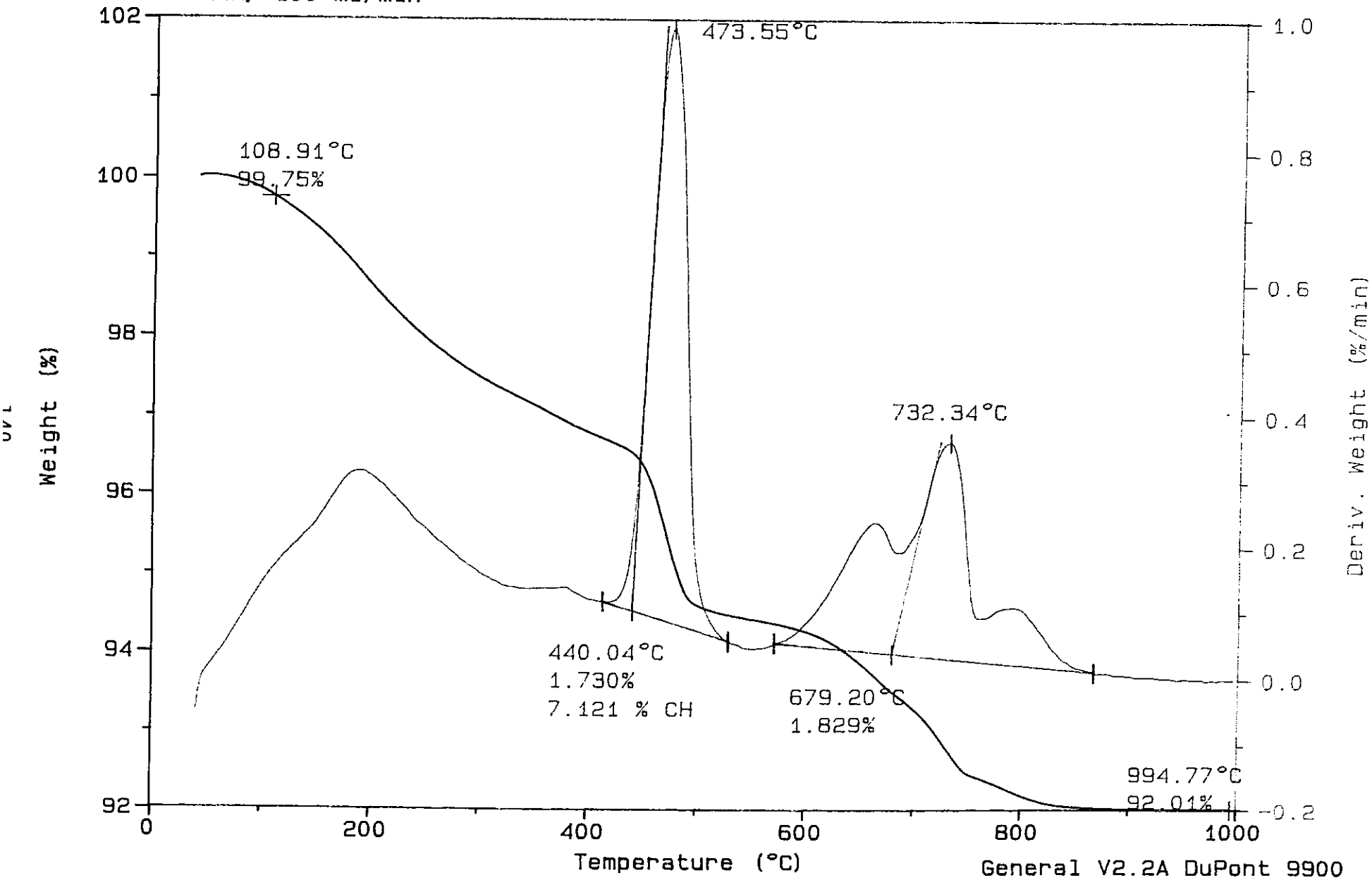

General V2.2A DuPont 9900

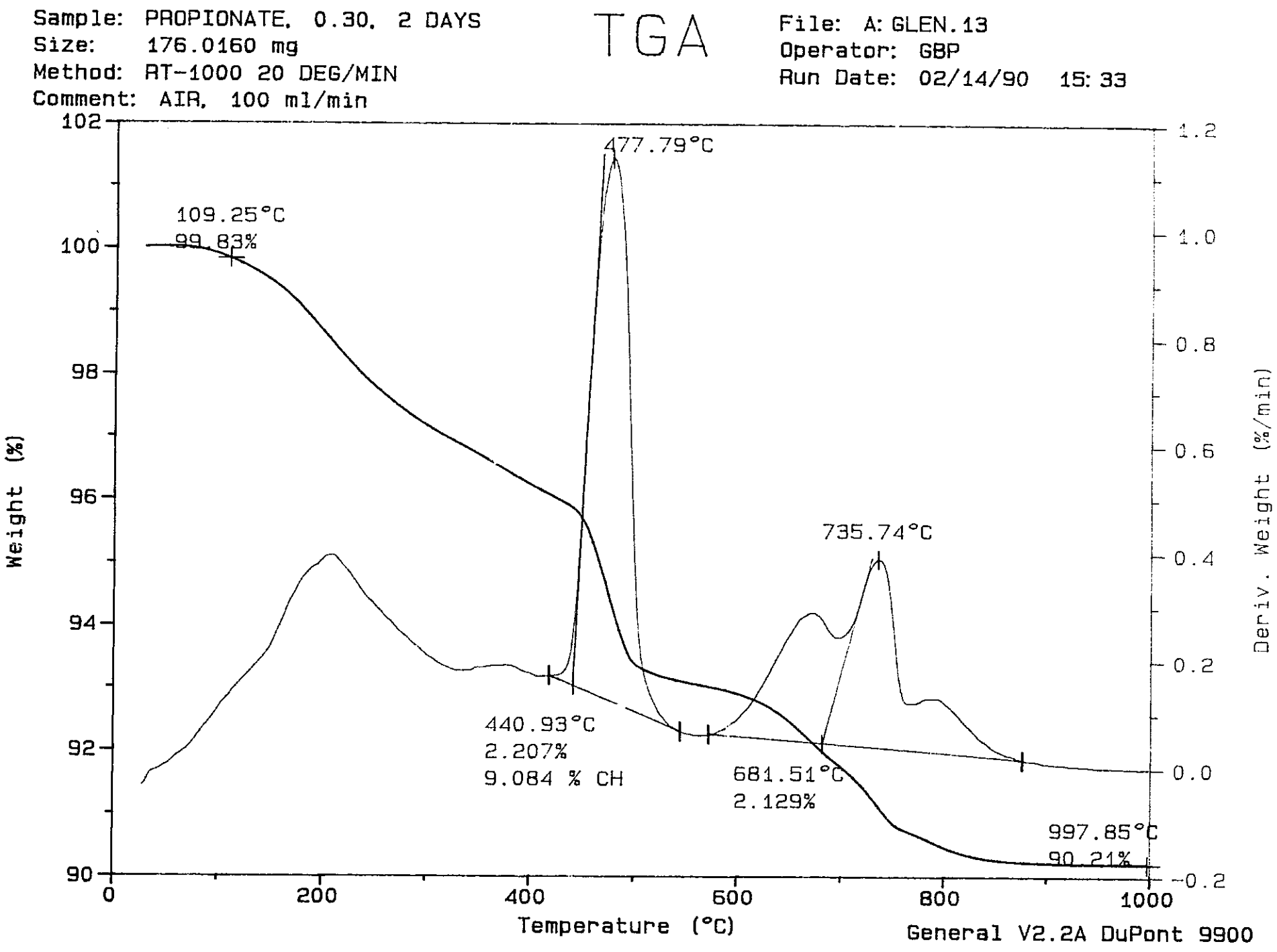
Sample: PROPIONATE, 0.30, 2 DAYS
Size: 176.0160 mg
Method: RT-1000 20 DEG/MIN
Comment: AIR, 100 ml/min
TGA
File: A:GLEN.13
Operator: GBP
Run Date: 02/14/90 15:33
477.79°C
109.25°C
99.83%
735.74°C
440.93°C
2.207%
9.084 % CH
681.51°C
2.129%
997.85°C
90.21%
Weight (%)
Deriv. Weight (%/min)
Temperature (°C)
General V2.2A DuPont 9900

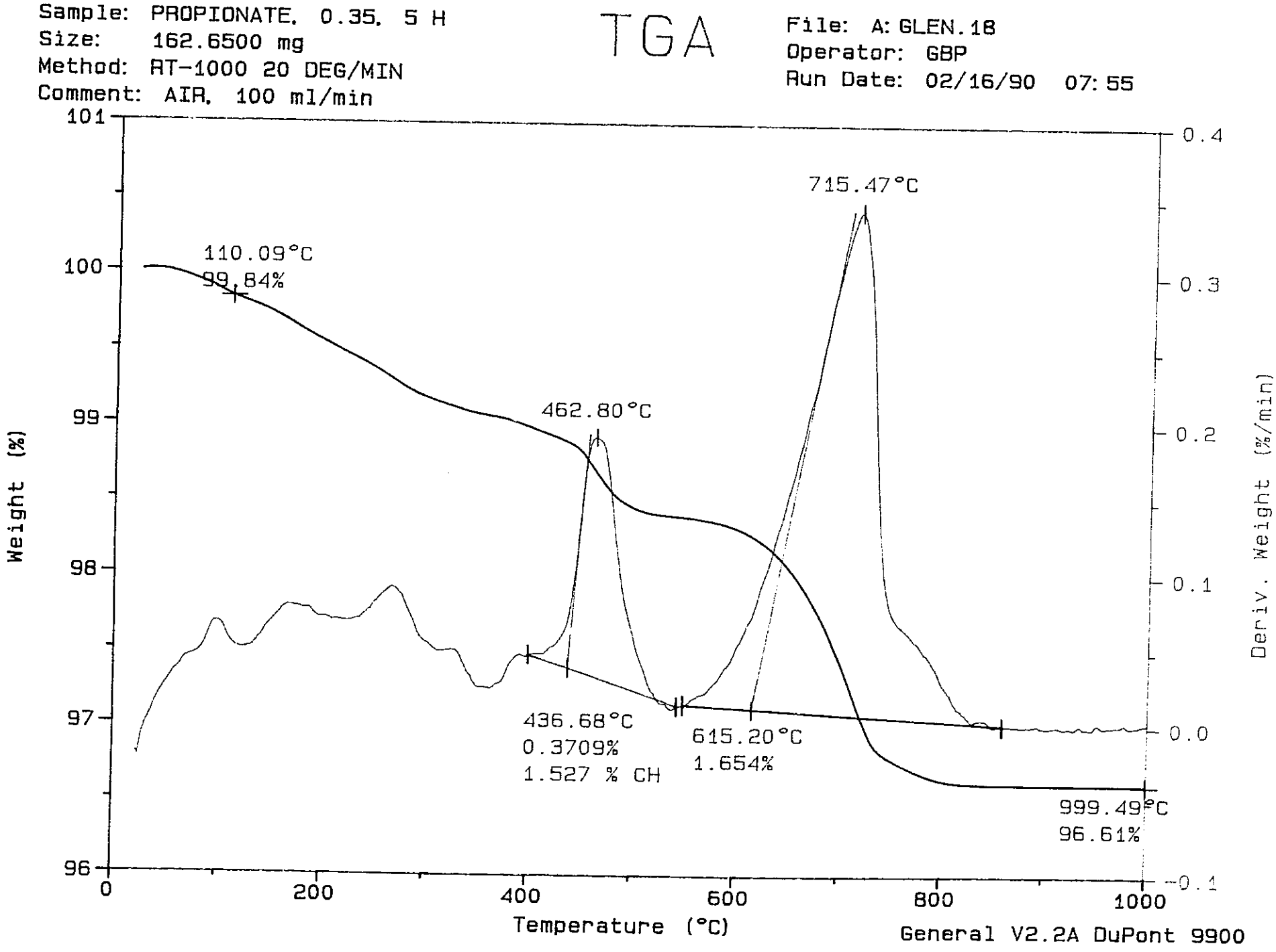
Sample: PROPIONATE, 0.35, 5 H
Size: 162.6500 mg
Method: RT-1000 20 DEG/MIN
Comment: AIR, 100 ml/min
TGA
File: A:GLEN.18
Operator: GBP
Run Date: 02/16/90 07:55
110.09°C
99.84%
462.80°C
715.47°C
436.68°C
0.3709%
1.527 % CH
615.20°C
1.654%
999.49°C
96.61%
Weight (%)
Deriv. Weight (%/min)
Temperature (°C)
General V2.2A DuPont 9900

Sample: PROPIONATE, 0.35, 9 H
Size: 155.5110 mg
Method: RT-1000 20 DEG/MIN
Comment: AIR, 100 ml/min

TGA

File: A:GLEN.19
Operator: GBP
Run Date: 02/16/90 09:49

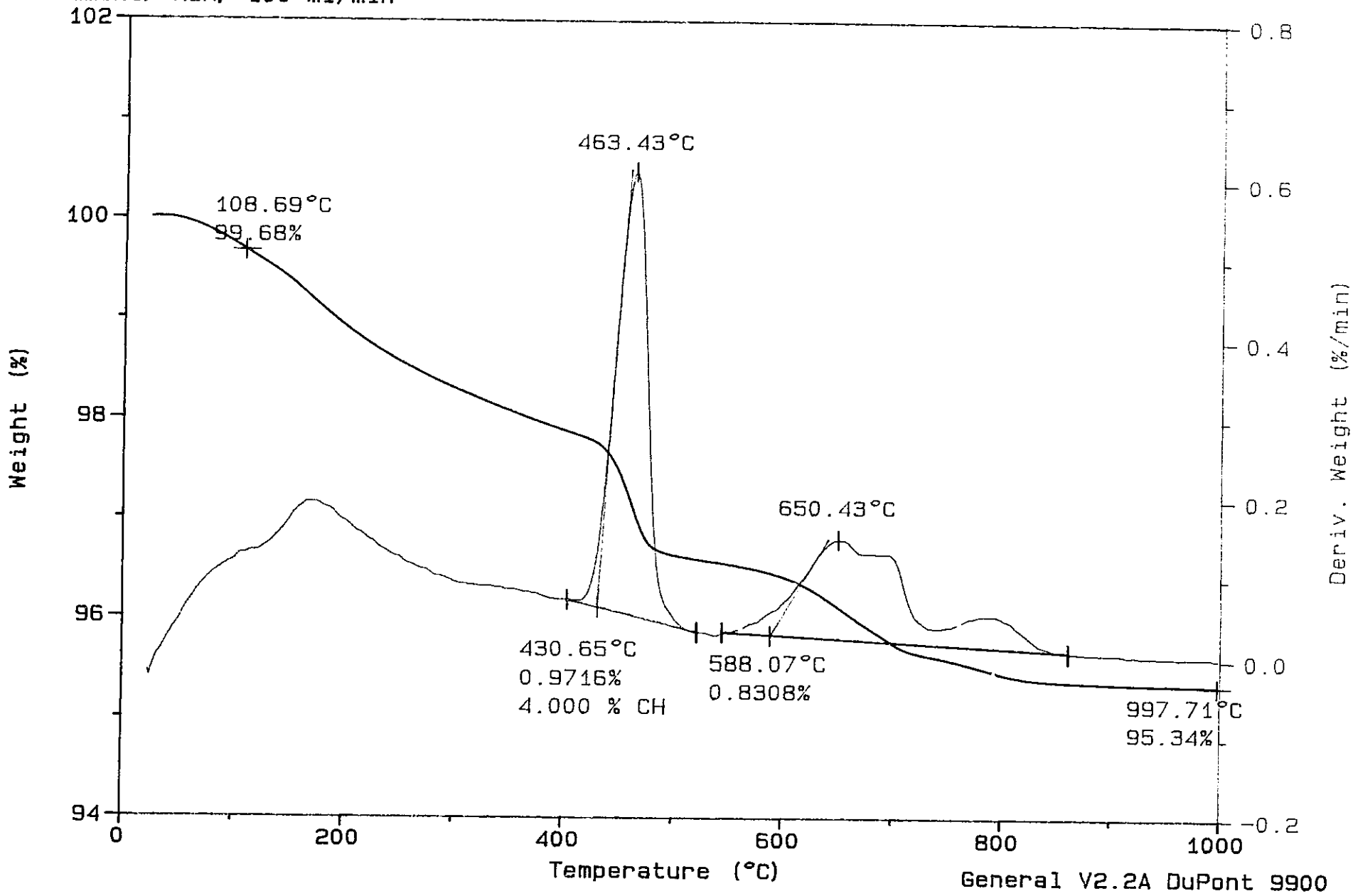

General V2.2A DuPont 9900

Sample: PROPIONATE, 0.35, 1 DAY
Size: 174.7060 mg
Method: RT-1000 20 DEG/MIN
Comment: AIR, 100 ml/min

TGA

File: A:GLEN.20
Operator: GBP
Run Date: 02/16/90 11:30

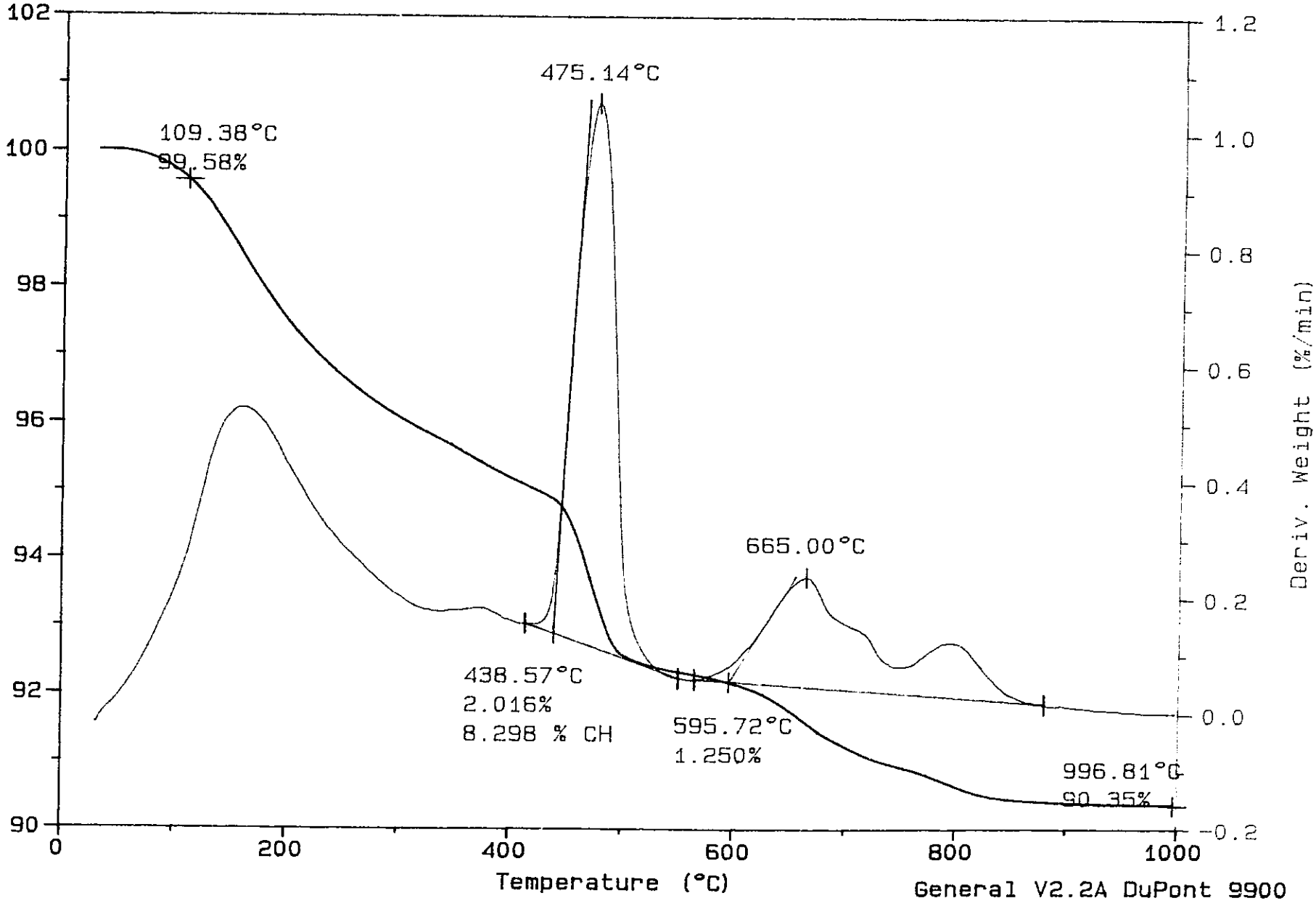

General V2.2A DuPont 9900

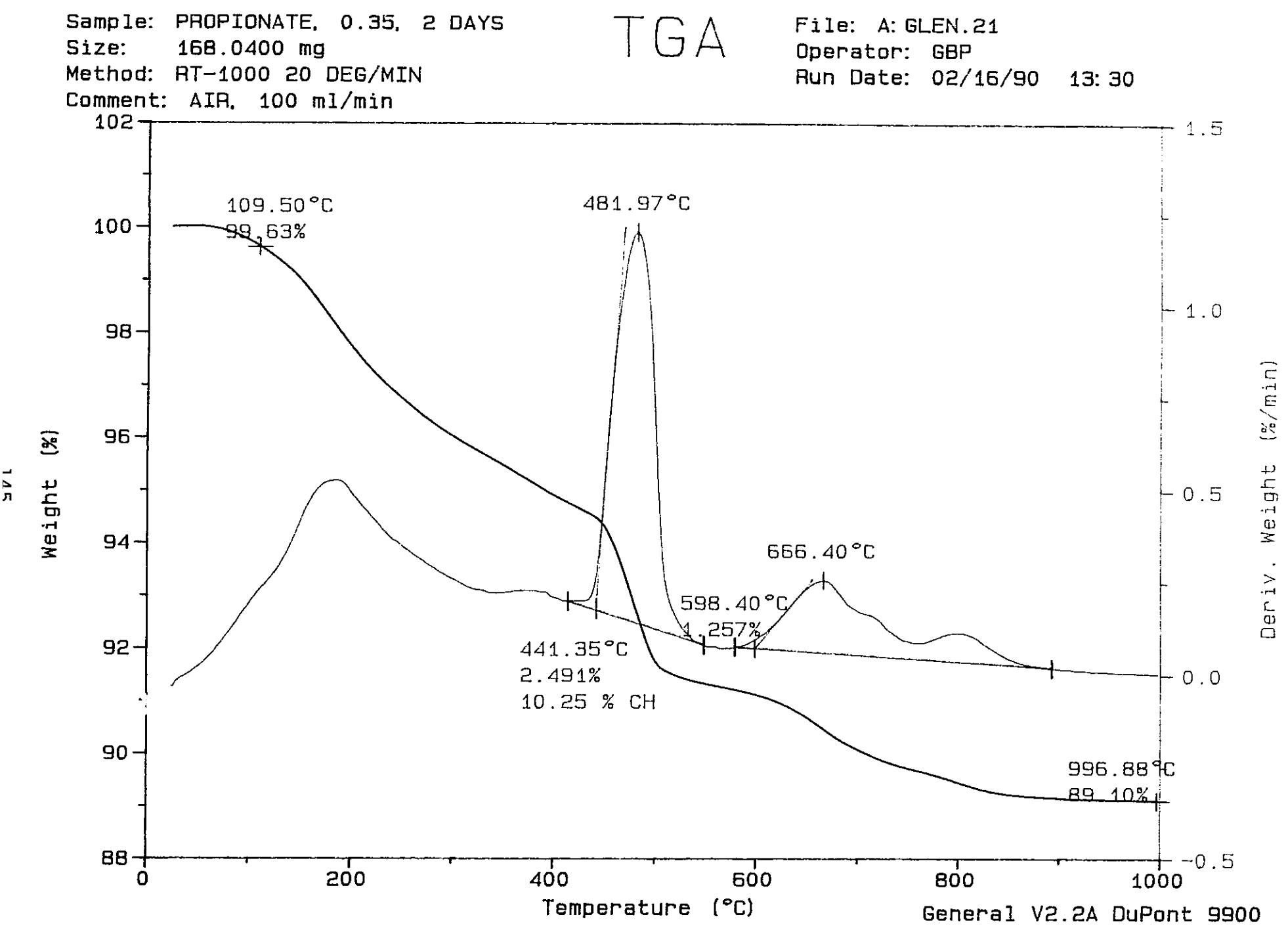
Sample: PROPIONATE, 0.35, 2 DAYS
Size: 168.0400 mg
Method: RT-1000 20 DEG/MIN
Comment: AIR, 100 ml/min
TGA
File: A:GLEN.21
Operator: GBP
Run Date: 02/16/90 13:30
109.50°C
99.63%
481.97°C
666.40°C
598.40°C
1.257%
441.35°C
2.491%
10.25 % CH
996.88°C
89.10%
Weight (%)
Deriv. Weight (%/min)
Temperature (°C)
General V2.2A DuPont 9900

Appendix B

Raw Data for Bond Strength vs. Paste Thickness Curves

Note: Above each set of data is a title which carries the following information: system name, w/c, hydration time, substrate type. The system names are abbreviated in the following manner:

Cement = Only Type 10 Portland Cement

CaCl2 = Cement + 2% $CaCl_2$

NaNO3 = Cement + 2% $NaNO_3$

Propionate = Cement + 2% $Ca(C_3H_5O_2)_2.H_2O$

SF = Cement + 10% Silica Fume

Clinker = Only Portland Cement Clinker

C3S = Only C_3S

C3S+Na = C_3S + 2% $NaNO_3$

C3S, 0.35, 1 d, steel

Thickness mm	Stress MPa
1.3665	0.4407
1.3513	0.5736
1.5773	0.4900
1.2624	0.7081
2.0472	0.2925
1.3627	0.6534
1.0224	0.7447
1.1074	0.5109
1.2624	0.4501
0.8039	0.8053
1.0224	0.8701
1.1303	0.5584
1.3640	0.6685

C3S, 0.35,2 days, steel

Thickness mm	Stress MPa
1.0046	0.5684
1.5253	0.6936
1.6167	0.3789
1.7132	0.3675
0.8623	0.7026
1.3703	0.4964

C3S, 0.35,7 days, steel

Thickness mm	Stress MPa
0.8649	0.6749
0.7264	0.5481
0.8052	0.7826
1.5812	0.2170
1.3843	0.1451
1.5875	0.2113
1.6154	0.2378
1.4122	0.2757
1.5469	0.1735
1.4453	0.5368

C3S, 0.35, 1 day, glass

Thickness mm	Stress MPa
0.8014	0.5736
1.5278	0.3058
1.8085	0.2279
1.2852	0.4938
1.5342	0.2716
1.1519	0.3761
1.2637	0.3400
0.9373	0.3001
0.7531	0.3438
0.9411	0.3001
0.9449	0.3969
1.4275	0.4691
0.9919	0.4407
1.2967	0.5204

C3S, 0.35, 2 days, glass

Thickness mm	Stress MPa
1.3373	0.1705
1.5392	0.1913
1.7564	0.1553
1.0935	0.3841

C3S, 0.35,7 days, glass.

Thickness mm	Stress MPa
0.9195	0.1508
0.9995	0.1319
1.5773	0.0846
1.3106	0.1300
1.1760	0.1054
1.4897	0.1167
1.3399	0.0846
1.2002	0.0903
1.0909	0.0865
1.0249	0.1073
1.1151	0.1300
1.2814	0.0770
1.2141	0.1527
1.1709	0.1091
0.9970	0.1091

C3S+Na, 0.35, 1 day, steel

Thickness mm	Stress MPa
0.9665	0.6226
1.1214	0.5129
1.1379	0.6605
1.0643	0.7233
1.1671	0.7681
0.5664	0.8591
1.3614	0.3918
1.5418	0.5053
1.1875	0.5488
1.0147	0.8970

C3S +Na, 0.35, 2 days, steel

Thickness mm	Stress MPa
1.0998	1.0018
1.4453	1.0398
1.3919	0.8667
1.4580	0.9446
0.9093	1.1522

C3S+Na, 0.35, 7 days, steel

Thickness mm	Stress MPa
1.1570	0.7267
0.4483	1.8485
0.7087	1.7382
1.1595	2.5594
1.1913	0.7116
1.6675	0.9095

C3S+Na, 0.35, 1 day, glass

Thickness mm	Stress MPa
1.5519	0.3374
1.4326	0.6705
1.5164	0.4472
1.3526	0.5475
0.9106	0.5229
0.9982	0.5021
1.1938	0.5153
0.8788	0.7784
0.7747	0.7274
0.7176	0.5191
0.9563	0.5418
0.9284	0.5872
1.3386	0.5570
1.0605	0.6175
1.1862	0.3867
1.2510	0.5948
1.8402	0.3942
1.3970	0.4624
1.7450	0.3110

C3S +Na, 0.35, 2 days, glass

Thickness mm	Stress mm
0.6388	0.6631
1.1684	0.3475
1.5126	0.1517
1.7374	0.1840
1.4872	0.3532
1.3703	0.1916
0.8928	0.3761
0.7684	0.5756
1.1252	0.5966
0.9233	0.5167
1.0782	0.5509
1.3780	0.1688
1.3017	0.3076

C3S+Na, 0.35, 7days, glass

Thickness mm	Stress MPa
1.1303	1.3032
1.3056	0.5082
1.2065	0.7309
1.1595	0.8901
1.1430	0.7612
0.9970	0.9246
0.7912	0.8846
0.8331	1.0598
1.2814	0.6909
0.8573	0.9377
0.8865	1.1528
1.5646	0.7081
1.3360	0.4247
1.4808	0.3165
1.5126	0.3068
1.5773	0.3599
1.7856	0.4268
1.7132	0.5061
1.7463	0.4268

Clinker, 0.30, 1 day, steel

Thickness mm	Stress MPa
0.9957	2.1188
0.6604	2.6001
1.1862	2.8104
0.6553	2.7518
1.4580	2.4105
1.4148	2.4450
1.7882	2.5601
1.4199	2.1112
1.2192	2.4788
1.9228	1.6982
2.0650	1.6658
2.1082	1.8444
2.1666	2.4374
2.3698	0.9274
2.1920	1.8217
2.6314	1.8217
2.2911	1.3004
0.9296	2.6780
0.9169	2.9642
1.0719	3.0717
0.7341	4.7334
1.7043	2.8007
1.5342	3.1965
1.3056	3.7385
1.5875	2.2760
2.3266	1.6320
2.1666	2.1306
1.8796	2.0940
2.1031	1.3287
1.4935	2.3195
1.7120	1.4652
1.6459	1.2852
1.6205	1.7306
1.5011	1.3818
1.9685	1.4466

Clinker, 0.30, 2 days, steel

Thickness mm	Stress MPa
0.7925	3.0924
1.0262	3.6219
1.7120	3.2496
1.3767	3.2303
1.2090	3.2151
1.2370	2.3064
2.0320	1.8582
1.9990	2.1967
1.8720	2.0719
2.2682	1.9320
1.9228	1.8734
2.4841	1.9223
2.2276	1.8299
1.7221	2.6560
0.9652	4.1377
1.0922	3.6743
1.0668	4.3735
1.0490	3.5082
0.9931	3.1248
1.3640	2.7766
1.3665	2.9242
1.3767	2.2816
2.0853	2.4008
2.1717	2.3422
1.9685	2.0037
1.4529	2.5615
1.5443	2.1547
1.9761	2.2098

Clinker, 0.35, 1 day, steel

Thickness mm	Stress MPa
1.1760	1.5914
0.9881	1.7713
1.3741	1.6348
1.8694	1.4514
1.8796	0.9625
2.3876	1.2976
2.0447	1.1990
2.1844	1.1046

Clinker, 0.35, 2 days, steel

Thickness mm	Stress MPa
0.9500	3.0117
1.0008	2.3395
1.5240	2.7863
1.6688	2.2367
1.0592	3.4489
1.7120	2.0133
2.0701	1.5024
1.7678	1.6196
2.1742	1.2845
1.9812	1.7410
1.6510	1.5307
1.5799	1.8451
1.5900	2.7787
1.9177	0.8543
2.0955	1.6403
2.2936	1.2880
2.0650	1.4280
2.1285	1.6844
2.2174	1.5417
1.8948	1.4114

Clinker, 0.30, 1 day, glass

Thickness mm	Stress MPa
0.6909	2.5691
1.2344	2.8897
0.8128	2.8725
0.6731	3.0014
1.2954	2.6904
1.5545	1.6355
1.0160	2.1981
1.3716	1.8099
1.5519	2.5767
1.6916	1.3363
1.8999	1.1846
1.5900	1.5479
1.4605	1.8320
1.9050	2.3643
1.5900	2.2981
2.1996	1.1977
1.1709	3.3365
1.0541	2.6339
1.1659	2.4629
0.8179	3.7950
1.0008	2.9497
1.1582	1.9120
1.0592	1.9534
1.3335	2.0540
1.4122	1.7851
1.9228	1.6279
1.6180	2.0292
1.7170	1.3211
2.0345	1.3245
2.1412	0.9612
1.8567	2.3043
1.7348	2.6642
2.4257	0.7453
2.2631	0.7771
2.0676	1.1880

Clinker, 0.30, 2 days, glass

Thickness mm	Stress MPa
0.6350	3.6468
0.6401	2.8194
0.5893	2.4884
0.8788	2.4898
0.6350	2.4257
1.0592	2.3043
1.1074	2.3995
1.4173	2.2967
1.1811	2.3084
1.2852	2.8931
1.6586	2.3160
1.5088	1.8672
1.5138	2.1112
1.4986	2.0354
2.3216	1.2666
1.9202	2.3215
1.9787	2.1154
1.7704	2.6153
2.5222	1.7555
0.7747	3.1165
0.7341	3.2834
1.1024	2.4919
1.0287	2.5112
1.1557	2.9221
1.3411	2.7952
1.1227	2.6456
2.0803	1.4583
1.5062	2.4974
1.7170	1.9713
1.8669	1.7803
2.2301	1.2156
2.3800	1.0280
1.9914	1.6114

Clinker, 0.35, 1 day, glass

Thickness mm	Stress MPa
0.8052	2.6187
1.3360	2.5374
1.4808	2.2850
1.4681	1.6162
1.6891	2.0878
1.9075	1.5645
2.1082	1.1742
2.0498	0.9329
1.7602	0.9350
2.1514	0.8570
1.3335	1.6769
1.6434	1.3976
2.0955	0.9770
1.8898	0.8040
2.0726	1.3866

Clinker, 0.35, 2 days, glass

Thickness mm	Stress MPa
0.4750	1.4197
0.9804	1.1846
0.9068	1.3307
0.9449	1.4742
1.7120	0.9881
1.5621	0.9839
2.2225	1.2680
2.3393	1.1073
1.5367	1.2128
1.9583	1.2190
0.7976	1.7203
0.6883	1.6789
0.8661	1.1184
0.7925	1.0922
1.3183	1.0012
1.2852	1.6541
1.4530	1.0163
1.5672	1.3363
1.3564	1.2907
1.9202	0.9274
1.4046	1.2039
1.7526	1.5727
2.1234	1.5141
2.1184	1.4080

SF, 0.30, 1 day, steel

Thickness mm	Stress MPa
1.1633	4.7003
0.9525	3.1724
1.3970	3.9922
1.7399	2.7683
2.0345	0.7274
0.9373	3.3220
1.1582	3.2710
0.8458	3.3317
1.3818	3.1365
1.3538	3.4930
1.5926	2.0526
2.5146	0.8129
1.8186	2.8842
1.9888	1.4907
2.1082	0.7157

SF, 0.30, 2 days, steel

Thickness mm	Stress MPa
0.8712	2.3946
0.7493	1.8982
1.9253	1.5507
1.3614	1.3500
1.8288	1.8941
1.7932	2.1995
1.1227	1.4900
1.0135	1.5734
2.4232	1.2721
2.6213	0.8226
2.5730	1.8451
0.9398	2.0023
1.3970	2.0857
1.2446	1.4107
0.8534	1.9968
0.8001	1.6589
0.9220	1.6024
1.7145	1.7844
1.2776	2.0306

SF, 0.30, steel, 7 days

Thickness mm	Stress MPa
1.7463	1.9582
1.7183	2.0906
1.1405	2.4036
1.1049	3.1483
0.7836	3.0007
1.8631	2.6953
1.7983	2.8449
2.7864	1.2756
2.4994	2.0947
2.2339	0.8908
2.5844	0.8377
1.5634	2.0547
1.9304	2.6746

SF, 0.35, 1 day, steel

Thickness mm	Stress MPa
1.0770	1.1315
1.0922	0.8874
0.7722	1.1804
0.9855	0.7419
0.8255	0.9384
1.3030	0.6454
0.9500	0.9232
1.1049	0.8646
1.2522	0.7171
0.9804	0.8757
1.6205	0.5054
1.6459	0.5054
1.2344	0.6564
1.4986	0.5109
1.2116	0.7943
1.9761	0.4785
2.4765	0.4523
1.7475	0.3330
2.4206	0.4827
1.7628	0.5695
0.8306	0.6261
1.1227	0.8288
1.5189	0.3785
2.0472	0.5695
2.6289	0.4489
1.8034	0.3634

SF, 0.35,2 days, steel

Thickness mm	Stress MPa
0.9525	3.9198
0.9804	3.0310
1.3005	1.8975
1.4351	2.4436
1.8593	1.6451
1.7678	1.9527
1.9990	1.4445
1.4986	1.4521
2.0625	1.5769
2.1361	2.0926
2.6289	1.6189
2.3470	0.9198
1.8821	2.8545

SF, 0.35, steel, 7 days

Thickness mm	Stress MPa
0.6934	6.6495
0.4813	4.4514
0.9601	4.3356
0.3801	1.5562
1.0135	2.0175
1.2573	1.0384
1.2840	1.7024
1.7932	1.0536
1.5697	0.9150
1.6358	1.2094
2.4663	0.6378
1.9431	0.6950
2.1933	1.5700
2.3343	0.8336

SF, 0.30, 1 day, glass

Thickness mm	Stress MPa
0.4674	1.9623
0.9423	1.7003
1.3741	1.2487
1.3843	2.2078
2.5324	1.3666
1.6078	1.6700
2.1438	0.5709
1.7526	1.0018
2.6264	0.3792
2.2631	1.1239
2.3241	1.4542
0.7493	1.9471
0.7112	1.9437
0.8433	1.4390
0.9855	1.4045
1.1582	2.3822
1.0973	2.2547
1.1532	1.3135
1.3868	1.1804
1.7882	0.9791
1.7069	1.5465
2.0625	0.5999
1.7297	1.9471
1.6053	1.0701
2.1996	0.5902
1.9304	1.2887
1.9507	1.2790
2.4130	0.9108
2.0193	1.5962

SF, 0.30, 2 days, glass

Thickness mm	Stress MPa
1.6510	1.2252
1.4275	0.8529
1.2471	1.5390
1.3005	1.6355
1.8796	0.6902
1.6637	1.6713
1.5494	2.0058
1.5621	2.0113
1.7145	0.9701
1.7374	0.8053
1.8999	0.4859
1.0998	2.8469
1.1506	1.7148
1.1100	2.3629
1.1074	2.4732
1.0566	2.3484
1.2040	1.7755
1.0693	2.1002
1.8644	0.7357
1.0744	1.5355
1.8085	1.4342
1.2979	2.9607
2.2428	0.5313
2.0498	1.3652
2.2758	1.2025
2.4359	0.4273
1.6713	1.4673

SF, 0.35, 1 day, glass

Thickness mm	Stress MPa
1.0973	1.6824
1.1024	2.4367
1.6053	1.3666
1.1227	1.6052
1.7221	1.5141
1.0973	1.5348
1.3208	2.0251
2.1234	1.6748
1.4961	1.1191
2.0320	0.7316
2.3444	1.1039
1.4732	1.4824
2.2352	0.8639
0.9093	3.1820
0.9627	2.9118
1.0439	2.3402
1.3386	2.2554
1.5265	1.5500
1.7297	1.4424
2.0015	1.5900
1.9660	0.9226
2.3063	0.9501
1.9101	0.8412
2.1996	0.4103

SF, 0.35, 2 days, glass

Thickness mm	Stress MPa
0.8484	2.2981
1.0490	2.7056
0.7849	1.8437
0.9246	1.8320
1.1735	1.9099
1.6434	1.9327
1.3919	1.2466
1.3157	1.3494
1.3233	1.1901
1.8466	1.1349
1.4122	1.1218
0.7239	2.7677
0.6375	3.0600
0.8941	2.9876
0.5842	2.7587
0.4191	3.4730
0.7417	1.8472
1.0719	1.2963
1.0693	1.2942
0.9703	1.6334
0.6807	2.0595
1.6358	0.8605
1.4072	2.2395
2.0244	1.0177
0.6731	2.7663
2.2454	1.4362
2.3063	1.2142

SF, 0.30, 7 days, glass

Thickness mm	Stress MPa
0.9995	2.4974
1.7259	1.6003
2.0320	1.2721
1.0795	3.3130
1.7856	2.2036
1.5608	1.4031
1.8453	2.1237
2.7178	1.2252

SF, 0.35, 7 days, glass

Thickness mm	Stress MPa
0.3937	2.8137
0.9411	2.6504
1.2256	1.5755
2.1425	1.3211
2.4943	1.3914
1.5354	1.5217
0.9398	1.9692
2.4105	0.2917
2.2568	0.6727
2.2835	0.9398
2.1019	0.8074
1.9977	0.7598

Cement, 0.30,1 day,steel,

Thickness mm	Streess MPa
1.9888	3.0435
1.9609	2.7242
2.2581	2.2891
1.8720	2.7580
1.7094	3.5868
1.0262	3.4406
1.7450	2.3098
1.7882	2.2209
1.9660	2.3229
2.0117	3.0476
1.8390	3.1345
1.7069	2.9393
2.0168	2.9662
1.4630	3.1965
2.0295	2.7808
1.7501	2.1223
1.3284	2.3719
1.5672	2.3326
1.1532	2.6691
1.2725	3.0662
1.5621	3.5523
1.4554	2.9283
1.3970	3.7757
1.4783	3.6013
1.2116	2.9393
1.4122	2.3457
1.3360	2.4195
1.1938	4.2487
1.5875	3.6088
1.7475	2.0657
1.6586	2.8828
1.2040	3.6509
1.6662	2.4367
1.5646	2.5594
1.6256	2.3912
1.8898	2.4064
1.3894	4.0591
2.0650	3.3213
1.8923	2.6863
1.9964	2.2092
1.4453	3.5599

Cement, 0.30, 2 days,steel

Thickness mm	Stress MPa
0.6299	1.5376
1.7196	1.5679
0.6883	1.7506
0.6248	2.2423
0.6375	1.5790
1.4249	1.5962
1.9634	1.2445
1.8567	1.3204
1.4173	1.3804
1.6840	1.5334
1.5926	1.3583
0.8153	1.7830
0.9500	1.4921
0.4470	1.8548
0.7087	2.2857
0.8026	1.6148
1.2040	1.3487
1.4275	1.3183
1.6104	1.7341
1.2116	1.9396
1.7907	1.5755
1.3132	1.6148
1.1278	1.4300
1.7094	1.3087
1.2954	1.3714
1.8542	1.1542
1.2649	1.7451

Cement, 0.30, 7 days,steel

Thickness mm	Stress MPa
0.9436	4.1184
1.2014	3.6916
0.8865	3.8543
0.9474	4.4273
1.4834	3.1683
2.0180	2.6711
1.5913	2.9517
1.7145	3.0428
1.8110	1.7927
2.1069	3.4337
0.5423	5.3416
0.9068	4.9603
1.1303	3.9302
1.2090	4.0632
1.1849	5.0589
2.0523	2.5360
1.4262	3.3896
1.4529	3.9205
1.5710	3.5109
1.8644	1.8444
1.4364	3.0538
2.0853	3.0048
1.7348	2.3788
1.9507	3.0524

Cement, 0.30, 6.5h, steel

Thickness mm	Stress MPa
0.8306	0.5719
1.2548	0.4158
1.3513	0.5166
1.2573	0.3734
1.5240	0.3552
1.1684	0.5476
1.4554	0.5900
1.9329	0.4681
1.9761	0.4287
1.6637	0.4938
1.4300	0.4060
1.6408	0.3552
1.3335	0.4900
0.6223	0.5817
1.3005	0.4931
1.1252	0.5400
0.9855	0.5067
1.5443	0.6097
1.0592	0.5029
2.1793	0.4128
1.1100	0.6120
1.9050	0.5385
1.6612	0.5294
1.9710	0.3476
1.8237	0.3809
1.9914	0.4378
1.7018	0.3476

Cement, 0.30, 4h, steel

Thickness mm	Stress MPa
1.0414	0.1242
0.8839	0.1439
0.9474	0.1340
0.8280	0.1681
1.2700	0.1189
1.7602	0.1016
1.4529	0.1106
1.4351	0.1076
1.5113	0.1371
2.1057	0.0834
2.3190	0.0751
1.6840	0.0894
2.1463	0.0713
2.0574	0.0856
1.9634	0.1227
1.8974	0.0849
1.7526	0.1091
1.4732	0.1121
1.4021	0.1151
1.8898	0.0932
2.1971	0.1106
1.9634	0.1114
2.5248	0.0738
1.9939	0.0751
2.0523	0.0864
2.7635	0.1008
2.7051	0.1068
2.0523	0.1242

Cement, 0.35, 2 days, steel

Thickness mm	Stress MPa
0.6934	2.0609
0.8103	1.7699
0.7417	1.5369
0.6731	2.3140
1.1303	1.0025
0.6553	1.4080
0.8331	2.1609
2.4130	0.0931
2.3165	0.1718
2.2225	0.1511
1.9177	0.1106
1.6078	0.6159
2.3089	0.3215
1.3081	0.6140
1.5977	0.0343
1.8263	0.1964
1.9990	0.1525
1.7983	0.2917
1.9583	0.0419
1.7069	0.5206
2.0422	0.3565
1.1176	1.0184

Cement, 0.35, 7 days, steel

Thickness mm	Stress MPa
0.4331	3.5137
0.8065	3.6847
1.0084	3.5799
0.5118	4.9389
0.9169	3.2744
0.8915	3.6481
1.3653	2.2498
1.6980	2.7187
1.5964	1.9996
0.9081	3.5040
0.8001	3.7164
1.1100	3.3579
1.2243	3.3241
0.8204	3.0717
0.7557	3.9977
1.3932	2.7035
1.0528	3.8667
1.8999	3.4096
1.6815	3.4661
1.7259	2.2574
1.8326	2.2995

Cement,0.35, 1 day,steel

Thickness mm	Stress MPa
1.3945	0.5408
1.2675	0.4691
1.0008	0.5843
1.7678	0.3257
1.0287	0.8715
1.1811	0.4540
1.1100	0.5408
1.4275	0.6485
1.2370	0.6992
1.1735	0.8826
0.7595	0.6654
0.8026	0.9281
1.0211	0.6712
1.0465	0.9260
0.9652	0.5446
1.2243	0.3408
0.9728	0.5201
1.2649	0.2643
1.3462	0.5342
1.3005	0.6083
1.3005	0.6740
1.3208	0.4493
0.7772	0.5626
1.3056	0.6060
1.4503	0.7667
1.1379	0.6513
1.6053	0.3190
1.1278	0.5248
1.0465	0.4776
1.3030	0.3945
1.0008	0.7419
1.7475	0.1227

Cement, 0.35, 7h, steel

Thickness mm	Stress MPa
0.7772	0.3822
1.1227	0.3875
0.7595	0.4132
1.4351	0.1838
1.4732	0.3474
1.3818	0.3284
1.4148	0.3185
1.8720	0.0845
1.6866	0.1845
1.1786	0.4420
1.0135	0.5200
0.6680	0.3723
1.0160	0.3679
0.6096	0.4693
1.0312	0.3837
1.6942	0.2997
1.0820	0.3307
1.9482	0.1655
1.6764	0.2852
1.6383	0.1368
1.7323	0.0974
1.7094	0.1860
1.5850	0.2830

Cement, 0.35, 4h, steel

Thickness mm	Stress MPa
1.4122	0.0825
1.2548	0.1029
1.3462	0.0992
1.5316	0.0938
1.4707	0.0931
1.4478	0.1006
1.4630	0.1044
1.3208	0.0825
1.3284	0.0969
1.7450	0.0779
1.7170	0.0712
1.5900	0.0946
1.0414	0.1158
1.0414	0.1173
1.3132	0.0916
1.5900	0.0832
1.1100	0.1067
1.4046	0.1241
1.6053	0.0832
1.3106	0.1347
1.3360	0.0969
1.6256	0.0946
1.3335	0.1150
1.1049	0.1014
1.5596	0.1036
1.7704	0.0923
1.1455	0.1324

Cement,0.30, 1 day, glass

Thickness mm	Stress MPa
1.0922	1.7748
1.0439	3.1869
1.1811	1.9554
1.4834	1.6872
1.1532	3.2972
1.4834	2.1223
1.6078	1.3623
1.4427	0.8522
1.3614	2.5663
0.9449	2.1940
0.4394	5.4781
1.2700	1.3590
1.4681	0.8522
1.6383	1.9265
1.4249	2.6953
1.2852	2.5167
1.2827	1.3494
1.3640	1.8754
0.7442	2.4601
1.3259	1.7975
1.4503	1.8775
1.3894	0.8184
1.3741	1.2701
0.6502	2.7939

Cement, 0.30, 2 days, glass

Thickness mm	Stress MPa
0.5588	4.5721
0.7061	2.0919
0.4267	2.9028
0.5639	3.3027
0.7010	3.3558
0.7341	1.9768
1.0998	2.1202
0.9296	1.7396
1.3360	1.1942
1.6916	0.6405
1.2217	2.1050
1.4961	1.8968
1.5494	0.5557
1.1582	2.7270
0.9119	2.3229
0.5258	2.6980
0.7112	2.9200
1.4783	0.7943
0.9804	1.7396
1.7780	0.9405
1.5875	1.8492
1.5113	2.1430
1.2903	2.3153
1.0820	2.9352
1.2548	2.3802
1.1735	2.5656
1.4503	0.9591
1.2217	2.7421

Cement, 0.30, 6.5 h, glass

Thickness mm	Stress MPa
0.9906	0.3829
1.2497	0.2848
1.0058	0.3740
1.1049	0.4195
0.5258	0.3967
1.1278	0.4898
1.0414	0.6340
1.7805	0.2145
1.7069	0.1689
1.5494	0.1822
2.1184	0.1234
2.2758	0.1898
2.2047	0.2088
2.1692	0.0892
1.5494	0.1689
1.4834	0.2088
1.5799	0.2297
1.6840	0.3379
1.6815	0.4627
1.6332	0.4385
1.5850	0.3550
1.5646	0.3132
1.1328	0.4822
1.7780	0.3625
2.1234	0.4005
2.1158	0.3854

Cement, 0.30, 4h, glass

Thickness mm	Stress MPa
0.7518	0.1364
1.0414	0.1598
0.8915	0.1515
1.3208	0.1069
1.3233	0.1484
1.4630	0.1151
1.2065	0.1364
1.0871	0.1386
1.7856	0.0865
1.8085	0.0661
1.8415	0.0668
1.9863	0.0721
2.0828	0.1114
2.2809	0.0645
2.6875	0.0486
2.4663	0.0199
2.3114	0.0305
1.0668	0.1069
1.7424	0.1484
1.7272	0.0743
1.9304	0.1061
1.9406	0.0812
1.4554	0.0932
2.2123	0.0532
1.9533	0.0827

Cement, 0.30, 7 days,glass

Thickness mm	Stress MPa
1.1468	1.9892
1.1836	1.4335
0.9423	2.3464
1.0122	1.7141
1.5164	1.5638
1.3132	1.5355
1.2522	1.9154
1.5075	1.6479
1.9037	1.4941
1.9279	1.3480
2.1577	1.7175
2.5235	1.6458
2.2225	1.5624
2.4270	1.5486
2.3000	1.4045
1.0655	1.5927
0.9411	1.9665
1.0744	2.1774
1.1532	1.6610
1.6269	1.6231
1.6370	1.2907
1.1265	1.6686
2.3178	1.3252
2.2073	1.3080
2.0523	1.7369
2.2009	1.3742
1.8644	1.5472
2.3851	1.5472

Cement, 0.35, 1 day,glass

Thickness mm	Stress MPa
1.1278	3.3089
0.4572	3.1414
0.3480	4.1018
1.5494	2.2250
1.1887	2.4732
1.4529	2.1243
1.3614	3.3903
1.4757	2.5022
1.8237	2.3712
1.1811	2.1774
1.3462	1.5397
0.8001	3.2951
0.4572	2.9973
1.2649	2.6422
1.2776	2.3181
1.7120	2.1168
1.1252	2.4167
1.3056	3.0579

Cement, 0.35, 2 days, glass

Thickness mm	Stress MPa
1.1252	1.1666
1.0185	1.1535
0.9677	1.8906
1.0109	1.3693
1.0185	1.5590
1.1989	1.8051
1.2624	1.9306
1.1151	1.9492
0.8255	1.5272
0.9347	2.7580
1.4859	1.4321
1.2319	0.6498
1.6053	0.9150
1.2014	1.1990
0.4343	3.3041
0.3683	3.3682
0.3556	4.4935
0.3454	3.9805
0.9830	2.4553
0.8839	1.6141
1.2700	0.8508
1.3716	0.9494
1.2624	1.3169
0.9017	1.6348
1.1735	0.5342
1.0236	1.0915
1.2751	1.3887
0.9398	1.3169

Cement, 0.35,7 h, glass

Thickness mm	Stress MPa
0.8230	0.3620
0.9068	0.3056
0.9093	0.3075
0.7163	0.3322
1.2878	0.1215
0.8661	0.3587
1.3691	0.2772
1.4910	0.3018
1.2090	0.1442
1.0820	0.1974
1.0592	0.3075
1.3106	0.2506
1.5545	0.2448
1.4097	0.2733
1.8898	0.1842
1.7399	0.2448
1.6688	0.2410
0.7391	0.3948
0.5867	0.7116
1.0617	0.5069
0.9500	0.2828
1.3335	0.2579
1.2192	0.2069
1.3691	0.2373
1.3665	0.2601
1.9812	0.2031
1.7399	0.1405
1.5824	0.2830
1.8796	0.1234
1.0516	0.4309
1.8872	0.1898
1.8567	0.1816

Cement, 0.35, 4h, glass

Thickness mm	Stress MPa
0.7950	0.0720
0.7925	0.0803
0.6350	0.0886
0.9017	0.0939
1.2471	0.0614
1.1735	0.0886
1.2268	0.0592
1.5824	0.0493
1.4275	0.0773
1.6815	0.0312
1.3970	0.0478
1.9609	0.0622
2.3673	0.0403
1.2598	0.0630
1.7018	0.0296
1.1836	0.0554
1.6815	0.0425
2.0142	0.0296
2.0447	0.0153
2.1234	0.0236

Cement, 0.35, 7 days, glass

Thickness mm	Stress MPa
1.3221	1.1818
1.2243	1.4514
1.4034	1.0377
1.6802	1.5859
1.7463	0.6470
1.7196	1.1418
0.5194	1.7589
0.4267	2.1478
1.1354	1.1439
1.5037	1.4342
1.9583	1.1687
1.4173	0.8026

Propionate, 0.30, 1 day,steel	
Thickness	Stress
mm	MPa
1.1278	3.0338
1.4478	1.2273
1.3386	2.8614
1.7856	1.5583
1.4554	1.9720
1.5621	2.0133
1.4326	2.8132
1.7272	2.3650
2.1285	1.8479
2.1412	2.2547
1.9558	2.6822
1.9558	1.0687
1.4376	3.1717
1.3564	2.3236
1.3589	2.7718
1.2116	2.6546
1.3462	2.5236
1.0693	2.7994
1.4199	2.8959
1.7450	2.0478
1.9533	2.4477
1.5316	2.2547
2.1107	2.1719
1.8313	2.1168
1.6662	2.2754
1.5316	2.8338
1.6053	2.1650
1.9685	1.5721
1.7018	2.4753
1.9050	1.8754
1.7704	2.4133
1.6916	1.7858
1.4910	2.3029
1.8034	2.1443
1.6383	2.5443
2.1057	2.3236
1.6688	2.4270
1.7805	2.0547
2.1209	2.5374
1.8948	1.5996
1.8466	2.2340
1.8669	2.2616
1.5392	2.0133
1.3868	2.1788
1.9101	2.4753

Propionate, 0.30, 1 day,steel	
Thickness	Stress
mm	MPa
1.9888	2.2478
1.9558	2.4960
1.4275	1.8272
1.7780	1.9789
1.9050	1.5721
2.0117	2.2340
1.7374	1.9168
1.3462	2.5167
2.1234	2.2850
1.5443	1.8417

Propionate, 0.30, 5.5h, steel	
Thickness	Stress
mm	MPa
0.7112	0.1333
1.6535	0.1076
1.2598	0.1083
1.2954	0.0969
1.2624	0.1303
1.1354	0.1280
1.6231	0.1500
1.1176	0.1151
2.6238	0.0818
2.0371	0.1265
1.4097	0.1432
1.8212	0.0856
2.2733	0.0628
1.1938	0.1569
2.1692	0.0567
0.5664	0.1462
0.7925	0.1698
1.3386	0.0841
1.1252	0.1318
1.1328	0.1091
1.4402	0.0939
1.7526	0.0856
2.1184	0.0878
1.8186	0.1159
2.5400	0.0249
1.9304	0.0605
2.3012	0.1038
1.8542	0.1273

Propionate, 0.30, 2 days,steel	
Thickness	Stress
mm	MPa
0.7493	1.2804
0.4826	1.4052
1.1506	0.9881
0.9855	1.1597
1.3056	0.8708
1.4681	1.0108
1.4046	1.0804
1.4275	1.2259
1.4986	0.8577
1.4326	1.0405
1.6561	1.4638
1.3208	1.5541
1.7755	1.3976
1.4427	1.5279
1.4376	0.8591
1.6891	0.9687
1.2192	1.6189
0.7620	1.1784
1.7297	1.0012
1.7831	1.1142
1.6104	0.9481
1.4427	1.1411
1.4072	1.2597
1.6586	1.1294
1.1963	0.9708
1.3081	1.1046
1.5900	1.2218
0.9017	2.1326
0.6477	2.3250
0.5334	2.7159
0.5842	1.6031
0.9119	1.4466
0.6858	3.6385
0.6833	1.7913
0.7391	2.6380
0.7544	1.7493
0.8814	1.9230
0.9169	2.5656
0.7417	1.2349
0.4064	3.6764

Propionate, 0.30,9 , steel	
Thickness	Stress
mm	MPa
0.8255	0.7447
0.8534	0.7405
1.1074	0.6626
1.1887	0.7950
0.8179	0.8633
1.6764	0.6357
1.0490	0.6206
1.4935	0.6929
1.6408	0.6061
0.7772	0.7605
2.7889	0.3110
2.3368	0.5723
2.0828	0.5006
2.8194	0.4813
1.5316	0.4647
2.1336	0.5847
1.7374	0.7260
2.3139	0.4206
1.8847	0.5192
1.8593	0.6323
1.1379	0.5578
1.2548	0.5185
1.0516	0.8784
1.3614	0.8695
1.2192	0.8557
1.4707	0.8336
1.7374	0.6095
1.5367	0.8274
1.8821	0.6971
1.9507	0.3716
1.5748	0.6847
1.9329	0.6047
1.7831	0.5923
2.4130	0.3792
2.4384	0.4392
1.8593	0.7150

Propionate, 0.35, 2 days,steel	
Thickness	Stress
mm	MPa
1.5088	0.8846
1.7450	0.7433
1.7094	0.9074
1.4529	0.9591
1.9761	0.8046
1.3640	0.9784
1.6129	0.9460
1.8898	0.8198
1.9685	0.3475
1.6586	0.8233
1.8948	0.6709
0.9322	1.0163
0.8661	2.3236
1.1024	0.9881
0.8661	1.2783
1.5189	0.8998
1.0668	1.5093
1.3462	1.5534
1.3183	0.8329
1.5316	1.1060
1.1328	0.9818
1.0211	1.6893
0.4877	2.2774
0.8458	1.7196
0.5207	2.0616
0.6782	1.7906
1.0109	2.4526
0.5131	2.4353
0.9423	2.2388
1.5291	0.6318
0.8255	2.1547
0.7671	1.9982
0.7493	2.2216
0.9779	0.9922
1.4529	1.3611
0.9957	1.4431
1.0312	1.8630
0.8890	0.1584
0.8788	2.2312
0.7899	1.6948
1.1125	1.6796
0.8306	2.1340
0.8484	1.8403
1.2802	1.9127

Propionate, 0.35, 1 day,steel	
Thickness	Stress
mm	MPa
0.9900	0.7185
1.1100	1.1928
1.3600	0.9708
0.9700	0.9460
1.2400	0.9439
1.1600	1.2080
1.0400	1.8954
1.2800	0.5337
0.9100	1.2997
1.1900	0.3289
1.2400	1.2825
0.7400	1.3790
1.0700	0.8874
1.0500	1.4438
0.8077	3.0669
1.3233	1.1239
1.1303	0.9494
1.4021	1.4500
1.7526	1.2439
1.1989	1.6679
1.7399	0.9646
1.2852	1.6134
0.7417	1.6893
1.0185	0.7640
0.9296	1.3273
0.7391	1.9147
0.6985	1.7175
1.1430	1.2701
0.4826	2.2250
0.8204	2.0644
0.9703	2.0547
0.8026	1.9051
1.0871	2.0092
0.7925	1.3797

Propionate, 0.35,9 h, steel	
Thickness mm	Stress MPa
0.6248	0.5201
0.6528	0.5817
1.1328	0.4151
1.0617	0.3345
0.7569	0.5079
1.2268	0.4950
1.1328	0.5346
1.1049	0.4303
1.2192	0.2576
1.2065	0.3132
1.0744	0.5923
1.5697	0.4029
1.2802	0.3907
1.7551	0.3778
1.5138	0.4440
1.5951	0.1991
1.7831	0.2972
1.8593	0.4143
1.5088	0.2150
2.4181	0.2302
1.3411	0.5011
0.8636	0.6297
0.7747	0.6547
1.5773	0.3869
1.6840	0.4379
1.7043	0.2819
1.0262	0.3801
1.4122	0.4851
1.8593	0.3915
1.4859	0.4341
1.7145	0.2903
1.9050	0.3040

Propionate, 0.35,5.5 h, steel	
Thickness mm	Stress MPa
0.7214	0.1069
0.8001	0.1153
0.8712	0.0842
1.5926	0.0432
1.2065	0.0956
0.8687	0.1418
1.8339	0.0614
1.9152	0.0303
1.1430	0.0675
1.9482	0.0432
1.3970	0.0622
1.9812	0.0250
1.7374	0.0296
1.8644	0.0394
1.8796	0.0561
0.7417	0.1023
1.2954	0.0561
1.3030	0.0538
1.8796	0.0584
1.5113	0.0364
1.2344	0.1047
2.2860	0.0463
1.9152	0.0326
2.0142	0.0264
1.1684	0.0569

Propionate, 0.30, 1 day, glass	
Thickness mm	Stress MPa
0.6858	2.1140
1.4834	1.9623
1.4046	2.3808
1.1989	2.0306
0.5334	2.9269
0.6731	2.4794
0.8636	2.1085
0.4775	2.1768
0.6452	2.7318
1.1557	2.0513
1.4630	2.3946
1.1659	3.0083
1.4732	2.1181
1.1354	2.8966
1.3208	2.4188
1.6154	2.0478
1.3056	1.8575
1.3081	1.8713
1.3157	2.6746
1.5621	2.5498
1.2598	3.0083
1.1100	2.7297
1.4300	2.8587
1.3284	2.9152
1.2624	3.0235
1.0109	2.1312
0.9144	2.9931
1.3462	1.9968

Propionate, 0.30, 2 day, glass	
Thickness	Stress
mm	MPa
0.6020	3.1227
0.4140	3.4806
0.7874	3.6716
1.3106	2.9014
1.2217	3.3717
1.0998	3.2655
1.3360	3.1138
1.3868	3.6847
1.1455	3.1345
1.0566	2.8649
1.2776	2.5139
1.4097	3.2200
1.4224	3.3448
1.8593	2.9524
1.9177	2.2126
2.0650	2.8063
1.4605	2.9407
1.8948	2.4381
1.5672	2.9373
1.1938	2.7304
1.2751	2.6884
1.2192	2.5105
0.9195	3.1096
0.5715	3.3034
0.6020	3.3979

Propionate, 0.30, 9h, glass	
Thickness	Stress
mm	MPa
0.7137	0.7343
0.5639	0.7778
0.8026	0.6143
1.3386	0.4240
1.3564	0.5357
1.3310	0.6447
1.3945	0.6702
1.3335	0.3482
2.0142	0.3703
2.1920	0.3882
1.4986	0.5695
2.1209	0.4737
1.5138	0.5585
1.2065	0.5619
0.5182	0.6206
1.5646	0.5199
1.4300	0.6171
1.0668	0.4392
1.0312	0.7474
1.4072	0.5854
1.4300	0.5413
1.4961	0.3992
1.6586	0.5550
1.6078	0.4661
1.6510	0.5406
1.5672	0.5668
1.8898	0.2537
1.9964	0.2951
1.8567	0.4406
1.8948	0.4992

Propionate, 0.30, 5.5h, glass	
Thickness	Stress
mm	MPa
0.7925	0.1738
0.8992	0.1383
1.3818	0.1420
1.3005	0.1156
1.3716	0.1163
1.4072	0.1035
1.9126	0.0936
1.8694	0.1322
0.7823	0.1618
1.3716	0.1300
1.4630	0.1602
1.4224	0.1285
2.1717	0.0982
1.8186	0.1269
1.7780	0.1564
1.2827	0.1511
2.2276	0.1080
2.3571	0.0474
2.0930	0.0769
2.4130	0.0860
2.2657	0.1072

Propionate, 0.35, 1 day, glass	
Thickness	Stress
mm	MPa
0.9728	2.2816
1.3589	2.0009
1.3360	1.6479
1.2116	1.8885
1.4884	1.5210
1.5138	1.6782
1.4351	1.7389
1.9050	0.7529
1.3665	2.3477
1.5113	2.1905
1.8034	1.7672
1.6408	2.3271
1.4986	2.0844
1.1760	1.9154
0.9500	2.7911
1.2522	2.4539
1.1176	1.9871
1.4884	1.5645
1.2268	2.4463
1.3005	2.5484
0.9398	2.0064
1.1938	2.0954

Propionate, 0.35, 2 days, glass

Thickness mm	Stress MPa
0.2997	2.5994
0.4369	2.9290
0.4242	2.8511
0.3810	3.3441
0.3505	2.5842
1.3208	1.6645
1.4554	1.5865
0.9728	2.9193
1.1227	2.7187
1.0236	2.7359
1.3818	1.6003
1.3208	2.2733
1.3081	2.0251
1.0363	2.1443
0.9093	2.3071
1.7348	2.1250
1.1709	2.2485
1.1735	2.5236
1.4986	1.7348
1.4605	1.7293
1.7526	1.6307
1.4249	1.7217

Propionate, 0.35, 5.5h, glass

Thickness mm	Stress MPa
1.3030	0.0643
1.1938	0.0590
1.2573	0.0984
1.4503	0.0984
0.8788	0.1029
0.9906	0.1151
2.1590	0.0182
1.3208	0.0825
2.0168	0.0242
1.2649	0.0613
0.9779	0.0719
0.8077	0.0961
0.8687	0.0923
2.0574	0.0348
1.7602	0.0447
1.5469	0.0613
1.6688	0.0394
1.9228	0.0439
1.5926	0.0560
2.0117	0.0598

Propionate, 0.35, 9h, glass

Thickness mm	Stress MPa
0.6198	0.3666
0.6350	0.3090
0.7899	0.4530
0.6528	0.4643
1.0211	0.2105
0.9144	0.3219
1.2827	0.2795
1.5494	0.1613
1.0084	0.3681
1.2344	0.3681
1.8288	0.0590
1.3818	0.2499
1.4935	0.1537
1.4046	0.3014
1.8618	0.1150
0.9220	0.1969
0.6248	0.3068
0.5232	0.3674
0.6604	0.5431
1.1125	0.3317
1.5799	0.2666
1.1557	0.2559
1.0109	0.2795
1.9888	0.0953
1.3208	0.1446
1.2573	0.2272
1.1557	0.1484

NaNO3, 0.30,1 day,steel

Thickness mm	Stress MPa
0.7518	2.7242
0.9195	4.6679
1.0363	4.2466
0.9017	2.4974
0.9855	3.3558
0.7950	3.6171
0.9246	3.0400
0.9296	4.3066
1.1608	3.4675
1.5570	3.2365
1.4707	2.0478
1.4630	3.7433
2.1082	3.3675
1.5189	3.3882
2.1539	2.3409
1.8415	2.7263
1.7323	3.4337
1.7424	1.9189
1.5037	2.9345
2.6010	1.9699
2.1285	1.9209
1.7018	2.0023
1.8618	2.8683
1.9583	1.8548
1.7120	3.8322
2.1082	2.2140
2.0549	1.6038
1.8618	3.1421
2.0193	2.2030
2.1133	2.8228
2.4562	2.6277
1.6662	2.6601
1.7983	1.9796
2.0015	2.0402
1.8847	2.0058
1.6383	2.2443
1.8796	1.9547
2.0574	2.2781
1.5850	2.7242
1.0109	2.4808
2.1158	1.7072
2.2936	2.4298
2.0980	2.2629
2.0269	2.5622
1.7577	2.3615
2.2174	2.3422

NaNO3,0.30, 1 day,steel

Thickness mm	Stress MPa
2.1844	2.3560
2.6797	2.3974
2.4054	1.7996
2.2454	2.6642
2.1438	2.7284
2.5629	1.7527
2.8931	1.6300

NaNO3, 0.30, 2 days,steel

Thickness mm	Stress MPa
0.6248	2.7070
0.4318	3.0000
1.3106	2.0409
1.4351	1.8196
0.9652	3.1627
1.7475	1.9996
1.2725	2.7808
1.4224	1.9616
1.7094	2.4064
1.5773	2.5105
2.2606	1.8106
0.4242	4.0784
0.4572	2.4139
0.9525	3.1758
1.1760	2.3967
1.4173	2.5711
1.6332	2.1850
1.7780	2.7146
1.2979	1.9596
1.6459	1.7824
1.4859	2.3422
1.4122	2.1319
1.7424	2.1057

NaNO3, 0.30,6.5 h, steel

Thickness mm	Stress MPa
0.8534	0.3449
0.8712	0.3814
0.9296	0.3814
0.8331	0.3973
0.7264	0.4702
1.1938	0.3411
1.5113	0.2910
1.5265	0.3122
1.2065	0.4117
1.8720	0.2895
1.4732	0.2575
1.9990	0.2796
1.8618	0.2819
1.7501	0.2203
1.5799	0.2211
2.1717	0.1922
1.7374	0.2720
2.1209	0.0646
0.8585	0.2963
0.8128	0.2811
0.7671	0.3950
0.8763	0.3479
0.9855	0.4041
1.4300	0.2712
1.2040	0.2689
1.3767	0.3190
1.6993	0.3168
1.2090	0.3137
1.9406	0.2462
1.5672	0.2203
1.6129	0.2469
1.2776	0.2257
1.4045	0.2598
2.1158	0.2180
2.3419	0.1231
1.2040	0.2142
1.6535	0.1451
2.0904	0.2317

NaNO3, 0.30, 4h, steel

Thickness mm	Stress MPa
0.8992	0.1429
0.9779	0.1444
0.9855	0.1489
1.2294	0.0828
1.2090	0.1094
1.1684	0.1125
1.0820	0.1315
1.0719	0.1178
1.5392	0.1079
1.2725	0.0889
1.7297	0.0654
1.9431	0.0927
1.7577	0.0958
1.9558	0.0395
2.5222	0.0327
1.8339	0.0767
2.3774	0.0167
1.3157	0.0843
0.7798	0.1527
0.7315	0.1748
0.9246	0.1087
1.0414	0.1330
1.6535	0.1238
1.7551	0.1216
0.9728	0.1162
1.6688	0.1018
1.5672	0.0843
2.1920	0.0532
2.0625	0.0638
2.0142	0.0912
1.9126	0.0798
1.8948	0.0904
2.0142	0.0547

NaNO3,0.30, 7 days, steel

Thickness mm	Stress MPa
0.6058	4.1232
0.9525	3.4282
0.8750	2.1554
0.9347	2.9166
1.2954	3.6537
1.4630	2.5201
1.1176	2.0513
1.3970	1.6086
1.0668	1.7968
1.3081	1.2687
1.7120	0.9625
1.7729	1.1549
1.8771	2.1402
1.4453	2.2678
1.8542	1.5879
2.7280	0.2434
2.1260	2.1140

NaNO3,0.35, 2 days, steel

Thickness mm	Stress MPa
0.8204	1.3673
0.6553	2.5670
0.9068	0.9143
1.2319	0.9143
0.6528	1.1411
1.4275	0.6826
1.4072	1.3749
1.6358	0.6199
1.1354	1.8727
1.3157	2.0457
1.5062	1.1928
1.8517	0.8798
2.0422	0.6492
1.0973	0.8688
2.2936	1.1777
0.7417	2.5967
0.8509	3.2296
0.9093	3.6330
1.5443	1.5397
0.9322	2.6380
0.8280	2.3636
1.0490	1.7120
1.3386	2.3560
1.2903	1.7631

NaNO3,0.35, 1 day,steel

Thickness mm	Stress MPa
1.2700	3.5916
0.9449	3.1641
1.1024	3.2420
1.1430	2.3284
1.2700	2.0913
1.5215	2.0699
1.7069	2.0147
2.3216	1.8458
1.8618	2.5415
2.0117	1.1901
1.8110	2.5836
0.9779	2.9531
2.1336	2.5911
1.4630	3.2275
1.6535	2.4429
1.1532	2.9586
1.7907	2.8642
1.2446	3.3606
1.1252	2.4601
1.2522	2.4188
1.4326	3.0931
1.0236	3.3434

NaNO, 0.35,4 h, steel

Thickness mm	Stress MPa
0.8382	0.1033
1.0058	0.1071
1.6002	0.0972
1.1963	0.1086
1.1735	0.1010
0.8992	0.1139
1.3640	0.1063
1.6104	0.0965
1.2268	0.1610
1.0795	0.1663
1.4478	0.1169
1.0262	0.1010
1.1100	0.1587
1.2497	0.1018
2.2682	0.0235
1.4732	0.1018
1.8542	0.0531
1.3640	0.1177
2.2530	0.0296
1.8745	0.0789
1.8618	0.0456

NaNO, 0.35 ,7 h, steel

Thickness mm	Stress MPa
0.5690	0.2659
0.7264	0.2841
1.0109	0.2097
1.1735	0.2355
1.1735	0.2910
1.0922	0.1801
1.3716	0.1945
1.4554	0.1383
1.2116	0.1786
1.7348	0.0829
0.9677	0.2165
1.6967	0.2013
0.7747	0.2530
0.6426	0.3061
1.1379	0.2219
1.2344	0.2226
1.0592	0.2963
1.2268	0.2819
1.0414	0.2537
1.8542	0.1558
1.0973	0.2689
1.4173	0.2157
1.3437	0.1998
1.3259	0.2112
1.3208	0.1960

NaNO3, 0.35, 7d, steel

Thickness mm	Stress MPa
0.4318	2.6394
0.3886	2.8683
0.4636	2.2402
0.5728	3.0807
0.8636	2.8214
1.9761	2.1588
1.9482	1.8368
1.8593	2.2740
2.4600	0.6226
1.8453	2.1795

NaNO3,0.30, 1 day, glass

Thickness mm	Stress MPa
0.7315	3.2524
0.9373	2.4725
0.6883	3.0607
0.8103	3.3096
0.3353	4.2225
1.2954	1.7879
1.3030	2.6801
0.9398	3.1083
1.0185	3.4103
1.2979	2.1319
1.5646	1.8030
1.4910	2.0809
1.5291	2.0009
1.7780	2.0009
1.2014	1.6507
1.9482	1.2611
0.5131	2.7732
0.5334	3.6557
0.5994	3.4551
1.1811	2.4994
0.9652	1.7196
1.2192	1.7899
1.3386	1.9113
1.2268	1.6127
0.9906	2.7656
1.1913	2.0127
1.2421	1.8754
0.9728	3.3703
1.1481	2.1933

NaNO3, 0.30, 2 days, glass

Thickness mm	Stress MPa
1.3132	1.5238
0.8712	1.9058
0.9042	2.1312
1.5570	1.9209
1.2471	1.5596
0.2921	2.9828
0.6223	2.0326
0.3200	2.3243
1.5062	1.4514
0.9703	2.1630
1.1278	1.4990
1.2624	1.3949
1.1328	2.2085
1.7043	1.7169
1.7653	1.5955
1.6942	2.3919
1.6866	1.9871
0.5893	2.6704
0.5639	3.3006
0.8661	2.4395
0.8585	3.2041
0.6934	2.7401
1.3894	1.9382
1.7780	1.9589
1.2954	2.4974
1.6256	2.1781
1.1989	2.4622
1.5596	1.8189
1.3513	2.0002
1.2954	1.9989
1.1328	2.2388

NaNO3, 0.30, 6.5h , glass

Thickness mm	Stress MPa
0.4724	0.4280
0.5639	0.3901
0.5131	0.3772
0.8255	0.4909
1.0871	0.2923
0.9017	0.4257
1.0414	0.4181
0.9017	0.4643
1.7602	0.5060
1.4224	0.4204
1.9482	0.2545
1.9177	0.2908
2.3038	0.3052
1.8618	0.2522
1.7780	0.4833
1.7094	0.4356
2.4663	0.2227
1.8821	0.3598
0.3683	0.5173
0.8509	0.2992
0.7010	0.5832
0.6299	0.4166
1.0566	0.2704
0.8407	0.4045
1.4910	0.3469
0.7696	0.4295
1.0617	0.5113
1.1735	0.3166
1.1836	0.3841
1.3716	0.2818
1.5519	0.3878
1.3919	0.4431
2.0523	0.3250
1.5113	0.3795
1.8593	0.2484
1.7297	0.4174
2.3495	0.3567

NaNO3, 0.30, 4h, glass

Thickness mm	Stress MPa
1.2268	0.0984
0.9042	0.1378
1.7272	0.0976
1.1506	0.1090
1.4808	0.0894
1.1862	0.1219
1.6104	0.1075
1.1760	0.1098
1.7424	0.1189
1.8466	0.0704
1.6510	0.0674
1.7882	0.0841
1.7374	0.0583
2.3495	0.0651
2.2098	0.0507
1.9126	0.0485
1.0287	0.1037
0.9576	0.1151
1.0668	0.1567
1.0947	0.1098
1.4275	0.0674
1.5113	0.0938
1.2192	0.1242
1.2700	0.1211
1.7018	0.0954
1.5621	0.0946
1.6891	0.0772
2.0066	0.0643
1.9837	0.0765
2.0726	0.0666
2.0447	0.0500
2.0091	0.0386

NaNO3, 0.30, 7days, glass

Thickness mm	Stress MPa
0.5220	2.4084
1.4745	1.6582
1.0782	2.2278
1.5634	2.0850
1.5900	1.7872
1.9164	1.9582
0.3353	2.1974
0.7544	1.7906
0.9106	1.6962
0.7772	1.9520

NaNO3, 1 day, 0.35, glass

Thickness mm	Stress MPa
0.4140	1.8451
0.9601	1.3397
0.4140	2.2016
0.5410	2.2678
0.4826	2.3374
0.9804	1.9458
1.1938	2.2885
1.6104	1.6196
1.1303	1.7672
1.2573	2.0099
1.2954	2.0230
1.5240	2.0595
1.1100	2.4305
1.6840	2.2016
1.4376	1.3487
1.3106	1.8623
1.4351	1.8375
1.8339	1.6086
0.3556	1.8341
0.3988	1.8658
0.5080	1.5934
0.3404	2.1312
0.5588	1.7486
1.1100	1.5417
1.1963	2.3374
1.2116	1.6162
0.9779	1.3845
1.0211	1.4397
1.0846	1.8679
1.2700	1.7582
1.0465	1.4928
1.2497	1.7355
1.5850	1.7617
1.5799	1.5859
1.4910	1.6500
1.9406	1.5135

NaNO3, 0.35, 2 days, glass

Thickness mm	Stress MPa
1.1709	1.1984
1.3462	0.7433
1.5088	0.6412
1.5850	0.5406
1.5646	0.9425
0.7239	1.3404
0.9830	0.8246
0.7137	1.5927
0.9347	1.5341
0.8153	1.2004
0.7722	0.9708
0.7366	1.4466
0.3988	2.8256
0.7874	1.4486
1.4402	0.7736
0.9169	0.9274
1.1481	1.0205
1.6434	0.3661
1.0541	1.0887
1.1709	0.5254
0.9373	1.1204
0.9525	1.5135
1.1024	0.7736
0.7849	2.8276
0.8941	2.2512
1.2294	1.8810
0.6350	2.4767
0.7214	2.1961
0.7874	2.9869
0.7010	2.0706
0.6858	2.2209

NaNO3, 0.35, 7h, glass

Thickness mm	Stress MPa
0.6858	0.2098
1.1252	0.1576
1.0414	0.1091
0.9017	0.1924
0.3556	0.3386
1.6662	0.1212
1.1684	0.1220
1.7272	0.0538
1.4097	0.1167
1.3259	0.1393
1.7399	0.0659
1.0668	0.1076
1.2217	0.1621
0.6477	0.1447
0.7239	0.2030
0.6274	0.1878
0.5664	0.1742
0.8026	0.2446
0.3454	0.2719
1.0947	0.1583
1.0160	0.1431
0.9398	0.1765
1.2090	0.1886
1.2090	0.2227
1.2700	0.1477
1.4351	0.1629

NaNO3, 0.35, 4h, glass

Thickness mm	Stress MPa
0.5690	0.0661
0.8966	0.0528
0.8280	0.1043
1.3208	0.0581
0.8280	0.0543
1.0592	0.0808
1.0719	0.0816
0.8890	0.0634
0.9144	0.0558
1.6154	0.0664
1.6256	0.0315
1.5443	0.0626
1.2700	0.0725
1.8034	0.0270
0.8407	0.0558
0.9601	0.0694
0.7950	0.0566
0.9195	0.0535
0.9855	0.0528
1.4376	0.0550
1.1278	0.0475
0.9398	0.0634
1.4148	0.0376
1.3462	0.0679
1.7450	0.0262
1.7094	0.0550
1.2192	0.0588
1.5062	0.0528

NaNO3, 0.35, 7 days, glass

Thickness mm	Stress MPa
0.5004	1.3914
0.3353	2.1974
0.7544	1.7906
0.9106	1.6962
0.7772	1.9520
1.1062	1.1508

CaCl2, 0.30 , 1 day,steel

Thickness mm	Stress MPa
1.1125	2.9738
0.9728	3.0372
1.4935	2.4250
1.4884	1.8244
1.0465	3.6481
2.0904	2.8738
2.4282	2.5346
2.1311	1.7941
1.8466	3.1317
2.2174	1.4307
2.4435	2.4877
2.4130	1.8637
2.4994	2.1257
1.9304	3.0697
1.4605	2.5063
1.9685	3.1317
2.8372	2.1574
1.6891	3.3786
1.5392	2.7697
1.4707	2.5380
1.2827	2.0223
1.6637	2.6001
2.1361	1.8299
1.7678	1.9389
2.5933	1.7789
2.2123	1.3666
1.8999	1.7265
2.2733	1.1949
2.4917	2.6360
2.1539	1.7810
1.7475	3.6778
2.3114	1.2921
1.5875	2.0726
1.5392	2.0540
1.0414	3.6254
1.9634	2.2781
1.9355	1.9671
1.5951	3.0924
2.2606	2.4801
0.9652	2.9469
1.4427	3.4220
1.5215	1.9596
1.7755	2.3705

CaCl2, 0.30, 2 days,steel

Thickness mm	Stress MPa
0.6528	4.4735
1.3818	2.8587
2.0676	2.3250
1.8085	2.3064
1.5113	1.8637
1.0414	2.3133
1.1328	3.6171
1.2319	2.8752
1.1278	3.3482
0.6960	2.2533
1.3487	3.6778
1.4859	2.8221
1.2090	3.1159
1.1532	3.6226
1.2624	4.1639
1.5519	2.2967
0.7823	2.4043
0.7544	2.4532
0.6375	2.2664
1.2548	3.4544
1.2954	2.7842
1.3792	2.8125
1.5011	2.8890
0.8331	3.9950
1.0795	3.2496

CaCl2, 0.30, 5h, steel

Thickness mm	Stress MPa
0.8128	0.4528
1.4630	0.2853
1.6205	0.2343
1.6078	0.2846
1.4580	0.3416
2.7330	0.1909
2.5121	0.1977
2.3952	0.2252
2.2962	0.2039
1.2141	0.2838
1.0363	0.2983
1.0109	0.4718
1.2878	0.3889
1.7602	0.2701
1.4834	0.3295
1.7602	0.3561
1.3208	0.2708
2.7432	0.1536
1.7577	0.2952
2.0066	0.2252
1.7780	0.3158
1.9964	0.3630
2.1946	0.2503
2.3546	0.2199
2.8626	0.1460
1.8542	0.3866
1.8618	0.4079

CaCl2, 0.30,3 h, steel

Thickness mm	Stress MPa
0.6934	0.1989
0.7874	0.2118
0.7874	0.1685
1.1557	0.1784
1.1557	0.1678
1.5189	0.1632
1.2294	0.1587
1.5672	0.1571
1.4224	0.1374
1.8161	0.1252
1.7424	0.1237
1.8364	0.1154
1.9050	0.1351
2.3139	0.0812
2.3876	0.0501
2.5146	0.1032
2.1692	0.0789
2.1742	0.0758
0.7722	0.1503
0.7620	0.1389
0.7214	0.1450
0.9525	0.1290
1.1684	0.1085
1.5596	0.0918
1.2548	0.1191
1.3894	0.1237
1.8796	0.1032
2.0396	0.0979
2.0269	0.1093
1.8440	0.0964
2.1336	0.0675
1.7526	0.0926
1.9964	0.0713
2.1006	0.0736
2.2784	0.1025

CaCl2, 0.35, 2 days,steel	
Thickness	Stress
mm	MPa
1.5088	0.8846
1.7450	0.7433
1.7094	0.9074
1.0465	0.5544
1.4529	0.9591
1.2548	0.2124
1.9761	0.8046
1.3640	0.9784
1.6129	0.9460
2.0244	0.1717
1.8898	0.8198
1.9685	0.3475
1.6586	0.8233
1.8948	0.6709
0.9322	1.0143
0.9398	0.8102
1.1430	0.3572
0.8661	2.3236
1.1024	0.9881
1.2040	0.3399
0.8661	1.2783
1.5189	0.8998
1.0668	1.5093
1.3462	1.5534
1.3183	0.8329
1.2217	0.2200
1.4199	0.2255
1.4656	0.2979
1.5316	1.1060
1.1328	0.9818
1.0211	1.6893
0.4877	2.2774
0.8458	1.7196
0.5207	2.0616
0.6782	1.7906
1.0109	2.4526
0.5131	2.4353
0.9423	2.2388
1.5291	0.6318
0.8255	2.1547
0.7671	1.9982
0.7493	2.2216
0.9779	0.9922
1.4529	1.3611
0.9957	1.4431
1.0312	1.8630

CaCl2, 0.35, 2 days,steel	
Thickness	Stress
mm	MPa
0.8788	2.2312
0.7899	1.6948
1.1125	1.6796
0.8306	2.1340
0.8484	1.8403
1.2802	1.9127
0.9931	3.0669
0.4343	4.9623
0.9754	4.1701
0.5766	2.9131
0.7264	2.5063
0.8966	0.7385
0.9093	1.2701
1.1836	2.2057
0.5207	2.8090
0.7569	1.7596
0.9347	1.0660
0.9195	1.6610
1.1074	3.8467
1.0008	1.5066
1.0617	0.2415
1.0439	3.4840
1.0516	2.9283
1.2751	3.1358
0.9576	2.6918
0.9195	1.8541
0.9093	2.0223

CaCl2,0.35,1 day, steel	
Thickness	Stress
mm	MPa
1.5240	1.6596
2.0955	2.0671
1.2395	2.4505
1.3233	1.2894
1.6840	0.7819
1.7958	2.6429
1.7297	2.1464
1.3741	2.2181
1.5799	1.6707
1.3818	2.0106
1.9304	1.9858
1.3056	2.2519
1.6561	1.7086
1.6688	0.8536
1.9888	0.7516
2.0320	1.7313
1.9837	0.7888
1.7145	0.6702
1.7323	0.7798
1.8440	1.3066
1.3208	1.5383
1.6205	1.8368
1.3183	1.9347
1.6891	2.1430
1.5215	1.6631
1.4326	1.5459
1.3538	2.1595
1.3792	2.6449
1.3284	2.3257
1.3335	2.2085
1.3665	2.8938
1.6586	2.2995
1.1938	3.0924
1.6154	2.8132
1.3360	2.3898
1.7120	1.2004
1.2014	2.9938
0.6807	2.8828
1.3081	2.8600
1.1735	3.5944
0.8077	3.4999
1.6002	2.6111
0.9017	2.6070
0.9322	2.2843
1.3157	3.2055
0.7315	2.4691

CaCl2,0.35, 1 day, steel

Thickness mm	Stress MPa
1.8212	2.0182
1.0947	3.8136
1.3538	2.7752
1.5291	1.2383
1.1405	1.4804
1.2243	1.7238
1.8593	1.3232
1.8466	1.9996
1.5113	2.3388

CaCl2, 0.35, 5.5h, steel

Thickness mm	Stress MPa
0.9728	0.1621
0.9423	0.1385
1.3995	0.0898
1.6053	0.0745
1.4580	0.0958
1.8034	0.1369
1.7348	0.0753
1.6307	0.1217
1.7704	0.1156
2.0193	0.0745
0.9322	0.1644
1.0211	0.2321
0.8331	0.1917
1.7653	0.0753
0.6985	0.2260
1.6510	0.0479
1.3005	0.1058
0.9474	0.1697
1.6789	0.1065
1.8313	0.0578
1.9126	0.0738
2.1361	0.0563
2.0574	0.0920
1.7882	0.1066

CaCl2, 0.35, 3.5h, steel

Thickness mm	Stress MPa
0.5334	0.0969
0.6274	0.1000
0.9906	0.0764
0.6934	0.1083
0.7874	0.1212
0.8331	0.1189
0.9754	0.1114
1.3894	0.1015
0.8001	0.1151
1.3030	0.1038
1.7145	0.0605
1.2700	0.0726
1.7602	0.0529
1.7526	0.0658
2.2606	0.0521
2.0828	0.0620
2.4714	0.0437
2.2809	0.0179
0.5842	0.1060
1.0770	0.1038
0.8484	0.1227
0.5080	0.1333
0.4953	0.1159
1.0541	0.0976
1.1684	0.0992
1.2014	0.0992
1.2903	0.1151
1.3665	0.0984
1.6027	0.0483
1.7932	0.0992
1.8059	0.0916
1.8872	0.0627
1.7577	0.0688
1.7272	0.0961
1.7958	0.0627
1.4935	0.0665

CaCl2, 0.30 1 day, glass

Thickness mm	Stress MPa
0.8179	3.3365
0.5334	3.4523
1.0008	2.1533
0.7214	3.5551
1.4707	2.0278
1.0922	1.5693
1.3919	1.4893
1.5138	2.0030
1.3411	2.4291
0.8712	2.3450
0.6121	3.4827
1.1887	2.8587
0.9855	2.5960
1.2370	2.7235
1.1532	3.0641
1.5113	1.7382
1.3233	1.7631
1.4732	2.0864
0.8712	3.5302
1.0363	3.0359
0.6350	3.2144
1.0033	2.6594
0.7696	2.8663

CaCl2, 0.30, 2 days , glass

Thickness mm	Stress MPa
1.8288	1.5603
1.3157	1.5603
1.4199	1.8292
1.6840	1.2183
1.8110	1.6189
0.8204	2.4877
0.7772	2.2264
1.0084	1.5755
1.4224	1.5721
1.2243	1.7120
1.3259	2.0299
1.3132	1.3976
1.2141	1.6817
0.8407	2.2002
1.3284	1.5169
1.4275	1.4224
1.4732	1.7968
0.8687	2.0561
1.0109	1.5603
0.8814	2.5139

CaCl2, 0.30, 5h, glass

Thickness mm	Stress MPa
0.9271	0.4094
0.9246	0.1820
1.1074	0.1880
0.7214	0.2510
1.2014	0.2411
1.3843	0.2320
2.0980	0.1911
2.0447	0.1539
1.8694	0.1494
2.4384	0.1220
1.8898	0.2404
1.8567	0.0599
1.3665	0.2237
0.9042	0.2570
0.6198	0.5428
0.7010	0.3798
1.4783	0.2077
1.6078	0.0978
1.3538	0.1342
1.1938	0.2040
0.8890	0.2639
1.5570	0.2062
2.0142	0.1501

CaCl2, 0.30, 3h, glass

Thickness mm	Stress MPa
1.0744	0.1114
1.5088	0.0766
1.4986	0.0985
2.1184	0.0932
1.8364	0.0652
1.4732	0.1175
1.7018	0.1175
2.4130	0.0303
1.8059	0.1008
2.0066	0.0698
2.1209	0.0561
2.1946	0.0516
2.2631	0.0842
1.2878	0.1099
1.1913	0.0978
1.3132	0.0879
1.9456	0.1008
1.8872	0.1069
1.7907	0.1076
1.8110	0.1091
2.0244	0.0970
2.1742	0.0485
2.0777	0.0675

CaCl2, 0.35, 1 day, glass

Thickness mm	Stress MPa
0.4140	2.0913
0.5029	1.1790
0.6655	1.3080
0.8433	1.1356
1.2522	0.9232
1.3640	0.7619
1.1735	0.6957
1.0414	1.0067
1.0516	1.0108
0.8534	1.4238
1.1278	1.0998
1.1328	1.1108
1.1582	1.1584
1.3716	0.7791
1.2776	0.9860
2.0574	0.7716
1.4834	1.1473
1.7069	1.0198
1.4681	0.7564
0.7823	1.6265
0.4547	1.3197
0.7163	1.3900
0.5842	1.3156
0.3480	1.3045
0.7214	1.3859
0.9576	1.3597
0.9144	1.4280
0.8941	1.2308
1.0439	0.8722
1.3995	0.8343
1.5773	0.5516
1.1379	0.6785
1.1430	1.0998

CaCl2, 0.35, 2 days, glass

Thickness mm	Stress MPa
0.9449	1.5955
1.2446	1.7127
1.7374	1.1135
0.6096	1.3045
0.6985	1.2356
0.7722	1.5334
0.9652	1.2246
0.3759	1.8244
0.4420	1.2687
1.6688	1.5727
2.0269	1.4480
1.4300	1.1604
1.2903	1.4404
2.0320	1.2287
0.9601	1.7624
0.7442	1.7810
0.9449	1.8079
0.7874	1.7810
1.0287	1.3121
0.5613	1.4086
0.8382	1.9478

CaCl2, 0.35, 5.5h, glass

Thickness mm	Stress MPa
0.6096	0.3040
0.7696	0.2624
0.7569	0.2100
0.5359	0.3973
0.6045	0.3063
1.5850	0.2586
0.9957	0.3442
1.1151	0.2806
1.3665	0.1683
1.3945	0.2464
1.9126	0.2290
1.5900	0.1698
1.4783	0.2631
1.8339	0.1304
0.4242	0.3427
0.5893	0.2479
0.5080	0.3396
0.4877	0.2715
1.1532	0.2775
0.8636	0.2297
1.1811	0.2972
1.2979	0.2214
1.3132	0.1797
1.3360	0.1850
1.6434	0.1971
1.7856	0.2335
0.8611	0.2994
1.8237	0.2017
1.7323	0.2692
1.1328	0.2912

CaCl2, 0.35, 3.5h, glass

Thickness mm	Stress MPa
0.6604	0.0622
0.7137	0.0538
0.9449	0.0622
0.8306	0.1000
0.9474	0.0819
1.3665	0.0629
1.2319	0.0356
1.3665	0.0531
1.5748	0.0652
1.2192	0.0879
2.0980	0.0152
1.5799	0.0417
1.8593	0.0553
0.7391	0.0751
1.1176	0.0812
1.0770	0.0402
1.5011	0.0652
1.1735	0.0523
1.6180	0.0349
1.8542	0.0349
1.3970	0.0243
1.8466	0.0341
1.1176	0.0660
1.5850	0.0227
1.4580	0.0561